Modeling the biomechanical behavior of a biprosthetic femur for the development of a numerical decision-making tool during implant placement

Ahmed Mohsen Mohammed Abdelkader

Ecole doctorale 269 Mathématiques,

Sciences de l'Information et de l'Ingénieur

En vue d'une soutenance le : 14/09/2021

par:

Ahmed MOHSEN MOHAMMED ABDELKADER

Pour obtenir le grade de : Docteur de l'université de Strasbourg

Modélisation du comportement biomécanique d'un fémur biprothésé pour le développement d'un outil numérique d'aide à la décision lors de la pose d'implant

Thèse dirigée par:

Pr. Nadia BAHLOULI	ICube, Université de Strasbourg
Pr. Sybille FACCA	ICube, Université de Strasbourg

Rapporteurs :

Pr. Laurent GORNET	GeM, Université de Nantes, CNRS 6183
Pr. Franck JOURDAN	LMGC, Université de Montpellier UMR 5508

Examinateurs :

Pr. Patrick CHABRAND	ISM, Université d'Aix-Marseille UMR 7287
Pr. Matthieu EHLINGER	ICube, Université de Strasbourg
Dr. Christophe CLUZEL	LMT - ENS-PARIS-SACLAY
Dr. João Pedro DE MAGALHÃES CORREIA	ICube, Université de Strasbourg

Doctoral school 269 « Mathematics,

Sciences of the Information and the Engineer

For a defense on 14/09/2021

By:

Ahmed MOHSEN MOHAMMED ABDELKADER

To obtain the degree of : Doctor of the University of Strasbourg

Modeling the biomechanical behavior of a biprosthetic femur for the development of a numerical decision-making tool during implant placement

Thesis directed byr:

Pr. Nadia BAHLOULI	ICube, university of Strasbourg
Pr. Sybille FACCA	ICube, university of Strasbourg

Rapporteurs :

Pr. Laurent GORNET	GeM, university of Nantes, CNRS 6183
Pr. Franck JOURDAN	LMGC, university of Montpellier UMR 5508

Examiners :

Pr. Patrick CHABRAND	ISM, Université d'Aix-Marseille UMR 7287
Pr. Matthieu EHLINGER	ICube, university of Strasbourg
Dr. Christophe CLUZEL	LMT - ENS-PARIS-SACLAY
Dr. João Pedro DE MAGALHÃES CORREIA	ICube, university of Strasbourg

Acknowledgement:

First of all, I would like to express my sincere thanks and gratitude to the thesis director Pr. Nadia BAHLOULI, and the thesis co-director Pr. Sybille FACCA my thesis directors for their efforts in providing useful suggestions, confidence and valuable guidance during each step of my work.

I would also like to thank NEWCLIP TECHNICS company represented by the general director Mr. Jean-Pierre PODGORSKI and the R&D department for the funding they provided for this thesis, and for the technical support.

A grateful thanks to Pr. Laurent GORNET and, Pr. Franck JOURDAN for agreeing to review this thesis. Their pertinent remarks helped me a lot to improve the quality of this work.

I would also like to thank the examiners Pr. Patrick CHABRAND, Pr. Matthieu EHLINGER, Dr. Christophe CLUZEL, and Dr. João Pedro DE MAGALHÃES CORREIA, to whom I extend my most respectful sentiments.

I also would like to thank Dr. João Pedro DE MAGALHÃES CORREIA. He had the biggest contribution numerically. He helped me to focus on what's important in the thesis. He was always offering advice and encouragement with a perfect blend of insight and humor. I'm proud of, and grateful for, my time working with him.

A huge acknowledgment is reserved to Dr. Christophe CLUZEL, who had the biggest contribution scientifically. His work ethics, scientific vision and process helped forge this work into its final shape, and I can only be thankful for his patience and help.

Words are not enough my thanks and gratitude to the whole ICube research team at the Boussingault site. Thanks to all my friends: Ali, Camille, Chrystelle, Hamdi, Mehdi.... And the list goes on for their honest support. Finally, i extend my thanks and gratitude to all of my family: my father's soul, my mother, my wife Anca, my daughter Myriam, my sister Eman and my brother Mohammed.

Contents

List of Figures

List of Tables

Résumé en français de la thèse

Sur l'étude d'un fémur bi- prothésé :

Modélisation et simulation de différents cas de chargements

Par : Ahmed ABDELKADER

Pr. Nadia BAHLOULI (1),

Le superviseur principal 1

Fournir les principales informations et données concernant la thèse, Examen et analyse des résultats. Suivi régulier des travaux de thèse en collaboration avec les différents encadrants et partenaires de la thèse. Correction des divers rapports, des PowerPoint, du manuscrit et de la soutenance.

Pr. Sybille FACCA (1,2)

Le superviseur principal 2

Fournir les principales informations et données concernant la partie anatomique /santé de la thèse.

Examen et analyse des résultats.

1. ICUBE Laboratory, University of Strasbourg - CNRS, 2 Rue Boussingault, 67000 Strasbourg, France.

2. Hand Surgery Department, Strasbourg University Hospital

Résumé en français de la thèse

Introduction :

L'arthroplastie totale de la hanche (ATH) et l'arthroplastie totale du genou (ATG) sont devenues des actes de plus en plus courants chez les personnes âgées. Cependant, il existe un risque élevé de fracture interprothétique (FI) pour les patients ayant subis sur la même jambe une arthroplastie de la hanche et du genou. Dans le cadre de cette étude, nous évaluons à partir de simulations numériques, la réponse mécanique d'un fémur avec arthroplastie totale de la hanche et du genou à la fois en compression et en flexion avec différentes conditions aux limites. Dans une première

analyse, une géométrie simplifiée du fémur a été utilisée pour bien comprendre les mécanismes de transferts de charges et l'influence de la distance des longueurs de tiges de prothèses. Puis une géométrie réelle a été modélisée pour introduire la notion de patient dépendant. La problématique va donc se focaliser sur l'analyse des facteurs de risque de survenue des fractures du fémur bi- prothésés en évaluant et caractérisant les contraintes locales subies par un ce fémur avec un focus sur les fractures inter-prothétiques. En effet, la mise en place d'une prothèse de hanche et de genou modifie l'élasticité de l'ensemble du fémur et du nouveau « couple » fémur prothèse. La distribution des contraintes en est affectée lors de chargements classiques. L'objectif est donc de comprendre les mécanismes de sur-contraintes et leurs effets sur la rupture de façon à pouvoir évaluer le risque fracturaire, en fonction de la zone de fémur « libre d'implant » dans le but de prévenir le patient. L'évaluation de ce risque aurait également pour intérêt de pouvoir adapter la longueur des implants prothétiques de primo-intention ou de révision, voire de remettre en cause les longueurs classiquement définies des pivots fémoraux de Prothèse totale de la hanche (PTH) ou Prothèse totale du genou (PTG). Pour réaliser cet objectif, nous proposons de développer un outil d'aide à la décision pour le chirurgien orthopédiste, afin de définir une géométrie optimale de la prothèse à implanter et de déterminer la nécessité d'implanter une plaque fémorale diaphysaire péri-prothétique préventive. Cet outil sera basé sur la modélisation par éléments finis qui est un outil d'ingénierie pour l'analyse structurelle qui a été utilisé pendant de nombreuses années pour évaluer le rapport entre le transfert de charge et la morphologie de l'os et afin d'optimiser la conception et la fixation d'implants orthopédiques.

La thèse se compose de 4 chapitres :

Chapitre un : Analyse bibliographique sur l'étude des fémurs biprothésés

Partie I : Os et fractures : contexte

Dans la première partie du chapitre, nous présentons successivement :

1. La structure de l'os.

2. Le comportement mécanique de l'os.

3. L'âge lié aux fractures du fémur.

4. Les fractures du fémur humain (proximales, de l'arbre et distales).

5. Le remplacement des articulations du fémur.

6. Les fractures péri-prothétiques et inter-prothétiques.

7. Le traitement inter-prothétique des fractures du fémur.

De cette partie bibliographique, nous retiendrons que l'os est un matériau hautement adaptatif et très sensible aux niveaux de chargements élevés et aux activités dynamiques. Il peut modifier ses propriétés et ses paramètres en réponse à la sollicitation mécanique. La résistance de l'os est déterminée par la composition et la structure de son matériau. La compréhension des propriétés mécaniques de l'os nécessite une connaissance détaillée de leurs interactions et de leurs organisations structurelles à différents niveaux d'échelle [Rho et al., 1998], [Ho Ba Tho et al., 2012]. Lorsque l'os est soumis à une charge externe ou à une énergie, le matériau osseux se déforme en suivant son comportement mécanique constitutif. La courbe contrainte-déformation peut expliquer ce comportement (figure 1). Au début, la réponse initiale est élastique. Ensuite, le matériau de l'os se déforme jusqu'à la rupture, en fonction de la charge appliquée. Le comportement mécanique d'un matériau peut être entièrement décrit par un groupe de propriétés matérielles. L'os présente des propriétés mécaniques remarquables. Il est utile d'évaluer et de comparer le comportement mécanique de l'os et d'autres matériaux sur la base d'indices de performance. En général, différents tests mécaniques peuvent être utilisés pour déterminer les propriétés de l'os telles que la résistance, la rigidité, la charge ultime et le travail à la rupture. Au niveau des tissus (macrostructure), le comportement de l'os peut varier en fonction des degrés de porosité et de densité de l'os cortical ou trabéculaire.

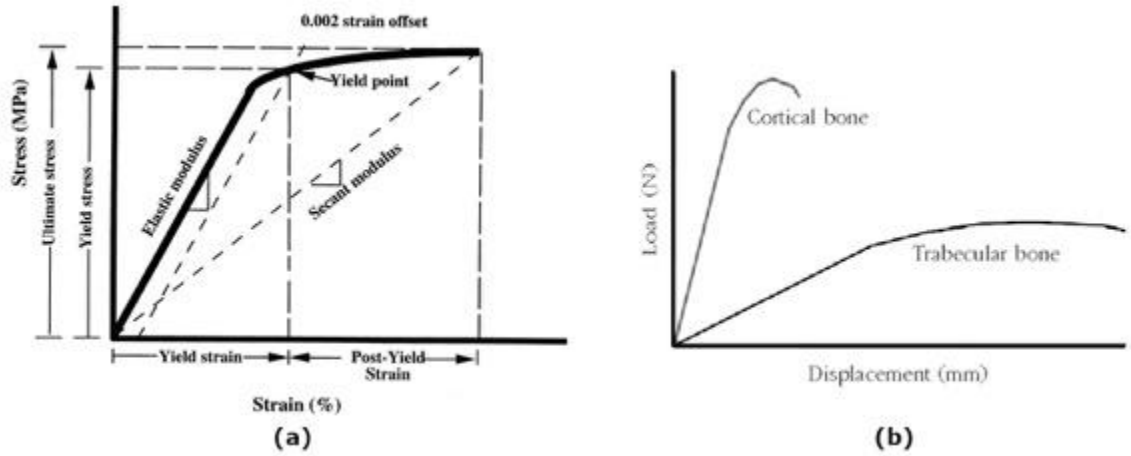

Figure 1: (a)Stress-strain curve of cortical bone [Vashishth et al., 2001]. (b) Load-displacement curve of biomechanical behavior of the different bone tissue (cortical and trabecular)

La réponse mécanique expérimentale est très sensible aux conditions aux limites et des erreurs d'identification sont courantes (figure1.a) [An et al., 2000], De plus, l'os dépend [Novitskaya et al., 2011], de la porosité [Carter et al., 1977], [Rho et al., 1998] et du contenu minéral [Currey, 2010]. La microstructure orientée de l'os cortical conduit à un comportement anisotrope. Le comportement élastique dépend donc de la direction le long de l'axe de l'os. Donald et al., 1975] ont étudié les propriétés anisotropes en compression et en traction de l'os cortical. Ils ont trouvé que le module d'Young et la résistance maximale dans la direction longitudinale sont deux fois plus élevés que dans les directions transversales. L'os trabéculaire, également appelé os spongieux, est un os très poreux renfermant de nombreux grands espaces qui lui donnent un aspect alvéolé ou spongieux. L'os trabéculaire présente une plus grande résistance à la charge de compression qu'à tout autre type de charge [Keaveny et al., 1994]. En test de compression, la résistance varie entre 1,5 et 9,3 MPa, et le module d'Young entre 10 et 1058 MPa en fonction de la région du squelette dont il est issu [Caeiro et al., 2013]. Figure 1.b : (a)Schéma des courbes de contrainte/déformation en compression et en traction pour un os cortical le long de l'axe d'un os long [Mercer et al., 2006]. (b) Comportement anisotrope des échantillons d'os cortical dans les différentes orientations de la charge lors d'un essai de traction (Frankel VH, Nordin M : Basic Biomechanics of the Skeletal System. Philadelphie, Lea et Febiger, 1980).

Partie II : Analyse par éléments finis et études des essais expérimentaux d'un fémur avec une prothèse totale de la hanche et du genou.

Dans la partie II, nous présentons une revue des méthodes numériques et expérimentales dans un fémur après PTH et PTG. Dans cette partie, nous avons passé en revue l'analyse par éléments finis et les tests biomécaniques qui étudient le risque de fracture d'un fémur humain après une ATH ou une ATG. Les principaux facteurs identifiés dans la littérature sont la faible épaisseur corticale, l'absence de fixation de la prothèse (descellement, ostéolise) et distance interprothétique. Différentes études de simulation par éléments finis et montages expérimentaux tels que le test du cantilever, le test de flexion quatre points, le test du cycle de marche et le test de la chute latérale ont été utilisés pour étudier l'effet de la distance IP sur le risque de fracture fémorale. Néanmoins, les auteurs ne parviennent pas aux mêmes conclusions. Il y a quelques contradictions dans les résultats entre l'étude FE de [Soenen et al., 2013] et l'essai expérimental de [Lehmann et al., 2012], [Weiser et al., 2014] utilisant l'essai de flexion quatre points. Cette contradiction peut être attribuée au chargement. Nous concluons que la littérature ne réussit pas

proposer une conclusion claire concernant le risque de fracture fémorale inter prothétique et le lieu de fracture. L'objectif des deux prochains chapitres est d'identifier l'influence des distances IP en utilisant différentes conditions de chargement et de prédire en termes de modèles de déformation les endroits critiques qui peuvent être exposés aux fractures. Une des solutions pour prévenir ce risque de fracture serait la mise en place d'une plaque verrouillée préventive.

Chapitre deux : Influence des prothèses sur la répartition des contraintes entre l'os et les prothèses "Une étude par éléments finis utilisant une géométrie simple".

Dans ce chapitre, nous allons analyser comment la distribution des contraintes entre le fémur et les prothèses varie en faisant varier les cas de chargement tout en maintenant une même distance inter prothétique. Ensuite, nous modifierons la longueur de la tige du genou pour faire varier la distance inter prothétique pour le même cas de charge. Ces simulations ont permis de sélectionner la meilleure méthode pour réaliser les essais de flexion pour l'étude de l'influence inter prothétique. L'objectif principal adopté pour ce travail est d'examiner plus en détail le risque de fracture présent dans les os fémoraux l'espace inter-prothétique de la PTH et de la PTG en utilisant la FEM, ceci, afin d'obtenir un aperçu qualitatif des différents facteurs qui engendrent le risque de fracture. Essentiellement, l'objectif à atteindre dans ce chapitre est de comprendre les effets de différentes distances IP dans un test de flexion. Il s'agit également d'analyser les différentes stratégies permettant d'imposer une charge mécanique contrôlée dans une géométrie réelle du fémur. Trois conditions différentes de charge mécanique sont proposées :

- Essai de flexion quatre points avec un moment constant dans toute la diaphyse moyenne du fémur.

- Essai de flexion quatre points avec un moment constant sur l'ensemble du fémur.

- Essai de flexion deux points

-

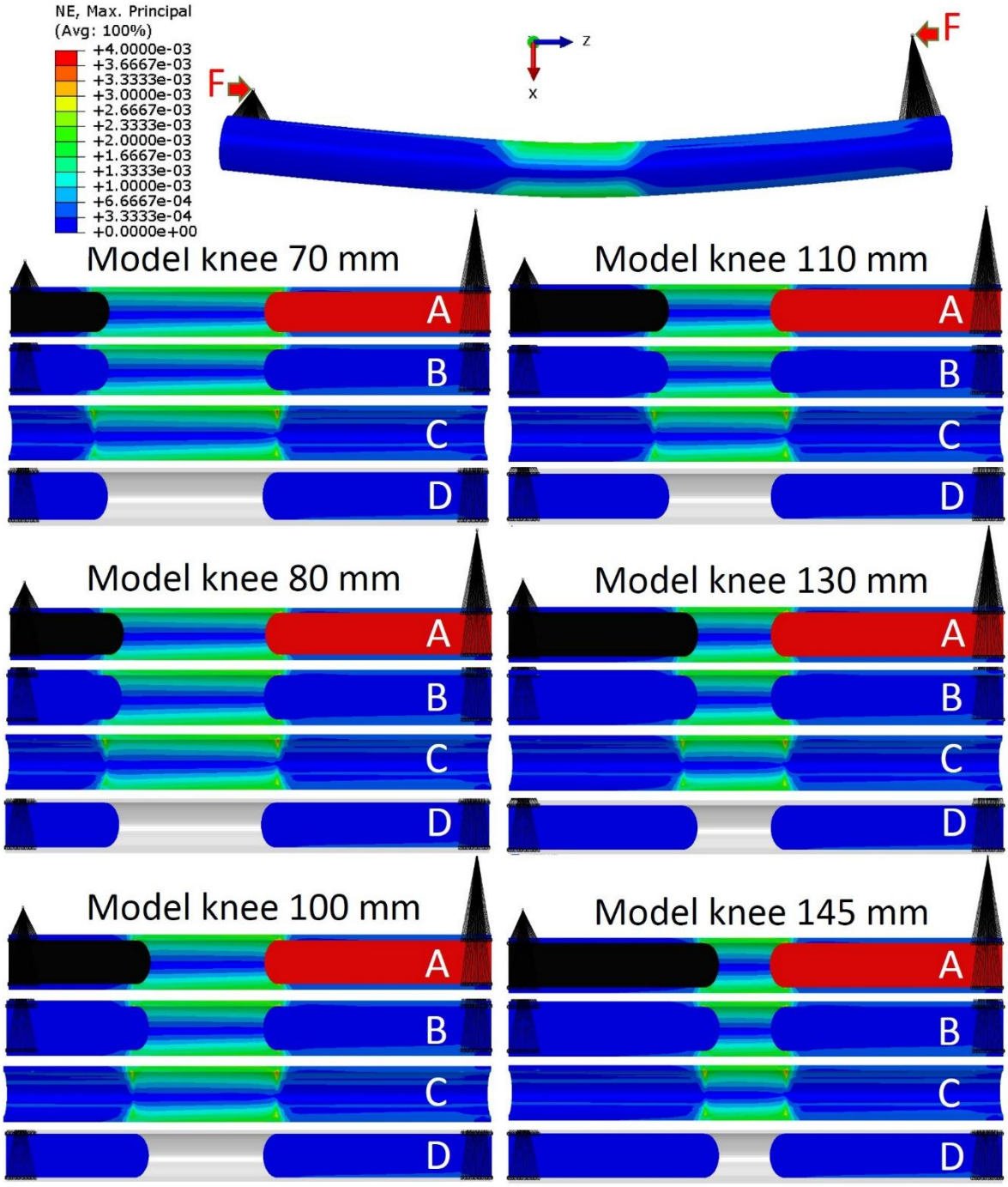

Figure 2: Le schéma représente les déformations principales maximales à la section transversale le long de la longueur des tiges implantées et du cylindre soumis à de la flexion deux deux points avec une configuration non symétrique : tandis que A représente la déformation du cylindre sans la montrer dans les tiges, B représente la déformation sur cylindre et les tiges implantées, C représente la déformation sur la cylindrique seulement et D représente la déformation sur les tiges implantées seulement

En utilisant une géométrie simplifiée, quatre cas de charges ont été simulées dans ce travail, dans le but de mieux appréhender les facteurs impliqués dans le risque de fracture (RF) dans le fémur humain. Les résultats montrent l'effet des différentes longueurs de tige lors de plusieurs essais de flexion. Néanmoins, ces simulations sont jugées encore trop simplistes pour en tirer des résultats concluants. Les résultats de cette étude montrent qu'avec un moment imposé fixé constant, la distance interprothétique n'a pas d'effet significatif sur le risque de développer une fracture IP du fémur. En utilisant une longueur de tige différente, l'élasticité du fémur change. Ainsi, dans la région où la tige prothétique est présente, la rigidité est plus élevée, et la déformation en flexion est donc plus faible que dans la région sans tige. L'existence de la tige prothétique entraîne une déformation plus faible dans les régions prothétiques que dans les régions de l'espace IP. On s'attend à ce que la fracture se produise dans la région de l'espace en fonction de la condition de charge. Dans des travaux récents, tels que [Weiser et al., 2014] ou [Quirynen et al., 2016], il a déjà été discuté que la distance IP joue un rôle mineur dans le risque de fracture. Il y avait des preuves statistiques que la surface de la section transversale corticale pourrait être le facteur le plus critique qui pourrait conduire à une telle augmentation du RF dans les os du fémur bi-prothétique de l'homme. L'étude réalisée par [Soenen et al., 2013], montrent l'importance de la distance dans les fractures IP. Il a donc été nécessaire de réaliser le test de flexion quatre points avec une charge constante au milieu de la tige fémorale simplifiée. Ainsi, nous avons pu étudier et analyser cette variabilité dans les résultats. Dans cet essai utilisant les conditions aux limites utilisées par [Soenen et al., 2013], le moment de flexion maximal était situé dans la zone entre les cylindres de chargement. Cependant, en raison des différences dans les longueurs des tiges, il y a 3 longueurs de tiges en dehors de la zone de flexion fournie par les cylindres de chargement. En fait, l'avantage de l'essai de flexion à 4 points est d'avoir un moment de flexion pur et constant entre les deux supports centraux. Malheureusement, dans le montage et l'utilisation de l'essai de flexion 4 points qui est présenté dans cet article [Soenen et al., 2013], l'information sur la transition du risque de fracture est simplement le passage de l'extrémité de la tige d'un côté à l'autre du support central distal et donc à une variation de la charge locale. La position de la surcharge n'est pas exactement à l'extrémité de la tige interne de la prothèse. Les modèles de bouts de tiges situés entre le support de chargement sont soumis à une surcharge est placée dans la zone centrale du moment maximal, alors que les modèles de bouts de tiges situés avant le support de chargement sont dans des zones de moindre moment. Ainsi, il n'y a pas d'uniformité de la charge dans la zone de transfert en

utilisant cet essai de flexion 4 points avec des appuis centraux qui sont proches les uns des autres. Ceci explique la légère différence des déformations principales maximales dans les intervalles IP. Et donc, en utilisant la géométrie réelle de l'os du fémur, la différence observée par [Soenen et al., 2013] pourrait être configurée.

Malgré les résultats obtenus dans ce chapitre, il faut garder à l'esprit que tous ces travaux de simulation étaient uniquement de nature qualitative : aucune géométrie réelle de l'os n'a été utilisée.

Chapitre trois : Analyse par éléments finis de la géométrie d'un fémur humain pour étudier le risque de fracture après une arthroplastie totale du genou et une arthroplastie totale du genou.

Dans le chapitre 3, nous analysons l'effet d'une géométrie réelle sur la distribution des contraintes pour des cas de chargements quasi statiques. Nous avons aussi analysé comment varie cette distribution en faisant varier les cas de chargements (flexion 4pt, flexion 2pt symétrique et non symétrique) en conservant une même distance inter prothétique. Puis nous modifions la longueur de la tige du genou pour faire varier la distance inter prothétique pour un même cas de chargement. Les paramètres fixés pour les comparaisons sont la Force maximale, le Déplacement maximale, l'Energie maximale. Afin de mener à bien ces simulations, nous avons défini la méthodologie suivante.

Le diagramme proposé juste à la page suivante correspond à la façon dont a été obtenue le maillage EF du fémur. Afin de mener à bien ces simulations, et pour permettre une personnalisation des simulations, le maillage du fémur est construit à partir d'un scan préalable. La démarche de construction du maillage suit le processus suivant :

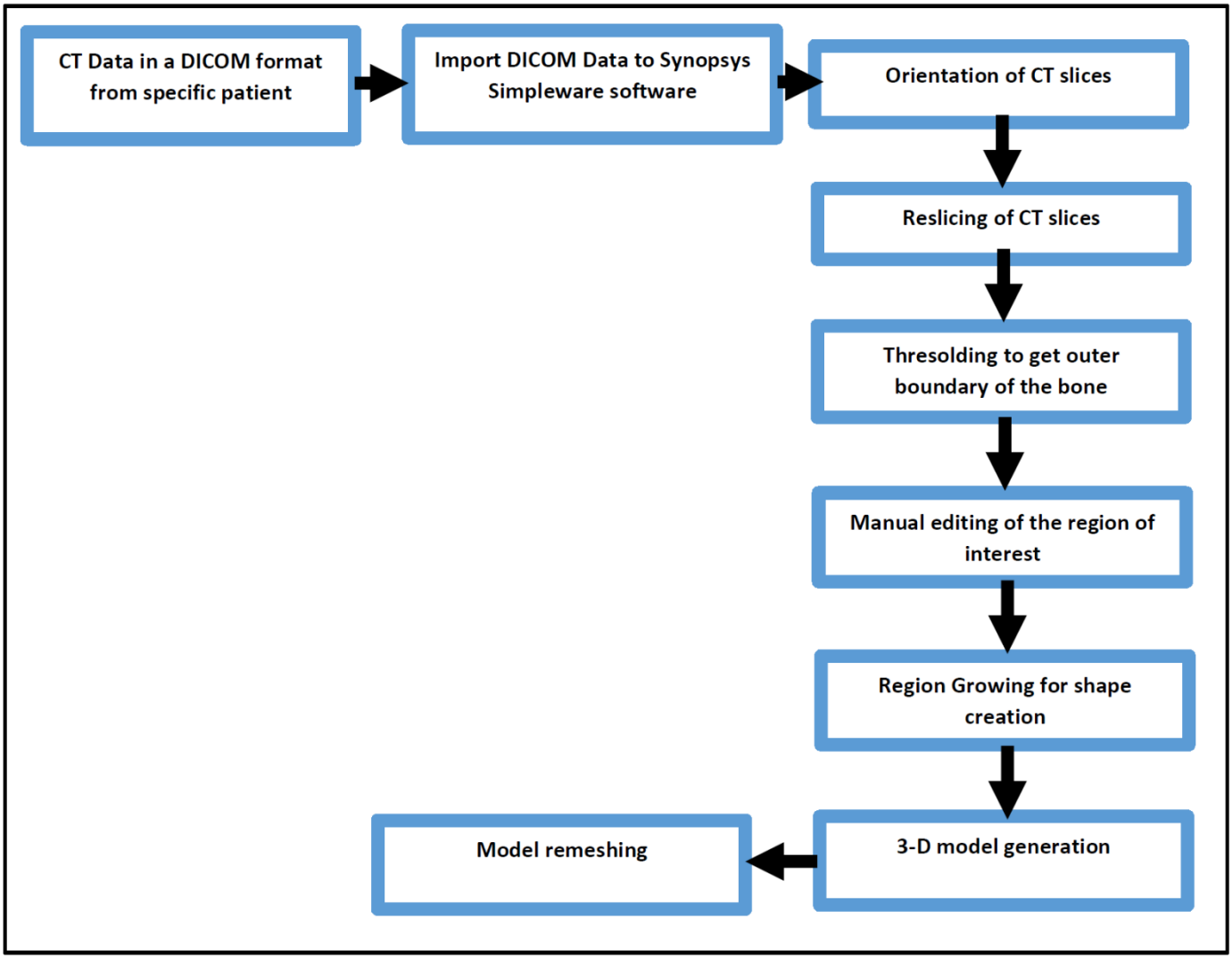

Géométrie du modèle

Les données géométriques de vrais os de fémur humain sous la forme de fichiers DICOM (Digital Imaging and Communications in Medicine) utilisant le scanner multi-couches haute résolution Ultra-Fast de GE sont obtenues aux US (hôpitaux universitaires de Strasbourg en modèles EF tridimensionnels à l'aide du système de contrôle d'image médical (figure 3), notamment de l'os cortical, de l'os spongieux et du canal intramédullaire (figure 4). Les données utilisées dans l'analyse appartiennent à un homme âgé de 56 ans, pesant 61 kg et dont la longueur totale du fémur est de 440 mm. Le remplacement total de la hanche à faible friction de Charnley a été utilisé avec une longueur de tige de 145 mm (tableau.2). La prothèse de la hanche placée et vérifiée par

le chirurgien orthopédique, telle que le centre de la tête de la PTH était apparié au centre de la tête fémorale en bonne santé. Deux groupes de tiges de genou ont été utilisés dans la simulation FE. Groupe 1 : six longueurs et diamètres de tige différents ont été modélisés : trois longueurs commerciales sur le marché (120, 160 et 220 mm) et trois longueurs intermédiaires non disponibles dans le commerce (140, 180 et 200 mm) [Soenen et al. , 2013] et groupe 2: six longueurs de tige différentes (120, 140, 160, 180, 200 et 220 mm) de même diamètre (tableau 2). La taille de l'espace inter prothétique était définie par la distance entre l'extrémité distale de la tige de la hanche et l'extrémité proximale de la tige du genou.

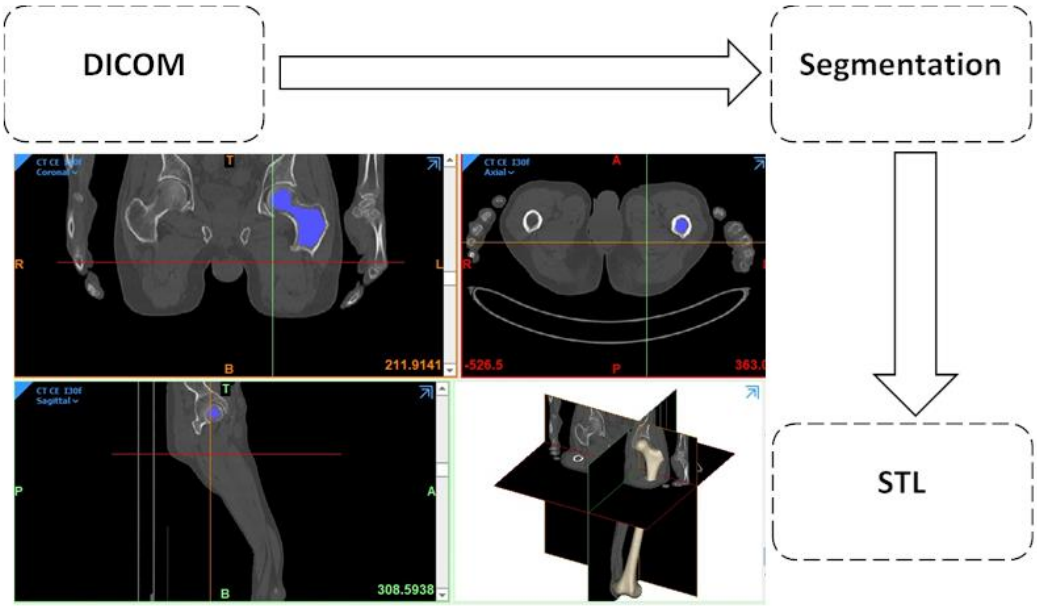

Figure 3 : Conversion des données DICOM en modèle 3-D.

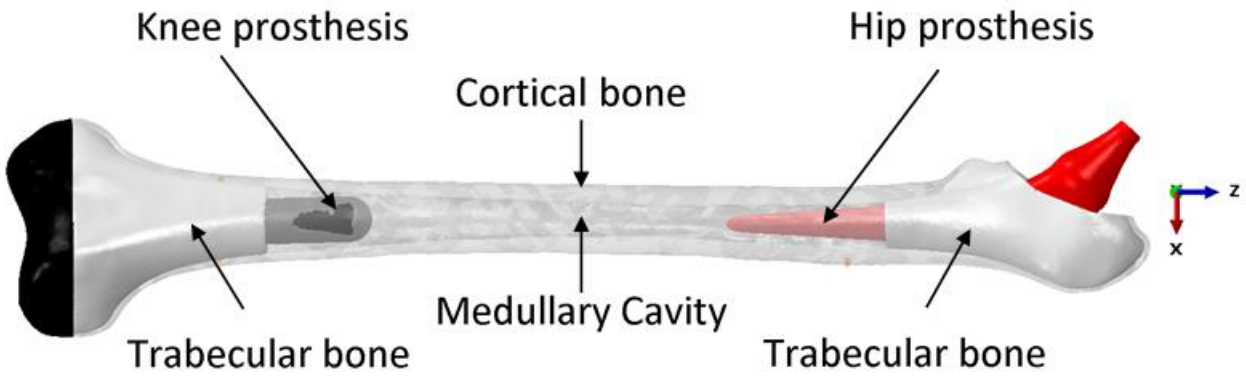

Figure 4 : Fémur avec remplacement de l'articulation de la hanche et du genou.

THA Stem length [mm]	TKA stem length [mm]	TKA stem diameters [mm]	Interprosthetic distance [mm]
145	120	22	130
145	140	22	110
145	160	20	90
145	180	18	70
145	200	16	50
145	220	15	30

Table 2 : Différentes configurations de modèles ont été utilisées dans les études.

Matériaux et propriétés

Les propriétés des matériaux osseux ont été simulées en tant qu'os synthétique équivalent gauche [Kayabasi et al., 2007], [Soenen et al., 2013]. Les propriétés des matériaux de l'os cortical sont supposées isotropes transvers : E1 = E2 = 11,5 GPa, E3 = 17 GPa, ν12 = 0,51, ν23 = ν13 = 0,31. Pour attribuer l'orientation des propriétés du matériau, l'axe Z a été pris parallèlement à l'axe anatomique du fémur. Le comportement mécanique de l'os trabéculaire est considérée élastique et isotrope linéaire avec des propriétés mécaniques: E = 2,13 GPa, ν = 0,3. La prothèse de hanche est en alliage chrome-cobalt, considérée comme un matériau homogène isotrope linéaire ayant comme propriétés mécaniques: E = 220 GPa, ν = 0,3. La prothèse du genou est fabriquée en alliage de titane, considérée comme un matériau homogène isotrope linéaire ayant comme propriété mécanique: E = 110 GPa, ν= 0,3. Aucune couche de ciment n'a été ajoutée alors qu'il était considéré que la prothèse était complètement liée à la surface de l'os, il n'y avait donc aucune tolérance entre la surface de l'os et la prothèse.

Un coefficient de frottement de 0,2 a été pris en compte pour le contact entre la prothèse de hanche et l'os, tandis qu'il est de 0,6 entre la prothèse du genou et l'os.

Tous les modèles ont été maillés à l'aide d'éléments tétraédriques quadratiques de type C3D10 d'une taille approximative de 1,5 mm. L'analyse par éléments finis a été réalisée avec (Abaqus 6.13, Dassault Systèmes Corp., Providence, RI, États-Unis).

Conditions aux limites

Trois conditions de chargement ont été utilisées dans les simulations par Eléments Finis pour étudier l'influence de la distance interprothètique."

• Test de flexion en quatre points sur l'étude de [Weiser et al., 2014] :

Les conditions aux limites étaient basées sur l'étude de [Weiser et al., 2014]. Après l'implantation des deux prothèses, le fémur a été encastré aux extrémités proximale et distale dans des supports en aluminium.

Le montage expérimental est composé de 4 cylindres montés dans le cadre de chargement, la distance entre les cylindres intérieurs étant de 253 mm et celle entre les cylindres extérieurs de 440mm. Les deux cylindres extérieurs sont utilisés pour maintenir et aligner le fémur et les cylindres intérieurs sont utilisés comme supports de chargement. Le côté distal du fémur a été contraint par le cylindre distal pour bloquer tous les déplacements du côté distal de manière isostatique, et bloquer la rotation autour de l'axe du fémur. Le côté proximal du fémur est contraint par le cylindre proximal dans la direction de la charge.

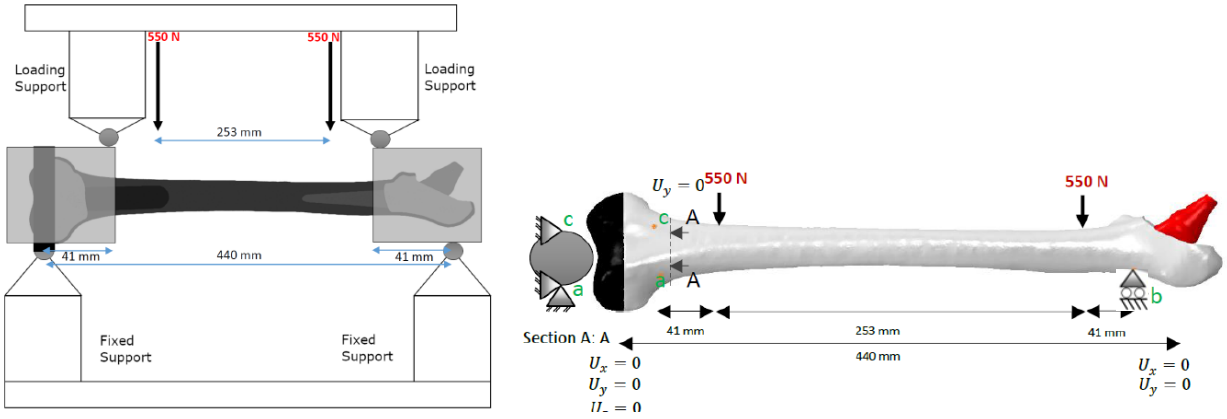

Figure 4 : Montage utilisé pour l'essai de flexion à 4 points et le modèle FE de l'essai de flexion à 4 points avec les conditions aux limite

Une charge constante de 550 N est appliquée à chacun des deux cylindres internes, Cette charge n'est pas suffisante pour briser le fémur pour toutes les différentes distances. La charge est appliquée en poussant depuis le côté médial du fémur pour générer une tension au niveau du côté latéral.

• Essai de flexion à deux points :

Un essai alternatif à l'essai de flexion à deux points, proposé par le Dr. CLUZEL, LMT Cachan, est une manière polyvalente d'appliquer un moment de flexion (avec une composante de compression qui peut être gérée avec la longueur des bras). Un essai symétrique et un essai non symétrique ont été appliqués au fémur avec une charge constante de 550 N.

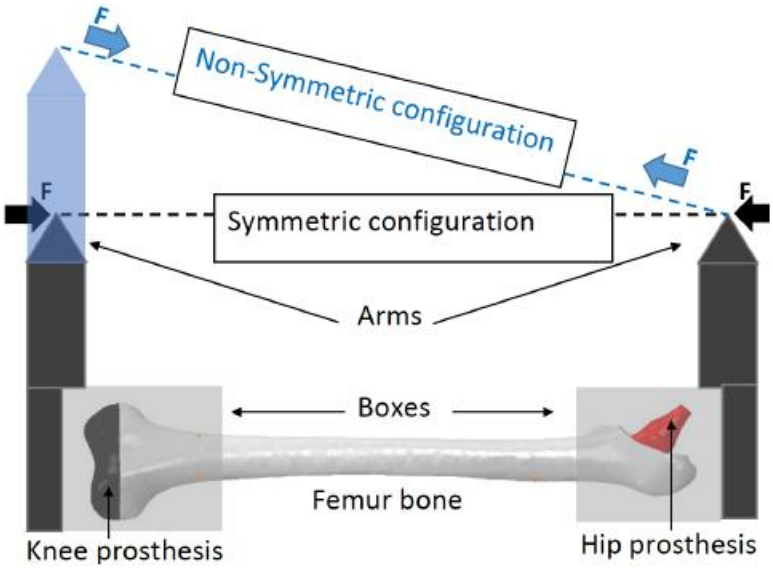

Pour réaliser un essai sur l'interaction entre une prothèse et un fémur, il est nécessaire de pouvoir imposer des conditions aux limites qui génèrent la charge souhaitée sans interférer avec la zone d'étude. Afin d'implémenter ces conditions aux limites dans le logiciel ABAQUS®, il a été décidé d'imiter les couvercles (boîtes) avec les bras proposés dans la description de la configuration et d'utiliser plutôt un couplage structurel distributif qui transférerait les forces appliquées à l'extrémité du bras dans un moment de flexion. En profitant de la nature distributive de ce couplage, il a été décidé de ne coupler que les degrés de liberté de translation du nœud de référence aux nœuds de couplage. Ainsi, bien que le nœud de référence soit libre de tourner (par exemple, de rouler), les nœuds de couplage sont translatés suivant le déplacement équivalent appliqué au nœud de référence. En utilisant cette approche, il a été possible d'économiser l'utilisation d'un plus grand nombre d'éléments dans la simulation, et donc de conserver un faible coût de calcul.

• Test de chargement de la marche :

Il était nécessaire de développer un profil de charge pour le fémur qui améliore la simulation des conditions de charge in vivo d'un patient ayant subi une arthroplastie totale du genou sur le même fémur et qui tienne compte de la relation entre les forces musculaires et articulaires. Ces conditions de charge sont considérées comme une simplification majeure de la situation de charge réelle in vivo et se traduisent généralement par des charges de flexion sur le fémur. Les conditions de charge musculosquelettique ont été calculées tout au long du cycle complet de la force de contact maximale du cycle de marche in vivo de la prothèse de hanche, en supposant un poids corporel de 81,5 kg (800 N). La force totale dans l'articulation de la hanche tenait compte de l'interdépendance des forces de contact musculaire et articulaire et de la charge musculosquelettique.

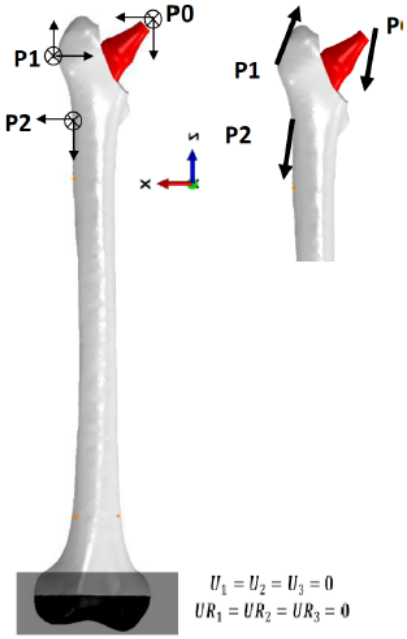

Point	P_0	P_1	P_2
F_x	518.3	-543.4	7.5
F_y	381.2	-133.8	-154.7
F_z	-2570	-677.2	-776.6

Figure 5 : Conditions limites du cycle de la marche pendant la marche.

Résultats

Pour les chargements de flexion pure, le risque de fracture est plutôt concentrée sur la face en tension en raison de la valeur de la contrainte limite en traction 30% inférieure à celle de compression [Bayraktar 2004]. Les comparaisons ne font donc intervenir que les écarts de contraintes positives d'une simulation à l'autre. Par contre, lors d'une analyse avec un chargement représentant la marche, la composante de contrainte de compression plus élevée que celle de traction peut générer une rupture de la face comprimée qu'il faut alors également vérifier. Pour quantifier le risque de fracture, certains auteurs [Bayraktar et al., 2004], [Schileo et al., 2008], utilisent un critère basé sur la contrainte principale maximale. Dans nos analyses, c'est un critère décrit dans [Nalla et al., 2003] basé sur la comparaison des déformations.

Critère principales maximale et minimale qui est utilisé :

$RF_t = {\varepsilon_{pp.max}}/{\varepsilon_{ultime.taction}}$ ou $RF_c = {\varepsilon_{pp.min}}/{\varepsilon_{ultime.compression}}$

Avec : $RF = sup(RF_t, RF_c)$

la déformation ultime en valeur absolue étant différente en traction et en compression [Bayraktar et al., 2004],[Ford et al., 2009].

- **Test de flexion classique à quatre points**

Sous cette condition de flexion quatre points, la déformation maximale de l'os cortical est toujours située entre les deux points intérieurs. Dans cette zone, pour une charge donnée, le moment est constant avec ou sans tige de renfort prothétique.

Pour les diamètres standard de la tige du genou des longueurs de tige différentes étaient utilisés. Le schéma de déformation principal maximal était situé sur le côté latéral dans la région de l'espace IP. Les schémas de déformation pour les différents modèles sont comparables et les valeurs maximales de déformation situées sur la surface latérale changent légèrement. Cependant, des écarts de propriétés mécaniques plus importants ont entraîné des contraintes plus élevées dans la région de l'espace vide. La valeur de contrainte principale maximale est située au niveau du contact entre l'extrémité de de la tige du genou et la couche d'os cortical interne.

Test de flexion en quatre points en utilisant des pots

Dans ce cas, le moment est constant entre les extrémités des tiges de prothèses car la longueur entre les appuis intérieurs est très grande par rapport à la longueur IP. Les déformations principales maximales sont toujours situées aux extrémités des tiges de prothèse, mais les écarts ne sont pas significatifs pour les différentes longueurs de tige distale.

Dans le cas de cet essai, dont les conditions aux limites sont issues de [Soenen 2013], le RF apparent est de 200% plus élevé pour les simulations avec une tige longues par rapport à une tige plus courte que 190mm. Les résultats montrent que la distance inter prothétique n'a pas d'effet significatif sur le risque de développer une fracture IP.

- **Test de chargement de la marche**

Les déformations maximales étaient situées plus distalement dans l'interstice en raison d'une modification du moment résultant par rapport à l'essai de flexion à 4 points. Le chargement anatomique a provoqué une torsion et une flexion, tandis que l'essai de flexion à 4 points n'a provoqué qu'une flexion. L'essai de flexion 4 points n'a provoqué que de la flexion. Les résultats montrent que la distance inter prothétique n'a pas d'effet significatif sur le risque de développer une fracture IP.

Discussion

Dans toutes les configurations testées, si le chargement imposé est une force instantanée en flexion pure ou en chargement équivalent à un cycle de marche, la longueur de la tige de prothèse de genou n'est pas liée de façon déterminante au risque de fracture. En utilisant une longueur de tige différente, l'élasticité du fémur change. Ainsi, dans la région où la tige prothétique est présente, la rigidité était plus élevée, de sorte que la déformation en flexion était plus faible que dans la région de l'intervalle. L'existence de la tige prothétique conduit à une contrainte moindre dans les régions prothétiques que dans les régions à IP. La fracture devrait se produire dans la région de l'espace IP en fonction de l'état de charge.

Pour valider la modélisation sans disposer de résultats d'essais sur pièces anatomiques, plusieurs simulations présentées dans [Soenen et al., 2013], [Weiser et al., 2014] et [Quirynen, 2016], ont été reproduites avec des conclusions similaires, sauf pour les essais de flexion 4 points de [Soenen 2013] qui donnent des résultats identiques mais des conclusions différentes.

• **Essai de flexion en quatre points proposé par [Soenen et al., 2013]:**

Le moment de flexion maximal se situait dans la zone située entre les supports de chargement. Cependant, pour ce test, les valeurs maximales de déformation principale étaient dans la zone de contact entre la pointe de la tige du genou et l'os cortical interne. L'avantage du test de flexion en 4 points est d'avoir un moment de flexion pur et constant entre les deux supports centraux. Malheureusement, lors de la configuration et de l'utilisation du cas de charge en flexion en 4 points présenté dans cet article [Soenen et al., 2013], les informations sur le risque de fracture sont simplement le passage de l'extrémité de la tige d'un côté à l'autre du point d'appui du montage. La position de la surcontrainte ne se situe pas exactement à l'extrémité de la tige interne de la prothèse. Les modèles d'embouts de tiges situés entre le support de chargement sont soumis à une sur contrainte qui est placée dans la zone centrale du moment maximal, alors que les modèles d'embouts de tiges situés avant le support de chargement sont dans des zones de moindre moment. Ainsi, il n'y a pas d'uniformité de la charge dans la zone de transfert en utilisant cette méthode de flexion 4 points avec des supports centraux rapprochés. Ceci explique la grande variation des valeurs de risque de fracture pour la distance entre les différents écarts.

• Essai de flexion en quatre points proposé par [Weiser et al., 2014]:

Le moment de flexion maximal se situait dans la zone située entre les supports de chargement. Dans cette configuration d'essai, la position de la sur contrainte se situe après la fin de la tige interne de la prothèse pour tous les modèles. Cela donne l'avantage d'avoir le même moment d'application. En conséquence, il y a une uniformité de la charge dans la zone de transfert en utilisant cette flexion 4 points.

Les résultats montrent que la distance inter-prothétique n'a pas d'effet significatif sur le risque de développer une fracture IP.

• Test du cycle de Cycle de marche sur sol plan proposé par [Soenen et al., 2013], [Quirynen, 2016] :

Les déformations maximales se situaient près du côté du genou dans le distance IP en raison d'un changement du moment résultant par rapport au Test de flexion 4 points. La charge anatomique a entraîné une torsion et une flexion, alors que l'essai de flexion 4 points n'a provoqué qu'une flexion. Pour ce cas de charge, la diaphyse subit une flexion dans un plan d'environ 30 degrés par

rapport à l'axe latéro-médial des essais de flexion pure précédents, ainsi qu'une torsion. Les résultats montrent que la distance inter-prothétique n'a pas d'effet significatif sur le risque de développer une fracture de l'IP. Les résultats montrent qu'une distance IP plus petite est préférable. Par conséquent, la zone de déformation résultante dans la diaphyse fémorale en utilisant une prosthèse du genou plus longue est plus faible qu'avec la petite.

Pour le groupe 2 qui utilise les mêmes diamètres de la tige du genou avec des longueurs de tige différentes, le schéma de déformation principal maximal est situé sur le côté latéral dans la région de l'espace IP. Les schémas de déformation des différents modèles sont comparables et les valeurs maximales de déformation situées sur la surface latérale changent légèrement.

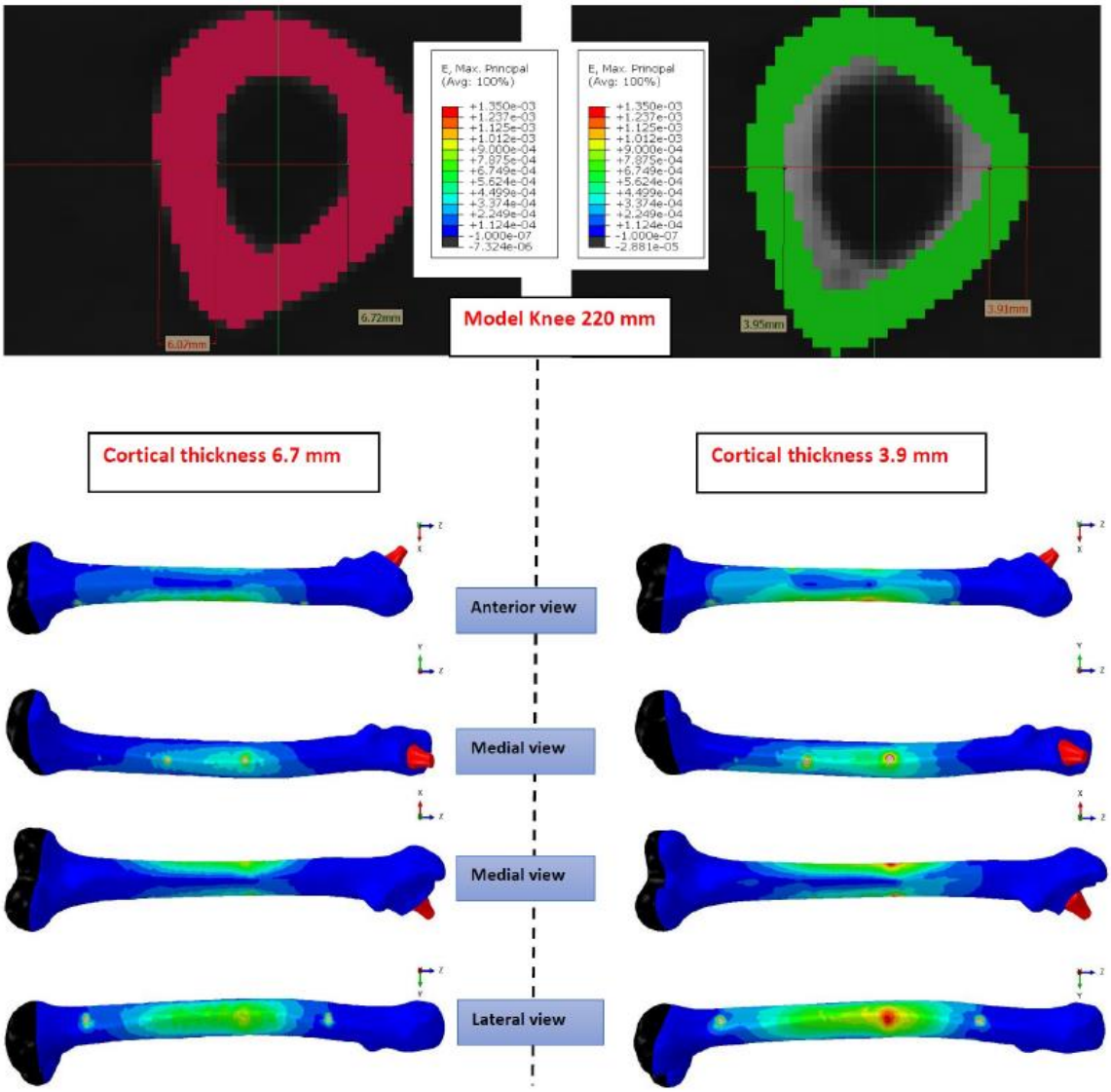

Figure 6: Distribution de la déformation principale maximale montrant l'effet de l'épaisseur de la paroi corticale pour une épaisseur moyenne de la tige fémorale corticale de 6,7 mm et 3,9 mm..

Les résultats de la modélisation sont en accord avec ceux de la littérature que cela soit pour le groupe 1 ou pour le groupe 2 de tiges de prothèses de genoux. Il est donc raisonnable d'exploiter cet outil pour l'étude des fémurs biprothésés. Nos conclusions sont que pour les chargements classiques de marche ou de flexion pure, les variations d'implantations de prothèses et notamment de longueur de tige de prothèse de genou, avec une force imposée constante ne modifient pas le risque de fracture. Par contre, l'exploitation du modèle montre que le risque de fracture est fortement dépendant de la qualité osseuse, et de l'épaisseur de la

partie corticale de la diaphyse. Si l'on se base sur ce critère pour implanter ou non une plaque de renfort, les résultats montrent que la personnalisation du modèle géométrique implanté dans notre démarche est indispensable. Une autre utilisation de cette modélisation élastique linéaire, est la possibilité de changer le paramètre fixe pour les comparaisons de RF avec différentes longueurs de tige de prothèse de genou. Le chargement peut être quantifié par une énergie cinétique quand il correspond à une chute en avant ou à un petit choc. L'implantation de double prothèse est souvent réalisée sur des personnes âgées dont la chute à partir d'une position debout est très courante et aboutit fréquemment à des fractures. Avec ce cas de charge dit faible énergie, pour estimer des risques de fractures, il est plus raisonnable de considérer que c'est le niveau d'énergie élastique avant rupture qui est une grandeur constante et non la force imposée qui ne correspond pas en flexion à une situation physiologique. Dans ce cas, les calculs éléments finis sont identiques, mais une quantification du déplacement des points de chargement permet de mesurer l'énergie introduite. L'utilisation de la linéarité du comportement permet de corriger les contraintes obtenues pour un niveau d'énergie donné. Dans ce cas, notre modèle permet une interprétation différente des résultats car la réduction de la distance interprotéthique est alors directement liée à une augmentation du risque de fracture. Cela montre que l'os entre les deux prothèses est la section la plus faible de la construction. Ainsi, nos résultats sont cohérents avec les résultats de [Iesaka et al., 2005], [Weiser et al., 2014], [Quirynen, 2016] alors que la prothèse n'agit pas comme un concentrateur de contrainte, ni augmente le risque de fracture. En outre, nos résultats suggèrent que la pointe de toute prothèse devrait être située dans une zone avec une épaisseur de paroi corticale suffisante. En conséquence, nous avons remarqué que les critères de sélection de l'espace IP devraient être basés sur la morphologie fémorale, et la qualité de l'os.

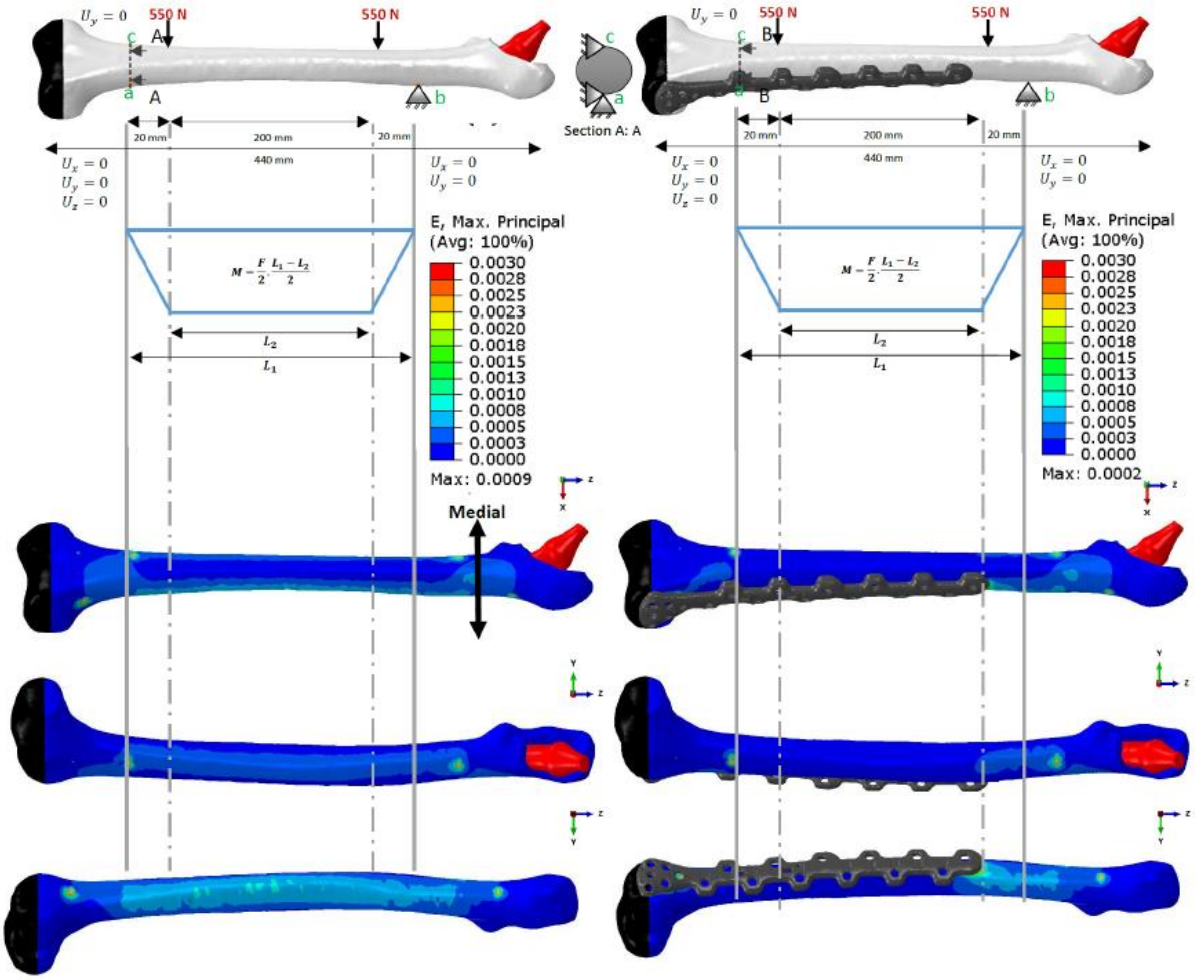

Figure 7 : Distribution maximale de la déformation principale obtenue dans les différents modes.

Si c'est l'énergie élastique du fémur avant rupture qui est le paramètre fixé de l'étude, il est évident que la présence d'une plaque augmente le moment à transmettre, mais diminue la contrainte vue par l'os cortical. Toutefois, pour aboutir à une quantification du risque de fracture, il faudrait s'assurer que les vis de fixation peuvent effectivement transmettre les charges de la plaque à l'os. Cette partie n'étant pas terminée, elle est à placer en perspective de ce travail.

Chapitre quatre : Simulation dynamique d'une chute vers l'avant : analyse du chargement de l' os fémoral humain pour étudier la zone de fracture critique"

L'objectif de cette étude numérique est d'étudier et de détecter les zones du moment de flexion élevé dans un fémur humain lors d'un choc de faible énergie d'une chute en avant. La détection de ces zones de moment maximum nous donnera la possibilité d'imposer ces moments en utilisant un dispositif expérimental développé en interne d'un test de flexion en deux points. La validation entre les simulations numériques et le travail expérimental donnera une information significative sur les zones de fracture possibles autour de l'implant du genou, donc elle sera utilisée pour atteindre l'objectif de recherche en concevant et en optimisant une plaque de fracture préventive qui pourra être utilisée dans un fémur avec ATH et ATG.

Géométrie du modèle et matériaux et propriétés :

L'épaisseur corticale du fémur a été mesurée et identifiée

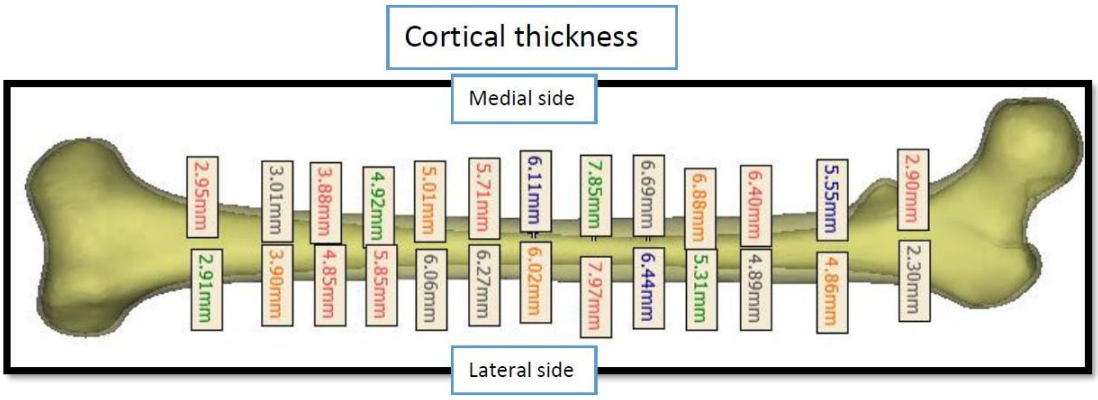

Figure 8 : Épaisseur de la paroi corticale le long du fémur sur les faces latérale et médiale.

Pour la géométrie et du modèle et les propriétés mécaniques, nous avons gardé le même fémur et les mêmes prothèses que celle utilisée dans le chapitre trois. Enfin, afin de mettre en œuvre le modèle dans la simulation par éléments finis, le sol est supposé être une surface rigide et l'écart entre la prothèse de genou et le sol est de 0,07 mm. La masse totale du fémur a été supposée être de 6 kg [lien NASA].

Conditions aux limites

Les conditions aux limites ont été choisies sur la base de l'étude expérimentale de [Choi et al., 2015] pour une chute volontaire vers l'avant. La caractérisation de la vitesse d'impact est mesurée en un point de la hanche (figure 9). Le premier point est l'analyse des images. La correspondance entre le nombre d'images et le temps est faite en supposant que les images sont prises à intervalles de temps réguliers, que la première est après le premier intervalle et que la dernière est le numéro 22 qui correspond à un temps de 533ms. Ce dernier point est cohérent avec les deux vitesses nulles. Dans la (figure 9) tirée de [Choi-2015]. Entre les images 5 et 11, l'intervalle calculé est de 22,3ms, tandis qu'entre 11 et 22, il est de 24,2ms. Il y a donc une certaine variabilité dans la mesure. Une conversion est donc proposée pour obtenir la meilleure des valeurs avec les deux échelles (figure 9). Les données sont fournies au point A et les vitesses correspondantes sont présentées en fonction du temps figure 9. Cependant, les deux fonctions moyennes décrivant les vitesses horizontale et verticale sont dérivées des données expérimentales de chaque image avec un bruit non négligeable. Les courbes sont données en (figure 10).

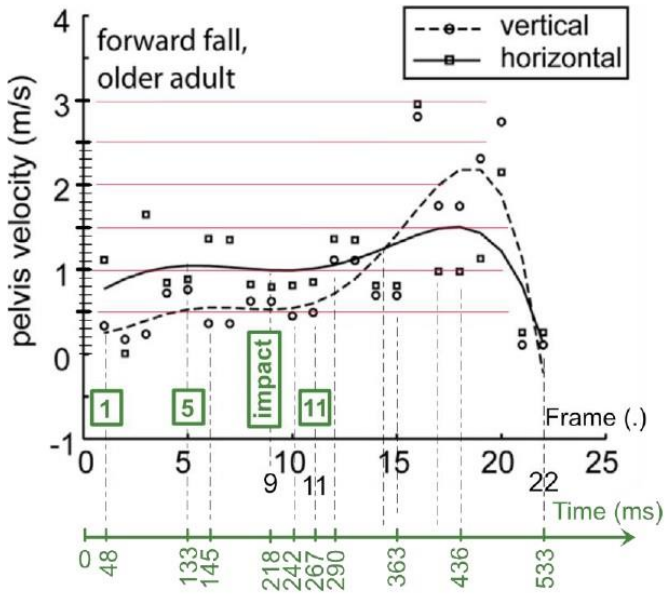

Figure 9 : Vitesses du bassin lors d'une chute volontaire sur le genou. Images extraites de [Choi et al., 2015]

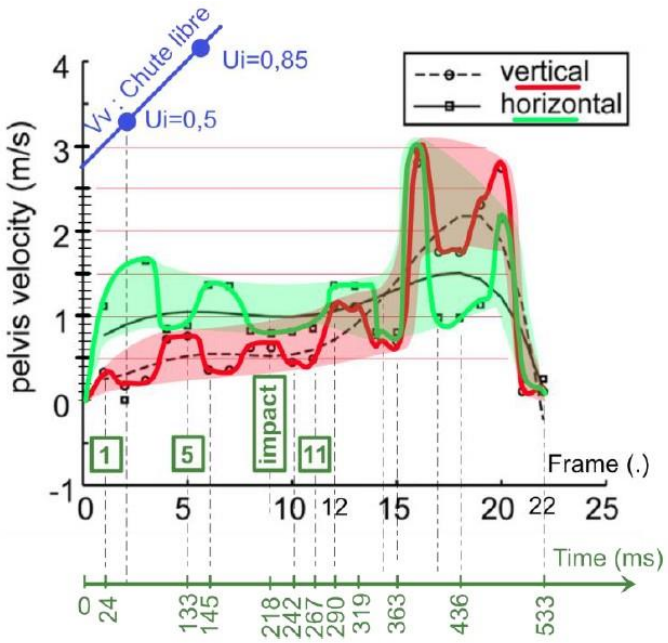

Figure 10 : Enveloppes des courbes de vitesse issues des courbes de [Choi et al., 2015].

La première image ne correspond pas au début de la chute, c'est pourquoi la courbe de chute libre est décalée. Le décalage est calculé à partir de l'angle du tibia de la première image. Pour effectuer un transfert des points de mesure et éviter l'utilisation des courbes moyennes de la figure 1, une option est de calibrer les images. Cette calibration est réalisée à partir de la grille de calibration de l'article avec un pas de 40cm. En dessinant un squelette sur les différentes images, il est possible de tracer les sauts de déplacement entre deux photos. Via les sauts temporels correspondants, il est possible de trouver des valeurs moyennes des vitesses qui sont raisonnables si elles varient peu entre les deux instants considérés. Les sauts de déplacement sont tracés en bleu sur (figure 11).

En supposant que les vitesses du point B1→9 est assez redondant jusqu'au moment de l'impact, le moment du choc est estimé en fonction de t5 avec :

$$\Delta t_{5\to 9} = \Delta t_{1\to 5}\left(\frac{U_{5\to 9}}{U_{1\to 5}}\right) = 78ms.$$

Le temps au moment du choc est donc : t5 = 211,6 ms. Cette valeur nous permet de placer correctement le point A9 entre A5 et A11 et donc d'ajouter la position du squelette au moment du choc (en jaune (figure 11)).

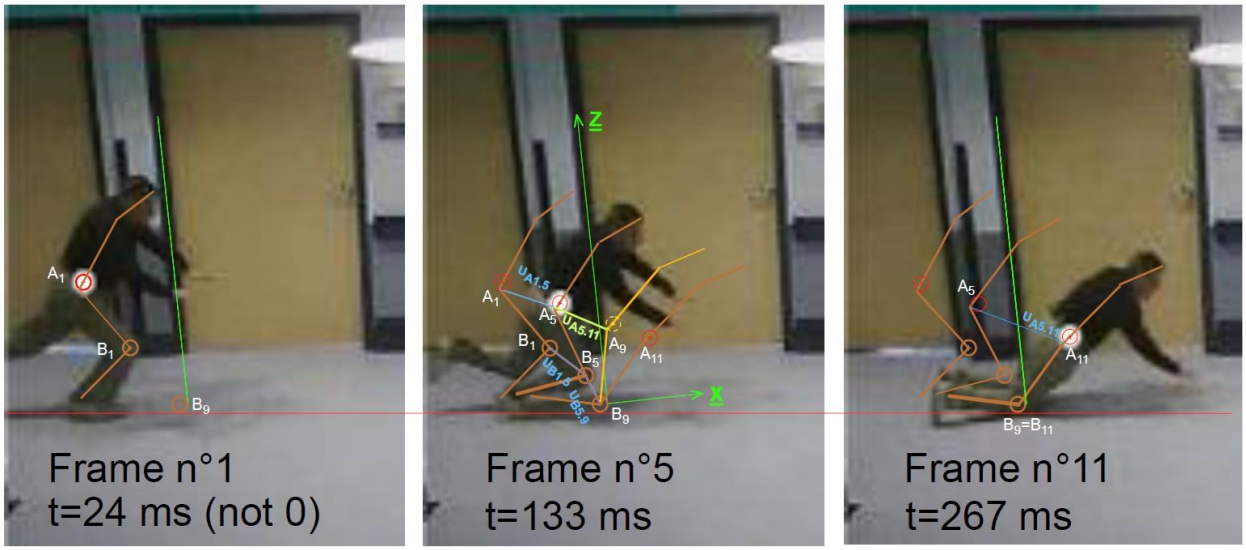

Figure 11 : cinématique de la chute via les images extraites de [Choi et al., 2015].

Au moment de l'impact, on trouve une vitesse angulaire de : ω9 = 487◦/s = 8,50 rd/s. Pour entrer les données dans la simulation de l'impact sur le genou qui est compatible avec un déplacement solide. On se base donc sur le torseur cinématique suivant :

$$\boldsymbol{\varepsilon_{femur}} = \begin{cases} \boldsymbol{\omega_{femur}}^{\underline{y}} \\ \underline{\boldsymbol{V}}\boldsymbol{A} \end{cases}$$

The velocity at point A: $\underline{VA} = \begin{pmatrix} v_{Ax} \\ v_{Ay} \\ v_{Az} \end{pmatrix} = \begin{pmatrix} 3.75\ m/s \\ 0 \\ -2\ m/s \end{pmatrix}$

Angular velocity : $\boldsymbol{\omega_{femur}} = 8.50\ rad/s$

Impact angel : $\boldsymbol{\theta_{femur}} = 102.5\ degre$

Enfin, afin de mettre en œuvre le modèle dans la simulation par éléments finis, le sol est supposé être une surface rigide et l'écart entre la prothèse de genou et le sol est de 0,07 mm. La masse totale du fémur a été supposée être de 6 kg [lien NASA].

Résultats

Nous avons analysé la distribution de la contrainte équivalente pendant le moment de la collision, l'analyse des contraintes nous permet de bien connaître la zone de concentration des contraintes. Dans les résultats présentés, nous déterminerons la distribution des contraintes pour quatre cas différents d'impact comme suit :

- Chute avant d'un fémur complet.

- Chute vers l'avant d'un os fémoral avec un TKR (uniquement le composant du genou).

- Chute vers l'avant d'un os fémoral avec THR et TKA (avec une prothèse de genou de 180 mm de long).

- Chute vers l'avant d'un os fémoral avec une THR et une TKA (avec une prothèse de genou de 220 mm de long).

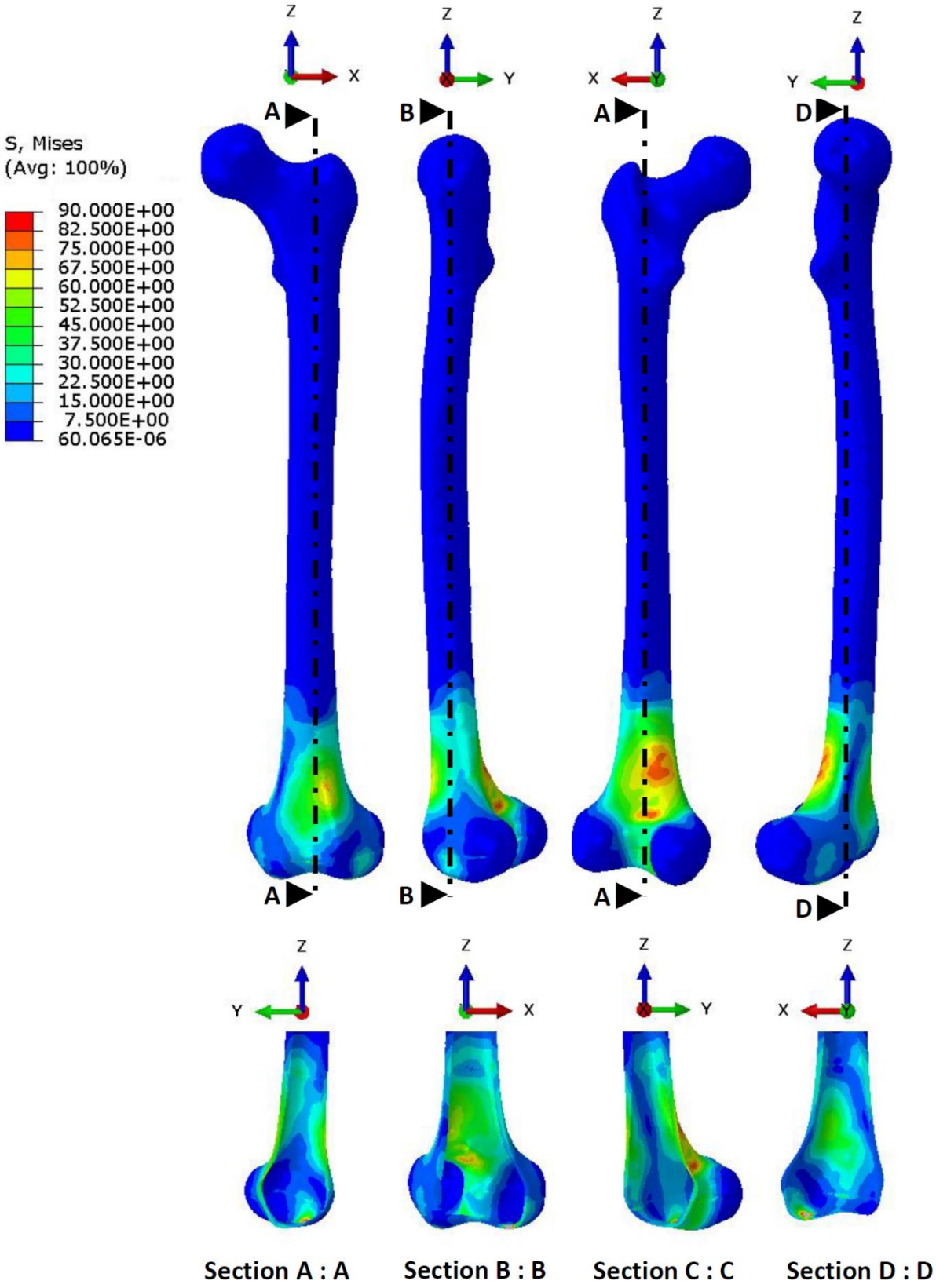

Figure 12 : Distribution de la contrainte de Von Mises équivalente [MPa] à l'extérieur et à l'intérieur de la couche corticale d'un fémur sans prothèse dans une simulation d'impact en chute avant au moment de l'impact.

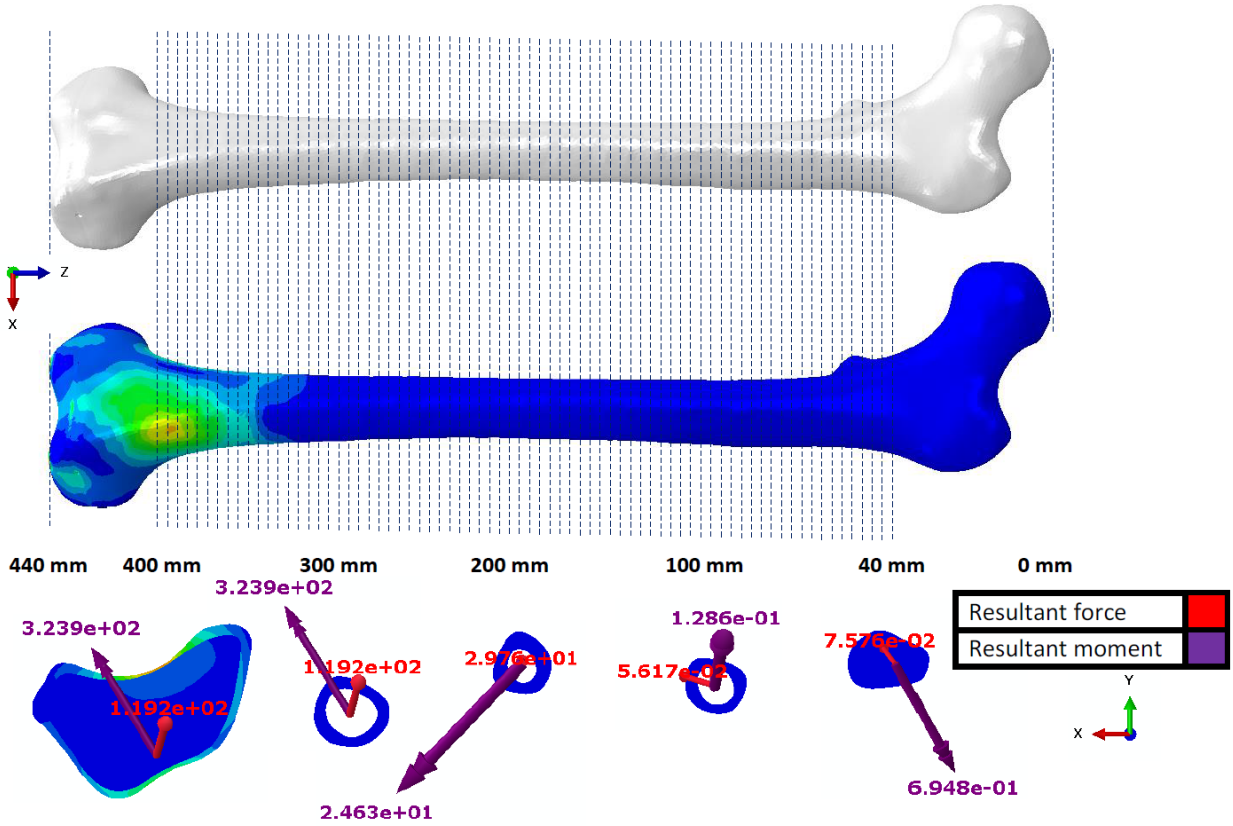

Figure 13 : La surface totale du fémur a été divisée en 73 sections de 40 mm à 400 mm avec un pas de 5 mm pour calculer le moment à chaque pas.

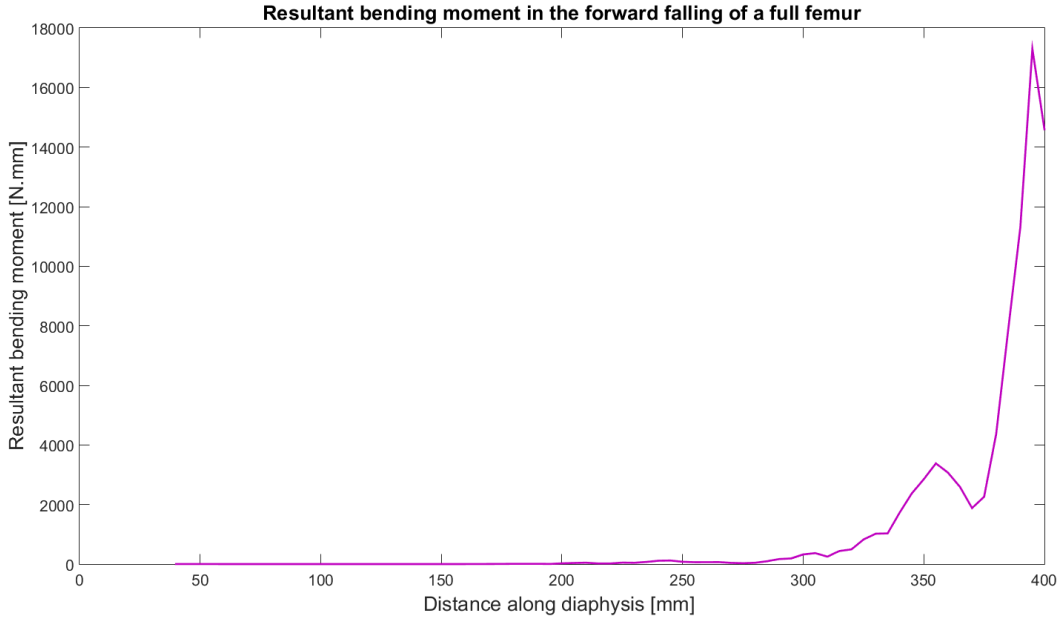

Figure 14 : Moment résultant sur un fémur sans prothèse après un impact en chute avant au moment de l'impact.

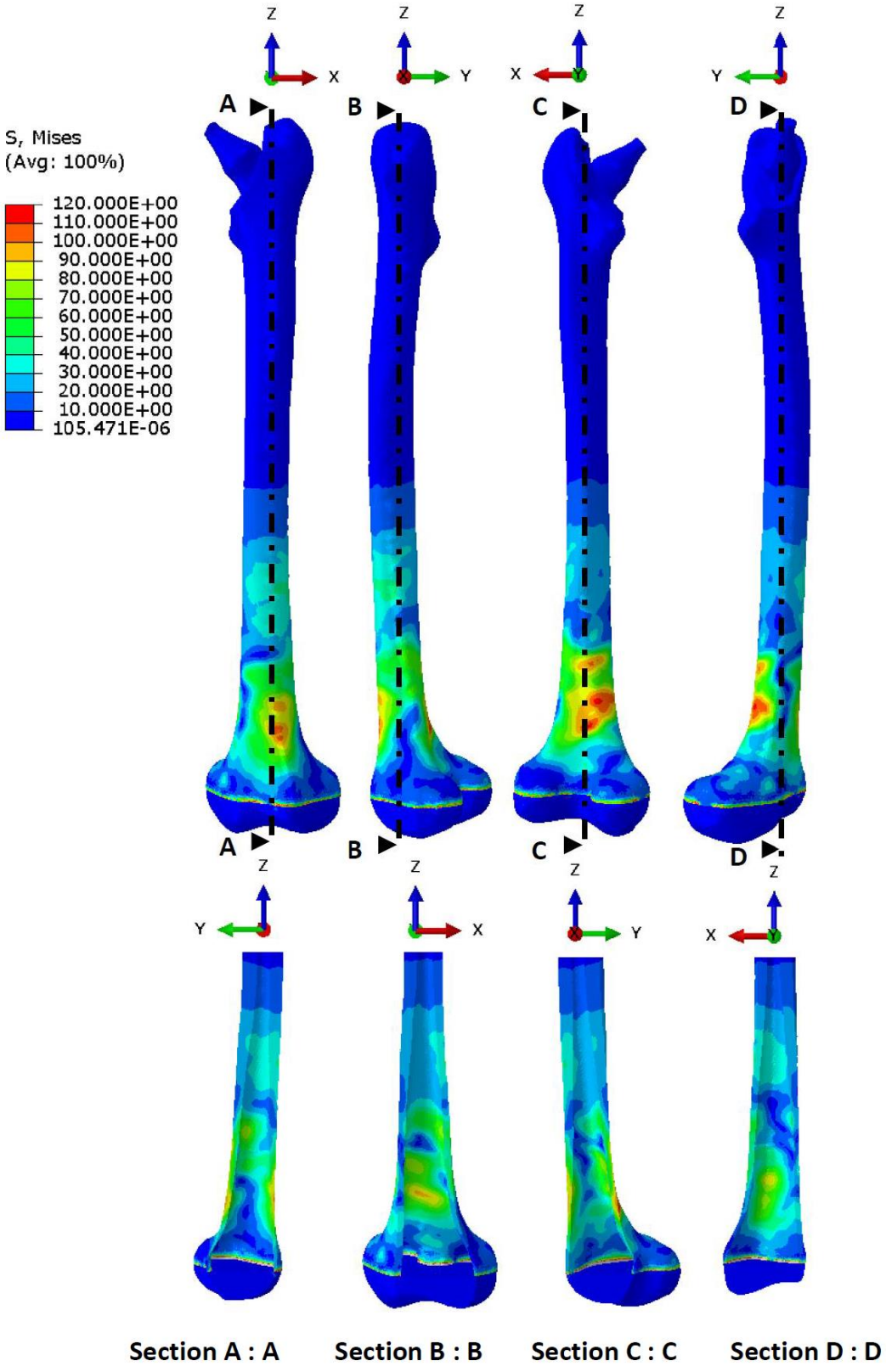

Figure 15 : Distribution de la contrainte de Von Mises équivalente [MPa] à l'extérieur et à l'intérieur de la couche corticale d'un fémur avec une prothèse de genou repliée (uniquement le composant du genou) lors d'une simulation d'impact frontal au moment de l'impact.

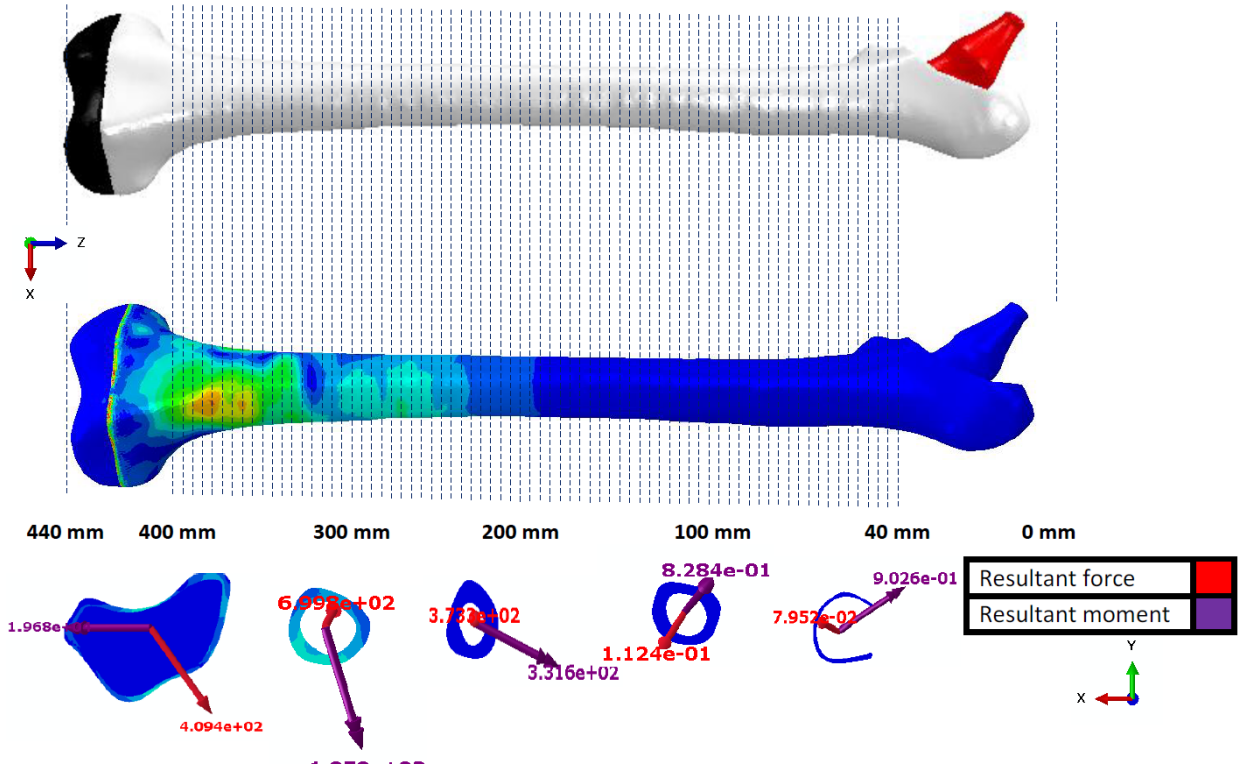

Figure 16 : Le fémur avec le seul composant du genou a été divisé en 73 sections de 40 mm à 400 mm avec un pas de 5 mm pour calculer le moment dans chaque pas.

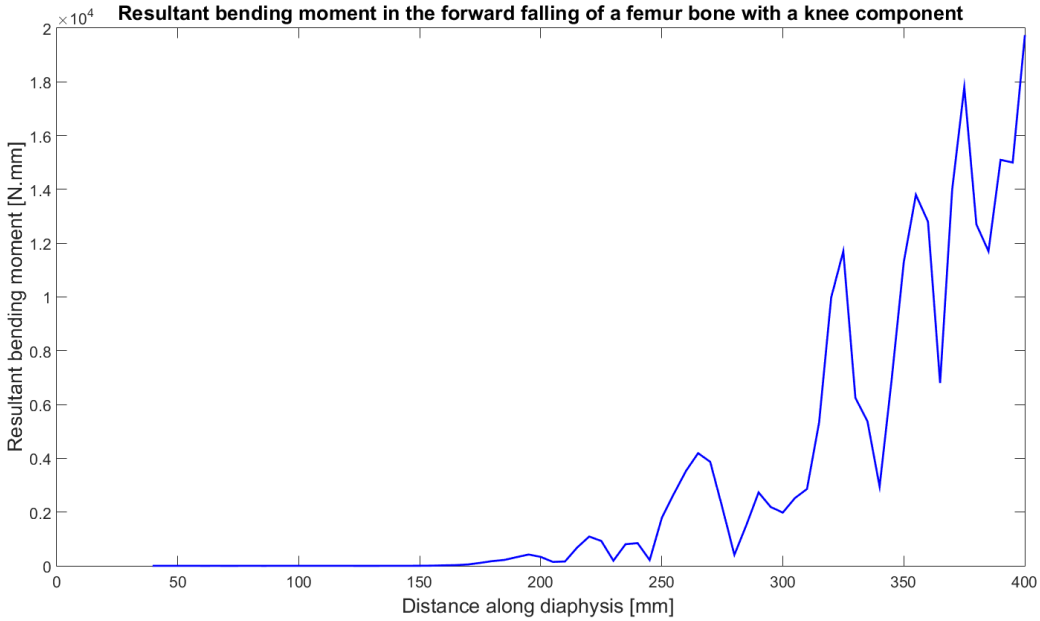

Figure 17 : Moment résultant sur un fémur équipé d'une prothèse de genou de remplacement (composant du genou uniquement) lors d'une simulation d'impact en chute avant au moment de l'impact

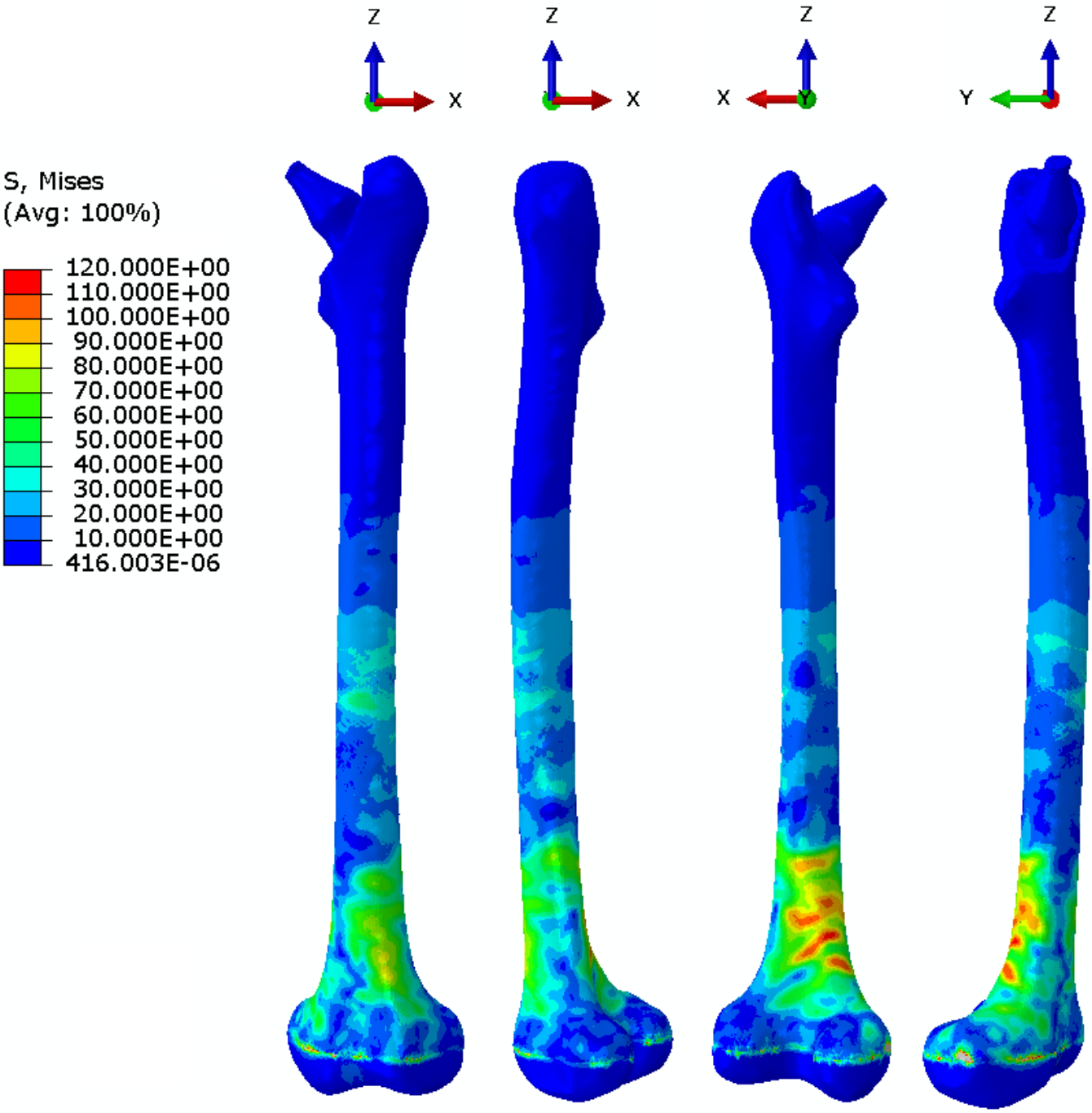

Figure 18 : Distribution de la contrainte de Von Mises équivalente [MPa] dans la surface externe de la couche corticale d'un fémur avec un remplacement THR et TKR (prothèse de genou de 180 mm de long) dans une simulation d'impact en chute avant au moment de l'impact

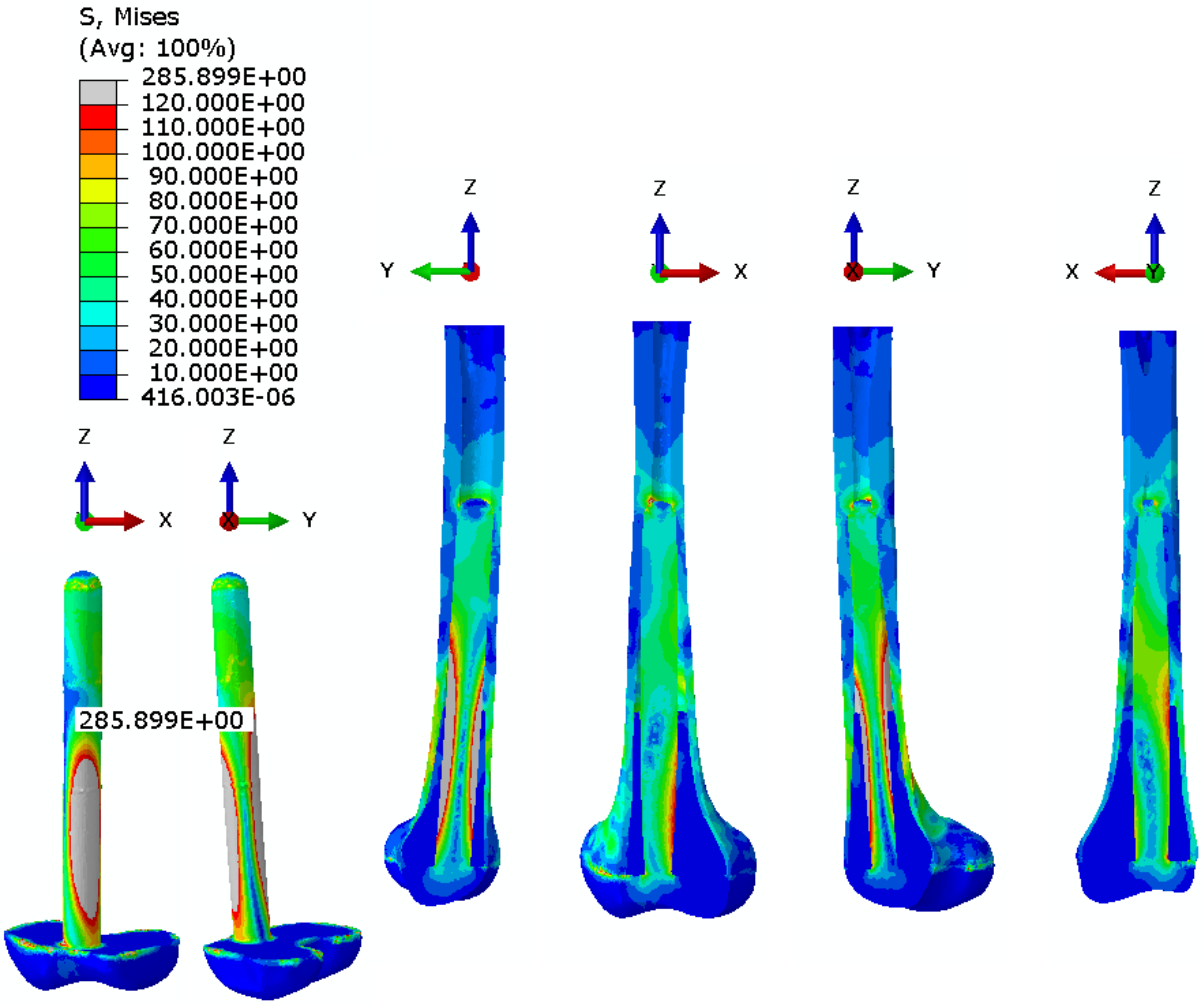

Figure 19 : Les coupes transversales du fémur avec une THR et une TKR (prothèse de genou de 180 mm de long) montrent la contrainte de Von Mises équivalente [MPa] à l'intérieur de la couche d'os cortical et la contrainte de Von Mises équivalente [MPa] sur la prothèse de genou.

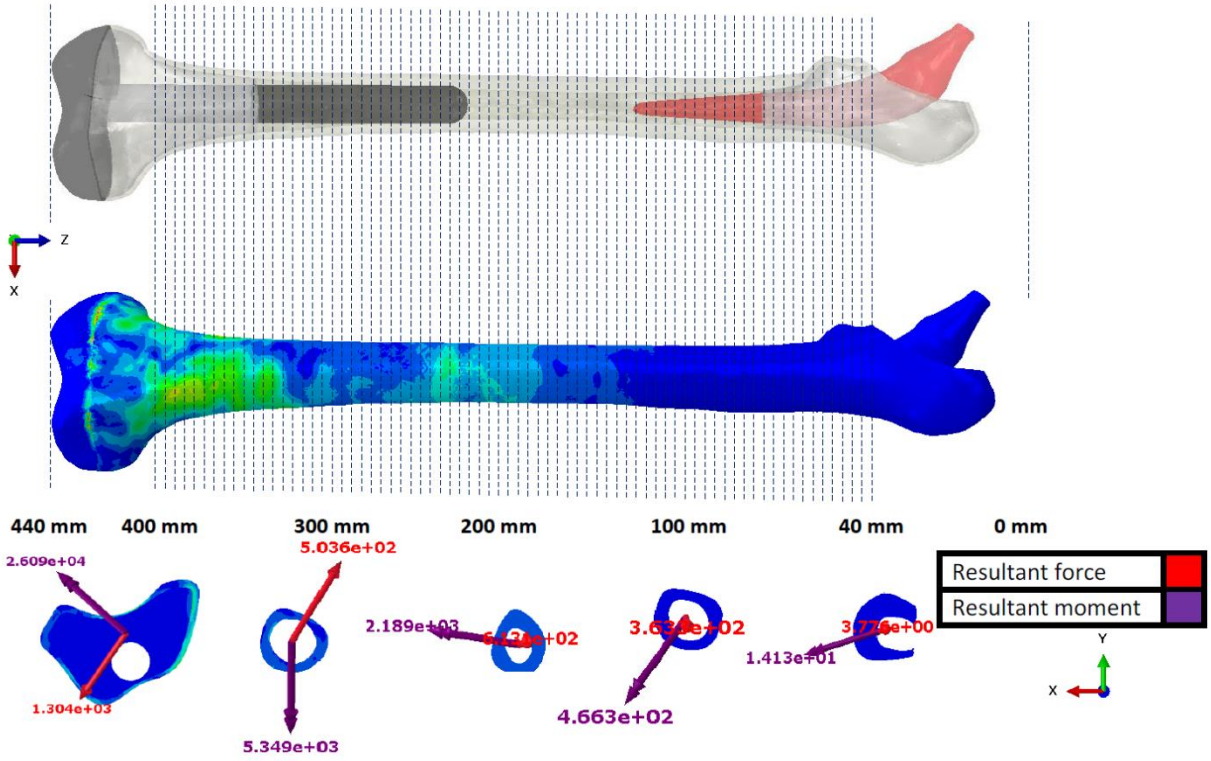

Figure 20 : Le fémur avec une THR et TKR (prothèse de genou de 180 mm de long) a été divisé en 73 sections de 40 mm à 400 mm avec un pas de 5 mm pour calculer le moment dans chaque pas

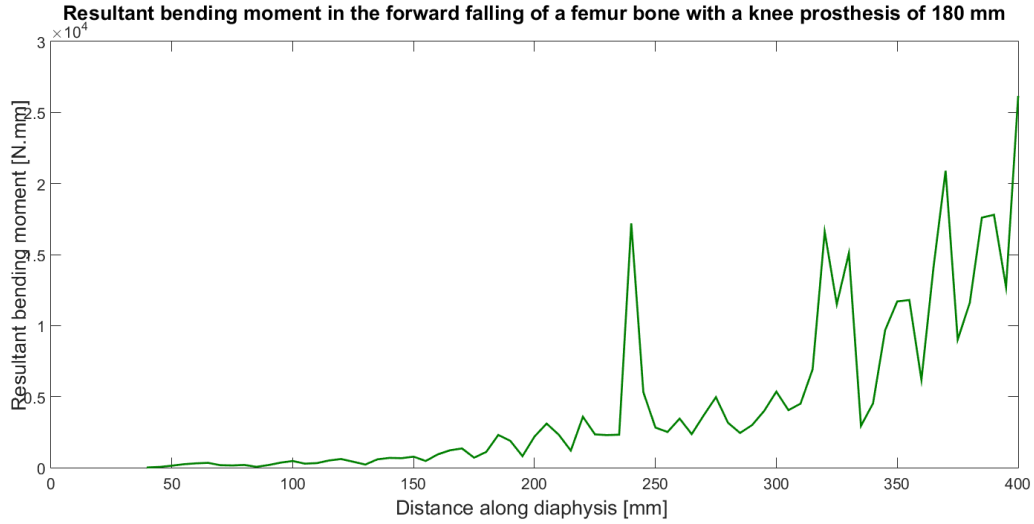

Figure 21 : Moment résultant sur un fémur équipé d'une prothèse de genou de 180 mm de long dans le cadre d'une simulation d'impact avec chute vers l'avant au moment de l'impact.

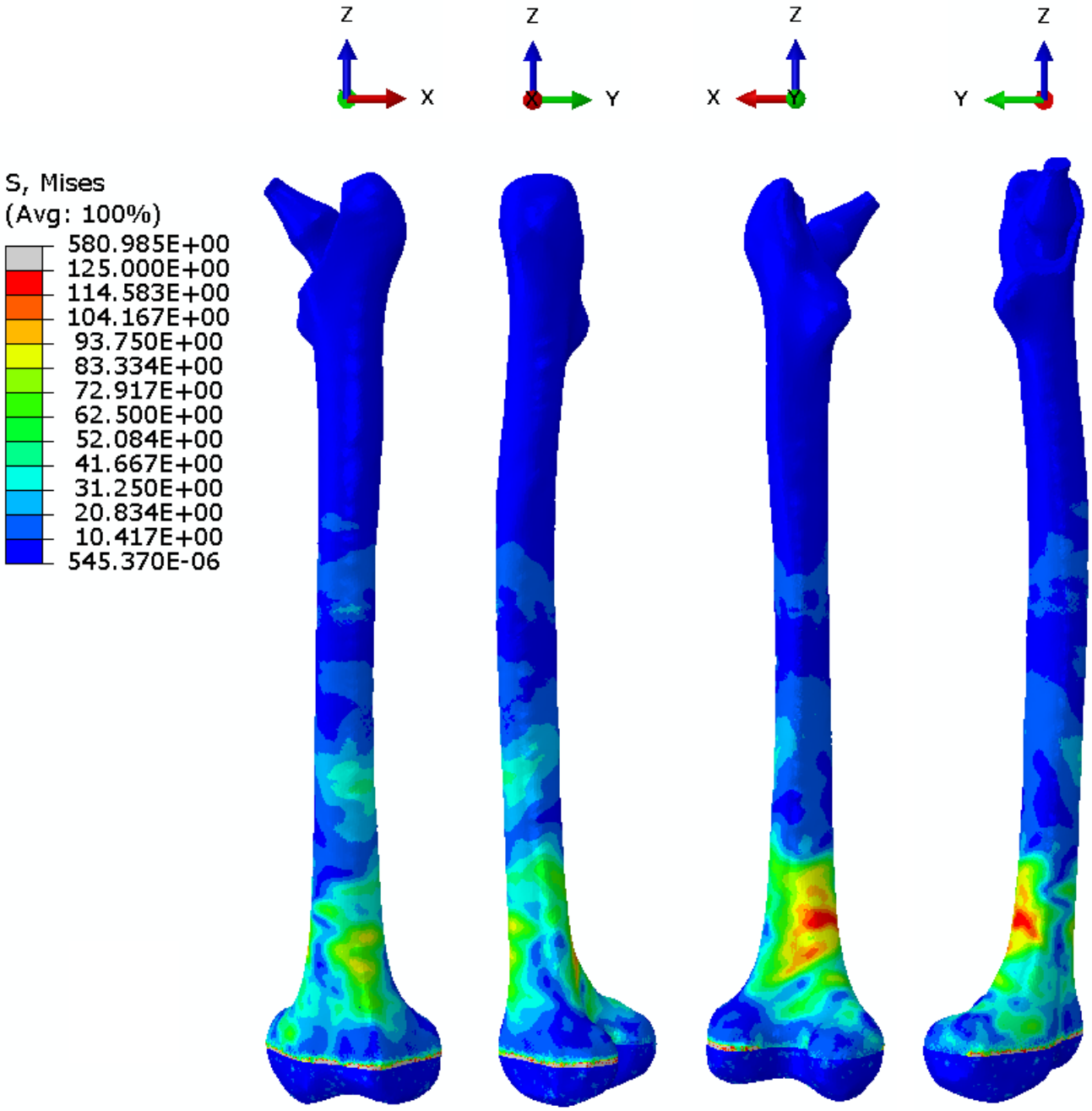

Figure 22 : Distribution de la contrainte de Von Mises équivalente [MPa] dans la surface externe de la couche corticale d'un fémur avec un remplacement THR et TKR (prothèse de genou de 220 mm de long) dans une simulation d'impact en chute avant au moment de l'impact.

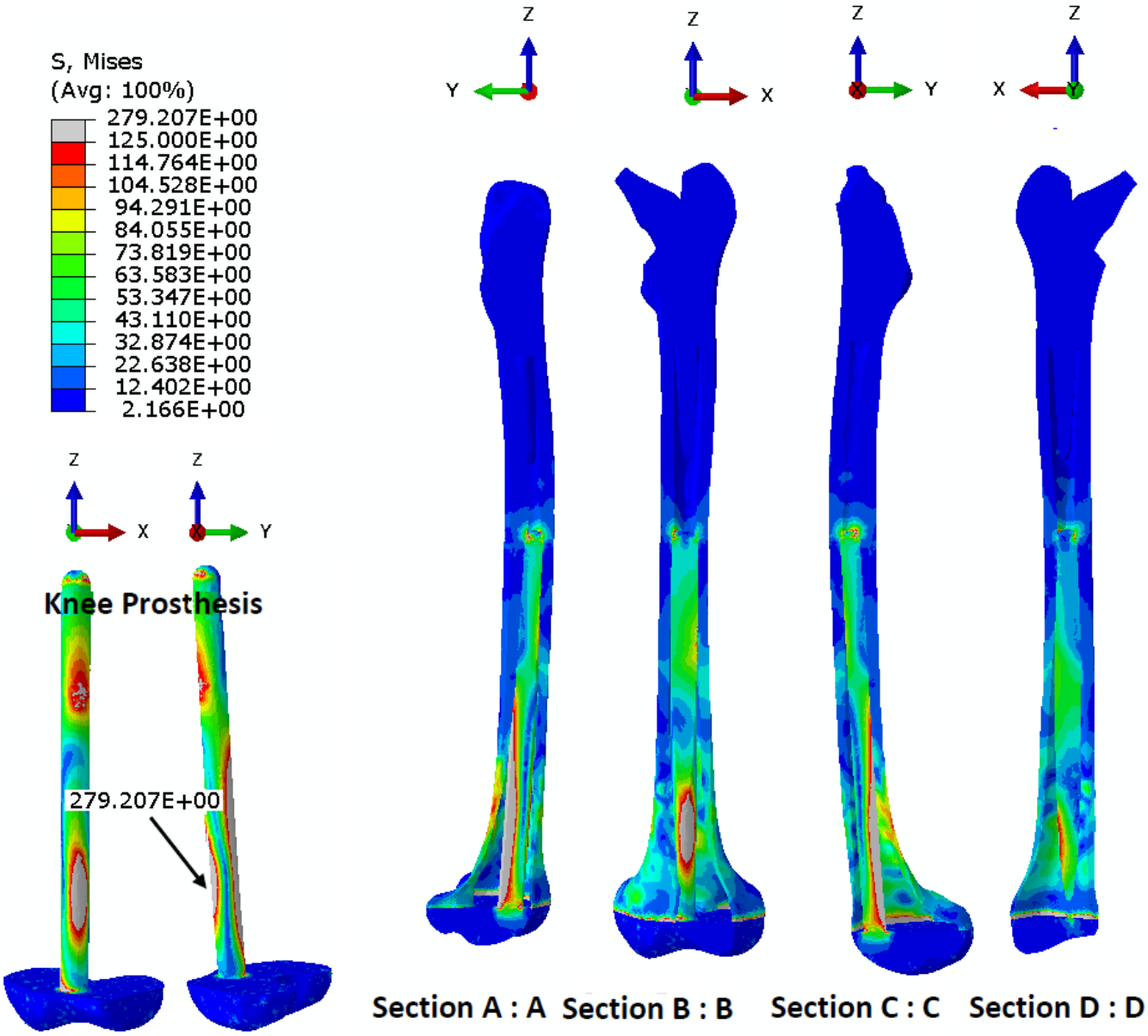

Figure 23 : Les coupes transversales du fémur avec une THR et une TKR (prothèse de genou de 220 mm de long) montrent la contrainte de Von Mises équivalente [MPa] à l'intérieur de la couche d'os cortical et la contrainte de Von Mises équivalente [MPa] sur la prothèse de genou.

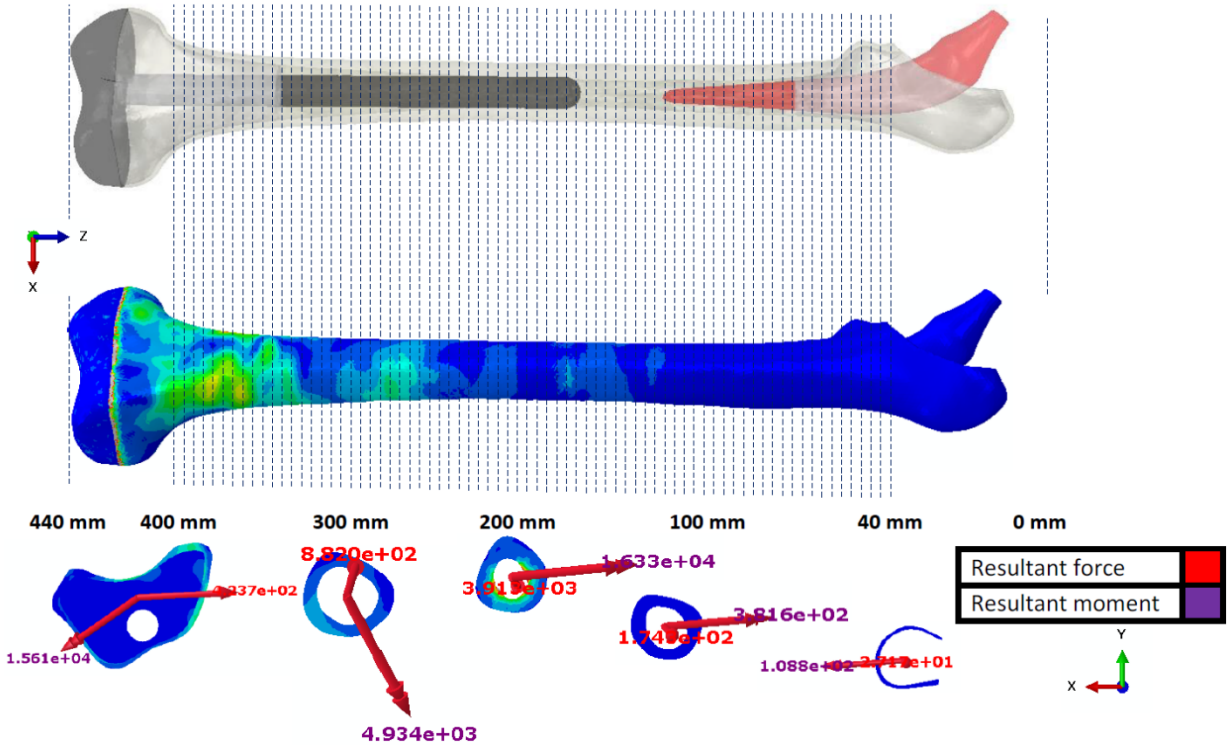

Figure 24 : Le fémur avec une THR et TKR (prothèse de genou de 220 mm de long) a été divisé en 73 sections de 40 mm à 400 mm avec un pas de 5 mm pour calculer le moment dans chaque pas.

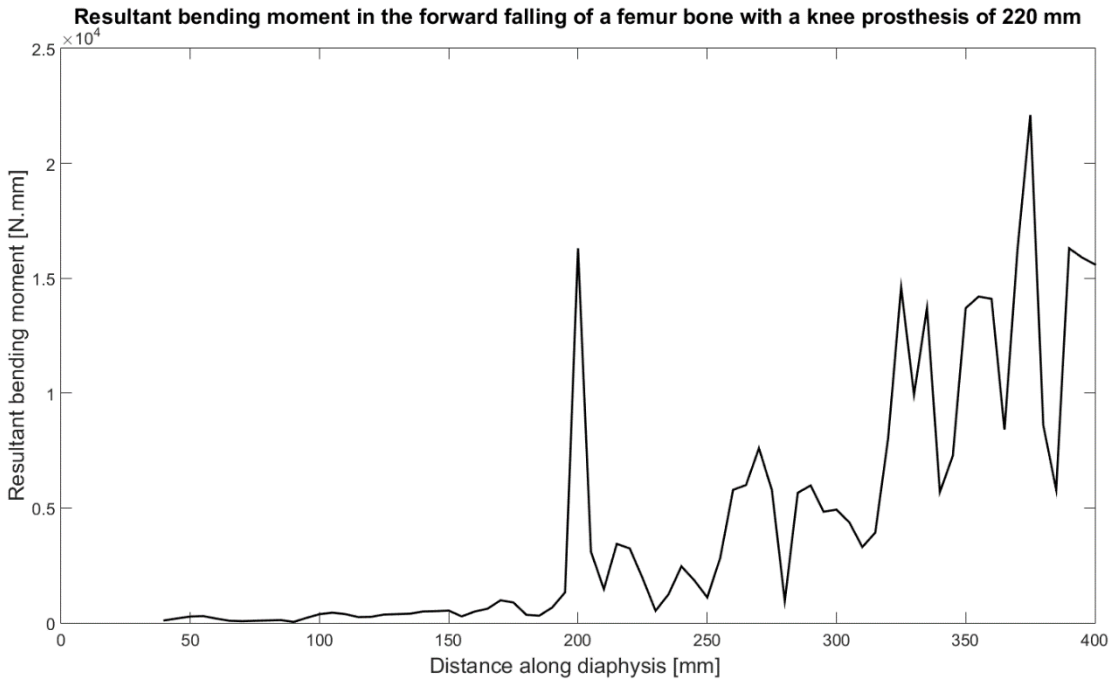

Figure 25 : Moment résultant sur un fémur équipé d'une prothèse de genou de 220 mm de long (THR et TKR) lors d'une simulation d'impact avec chute vers l'avant au moment de l'impact.

On note la distribution des contraintes pour les quatre modèles d'impact au moment de la collision de

0.34 ms

Pour toutes les simulations les résultats (figure.12), (figure.15), (figure.17), (figure.18), (figure.19), (figure.22), (figure.23) montrent que les contraintes maximales sont concentrées distalement autour de la tige du fémur près du genou alors que la partie distale reçoit la première charge de l'impact. Afin de tracer le moment résultant à travers le fémur pour chaque cas (figure.13), (figure.16), (figure.20), (figure.24) ; l'os du fémur a été divisé en 73 sections et le moment est calculé à chaque section (figure.14), (figure.17), (figure.21), (figure.25).

Ces résultats sont en accord avec le point de vue médical, alors que la chute vers l'avant d'un fémur lors d'une arthroplastie totale de la hanche et du genou provoque une fracture du fémur dans la partie distale autour de la prothèse du genou.

General introduction:

Total hip arthroplasty (THA) and total knee arthroplasty (TKA) have become increasingly common procedures in the elderly. However, there is a high risk of interprosthetic fracture (IPF) for patients who have undergone hip and knee arthroplasty on the same leg. In this study, we use numerical simulations to evaluate the mechanical response of a femur with total hip and knee arthroplasty both in compression and in flexion with different boundary conditions. In a first analysis, a simplified geometry of the femur was used to fully understand the load transfer mechanisms and the influence of the distance of the prosthesis stem lengths. Then a real geometry was modeled to introduce the notion of dependent patient. The problematic will thus focus on the analysis of the risk factors of occurrence of fractures of the bi-prosthetic femur by evaluating and characterizing the local stresses undergone by this femur with a focus on the inter-prosthetic fractures. Indeed, the positioning of a hip and knee prosthesis modifies the elasticity of the whole femur and of the new femur-prosthesis "couple". The distribution of stresses is affected during conventional loading. The objective is therefore to understand the mechanisms of overstress and their effects on fracture so as to be able to assess the risk of fracture, depending on the area of the femur "free of implant", with the aim of preventing the patient. The evaluation of this risk would also be of interest to adapt the length of the prosthetic implants of primary or revision, or even to question the classically defined lengths of the femoral pivots of total hip replacement (THR) or total knee replacement (TKR). To achieve this objective, we propose to develop a decision support tool for the orthopaedic surgeon, in order to define an optimal geometry of the prosthesis to be implanted and to determine the need to implant a preventive peri-prosthetic diaphyseal femoral plate. This tool will be based on finite element modeling which is an engineering tool for structural analysis that has been used for many years to evaluate the relationship between load transfer and bone morphology and to optimize the design and fixation of orthopedic implants.

The thesis consists of 4 chapters:

Chapter one: Literature review on the study of biprosthetic femurs.

Part I: Bones and fractures: background :

In the first part of the chapter, we present successively :

1. The structure of the bone.
2. The mechanical behavior of the bone.
3. Age related fractures of the femur.
4. Fractures of the human femur (proximal, shaft and distal).
5. Joint replacement of the femur.
6. Periprosthetic and interprosthetic fractures.
7. Interprosthetic treatment of femoral fractures

Part II: Finite element analysis and experimental test studies of a femur with a total hip and knee replacement.

In Part II, we present a review of numerical and experimental studies dedicated to femur after THR and TKR. In this part, we reviewed the finite element analysis and biomechanical tests that investigate the fracture risk of a human femur after THA or TKA. The main factors identified in the literature are thin cortical thickness, lack of fixation of the prosthesis (loosening, osteolization) and interprosthetic distance. Various finite element simulation studies and experimental setups such as the cantilever test, the four-point bending test, the gait cycle test, and the lateral drop test have been used to investigate the effect of IP distance on femoral fracture risk. Nevertheless, the authors do not reach the same conclusions. There are some contradictions in the results between the FE studies and the experimental tests using the four-point bending test. This discrepancy can be attributed to loading. We conclude that the literature fails to propose a clear conclusion regarding interprosthetic femoral fracture risk and fracture location. The objective of the next two chapters is to study different loading conditions and to predict in terms of deformation patterns the critical locations that may be exposed to fractures. One of the solutions to prevent this risk of fracture would be the implementation of a preventive locked plate.

Chapter Two: Influence of prostheses on the stress distribution between bone and prostheses "A finite element study using simple geometry".

In this chapter, we will analyze how the stress distribution between the femur and the prostheses varies by varying the loading cases while maintaining the same interprosthetic distance. Next, we will change the length of the knee stem to vary the interprosthetic distance for the same loading case. These simulations allowed us to select the best method to perform the bending tests for the study of the interprosthetic influence. The main objective adopted for this work is to examine in more detail the femoral bones in the interprosthetic space of THR and TKR using FEM, in order to obtain a qualitative overview of the different factors that generate the fracture risk. It is also to analyze the different strategies to impose a controlled mechanical load in a real femur geometry. Three different mechanical loading conditions are proposed:

- Four-point bending test with constant moment throughout the mid-diaphysis of the femur.
- Four-point bending test with a constant moment over the total femur.
- Two-point bending test with symmetric configuration.
- Two-point bending test with non-symmetric configuration.

Using a simplified geometry, four load cases were simulated in this work, with the aim of better understanding the factors involved in fracture risk (FR) in the human femur. The results show the effect of different stem lengths in several bending tests. Nevertheless, these simulations are still considered too simplistic to draw conclusive results.

Chapter Three: Finite element analysis of human femur geometry to study fracture risk after total knee replacement and total knee arthroplasty.

In Chapter 3, we analyze the effect of a real geometry on the stress distribution for quasi-static loading cases. We also analyzed how this distribution varies by varying the loading cases (4pt bending, 2pt symmetrical, non-symmetrical bending and gait cycle test) while keeping the same interprosthetic distance. Then we modify the length of the knee stem to vary the interprosthetic distance for the same loading case. The parameters fixed for the comparisons are the Maximum Force, the Maximum Displacement, the Maximum Energy.

Geometric data of real human femur bones in the form of DICOM (Digital Imaging and Communications in Medicine) files using GE's high-resolution Ultra-Fast multi-layer scanner are obtained at the US (University Hospitals of Strasbourg in three-dimensional FE models using the medical image control system, including cortical bone, cancellous bone, and intramedullary canal. The data used in the analysis belong to a 56-year-old male, weighing 61 kg, with a total femur length of 440 mm. The Charnley low-friction total hip replacement was used with a stem length of 145 mm. The hip prosthesis placed and checked by the orthopedic surgeon, such that the center of the hip prosthesis head was matched to the center of the healthy femoral head. Six different knee stem in the lengths and the diameters were modeled: three are commercially available (120, 160 and 220 mm) and three are not commercially available (140, 180 and 200 mm).

Chapter Four: Dynamic simulation of a forward fall: loading analysis of the human femoral bone to study the critical fracture zone

The objective of this numerical study is to investigate and detect the areas of high bending moment in a human femur during a low energy impact of a forward fall. The detection of these areas of maximum moment will give us the ability to impose these moments using an experimental setup developed in-house of a two-point bending test. The validation between the numerical simulations and the experimental work will give significant information about the possible fracture zones around the knee implant, so it will be used to achieve the research objective by designing and optimizing a preventive fracture plate that can be used in a femur with Total hip and total knee replacement.

Introduction générale:

L'arthroplastie totale de la hanche (ATH) et l'arthroplastie totale du genou (ATG) sont des interventions de plus en plus courantes chez les personnes âgées. Cependant, il existe un risque élevé de fracture inter-prothétique (FIP) pour les patients qui ont subi une arthroplastie de la hanche et du genou sur la même jambe. Dans cette étude, nous utilisons des simulations numériques pour évaluer la réponse mécanique d'un fémur ayant subi une arthroplastie totale de la hanche et du genou à la fois en compression et en flexion avec différentes conditions aux limites. Dans une première analyse, une géométrie simplifiée du fémur a été utilisée pour bien comprendre les mécanismes de transfert de charge et l'influence de la distance des longueurs de tige de la prothèse. Ensuite, une géométrie réelle a été modélisée pour introduire la notion de patient dépendant. La problématique portera donc sur l'analyse des facteurs de risque d'apparition de fractures du fémur bi-prothétique en évaluant et caractérisant les contraintes locales subies par ce fémur avec un focus sur les fractures inter-prothétiques. En effet, la mise en place d'une prothèse de hanche et de genou modifie l'élasticité de l'ensemble du fémur et du nouveau " couple " fémur-prothèse. La distribution des contraintes est affectée lors d'un chargement conventionnel. L'objectif est donc de comprendre les mécanismes de surcontraintes et leurs effets sur la fracture afin de pouvoir évaluer le risque de fracture, en fonction de la zone du fémur " libre d'implant ", dans le but de prévenir le patient. L'évaluation de ce risque serait également intéressante pour adapter la longueur des implants prothétiques de première ou de révision, voire pour remettre en cause les longueurs classiquement définies des pivots fémoraux des prothèses totales de hanche (PTH) ou de genou (PTG). Pour atteindre cet objectif, nous proposons de développer un outil d'aide à la décision pour le chirurgien orthopédiste, afin de définir une géométrie optimale de la prothèse à implanter et de déterminer la nécessité d'implanter une plaque fémorale diaphysaire préventive péri-prothétique. Cet outil sera basé sur la modélisation par éléments finis, qui est un outil d'ingénierie pour l'analyse structurelle utilisé depuis de nombreuses années pour évaluer la relation entre le transfert de charge et la morphologie osseuse et pour optimiser la conception et la fixation des implants orthopédiques.
La thèse est composée de 4 chapitres:

Chapitre 1 : Revue de la littérature sur l'étude des fémurs biprothétiques.

Partie I : Os et fractures : contexte :

Dans la première partie du chapitre, nous présentons successivement :

L'étude des fémurs bipèdes. 1. La structure de l'os.

2. Le comportement mécanique de l'os.
3. Fractures du fémur liées à l'âge.
4. Fractures du fémur humain (proximal, diaphragme et distal).
5. Remplacement de l'articulation du fémur.
6. Fractures périprothétiques et interprothétiques.

7. Traitement interprothétique des fractures du fémur.

Partie II : Analyse par éléments finis et études expérimentales d'un fémur avec prothèse totale de hanche et de genou.

Dans la partie II, nous présentons une revue des méthodes numériques et expérimentales d'un fémur après THR et TKR. Dans cette partie, nous avons passé en revue l'analyse par éléments finis et les tests biomécaniques qui étudient le risque de fracture d'un fémur humain après une ATH ou une ATG. Les principaux facteurs identifiés dans la littérature sont la faible épaisseur corticale, le manque de fixation de la prothèse (descellement, ostéolisation) et la distance interprothétique. Diverses études de simulation par éléments finis et montages expérimentaux tels que le test du cantilever, le test de la flexion à quatre points, le test du cycle de marche et le test de la chute latérale ont été utilisés pour étudier l'effet de la distance IP sur le risque de fracture fémorale. Néanmoins, les auteurs ne parviennent pas aux mêmes conclusions. Il y a quelques contradictions dans les résultats entre les études FE et les tests expérimentaux utilisant le test de flexion à quatre points. Cette divergence peut être attribuée au chargement. Nous concluons que la littérature ne parvient pas à proposer une conclusion claire concernant le risque de fracture fémorale interprothétique et la localisation de la fracture. L'objectif des deux prochains chapitres est d'étudier différentes conditions de chargement et de prédire en termes de modèles de déformation les endroits critiques qui peuvent être exposés aux fractures. L'une des solutions pour prévenir ce risque de fracture serait la mise en place d'une plaque verrouillée préventive.

Chapitre 2 : Influence des prothèses sur la distribution des contraintes entre l'os et les prothèses "Une étude par éléments finis utilisant une géométrie simple".

Dans ce chapitre, nous allons analyser comment la distribution des contraintes entre le fémur et les prothèses varie en faisant varier les cas de chargement tout en maintenant la même distance interprothétique. Ensuite, nous changerons la longueur de la tige du genou pour faire varier la distance interprothétique pour le même cas de charge. Ces simulations nous ont permis de sélectionner la meilleure méthode pour réaliser les tests de flexion pour l'étude de l'influence interprothétique. L'objectif principal adopté pour ce travail est d'examiner plus en détail le risque de fracture présent dans les os fémoraux dans l'espace interprothétique de la THP et de la TKP en utilisant la FEM, afin d'obtenir un aperçu qualitatif des différents facteurs qui génèrent le risque de fracture. Il s'agit également d'analyser les différentes stratégies pour imposer une charge mécanique contrôlée dans une géométrie réelle du fémur. Trois conditions de chargement mécanique différentes sont proposées :

- Essai de flexion en quatre points avec un moment constant sur la diaphyse moyenne du fémur.
- Essai de flexion à quatre points avec un moment constant sur l'ensemble du fémur.
- Essai de flexion en deux points avec configuration symétrique.
- Essai de flexion en deux points avec configuration non symétrique.

En utilisant une géométrie simplifiée, quatre cas de charge ont été simulés dans ce travail, dans le but de

mieux comprendre les facteurs impliqués dans le risque de fracture (FR) du fémur humain. Les résultats montrent l'effet de différentes longueurs de tige dans plusieurs essais de flexion. Néanmoins, ces simulations sont encore considérées comme trop simplistes pour en tirer des résultats concluants.

Chapitre 3 : Analyse par éléments finis de la géométrie du fémur humain pour étudier le risque de fracture après une arthroplastie totale du genou et une arthroplastie totale du genou.
Dans le chapitre 3, nous analysons l'effet d'une géométrie réelle sur la distribution des contraintes pour des cas de chargement quasi-statique. Nous avons également analysé comment cette distribution varie en faisant varier les cas de chargement (flexion 4pt, symétrique 2pt, flexion non symétrique et test du cycle de marche) tout en gardant la même distance interprothétique. Ensuite, nous modifions la longueur de la tige du genou pour faire varier la distance interprothétique pour le même cas de charge. Les paramètres fixés pour les comparaisons sont la force maximale, le déplacement maximal et l'énergie maximale.
Les données géométriques de véritables os fémoraux humains, sous forme de fichiers DICOM (Digital Imaging and Communications in Medicine), sont obtenues à l'aide du scanner multicouche haute résolution Ultra-Fast de GE dans des modèles FE tridimensionnels utilisant le système de contrôle des images médicales, incluant l'os cortical, l'os spongieux et le canal intramédullaire. Les données utilisées dans l'analyse appartiennent à un homme de 56 ans, pesant 61 kg, avec une longueur totale du fémur de 440 mm. La prothèse totale de hanche à faible frottement de Charnley a été utilisée avec une longueur de tige de 145 mm. La prothèse de hanche a été placée et vérifiée par le chirurgien orthopédiste, de sorte que le centre de la tête de la prothèse de hanche correspondait au centre de la tête fémorale saine. Six tiges de genou différentes en termes de longueur et de diamètre ont été modélisées : trois sont disponibles dans le commerce (120, 160 et 220 mm) et trois ne le sont pas (140, 180 et 200 mm).

Chapitre 4 : Simulation dynamique d'une chute avant : analyse de la charge de l'os fémoral humain pour l'étude de la zone de fracture critique".
L'objectif de cette étude numérique est d'examiner et de détecter les zones de moment de flexion élevé dans un fémur humain pendant un impact à faible énergie d'une chute avant. La détection de ces zones de moment maximal nous donnera la possibilité d'imposer ces moments à l'aide d'un montage expérimental développé en interne d'un test de flexion à deux points. La validation entre les simulations numériques et le travail expérimental donnera des informations significatives sur les zones de fracture possibles autour de l'implant du genou, et sera donc utilisée pour atteindre l'objectif de recherche en concevant et en optimisant une plaque de fracture préventive qui peut être utilisée dans un fémur avec une prothèse totale de la hanche et du genou.

Chapter 1

Part I : Bone and fractures: background

Abstract:

Bones are living tissue. They have their own blood vessels and are made of living cells, which help them to grow and to repair themselves. As well, proteins, minerals, and vitamins make up the bone. They are complex stiff tissue able to resist internal muscle forces and external forces. Bones provide protection for vital structures, mechanical of basic movement, mineral storage, and blood production. A bone fracture can be the result of a high force impact or stress or low energy impacts as a result of medical conditions that weaken the bones such as osteoporosis and bone cancer. The bone fracture risk also increases during the aging process, while bone mineral density (BMD) decreases and continuously bone fragility increases. Femur fractures considered to be one of the most common orthopedic problems caused by the decline of the BMD.

This chapter will introduce:

1. Structure of the bone.
2. Mechanical behavior of the bone.
3. Age-related to femur bone fractures.
4. Fractures of the human femur (Proximal, Shaft and distal).
5. Femur joints replacement.
6. periprosthetic and Interprosthetic fractures.
7. Interprosthetic femur fractures treatment.

Résumé:

Les os sont des tissus vivants. Ils ont leurs propres vaisseaux sanguins et sont constitués de cellules vivantes qui les aident à se développer et à se réparer. Les protéines, les minéraux et les vitamines constituent l'os. Ce sont des tissus rigides complexes capables de résister aux forces musculaires internes et externes. Les os protègent les structures vitales, participent à la mécanique du mouvement de base, au stockage des minéraux. Une fracture osseuse peut être le résultat d'un traumatisme

direct d'une contrainte élevée indirect ou d'un impact de faible énergie mais associé à des conditions locales défavorables (ostéoporose, maladie osseuse) qui affaiblissent les os. Le risque de fracture osseuse augmente également pendant le processus de vieillissement, tandis que la densité minérale osseuse (DMO) diminue avec en parallèle une fragilité osseuse qui augmente continuellement. Les fractures diaphysaires du fémur sont relativement rares et sont considérées comme graves car peuvent engager le pronostic fonctionnel voire vital (perte sanguine de 1.5 litre) du patient. Les fractures fémorales sur implant représentent une entité particulière, qui survient essentiellement chez le patient âgé, favorisées par la baisse de la DMO et les modifications osseuses locales due à la présence des implants prothétiques.

Le présent chapitre vous présente :

1. La structure de l'os.
2. Le comportement mécanique de l'os.
3. L'âge lié aux fractures du fémur.
4. Les fractures du fémur humain (proximales, de l'arbre et distales).
5. Le remplacement des articulations du fémur.
6. Les fractures périprothétiques et interprothétiques.
7. Le traitement interprothétique des fractures du fémur.

1.1 The structure of the bone

Bones, muscles, and joints work together to hold our bodies and support freedom of movement. They provide the structure for our bodies. Skeletal elements protect various vital organs, such as the brain and the heart. The bone structure has a decisive impact on its mechanical properties. Bones are made of two components: organic, which is responsible for elasticity, and inorganic, which responsible for hardness. The total number of bones in the adult human skeleton is 206 bones, which classification can be based on their size, shape, location, and structure.

In order to understand the mechanical properties of bone material, bone can be considered as an assembly of different levels of hierarchical structure. This levels can be classified based on the scale from nano to micro (figure.1.1.1) in to five groups [Rho et al., 1998] :

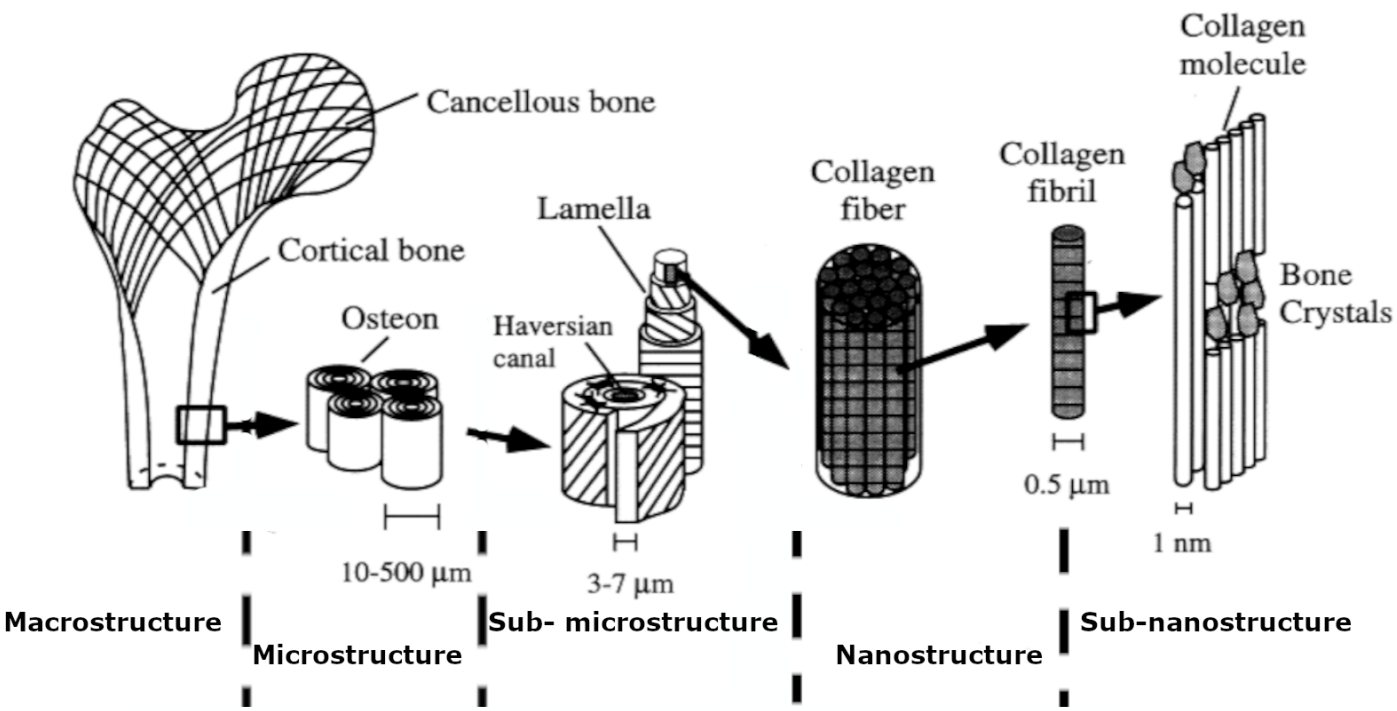

Figure 1.1.1: Hierarchical structure of bone [Rho et al., 1998]

- **The macrostructure level:** This level (the whole bone level), with size from to 10 mm up to several centimeters, consists of cortical and trabecular bone (figure.1.1.2). While the cortical bone is about 80 % volume of the total skeleton and the trabecular bone is about 20 % volume.
- **The microstructure level:** This level, with size to (10-500) μm, consists of haversian systems,

randomly arranged osteons, single trabeculae.

- **The sub-microstructure level:** This level (lamellae level), with size to (1-10) μm, consists of several structures of oriented fibrils, depending on the location in the bone (parallel, circumferential, twisted) with respect to the longitudinal axis of the diaphysis.
- **The nanostructure level:** This level, with size from a few hundred nanometers to 1 μm, consists of fibrillar collagen and embedded mineral.
- **The subnanostructure level:** This level, with size less than few hundred nanometers, consists of fibrillar collagen and non-collagenous organic proteins.

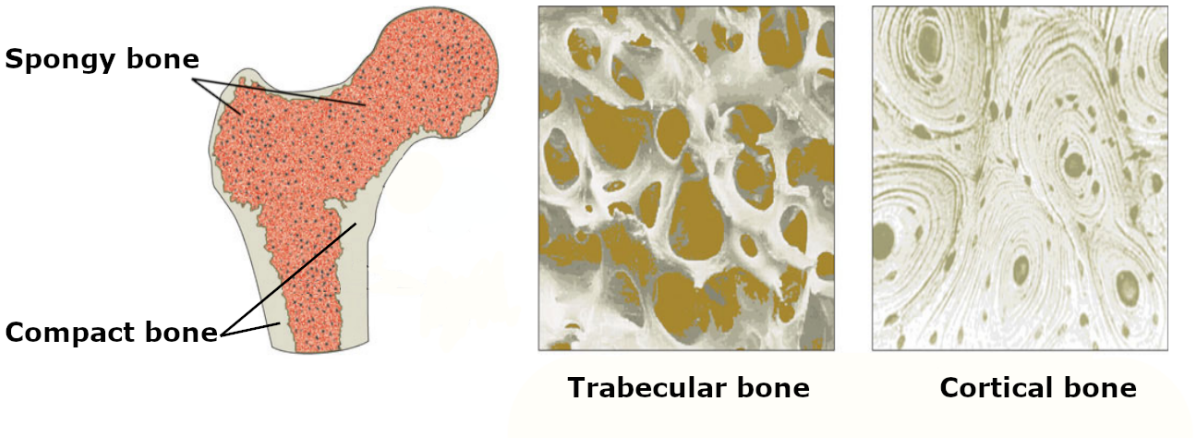

Figure 1.1.2: *Bone section cortical and trabecular. Resource of the images: https://2012books.lardbucket.org/books/an-introduction-to-nutrition/s13-01-bone-structure-and-function.html*

1.2 Mechanical behavior of the bone

Bone is a highly adaptive material and very sensitive to high load levels and vigorous activities. it could change in the properties and it's settings in response to the mechanical demand. Bone strength is determined by its material composition and structure. The understanding of the bone mechanical properties requires detailed knowledge of their interactions and structural organizations at different scale levels [Rho et al., 1998], [Ho Ba Tho et al., 2012]. The cortical bone highlights two main parts in the stress-strain curve (figure.1.2.1). In the beginning, the initial response is linear elastic. Then a non linear behavior os is observed until the material of the bone goes to the yield befor reaches the fracture. The mechanical behavior of a material may be completely described by a group of material properties. Bone shows remarkable mechanical properties, as can be seen in the chart presented in (figure.1.2.2). It is helpful to evaluate and compare the mechanical behavior of bone and other

materials on the basis of so-called performance indices. Different mechanical tests can be used to determine the properties of the bone such as strength, stiffness, ultimate load and work to failure. At the macroscopic level, bone can vary in its behavior depending on the porosity and density degrees in cortical or trabecular bone.

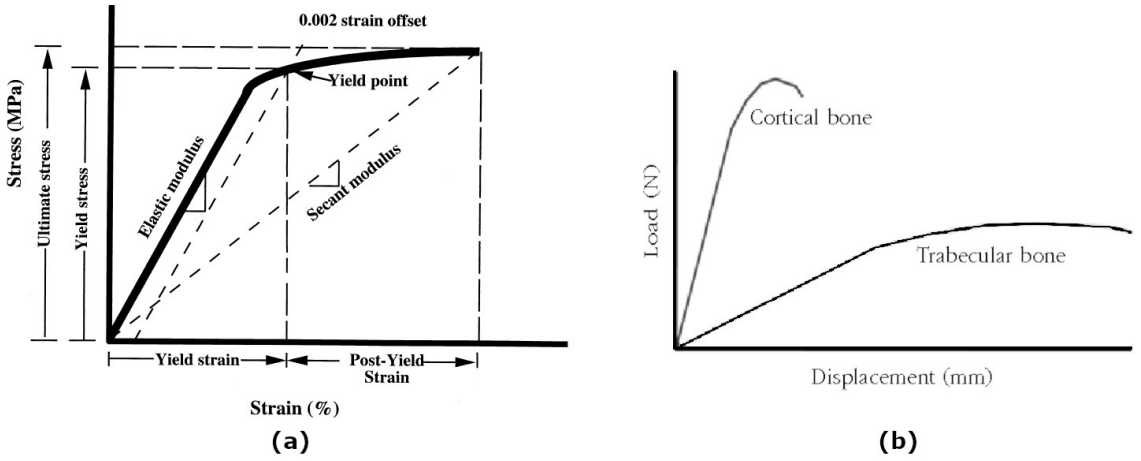

Figure 1.2.1: *(a)Stress-strain curve of cortical bone [Vashishth et al., 2001]. (b) Load-displacement curve of biomechanical behavior of the different bone tissue (cortical and trabecular)*

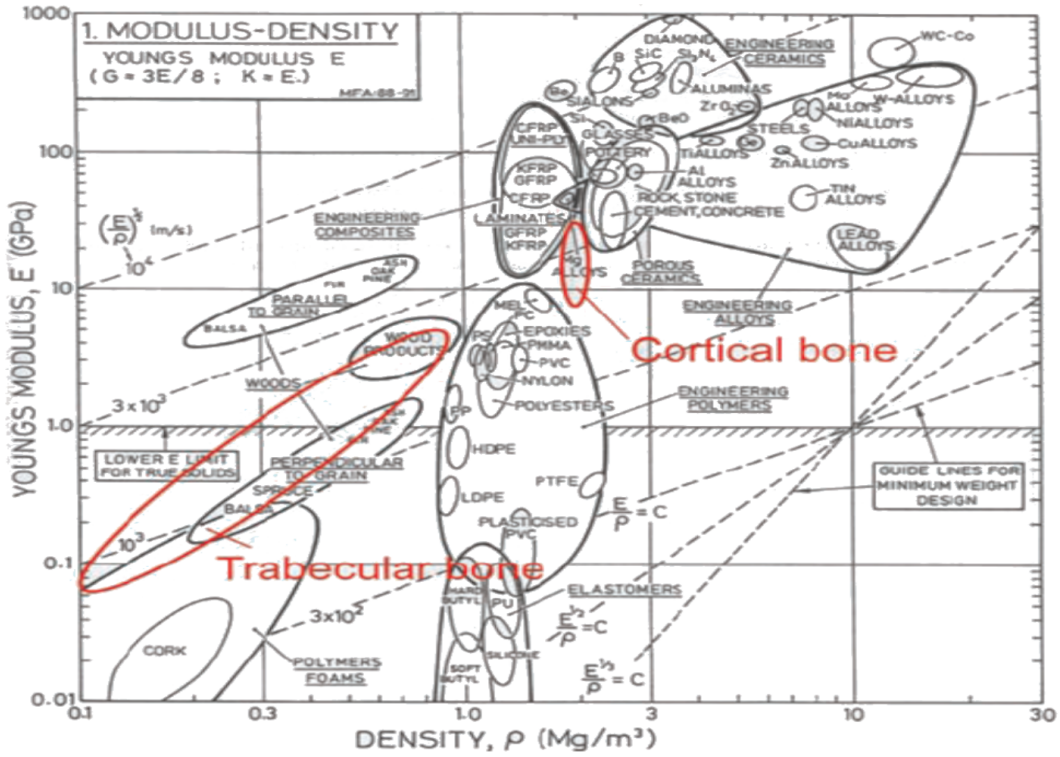

Figure 1.2.2: *A material property chart for bone tissue and engineering materials, plotting Young's modulus against density ([Kulin et al., 2011])*

• 1.2.1 Mechanical behavior of the cortical bone

The mechanical properties of cortical bone highly dependse on the experimental conditions of test method (figure.1.2.3.a) [An et al., 2000] , [Novitskaya et al., 2011], the porosity [Carter et al., 1977], [Rho et al., 1998] and the mineral content[Currey, 2010]. The oriented microstructure of cortical bone leads to anisotropic behavior :

1.2.1.1 Anisotropic behavior

Theelastic behavior depends on the direction along the bone axis (figure.1.2.3.b). [Donald et al., 1975] studied the anisotropic compressive and tensile properties of cortical bone. They found that the Young's modulus and maximum strength in the longitudinal direction are twice those in the transverse directions.

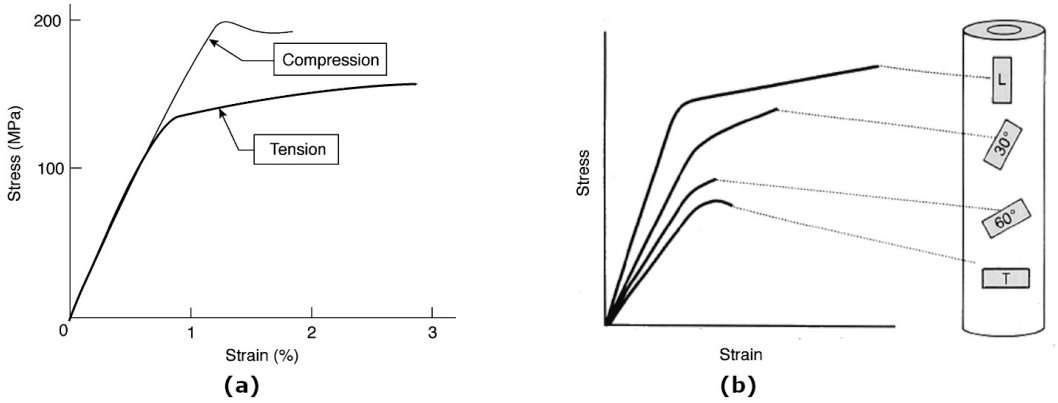

Figure 1.2.3: *(a)Schematic of the compressive and tensile stress/strain curves for cortical bone along the axis of a long bone [Mercer et al., 2006]. (b) Anisotropic behavior of cortical bone specimens in the different orientation of load in tensile test (Frankel VH, Nordin M: Basic Biomechanics of the Skeletal System. Philadelphia, Lea and Febiger, 1980)*

Several authors [Katz and Ukraincik, 1971], [Donald et al., 1975], [Yoon and Katz, 1976] assumed bone to be transversely isotropic with the long bone axis. [Peng et al., 2006] recognized bone material as an orthotropic material. The elastic properties of human cortical bone obtained in the literature with conventional mechanical tests (tension, compression, torsion tests) as well as ultrasounds and acoustic microscopy measurements. The results of recently reported measurements of the elastic modulus obtained alond the longitudinal direction of the bone by different experimental techniques for cortical bone summarized in (Table.1.2.1).

Experimental test	Modulus of elasticity (GPa)	Sample condition	Reference
Compression	19.9 ± 1.8	Wet.	[Bayraktar et al., 2004]
	16.2 to 17		[Keller, 1994]
Tension	16.7	Wet.	[Currey, 2004]
	16.6 ± 1.8		[Neil et al., 2004]
Torsion	4.7 ± 0.7	Wet.	[Currey, 2004] [Neil et al., 2004]
Ultrasound	13.9	Wet	[Bayraktar et al., 2004]
	32.5 ± 0.5	Fresh	[Hunt et al., 1998]

Table 1.2.1: Elastic modulus obtained by different experimental techniques for human cortical bone.

1.2.1.2 Strain rate sensitivity,

The mechanical behavior of bone varies depending on factors like loading condition and strain rates. The earliest and most widely cited on a wide range of strain rates studies were undertaken by [McElhaney, 1966] (figure.1.2.4) while the loads were applied in the direction of the longitudinal axis of the bone..

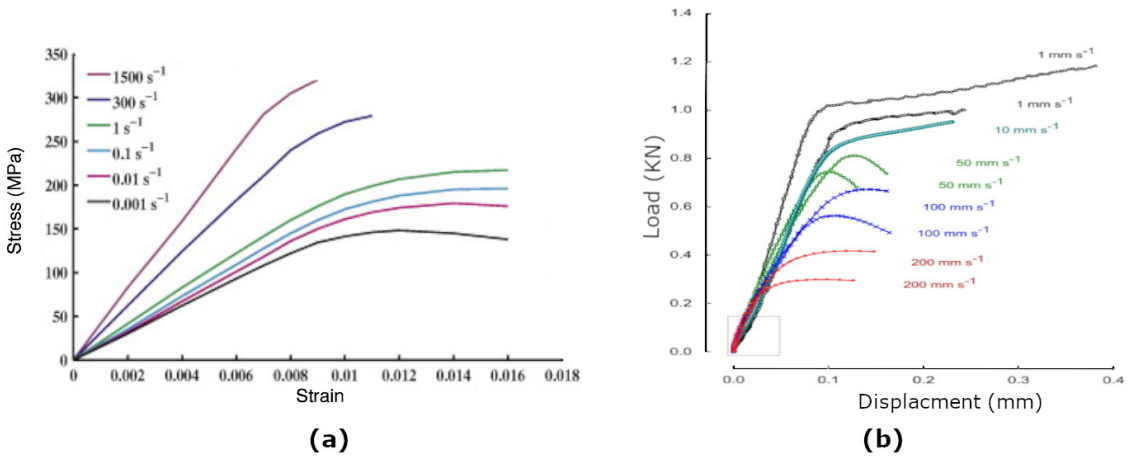

Figure 1.2.4: Viscoelasticity property of cortical bone (a) Schematic of the compressive stress/strain curve for cortical bone under different strain rates [Johnson et al., 2010]. (b) Schematic of the tensile force-displacement curve for cortical bone under different strain rates [Zioupos et al., 2008]

The human cortical bone samples from the femur were tested in uniaxial compression test at rates ranging from 0.001 to 1500 s^{-1}. They found that with increasing the strain rate there is an increase in yield and pre-yield properties (stress, σ ; strain, ε ; elastic modulus, E). Another study by [Hansen et al., 2008] reported results from tests on specimens of human

femoral cortical bone loaded in tension at rates ranging from 0.08 to 18 s^{-1}. They found that the Young' modulus, E in tension generally increased, stress, σ at yield and failure and strain at failure decreased for rates higher than 1 s^{-1}.

1.2.2 Mechanical behavior of the trabecular bone

Trabecular bone, also called cancellous bone or spongy bone is a highly porous bone enclosing numerous large spaces that give a honeycombed or spongy appearance (figure.1.2.5.a). It makes up about 20% of the human skeleton. It also can be described as heterogeneous, and anisotropic material [Oftadeh et al., 2015]. The main function of the trabecular bone is to transfer mechanical loads from the articular surface to cortical bone. The mechanical properties of trabeculalr bone dependent on the experimental conditions of the tests (figure.1.2.5.b). Several numerical studies done by [Bayraktar et al., 2004], [Verhulp et al., 2008], [Vanderoost et al., 2011] and experimental tests done by[Goldstein, 1987],[Ashman et al., 1988], [Du et al., 2006], [Kefalas et al., 2012], [Lakatos et al., 2014] have been used in order to investigate the mechanical properties of trabecular bone. The material properties of the trabecular bone are important for characterizing various bone pathologies,microlevel stress analyses, and bone adaptation around implants (For example there are two types of adaptations: either the bone has been forced to bring in the prosthesis so there is an over-stress at the level of the cortical in contact with the prosthesis and therefore thinning of the cortical because it hurts. Then there can be a secondary bond when not using cement (free space between bone and prosthesis) which will be filled by secondary bond) because they are affected by disease sooner than cortical bone. For example there are two types of adaptations: either the bone has been forced to bring in the prosthesis so there is an over-stress at the level of the cortical in contact with the prosthesis and therefore thinning of the cortical because it hurts. Then there can be a secondary bond when not using cement (free space between bone and prosthesis) which will be filled by secondary bond.

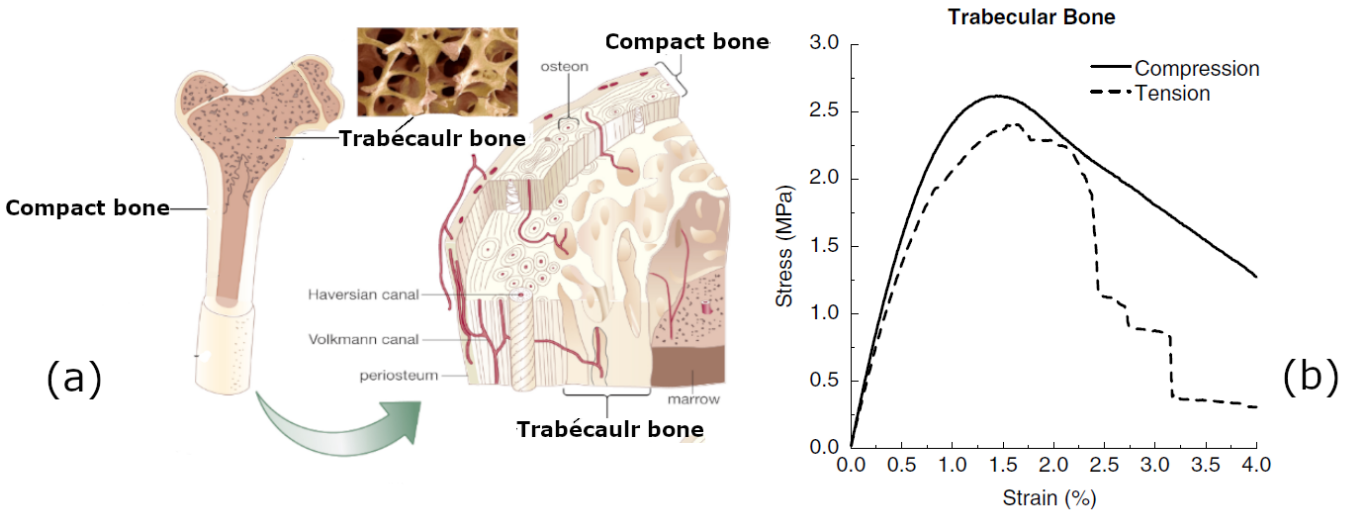

Figure 1.2.5: *a) A cross section of the interior human femur showing the largely contains of the trabecular bone. b) Stress–strain curves for trabecular bone in both compression and tension test ([Brown et al., 2013])*

The trabecular bone has a greater resistance to compression load than to any other type of load [Keaveny et al., 1994]. In compression test the resistance varies between 1.5 to 9.3 MPa, and the Young's modulus between 10 and 1058 MPa as a function of the region of the skeleton from which is comes [Caeiro et al., 2013].Elastic modulus obtained by different experimental techniques for trabecular bone summarized in (Table.1.2.2).

Test type	Modulus of elasticity (GPa)	Sample condition	Reference
Compression	3.47 ± 0.41	Wet	[Hong et al., 2007]
	0.44 ± 0.27		[Lotz et al., 1990]
Tension	10.4 ± 3.5	Dry	[Rho et al., 1993]
	2.4 ± 0.8	Wet	[F. Morgan et al., 2001]
Torsion	0.29 ± 0.18	Wet	[Bruyère Garnier et al., 1999]
Ultrasound	1.3	Wet	[Turner et al., 1999]
	13 ± 1.47	Wet	[Ashman and Rho, 1988]

Table 1.2.2: *Elastic modulus obtained by different experimental techniques for human trabecular bone.*

1.3 Femur bone specification

The femur is the largest and strongest bone in the body. Thus, it requires maximum amount of forces to break the bone. The ability of bones to resist fracture depends on their mass, material properties, geometry and tissue quality when subjected to loading [Forwood, 2001]. The femur is divided in to proximal region, shaft region and distal region. The proximal femur consists of a femoral head, a

neck and trochanteric (greater trochanter and lesser trochanter) region (Figure.1.3.1) . The head of the femur articulates with the acetabulum in the pelvic bone forming the hip joint, while the distal part of the femur articulates with the proximal tibia forming the knee joint. The knowledge of the femur macroscopic architecture is an important factor for femoral fracture occurrence (Figure.1.3.1). While the existence of a cantilevered neck and neck cephalic region explains the fractures of the femur neck and, the wears at the bottom of the condyle (knee) explains the fractures below close to the knee. The specification of the femur bone is varying according to the age, gender, and ethnicity [Nelson et al., 2000],[Nelson et al., 2004],[Travison et al., 2008],[Beck et al., 2009],[Zhang et al., 2010]

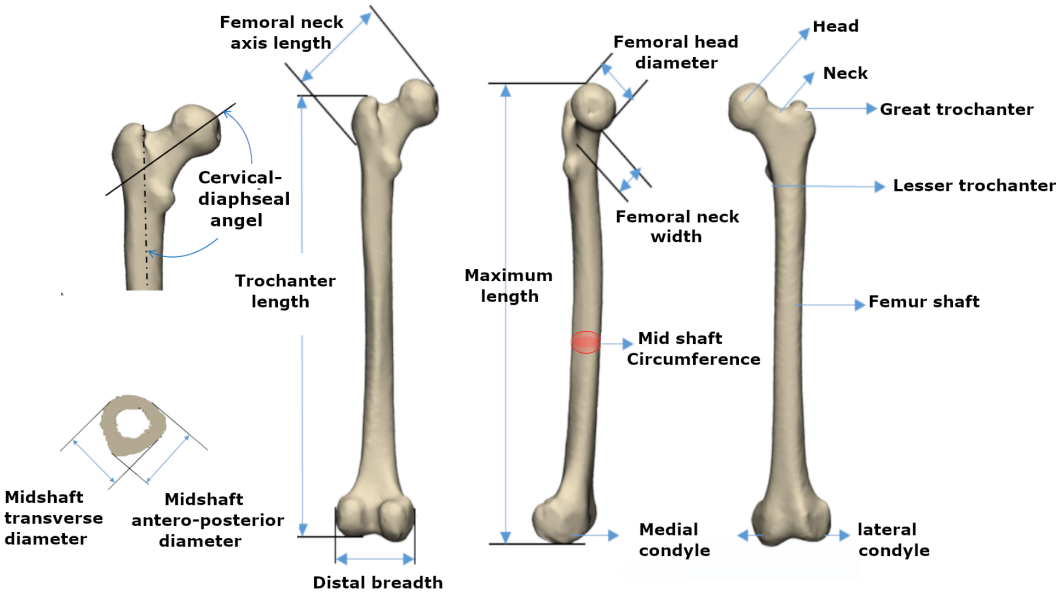

Figure 1.3.1: Human femur Anthropometry

1.4 Femur bone fractures

Fracture is a loss of continuity partially or completely. It can be classified based on the shape or pattern of the fractured fragments (transverse, oblique, spiral, and butterfly) [Oryan et al., 2015]. Different bone fractures are occur as a result of:

1. Violent trauma on normal bone.
2. Repeated microtrauma on normal bone: stress fracture.
3. Minimal trauma to a diseased bone: pathological fracture..
4. Fracture due to bone insufficiency : low-energy trauma on porous bone.

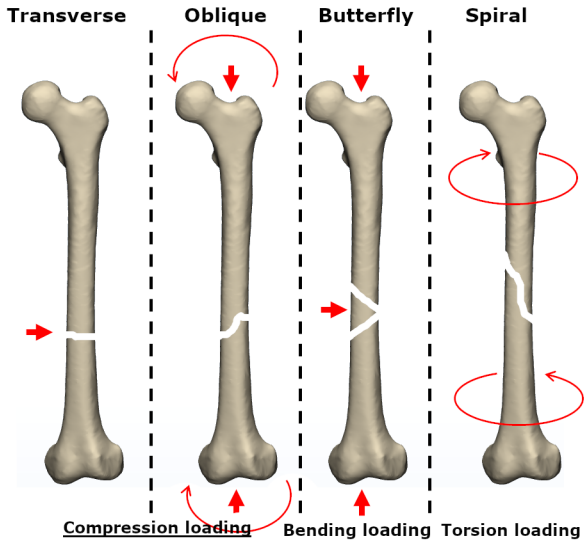

Figure 1.4.1: Classified of femoral fractures based on the shape or pattern of the fractured fragments

There are different types of fracture and with each type it is necessary to associate an injury mechanism (compression causes a transverse or oblique fracture, the bending will be the cause of a third fragment) and the torsion will cause a spiral fracture (Figure.1.4.1).

1.4.1 Age related to femur bone fractures

Due to the physiological changes in the bone, osteoporosis occurs with aging, which induces bone fragility and therefore potentially leads to bone fracture [Reginster et al., 1999], [Lau et al., 2011]. Bone mineral density (BMD) is the most widely used clinical measure of bone quantity and it is considered to be one of the factors which, used as a predictor of bone fracture (Figure.1.4.2). [Kurtz et al., 2007].

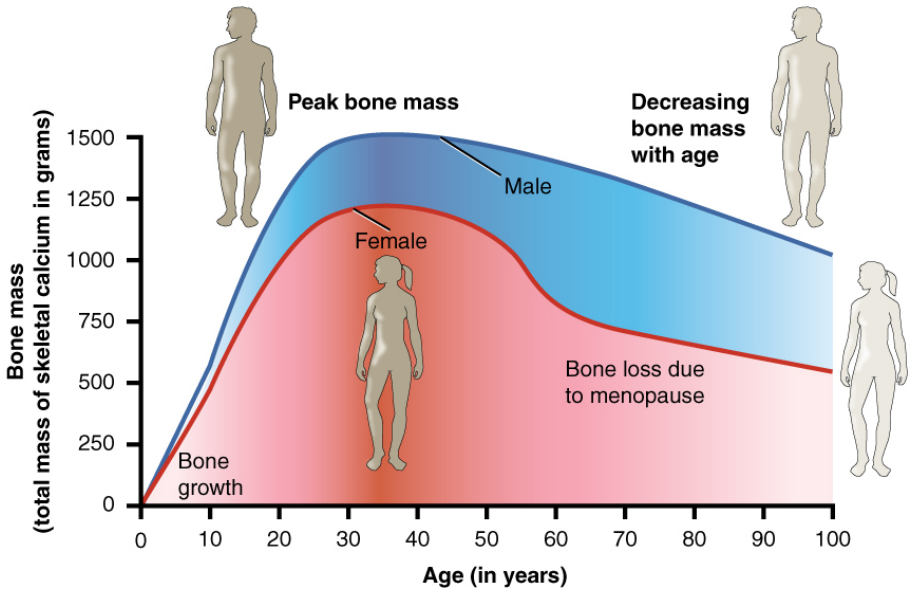

Figure 1.4.2: Bone mass in male and female as it relates to age. Resource of the image: https://commons.wikimedia.org/wiki/File:615_Age_and_Bone_Mass.jpg.

1.4.2 Fractures of the femur shaft

The femoral shaft fractures are the fractures located below the lesser trochanter of the femur and above the distal [?]. Direct-high-energy trauma and the fall on the affected limb are the main reasons of the femoral shaft fractures [Arneson et al., 1988], [Weiss et al., 2009], [Neumann et al., 2015]. Limited attention has been given to low-energy violence as a cause of these fractures among the elderly people [Arneson et al., 1988], [Bengnér et al., 1990], [Salminen et al., 1997], [Weiss et al., 2009]. The AO-OTA system by [Muller, 1990] is used to classify the femoral shaft fractures as a simple, wedge and complex fractures (figure.1.4.3).

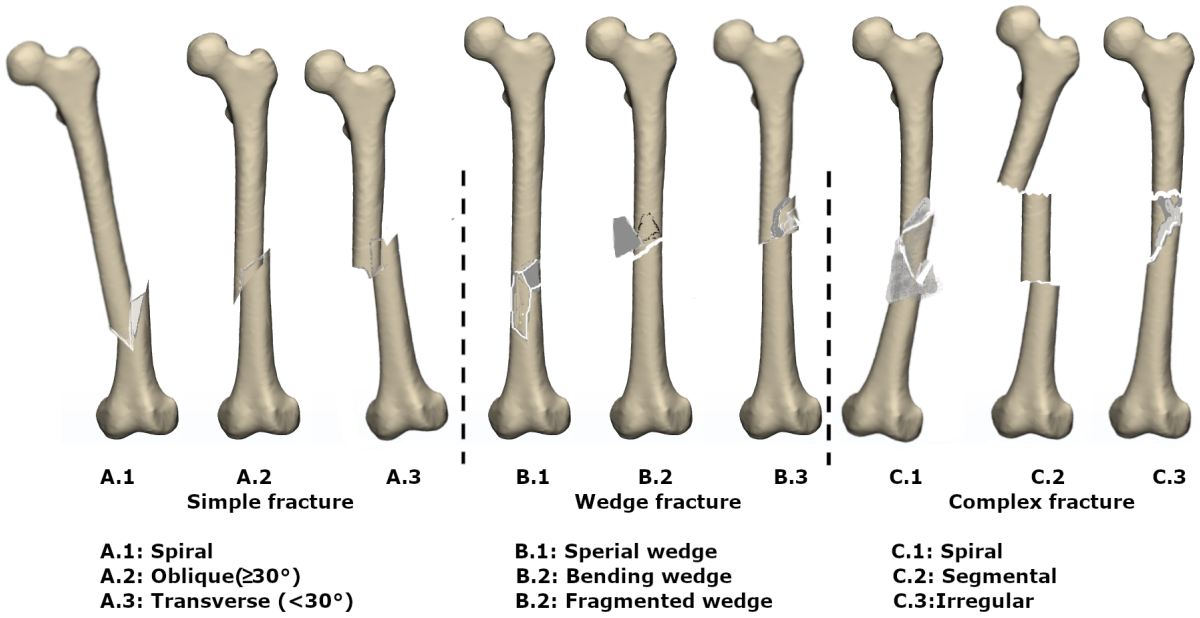

Figure 1.4.3: AO-OTA classification of the fractures of the femoral shaft by Muller

1.4.3 Fractures of the proximal femur

No mention of these fractures because it is far from our research and, in addition to having a hip prosthesis, which means no more fractures.

1.4.4 Fractures of the distal femur

Distal femoral fractures are the fractures within the distal 15cm of the femur, which includes the metaphysis, epiphysis, and the articular surface. Frequently, They do occur following low energy incidents such as a simple fall for aged people. But this kind of fracture will often happen to younger people at high energy (accident ou traumatisme). Fractures are classified according to the antomical location: supracondylar, condylar or intercondylar. Another description can be based on the fracture pattern: oblique, spiral or transverse fractures. The AO/OTA fracture classification system by [Muller, 1990] (figure.1.4.4) is the most universally used [Gwathmey et al., 2010] to describes these fractures.

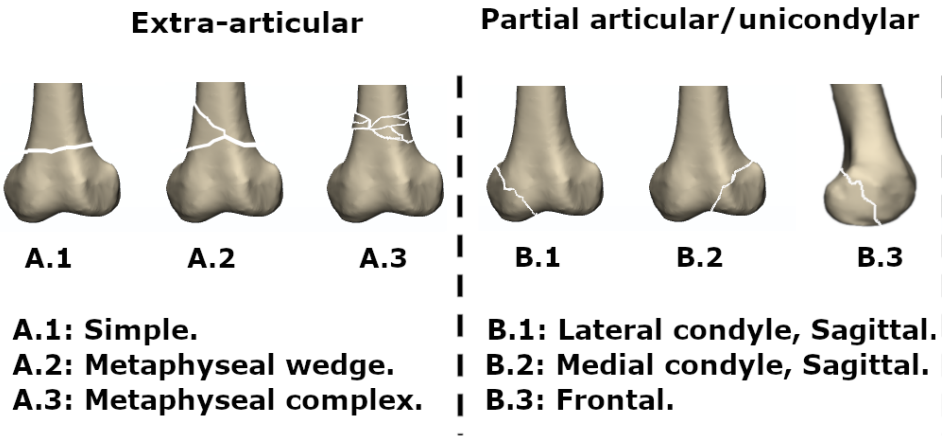

Figure 1.4.4: AO-OTA classification of distal femoral fractures by Muller

1.5 Joints replacement : hip and knee

Osteoarthritis is a classic disease that appears and develops with aging[M.Dowsey et al., 2013]. It is responsible for the disability in over 43 million people worldwide, about 50% of this number of whom are older than 60 years old [World Report on Disability, 2012]. This number is expected to continue to increase to make osteoarthritis the fourth leading cause of disability by the year 2020[D.Woolf et al., 2003]. Osteoarthritis is a wear and tear destroys of the cartilage. This can result in painful bone-on-bone contact, along with swelling and loss of motion. In order to relieve this pain, the total joint replacement (TJR) is mandatory [Wang et al., 2009].

Total joints replacement is a surgical operation in which the joint is replaced by a prosthetic implant.

This surgery is always performed to relieve arthritis pain or treat severe physical joint damage. A femur bone joint replacement could be total hip or total knee arthroplasty. Total hip replacement (THR) operation is by removing the damaged bone and cartilage (femoral head) and replaced with prosthetic components (figure.1.5.1). Total knee replacement (TKR) operation is by removing the damaged bone and cartilage (distal femur and proximal tibia) and replaced with an implant (figure.1.5.2).

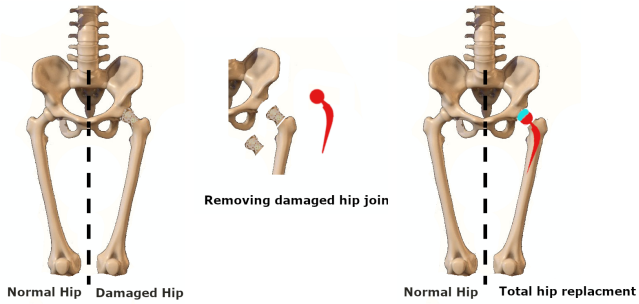

Figure 1.5.1: Prosthesis placement in the hip to replace the arthritic hip joint.

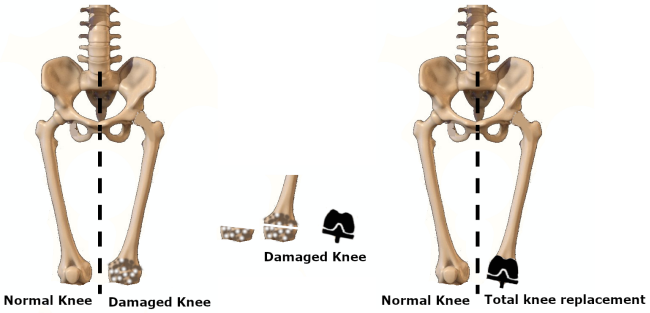

Figure 1.5.2: Prosthesis placement in the knee to replace the arthritic knee joint.

1.6 Periprosthetic fractures

A patient, especially an older patient, is more likely to suffer a femoral fracture. This fracture can occur on a prosthetic femur. If there is a hip and knee prosthesis, then it is called an interprosthetic fracture [Mamczak et al., 2010], [Solarino et al., 2014]. Different factors may lead to the occurrence of this type of fracture; such as the distance between the two prostheses which are known as the inter-prosthetic (IP) distance, Stem stability and cortical thickness area. The incidence of the periprosthetic fractures is estimated between 0.3 to 5.5 % for TKA placement [Rorabeck et al., 1998], between 0.1 to 6 % for THA placement [Berry, 1999],[Hou et al., 2011a] and 1.25 % for the IP fractures. The number of patients who have undergone ipsilateral THA and TKA procedures continues to rise and the number of inter-prosthetic fractures is increasing, likewise [Garellick et al.,], [Scolaro et al., 2017],[Soenen et al., 2011]. These IP fractures are a great challenge because of the type of these fractures, their locations, bone stock and the stability of the prosthesis.These periprosthetic fractures frequently occur in elderly people and therefore in fragile and osteoporotic bones. Thus they are most often secondary to a fall from a height and therefore a low energy trauma. Different classifications have been suggested to describe the periprosthetic femoral fractures (PFF).

1.6.1 Hip periprostetic fracture

The Vancouver classification system probably comes closest to the ideal for the periprosthetic hip fractures [Duncan and Masri, 1995]. The Vancouver classification was developed on the basis of fracture location with respect to the prosthesis, stem stability, and the quality of the remaining bone (figure.1.6.1). It can be classified into intraoperative periprosthetic fractures and postoperative periprosthetic fractures (figure.**??**). This classification has been improved by SOFCOT [Soenen et al., 2006].

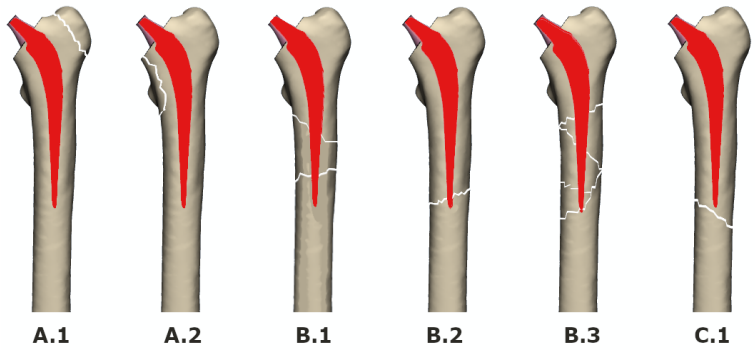

Figure 1.6.1: Vancouver classification of intraoperative femoral periprosthetic fracture. While A.1, A.2: Fractures located in the trochanteric region. B.1, B.2 and B.3: Fractures located around the stem (1= stem well fixed, 2= stem loose but good bone stock, 3=poor surrounding bone stock). C.1: Fractures loacted distal to the tip of the stem

1.6.2 Knee periprostetic fracture

The Rorabeck and Taylor [Rorabeck and Taylor, 1999] classification system is the most commonly used for supracondylar femoral fractures after total knee arthroplasty (figure.1.6.2). This classification takes into account fracture displacement and prosthesis stability condition. The description of these fractures have been described by SOFCOT [Soenen et al., 2006],[Ehlinger et al., 2013] , [Ehlinger et al., 2019]

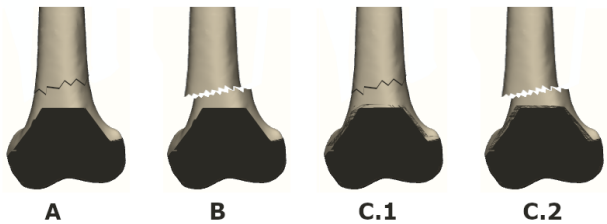

Figure 1.6.2: Lewis and Rorabeck classification of supracondylar periprosthetic fractures proximal to total knee arthroplasty. While A: Undisplaced fracture (prosthesis intact). B: Displaced fracture (prosthesis intact). C.1, C.2 and B.3: Fractures located in diaphysis, around oer just distal to the prosthesis. C: Displaced or undisplaced fracture (Prosthesis loose or failing)

• 1.6.3 Interprosthetic fracture

There are several classifications that describe the knee and the hip periprosthetic fractures; however, there is no complete and specific classification system for inter-prosthetic femoral fractures [Hou et al., 2011b], [Mamczak et al., 2010], [Platzer et al., 2011]. The classification system done by [Pires et al., 2014] classifies the inter-prosthetic fractures based on fracture site, the viability of inter-prosthetic bone fragment, and prostheses stability (figure.1.6.3).

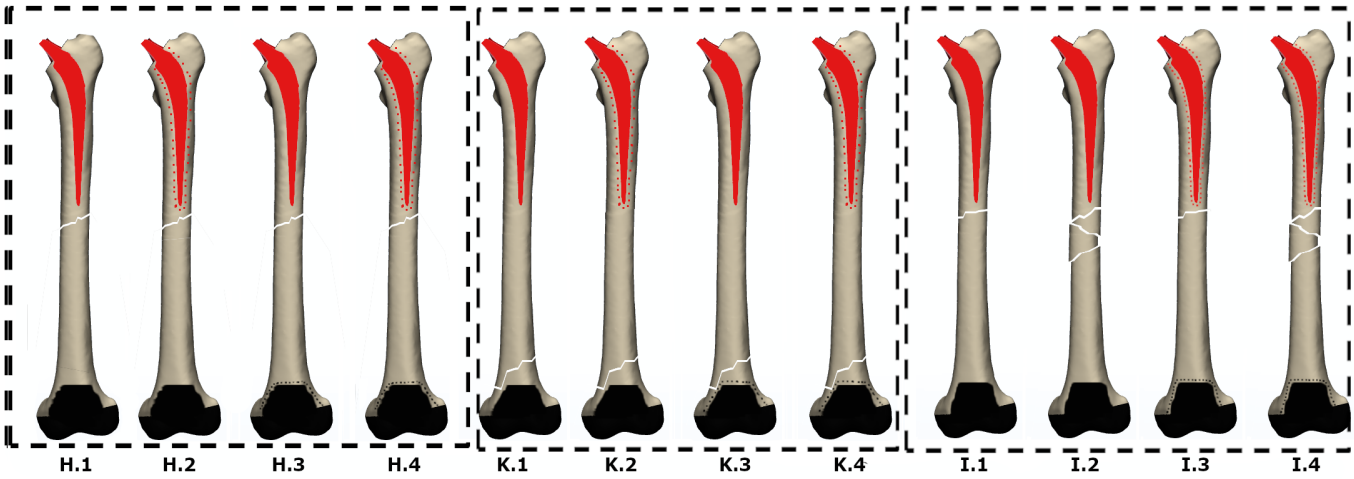

Figure 1.6.3: Piresa et.al classification of interprosthetic femur fractures. While H: Interprosthetic fracture surrounding hip: (H.1 Stable prostheses, H.2 Unstable hip prosthesis; stable knee prosthesis, H.3 Stable hip prosthesis; unstable knee prosthesis and H.4 Unstable hip and knee prostheses. K: Interprosthetic fracture surrounding knee: K.1 Stable prostheses, K.2 Unstable hip prosthesis; stable knee prosthesis, K.3 Stable hip prosthesis; unstable knee prosthesis and K.4 Unstable hip and knee prostheses. I: Interprosthetic fracture with femoral extension stem: I.1 Stable prostheses with viable bone between the prostheses, I.2 Stable prostheses with unviable fragment due to lack of bone interval between prostheses ends, I.3 Unstable prostheses (hip, knee or both) with viable bone between the prostheses. I.4 Unstable prostheses (hip, knee or both) with unviable fragment due to lack of bone interval between prostheses ends.)

It was described by the French teams from Lille and Strasbourg, a particular case of inter-prothetic fracture, which makes the link between the classification and fracture around hip prostheses and the classification and fracture around knee protheses. This type is defined as a femoral interprosthetic fracture located on a region free of any prosthetic implant, with a length inferior to one third of the diaphysis [Soenen et al., 2011].

1.7 Interprosthetic femur fractures treatment

The treatment of inter-prosthetic femoral fractures after total hip and total knee replacement is a challenge especially for the aged people due to the combination of fractured bone and prosthesis with further complications like osteoporotic bone and cement used for prosthesis fixation [Wähnert et al., 2014]. The inter-prosthetic fracture treatment is thought to show similarities with the reconstruction of peri-prosthetic fractures [Hou et al., 2011b]. The selection of the appropriate fracture fixation method depends on the type and the location of the fracture and the stability of the prosthesis. Fixation using plates and screws (ORIF) are used for fixation and conservative treatment of the IP fractures. This treatment places a plate overlapping the region of the fracture and repositions the broken bone fragments to their initial position (figure.1.7.1.I). Specialized plates been developed for femoral fractures. The locking plates are mostly system used for conservative treatment [Wang et al., 2019]. LCP plates (figure.1.7.1.II)have been proven to be biomechanically superior compared to other types of fracture fixation [Choi et al., 2010], [Solarino et al., 2014], [Stoffel et al., 2016].

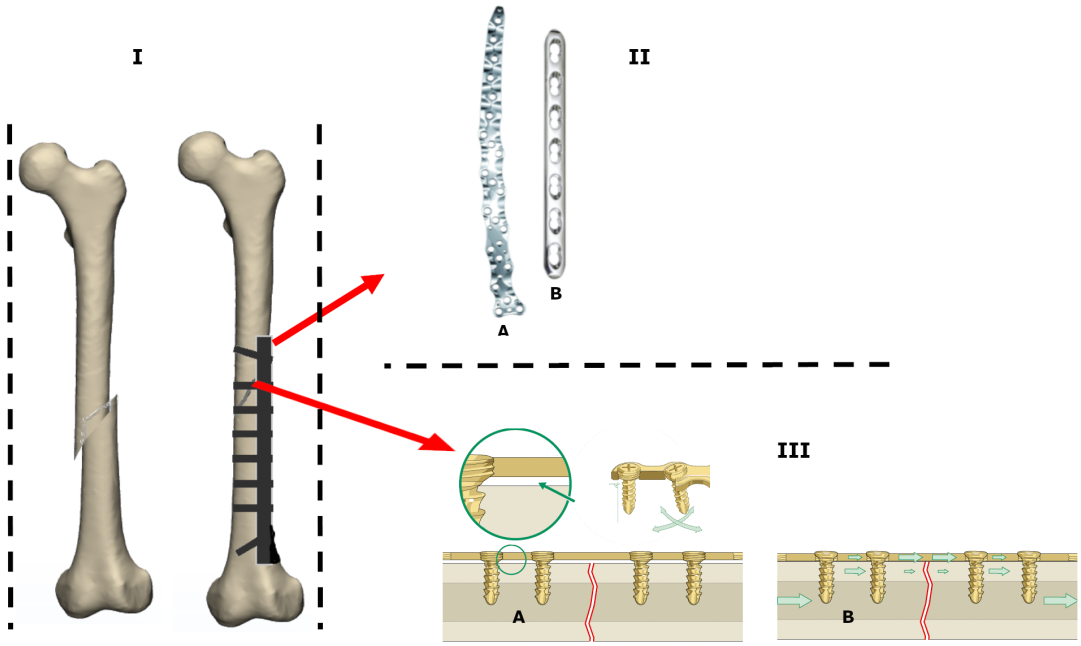

Figure 1.7.1: I) Fracture treatment with a fixation plate. II) Types of fracture fixation plates are commonly used in clinical practice. A) NCB plate, B) LCP plate, III) A) The interference between the LCP plate and the bone surface. B) The nonlocking screws, which permit greater angulation. B)Transmission of the load directly from the bone to the screws, then onto the plate

One of the advantages of the locking plat that attempts to preserve that attempts to preserve the vascularization of the periosteum by reducing the contact with the bone (figure.1.7.1.III.A), dans le but de favoriser la consolidation, the locking plate can be applied as a compression plate [Wagner, 2003](figure.1.7.1.III.A). locking screws provide axial and angular stability indépendante de la qualité

osseuseThus, the loading forces are transmitted directly from the bone to the screws, then onto the locking plate, across the fracture and again through the screws into the bone (figure.1.7.1.III.B). The plate length should overlap the fracture area (at least two femoral diameters at both proximal and distal sides) [Mamczak et al., 2010], [Hou et al., 2011a], [Platzer et al., 2011].

One of the preferred treatment algorithm based on the classification is done by [Pires et al., 2014]. This algorithm (figure.1.7.2) guides treatment on the basis of key factors, such as implant stability and the presence of a stemmed total knee arthroplasty implant.

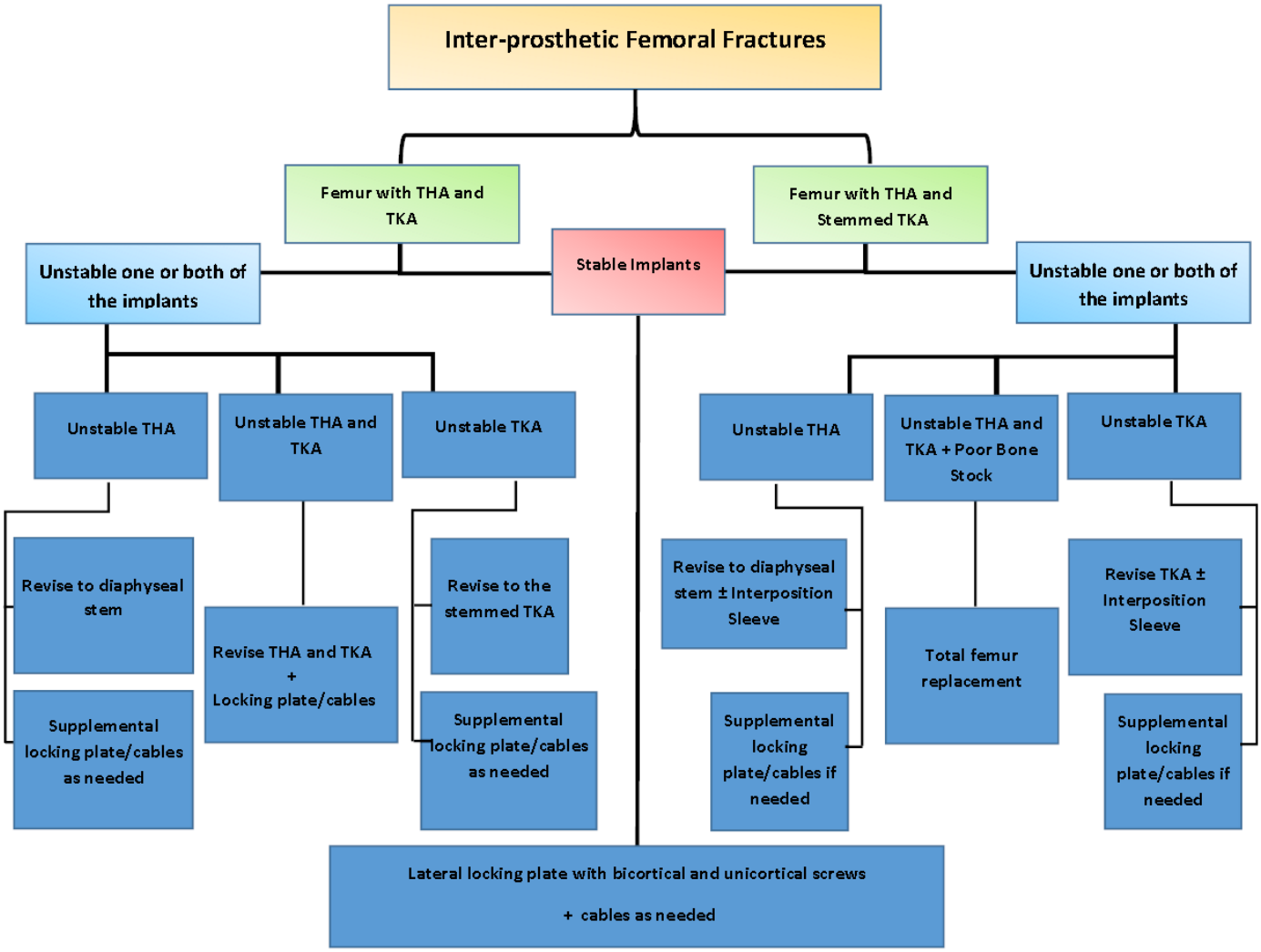

Figure 1.7.2: *[Pires et al., 2014] management strategy for fixation of interprosthetic femur fractures based upon fracture location, implant stability, and bone stock*

Note: The situation that interests us is the inter-prosthetic fractures on non-unsealed (stable) prostheses, which corresponds to the middle case (red frame).

Part II : Finite element analysis and experimental testing review of a femur with a total hip and knee replacement

Abstract:

There are two general approaches for studying bone fractures and healing processes: Computational methods and experimental methods. Each of these methods has benefits and limitations. Patients with both joints replacements in the same leg are at the risk of IP fracture. The hip and knee prosthesis modifies the behavior of the femur and its mechanical strength, which can be studied by analyzing the risk of fracture of a biprosthetic femur. Different solutions can be considered to prevent this type of fracture; one of them is the optimization of the inter-prosthetic (IP) distance. In this part, we introduce a review of the computational and experimental methods in a femur after THA and TKA.

Résumé:

Il existe deux approches générales pour étudier les fractures osseuses et les processus de guérison : Les méthodes de calcul et les méthodes expérimentales. Chacune de ces méthodes présente des avantages et des limites. Les patients ayant subi une arthroplastie des deux articulations dans la même jambe sont exposés au risque de fracture IP. Les prothèses de la hanche et du genou modifient le comportement du fémur et sa résistance mécanique, ce qui peut être étudié en analysant le risque de fracture d'un fémur biprothétique. Différentes solutions peuvent être envisagées pour prévenir ce type de fracture ; l'une d'entre elles est l'optimisation de la distance inter-prothétique (IP). Dans cette partie, nous présentons une revue des THR et TGR.

1.8 Introduction

The implantation of two femur prostheses (hip and knee) strongly modifies the distribution of stresses in the femur. Having access to these stresses and understanding the influence of geometries on their distribution in the bone is important both to analyze the direct mechanical risk of fracture under extreme stress, but also to ensure that the stresses remain within an acceptable range both to ensure natural bone remodeling ($\sigma_{inf} \lesssim \sigma$), and to avoid overload necrosis ($\sigma \lesssim \sigma_{sup}$). The values of σ_{inf} and σ_{sup} are material criteria to be defined according to bone quality (porosity and mineralization) and customized for each individual. They are the subject of numerous works described but this will not be dealt with in this thesis.

On the other hand, the determination of the distribution of stresses σ, in fact associated with $\sigma_{(Position,Load)}$ involves a structural problem. Whether by a numerical or experimental approach, it seems useful to differentiate two levels of analysis (figure.1.8.1):

- 1st study of the load distribution between bone and prostheses.
- 2nd study of the load transfer between the bone and the metal parts by direct contact, via cement or screws.

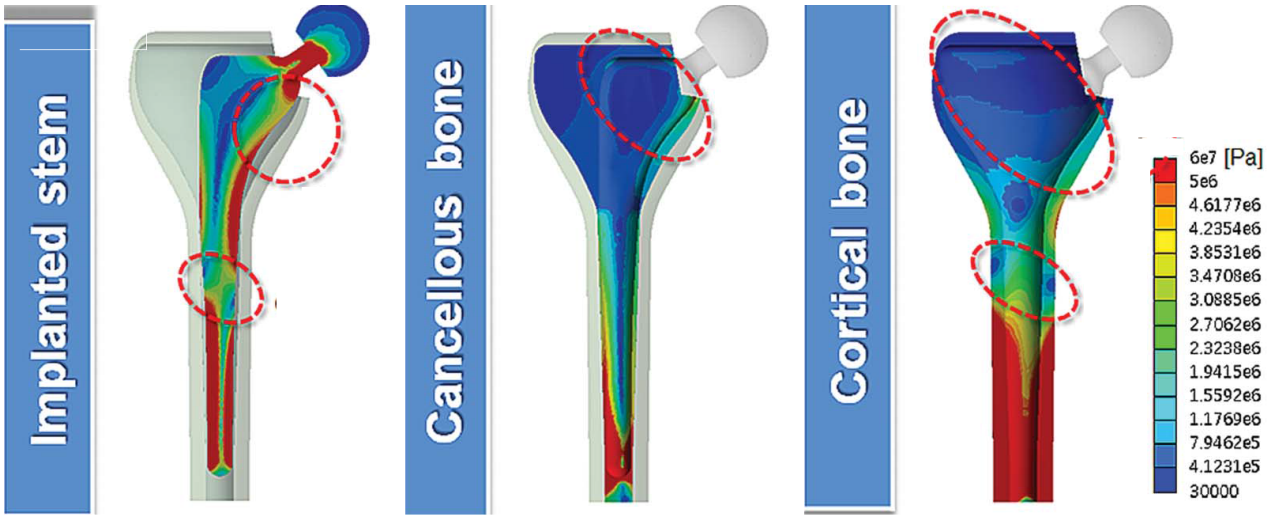

Figure 1.8.1: *[Mu Jung and Sang Kim, 2014] Equivalent stress distribution at the cross-section along the length of the implanted stem, cancellous bone and cortical bone.*

A joint replacement by a metalic prosthesis has an obvious effect on the loading of the implants and the deformation of the bone. As an example the complication of THR using a cementless fixation while, the bone resorpation around the implant results a failure of the bound at the porsthesis-bone interface [Agarwal, 2004]. The loading which transfer to the bone could change if the load

was partially absorbed by the prosthesis, and therefore the stress distributed at the bone–implant interface will decrease and causes a stress shielding loading effect. This could make the bone more porous and thinner as a natural adaptation process corresponding to the decreased carrying load [Mu Jung and Sang Kim, 2014].

The computational modeling of biological systems using the FEA has become an important tool for understanding bone mechanics. It allows simulation of the mechanical behavior of tissues to accomplish experimental investigations or when this mechanical behavior is experimentally unobtainable. Under given boundary conditions, it has been shown that the numerical simulation using the finite element method (FEM) is a useful method to predict the femur fractures. The use of finite element analyses in biomechanics applications was limited in the two-dimensional approaches and linear analyses. Nowadays, the use of it becomes more widespread and more specialized in three-dimensional approaches and nonlinear analyses. Two, and three-dimensional FE models have been shaped up to predict femoral fractures. In the pre-processing stage, the geometrical FE model is required to be generated. This geometry can be acquired from Dual-Energy Xray Absorptiometry (DXA) or computed tomography (CT) scans as a 2D model [Testi et al., 1999], [Op Den Buijs and Dragomir-Daescu, 2011], [Bettamer et al., 2017] or as a 3D model [Lotz et al., 1991], [Mirzaei et al., 2012], [Grassi et al., 2017] . It could be also acquired by using 3D mesh-based Voxel FE models [Keyak, 2001], [Carballido-Gamio et al., 2015], [Luo, 2017] or the stereo-radiography reconstruction technique [Laporte et al., 2003], [Bras et al., 2004]. Following the geometrical stage, the mesh generation stage is carried out then the material properties assignment for each element in the mesh. Finally, depending on the required FE test the loads and boundary conditions are applied to the model (figure.1.8.2). One of the most advantages of using the FEM is once, the geometry of the model developed, it is relatively straightforward to alter the meshing, boundary conditions, and both testing and physiologic loading regimes can be applied. In almost all studies, FE models assumed the femur had linear, isotropic, and elastic properties [Wang et al., 2019]. In addition, FE modeling can also provide a worthy vision for the design, optimization, prediction and treatments. In spite of that benefits, FE modeling methods have their own limitations in clinical applications. Consequently, using FE modeling need to be further improved and validated in order to achieve clinically relevant results [Pivonka and Dunstan, 2012]. This review aims to summarize the present biomechanical studies on the parameters that could increase the fracture risk of the human femur after THA and TKA such as cortex thickness and IP distance.

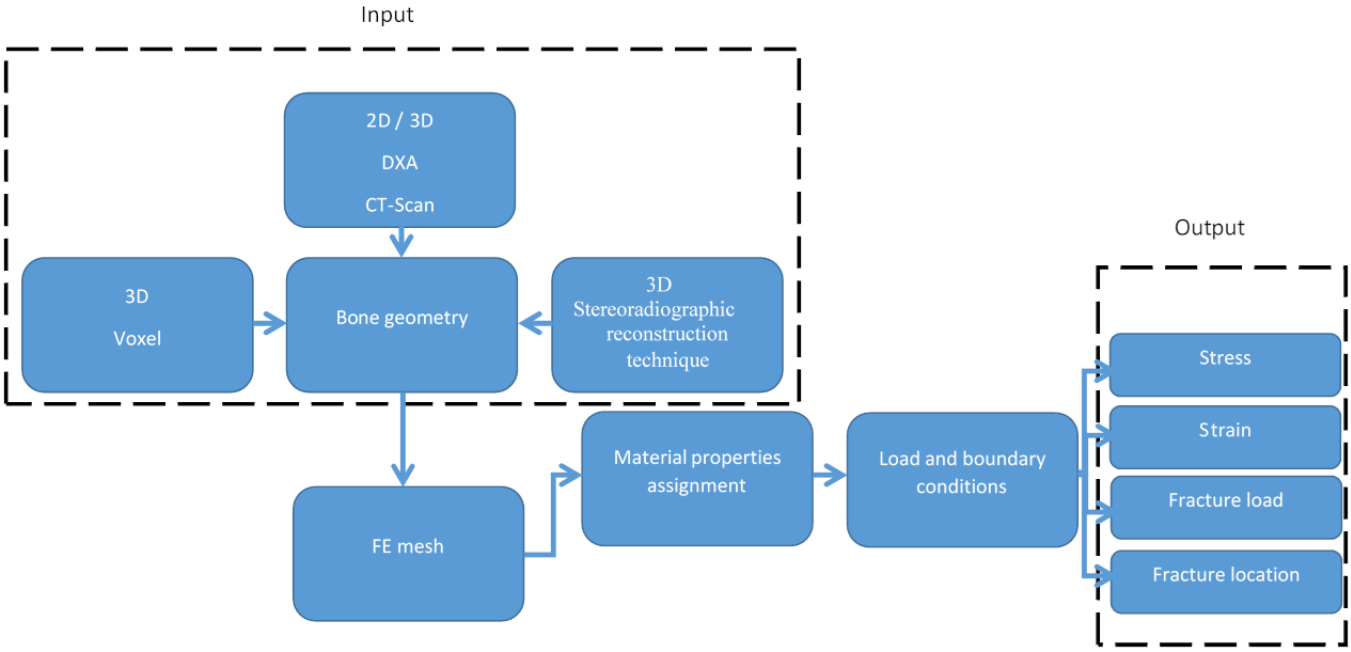

Figure 1.8.2: *A Schematic summary the finite element modelling of bone.*

Interprosthetic (IP) femur fractures are the fractures occurring between a total hip arthroplasty and a total knee arthroplasty (figure.1.8.3). As the rate of total joint replacement increases, these fractures are likely to increase. The incidence of inter-prosthetic fractures in patients with ipsilateral prosthesis placement is 1.25% [Kenny et al., 1998]. Patients with the both joints replacements in the same leg are at the risk of periprosthetic and inter-prosthetic (IP) fractures [Mamczak et al., 2010], [Solarino et al., 2014]. Different factors may lead to the occurrence of this type of fracture; such as the distance between the two prostheses which known as the IP distance [Soenen et al., 2013], stem stability [Iesaka et al., 2005] and cortical thickness area [Valle Cruz et al., 2016].

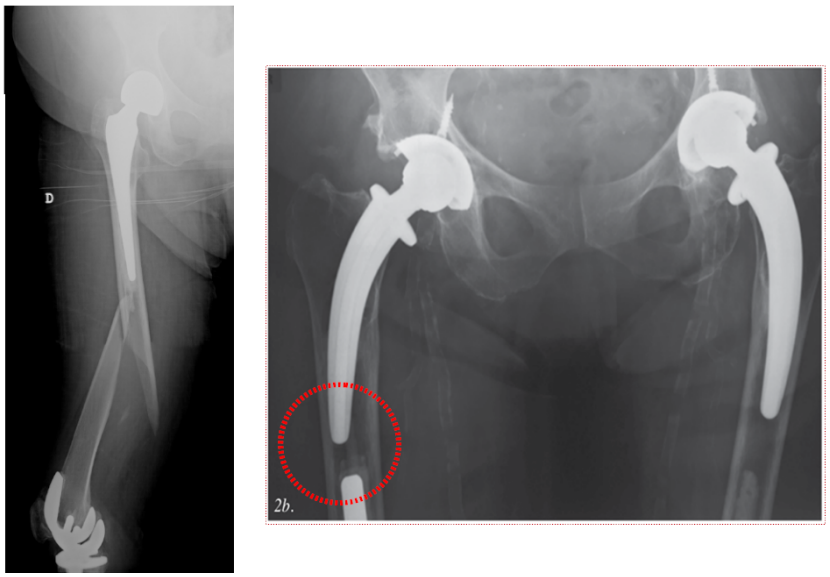

Figure 1.8.3: *Interprosthetic diaphyseal fracture. image source: [Albareda et al., 2017]*

Different numerical and experimental tests such as cantilever test, 4-point bending test, gait cycle test and side falling test have been used to study the risk of fracture of bi-prosthesis femurs. However, the authors do not reach the same conclusions [Iesaka et al., 2005], [Soenen et al., 2013], [Weiser et al., 2014], [Quirynen, 2016]. The aim of this part is to provide an updated review of current research relating to the influence of the IP distance in the risk of fracture in the human femur bone. In The thesis we will purely focus on numerical analysis. However, the bibliographical analysis will focus on numerical studies and on experimental studies, as studies on biprosthetic femurs are limited.

1.9 Finite element simulation of femur bone with THA and TKA

A first study analyse the effect of the presence of two prostheses [Iesaka et al., 2005] on a simplified geometry of the femur by a finite-element analysis. The load applied in this study is a cantilever test. The effects of gap size, stem stability and cortical thickness between two press-fit, ipsilateral intramedullary stems were investigated in terms of the stress results. The femur was represented in a simple geometry as a hollow cylinder with isotropic material properties with a length of 300 mm and the intramedullary stems by two solid cylinders with rounded tips with the same diameter of 14 mm (figure.1.9.1). The contact between the bone and the stem is considered to be a tie contact. A stem with a length of 100 mm was inserted into the femoral cavity from the fixed end, while the other stem, inserted from the loaded end with a varied length depending on the simulated gap (1, 10, 35, or 85 mm). Cortical bone was modeled with a femoral cortex thickness of 3, 5, 7 mm.

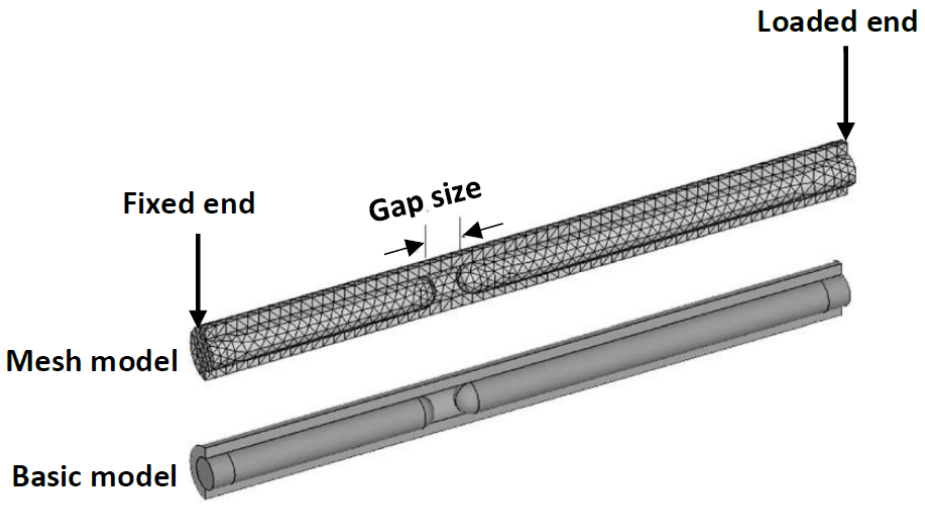

Figure 1.9.1: Finite-element model and the mesh model proposed by [Iesaka et al., 2005]

They concluded that: there was no influence of the size of the IP gap on the maximal tensile stresses; the stress riser effect of an intramedullary metal stem is dependent on stem stability "the stress at the well-fixed stem tip did not exceed the stress of the control model (a femur with no stem inside)", while there were a stress rise effect in case of the loose (unstable) stem; finally the bone cortex thickness had an important effect on tensile stress distribution. There were still some limitation of this study such as the bone cylinder assumed to be cortical bone only, isotropic behavior of the bone modeled, only simple geometry was used while the bone and prosthesis geometry was neglected, the contact conditions were limited while it was assumed a complete bonding condition between the stems and the bone, and only bending moment condition was used in this FE study. A second study was done by [Soenen et al., 2013]. The FE analysis of the femur was represented by a three-dimensional (3D) femur including cortical bone, trabecular bone, and intramedullary canal. The femur model was equiped with a THR and TKR. The length of the hip stem was fixed, while the length of the knee stem was varied to create gaps of (50, 70, 90, 110, 130 and 150 mm). Strain fracture criteria have been used to determine and describe the risk of fracture (RF) [Nalla et al., 2003]. While RF was defined as the ratio between the maximum principal strain in the femur shaft and the corresponding ultimate strain [Bayraktar et al., 2004], [Schileo et al., 2008a]. When RF is larger than 1, this indicates a fracture. While if it is less than 1, this indicates no fracture. This FE model was analyzed during different loading conditions "four-point bending, gait cycle loading and sideways falling test" (figure.1.9.2). During gait cycle and sideways falling no difference in RF among different stem lengths was shown. However, a clear threshold appears during four-point bending.

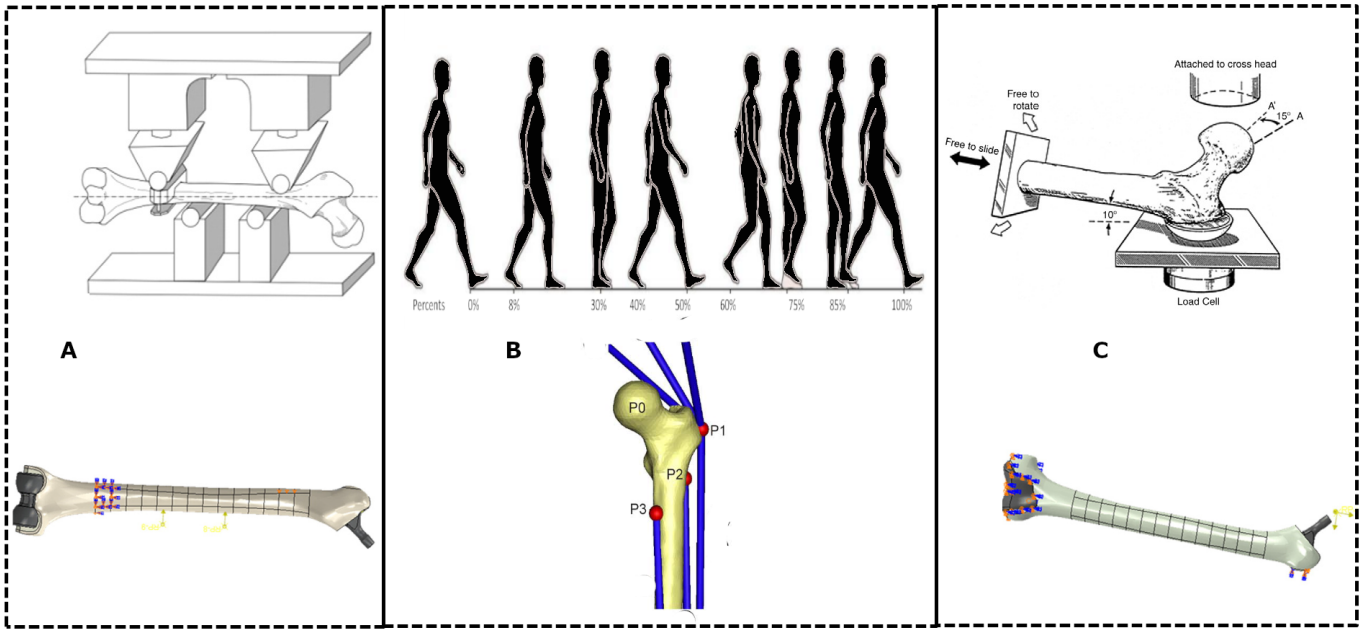

Figure 1.9.2: Finite-element model represent the experimental setup for "A. four-point bending, B. gait cycle loading and C. sideways falling test by [Soenen et al., 2013]

They concluded that: The IP distance has an influence on the risk of a fracture in the 4-point bending test (the less distance between the stems tips the higher fracture risk); Standard walking (gait loading) and sideways falling results did not show an increased risk for fracture, not even in osteoporotic patients while, femur without prosthesis displayed higher strains than a femur with ipsilateral prostheses when subjected to the same loads. The limitations of this study were that the femur length and cortical thickness did not investigate during this study. Homogenous density distribution for the cortical and trabecular bone has been assumed in the study. Finally, for the four points bending test, the analysis of the results shows that the bending moment which has been used for each IP distance is different and thus this discrepancy appeared in the results (this result analysis will be explained in details in the next chapters).

A third study was done by [Quirynen, 2016]. Under a finite element study, the effect of the neck length of a THA, IP distance, and gap location on strains in the femoral cortex were investigated. Three different loading conditions were applied: Mechanical axis loading, walking and stair climbing (figure.1.10.4). A 3D model of a left femur saw-bone obtained by CT-scan was used in this study. The femur image Digital Imaging and Communications in Medicine (DICOM) data were segmented into the cortical bone, trabecular bone and intramedullary. The cortical bone material properties were modeled as transversely isotropic. The trabecular bone material properties were considered to be linear isotropic. The THA was made from Cobalt Chrome and was considered linear isotropic material properties. The TKA was made from titanium with linear isotropic material properties.

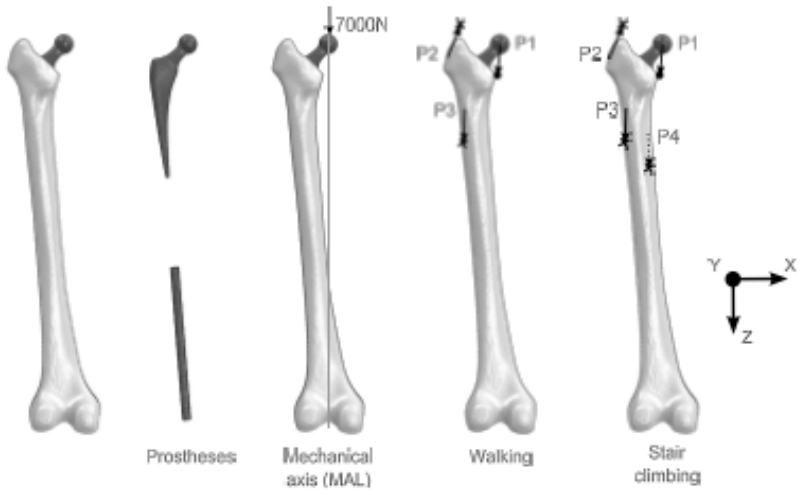

Figure 1.9.3: : Finite element models representing three different loadings; load along the mechanical axis of the femur, walking and stair climbing by [Quirynen, 2016]

The TKA stem was modeled as a cylinder and placed into the femur model to create an IP gap. The prosthesis was modeled to be fully fixed to the bone to simulate the use of bone cement. The stem length of the TKA was varied to create gaps of 15, 30, 50, 100 and 150 mm with a primary

length of the THA 140 mm and 200 mm of THA revision. As a result of his work, he concluded that: The longer neck length of the THA had an obvious effect in the increasing of the femoral strains while a longer neck length created a larger lever arm and consequently increased the resulting moment; Larger gaps resulted in higher femoral strains than smaller gaps; The placement of a TKA did not act as a stress riser while all the models with THA and TKA have a lower femoral strain than the model with THA only.The limitations of this study were that bone remodeling is not taken into account.; The femur length and cortical thickness were not investigated; The intramedullary canal was filled with cement this could affect the bending stiffness and resulting strains between the different IP gap models; Finally, the prostheses were modeled as a fully bonded to the bone which neglects the effect of the stem sliding inside the bone.

1.10 Experimental testing of femur bone with THA and TKA

A first biomechanical study was done by [Iesaka et al., 2005] using a Sawbones femur with the presence of two cobalt-chrome alloy metal stems to investigated the effect of the stem tips to act as a stress riser and the effects of gap size, cortical thickness, and stem stability on femoral stresses. The femur was connected to strain gauges. This study was a validation of an initial theoretical FEA. The study was done under a cantilever-bending test to determine the level of the femoral stresses (figure.1.10.1). The Sawbones femoral shaft used in this test as a hollow cylinder with 250 in length. The femur cylinder shaft was reamed to make a cavity of a 12.6 mm in diameter from both ends for the insertion of rods of the same diameter. One stem was implanted in the femoral shaft with a depth 100 mm from the end of the Sawbones femur and fixed on a vice.

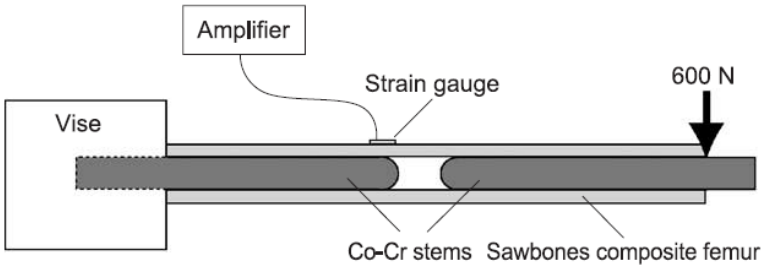

Figure 1.10.1: : A schematic of the cantilever experimental setup used by [Iesaka et al., 2005].

The second stem was inserted at the free end with an ipsilateral stem of varying lengths to create IP gaps of 1, 5, 10, 35, and 85 mm. The structure of the femur including the stem was loaded under a cantilever bending test by application of a 600-N load to the free end using MTS servohydraulic

testing machine. the deformation values in terms of the strains were measured using the strain gauges. They conclude that the IP gap did not act as a stress riser, while the values of the different stem sizes fell within 5% of the control model (Femur without stems). Limitations of the study were that shape the influence of both femur and prosthesis were not taken into consideration, while the used geometry was simple. Also applying the load from one side as the cantilever test is not enough to mimic the real loading in the human femur (I.e. anatomical loading). A second study was done by [Lehmann et al., 2012] to evaluate the risk of stress risers for IP fractures of the femur. A total number of 30 frozen human cadaveric femurs were divided into three groups (figure.1.10.2.A): 1) femurs with a hip prosthesis, 2) femur with a hip prosthesis and a distal femur nail and 3) femur with both a hip prosthesis and knee prosthesis. The construct was loaded under the four-point bending test (figure.1.10.2.B). The osteoporotic bone model was chosen in this study, while patients with osteoporosis have a higher risk of periprosthetic fractures. All the femurs were implanted with a Synergy Cemented Hip Stem. The femur was loaded between the middle two supports with a constant bending moment. They concluded that the highest risk for a fracture in the femur with a hip prosthesis and a distal femur nail. The femurs with a hip prosthesis showed a fracture strength higher than the femurs with a hip prosthesis and distal nail. The femurs with both a hip prosthesis and knee prosthesis showed the highest fracture risk. These results showed that the presence of both hip and knee prostheses in the same femur does not have an influence on the fracture risk, but vise versa it is preferable over the femurs with hip prosthesis only to hip prosthesis with a distal nail. The limitation of this study that they did not envisage the IP gap variation.

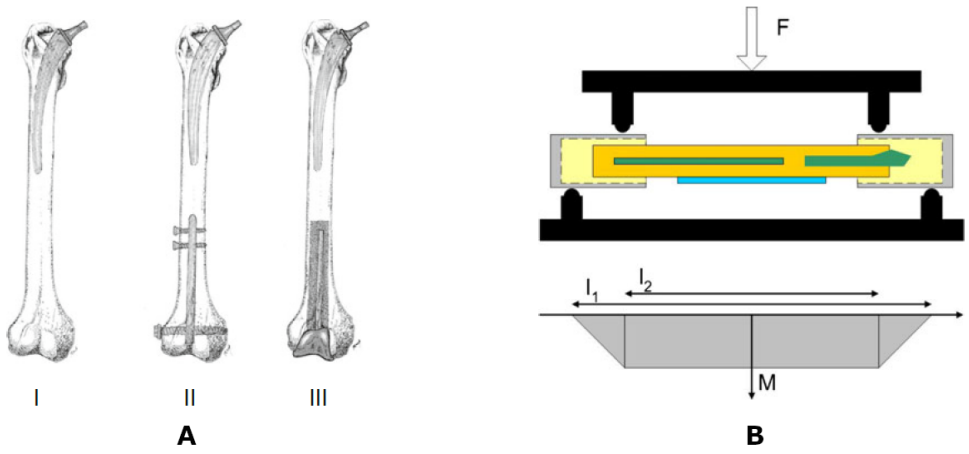

Figure 1.10.2: *A schematic of the four-point bending test setup used by [Lehmann et al., 2012].*

A third study was done by [Weiser et al., 2014] to evaluate the influence of IP distance, cortical thickness and bone mineral density on the IP femoral fractures. A total of 18 frozen human cadaveric femurs were implanted with a hip and a knee prosthesis. Femurs specimens were collected from

donors with expected osteoporotic. the femurs were divided into three groups based on the cortical thickness. Different IP gap size has been used to investigate its influence to 35 mm, 80 mm and 160 mm. A cemented hip prosthesis and knee prosthesis of different stem lengths were used. the femur was embedded in aluminum pots at proximal and distal ends using polyurethane. The four-point bending test applies with a constant moment throughout the total construct by using a servo-hydraulic testing machine (figure.1.10.3). The pots were placed on the outer support and loaded with the constant moment between the two inner supports, thus the bending moment is the same for all the IP gaps. The load was applied with a constant speed of 0.1 mm/s until fracture occurred.

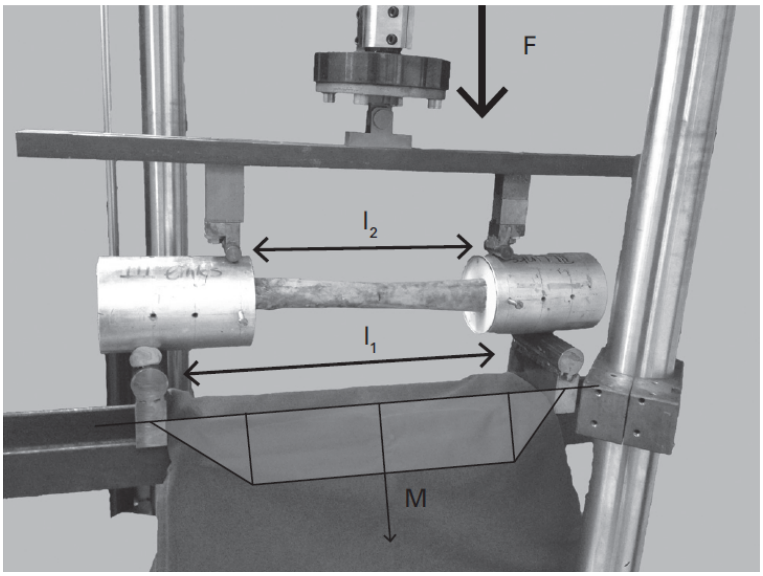

Figure 1.10.3: *A schematic of the four-point bending test setup used by [Weiser et al., 2014]. Femur was loaded with a constant bending moment between the inner supports. L1: distance between the outer supports; L2: distance between the inner supports; F: applied force; M: bending moment.*

They concluded that there is no influence on the IP gap size and mean fracture strength. The section of the femur bone between the two prostheses was the weakest section of the construct, while all the fractures happened in it. The fractures were happened around the tips of the prosthesis, whether the IP distance was short or long. Finally, the cortical thickness clearly shows a significant effect on the fracture risk. The limitation of this study that they only used the four-point bending test with acting force from lateral side to medial side of the femur. The loosening of a prosthesis was not considered. A final study was done by [Quirynen et al., 2016] using a Sawbones femur with the presence of THA and TKA prostheses to evaluate the effect of the inter-prosthetic gap distance on the fracture strength and quantify fracture morphology. Six primary THA stems of 14 cm length and six revision THA stems of 20 cm length were used. The TKA prostheses stem length was varied from 10 to 20 cm. Thus, seven IP gaps created in this study 0, 1.5, 3, 5, 10, 15, 20 cm. The construct was loaded at the hip prosthesis head along the mechanical axis of the femur using a 250 kN mechanical testing machine. The femur was distally fixed with a v-shaper holder to constrain the movement in

the sagittal plane. Thus the resulted load was a combined compression and bending (figure.1.10.4). All specimens were loaded to failure following a compressive loading protocol.

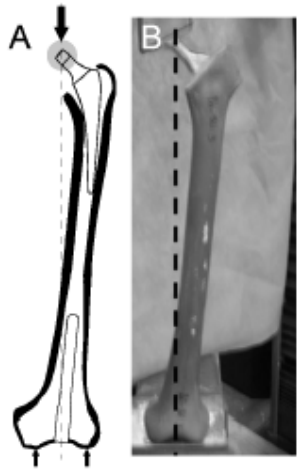

Figure 1.10.4: *A and B schematic and the experimental setup of the test done by [Quirynen et al., 2016] with indicated load axis (the mechanical axis of the femur)*

They concluded that the IP gaps did not have an influence on the fracture risk. in fact, using longer stem length with smaller gaps require higher forces to fracture, thus do not have increased fracture risk. All specimens failed at the level of the IP gap, close to the tip of the hip prosthesis. The limitation of this study that the resultant moment was always higher in the hip side while the distal side was fixed, that could explain that all the fractures happened in the tip of the hip stem. Finally using Sawbones are not representative of osteoporotic bone quality.

1.11 Discussion and conclusion

In this chapter, we highlight the strong influence of the prosthesis on the stress distribution on femur. Thus we focus on the FEA and the biomechanical testing which investigate the risk of the fracture of a human femur after THA and TKA. However, the biomechanical studies are limited but some parameters which can lead to the inner prosthetic femoral fracture risk have already been concluded, such as the effect of the cortical thickness, the stem stability, and the IP gap. Orthopedic surgeons have doubts and fear that the distance between the stem tips may correlate with the femoral fracture risk [Soenen et al., 2013] and the short distance between the tips of two stemmed implants in the same femur may predispose to fracture. Different computational and experimental tests such as cantilever test, four-point bending test, gait cycle test and side falling test have been used to study the effect of the IP gap on the femoral fracture risk. Nevertheless, the authors do not reach the same conclusions (tabel.1.11.1). There is an obvious contrast in the results between the FE study by [Soenen et al., 2013] and the biomechanical test by [Lehmann et al., 2012], [Weiser et al., 2014]

using the four-point bending test. This contrast because of the different place of loading (bending moment zone). The literature review shows that, there is no influence of the IP distance as long as we did not modify the maximum bending moment zone. The aim of the next chapters by using finite element analysis is in chapter 2, analyze the stress distribution between the bone and the prosthesis for quasistatic loading cases and for this we will use a simplified geometry.

Authors	Analysis type	Specimen type and number	loading conditions	Position of the femur	IP gap influence in FR
[Iesaka et al., 2005]	FE analysis. Experimental test.	Simple cylinder geometry.	-Cantilever-bending.	Measuring the stresses on the tensile surface.	-No.
[Soenen et al., 2013]	FE analysis.	Left mechanical-equivalent synthetic bone	-Gait (walking) -Sideway falling -4-Point bending.	. -Applied in three regions in the proximal part of the femur as described in [Heller et al., 2005]. .- - - - - - - - - - - - - - - -Four configurations of the four point bending test (medio-lateral, latero-medial, postero-anterior, antero-posterior) bending. .	-No. -No. -Yes.
[Weiser et al., 2014]	Experimental test.	. -18 human femurs. .	-4-Point bending.	-Medio-lateral bending	-No.
[Lehmann et al., 2012]	Experimental test.	. -30 human femurs. .	-4-Point bending.	-Medio-lateral bending	-No.
[Quirynen, 2016]	FE analysis.	-Simple cylinder geometry. -Left femur Sawbones	-Gait (walking) -Gait (stair climbing) -2-Point bending.	. For both walking and stair climbing, b²oundary conditions and load application points as described in[Heller et al., 2005] -Mechanical axis loading as described in [Talbot et al., 2008]. .	-Yes. -Yes. -Yes.

Table 1.11.1: Overview of relevant literature: Experimental tests and finite element analysis on Inter-prosthetic distance sensitivity of the femur after total hip and knee arthroplasty.

Chapter 2

Influence of prostheses on stress distribution between the bone and the prostheses "A finite element study using a simple geometry"

Abstract:

The numbers of IP fractures continue to rise. A few biomechanical studies were performed to analyze the sensitivity of the IP distance. Nevertheless, there is still a contradiction between the experimental and computational studies. Bending tests are commonly used to evaluate the mechanical behavior of the bones. In particular, the 4-point bending test has been usually used to study the risk of fracture of the femur after THA and TKA. The purpose of this chapter is to evaluate this sensitivity by using different mechanical load conditions.

Résumé:

Le nombre de fractures IP continue d'augmenter. Quelques études biomécaniques ont été réalisées pour analyser la sensibilité de la distance IP. Néanmoins, il y a toujours une contradiction entre les études expérimentales et informatiques. Des tests de flexion sont couramment utilisés pour évaluer le comportement mécanique des os. En particulier, l'essai de flexion en 4 points a été généralement utilisé pour étudier le risque de fracture du fémur après THA et TKA. Le but de ce chapitre est d'évaluercette sensibilité en utilisant différentes conditions de charge mécanique.

2.1 Introduction

In this chapter, we will analyze the distribution of stresses between the bone and the prosthesis for quasistatic loading cases and for this we will use a simplified geometry. We will analyze how this distribution varies by varying the loading cases (4pt bending, 2pt symmetrical and non-symmetrical bending) while keeping the same interprosthetic distance. Then we will modify the length of the knee stem to vary the interprosthetic distance for the same loading case. In this we will focus our attention on the four point bending test results of [Soenen et al., 2013], in order to well understand the discrepancy between his finite element result and the expermintal results of [Iesaka et al., 2005], [Lehmann et al., 2012], [Weiser et al., 2014] . These simulations helped to select the best method in order to make the bending tests for the study of the inter-prosthetic sensitivity. The main objective adopted for this work is to further scrutinize the risk of fracture present in THA and TKA femur bones using the FEM, in order to obtain a qualitative insight into the different factors that arise the fracture risk. This analysis will help us to understand the effects of different IP distances in a bending test. Also, to analyze different strategies in order to impose a controlled mechanical load in a real femur bone geometry.

Four different mechanical-load conditions are proposed:

- Four-point bending test with a constant moment throughout the mid-diaphysis of the femur.
- Four-point bending test with a constant moment throughout the full femur.
- Two-point bending test with a symmetric configuration.
- Two-point bending test with a non-symmetric configuration.

2.2 Materials and methods

A cylindrical shaft recalling the femur diaphysis was modeled with an inner and outer diameter of 20 mm and 25 mm. The total length of the cylinder was set to 340 mm (figure.2.2.1).

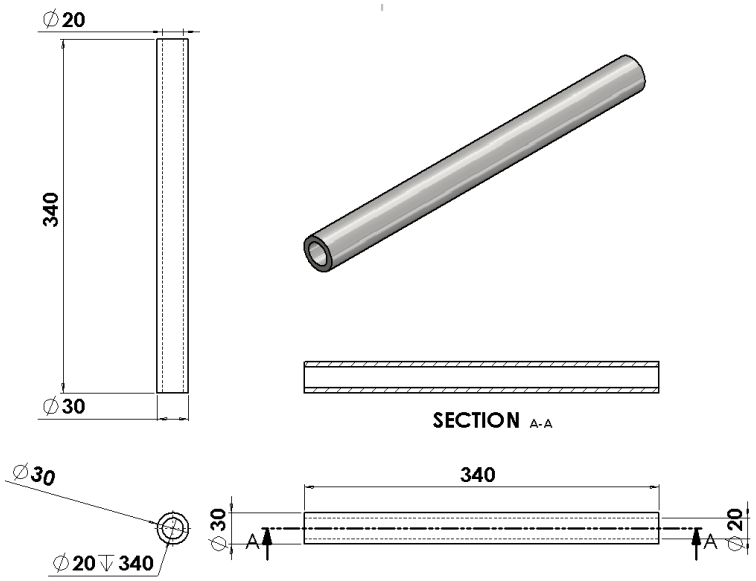

Figure 2.2.1: *Simple geometric model representing the femur bone.*

The hip and the knee stems were modeled as a cylinder of 20 mm in diameter with spherical tips to match geometrically with the inner cylindrical shape of the shaft. The total length of the hip stem was fixed to 160 mm, while for the knee stems, six different lengths were used (70 mm,80 mm,100mm,130 mm and 145 mm) to create different configurations of the inter prosthetic distances (figure.2.2.2). The design of all the components was made in the CAD software SolidWorks® 2016 (Dassault Systèmes©). Then the resulting geometry was meshed. As the geometries were near fully mappable, the selected mesh used primarily hexahedral/wedge elements for all the components. Only the ends of the stems were meshed using a tetrahedral unstructured technique.

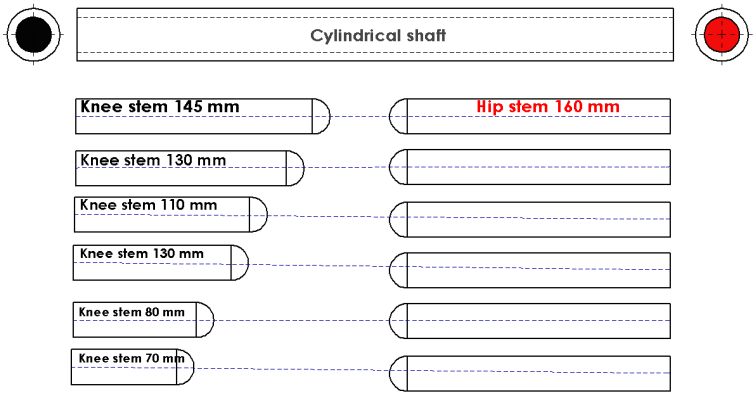

Figure 2.2.2: *A schematic represent the cylindrical bone shaft and the different stems used in the FE simulations. While the hip stem length was fixed and different knee stem lengths used to create the different IP gaps.*

Pre-processing, solving and post-processing tasks were performed in the Abaqus® CAE 6.14-1 (Dassault Systèmes ©) in order to perform the numerical simulations. All the meshed parts were imported using the standard Abaqus input file format. Hence, no geometry was treated in the

Abaqus, but rather the orphan meshes. For the material assignment, two different properties were considered for the bone shaft, for the stems. The mechanical behavior of bone and stems were assumed linear elastic. The bone shaft material properties were considered transversely isotropic: $E_1 = E_2 = 11.5$ GPa, $E_3 = 17$ GPa, $\nu_{12} = 0.51$, $\nu_{23} = \nu_{13} = 0.31$. To assign the material properties orientation, the Z-axis was taken parallel with the longitudinal axis of the cylindrical shaft. The stems material was considered as titanium alloy which is considered linear isotropic material with a mechanical property: $E = 110$ GPa, $\nu = 0.3$. It has been considered that there is no tolerance between the bone inner surface and the prostheses. A coefficient of friction of 0.2 was considered for the contact between the hip stem and the shaft, while it is 0.6 between the Knee stem and the shaft. While if we put in an embedding (no friction properties in a contact property definition) then we will have an overcontracting at the point of contact between the inner cortical bone and the prosthesis which is too strong, so we have to leave a very slight sliding between bone and prosthesis. In addition, the prosthesis is extremely rigid with respect to the bone, so it must not be embedded.

2.3 Loads and Boundary conditions

Four different FE models with different boundary conditions were used to study the sensitivity on the IP distance as following.

- Four-point bending test with a constant moment throughout the mid-diaphysis of the femur.
- Four-point bending test with a constant moment throughout the full femur.
- Two-point bending test with a symmetric configuration.
- Two-point bending test with a non-symmetric configuration.

• 2.3.1 Four-point bending test with a constant moment throughout the mid-diaphysis of the cylindrical shaft

The boundary conditions that were selected were based on the study of [Soenen et al., 2013]. While the four-point bending test applies a constant moment throughout the mid-diaphysis of the cylindrical shaft. The configuration of the test (figure.2.3.1a) consists of 4 cylinders mounted in the loading frame with 113.33 mm apart from each other (figure.2.3.1b).

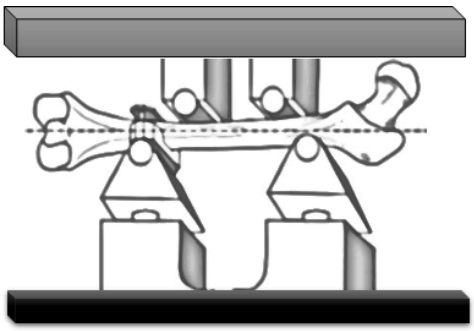

(a) *Set-up used for the four point bending test by ([Soenen et al., 2013]).*

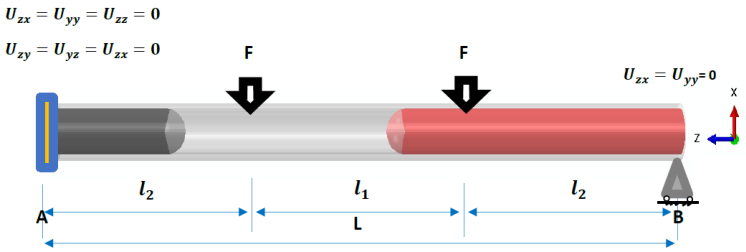

(b) *FE model of the 4 point bending test through out the mid-diaphysis of the femur*

Figure 2.3.1: Four-point bending test with a constant moment through out the mid-diaphysis of the femur

The two outer cylinders are used for holding and aligning of the shaft and the inner cylinders are used as a loading supplier. The shaft from the knee stem side is constrained by the distal cylinder to lock all distal side displacement iso-statically, and lock the rotational around the femur axis. The other side of the shaft is constrained by the other outer cylinder in the load direction. A constant load of 550 N is applied at each of the two internal cylinders.

2.3.2 Four-point bending test with a constant moment through out the total cylindrical shaft

The boundary conditions were selected based on the study of [Weiser et al., 2014]. After implantation of both prostheses, the shaft was embedded in aluminum pots on both ends. In this way of the four-point bending test, a constant moment throughout the total cylindrical shaft. The configuration of the test (figure.2.3.1a) consists of 4 cylinders mounted in the loading frame. A distance of 273.33 mm between the inner cylinders and a distance of 33.33 mm between each of the outer cylinders and the proximity to the inner cylinders (figure.2.3.2b).

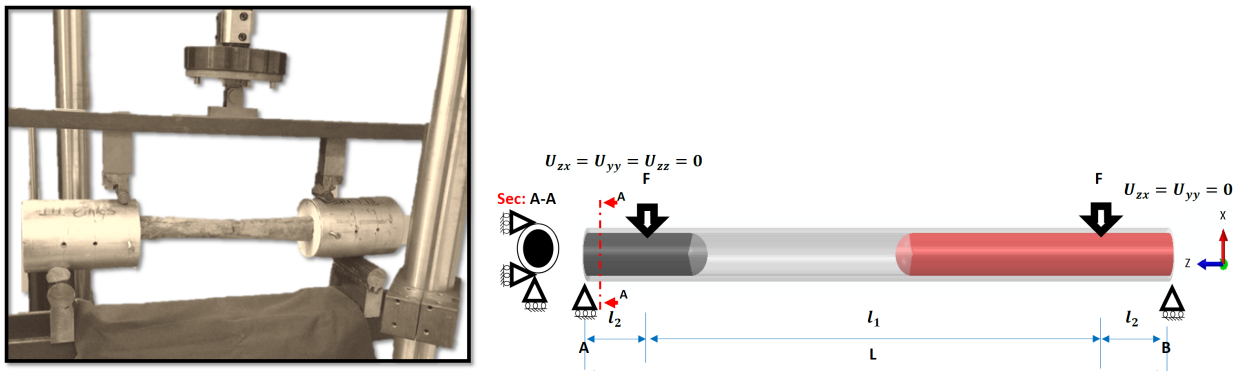

(a) Set-up used for the four-point bending test by([Weiser et al., 2014])

(b) FE model of the 4 point bending with a constant moment through out the total cylindrical shaft

Figure 2.3.2: Four-point bending test with a constant moment with a constant moment through out the total cylindrical shaft

The two outer cylinders are used for holding and aligning of the shaft and the inner cylinders are used as a loading supplier. The shaft from the knee stem side is constrained by the distal cylinder to lock all distal side displacement iso-statically. The other side of the shaft is constrained by the other outer cylinder in the load direction. A constant load of 550 N is applied at each of the two internal cylinders.

• 2.3.3 Two-point bending test with symmetric and non-symmetric configurations

The 4-points tests are not meant to be the only configurations whose aim is to transmit a flexural moment all along a shaft, although their advantages are evident. An alternative configuration of two point bending test has been developed by Dr. Christophe Cluzel to apply a flexural moment with a symmetric, non-symmetric way (figure.2.3.3). In order to implement it in the ABAQUS® software, it was decided to mimic the lids (boxes) with the arms proposed in the configuration description and rather use a structural distributing coupling that would transfer the forces applied at the tip of the arm in a flexural moment.

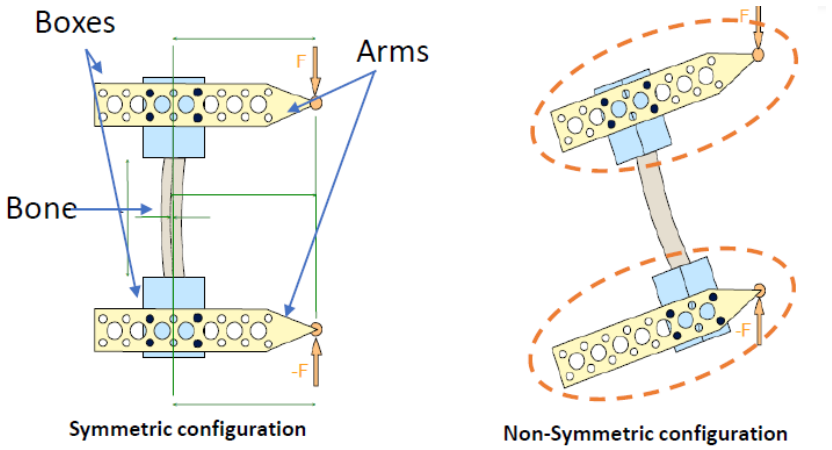

Figure 2.3.3: A schematic represent the diffrent configurations of the two-point bending test "Rigid-Orthogonal-Heels flexion (ROHF) test configuration.

In general, the structural distributing coupling method couples the translation and rotation of a reference node to the translation and rotation motion of the coupling nodes. So, in this method, the transmission of loads is enforced through weight factors at the coupling nodes. Taking advantage of the distributing nature of this coupling, it was decided to couple only the translational degrees of freedom from the reference node to the coupling nodes. Thus, although the reference node is free to rotate (e.g. to roll), the coupling nodes are translated following the equivalent displacement applied at the reference node. Using this approach, it was possible to save the use of more elements in the simulation, and hence, it was kept a low computational cost. A constant load of 550 N is applied at each of the two-moment arms on the symmetric configuration and nonsymmetric configuration (figure.2.3.4).

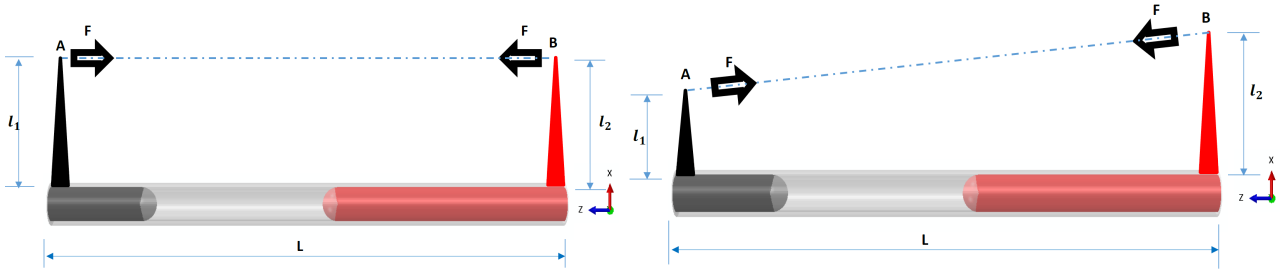

(a) FE model of the 2-points symmetric bending test with the boundary conditions

(b) FE model of the 2-points Non-symmetric bending test with the boundary conditions

Figure 2.3.4: FE model of the 2-points Symmetric (a) and, Non-symmetric (b) bending test with the boundary conditions

2.4 Results

For this analysis, quasi-static conditions were supposed as fact, as no time-dependent properties were configured. The tensile strains along the cylindrical shaft surface have been determined by finite-element analysis. While it has been decided to study the strains only in the tensile side since the ultimate tensile strain is 30% lower than the ultimate compressive strain in the cortical layer of the femur [Bayraktar et al., 2004]. Four different configurations (two for the four-point bending test and two for the two-point bending test) were successfully solved and give different results due to the varying of the boundary conditions.

2.4.1 Four-point bending test with a constant moment through out the mid-diaphysis of the cylindrical shaft:

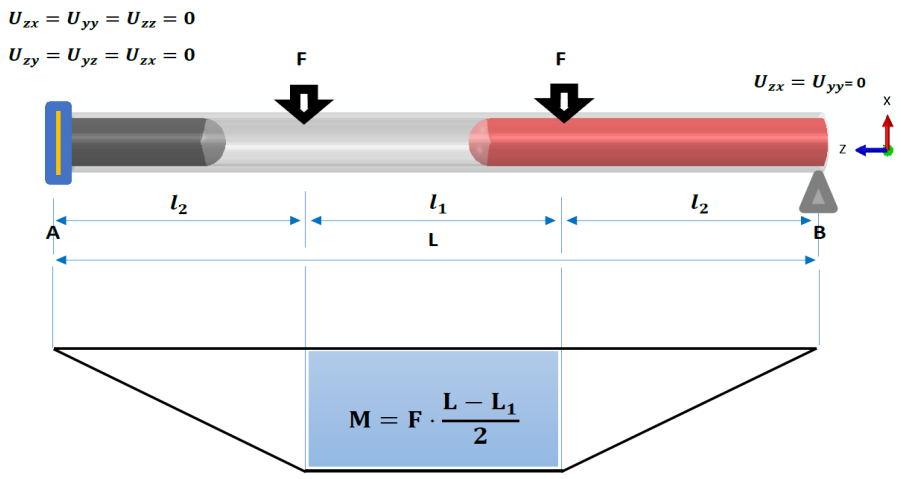

Figure 2.4.1: Moment in the 4-point bending test with a constant moment throughout the middle of the cylindrical shaft, While L: distance between the two outer cylinders and L_1 distance between the two inner cylinders .

In this loading condition, the maximum momentum area always located between the two loading forces which induce a constant moment in the middle of the shaft, whatever was the IP gap (figure.2.4.1). The two loading cylinders are pushing a side of the cylindrical shaft to generate tension at the other side. The maximum principal strains values were located in the IP gaps region. The maximum principal strains for the different models are varies between 0.003 to 0.0037 and depend on the distance between the stem tips (figure.2.4.2).

Figure.2.4.3 shows the maximum-principal strains values at the cross-section along the length of the implanted stems and the cylindrical shaft obtained in all FE analyses. The inner loading cylinders creat a bending moment. However, the loading is the same of all the different gaps between the stem tips but the moment changes due to nature of this assemply of the test and the position

of the loading supports relative to the stem length (figure. 2.4.3), while it is clear the different in the strains ditributions between the models of knee stem length of 70,80,100) mm and the length of (110,130,145) mm.

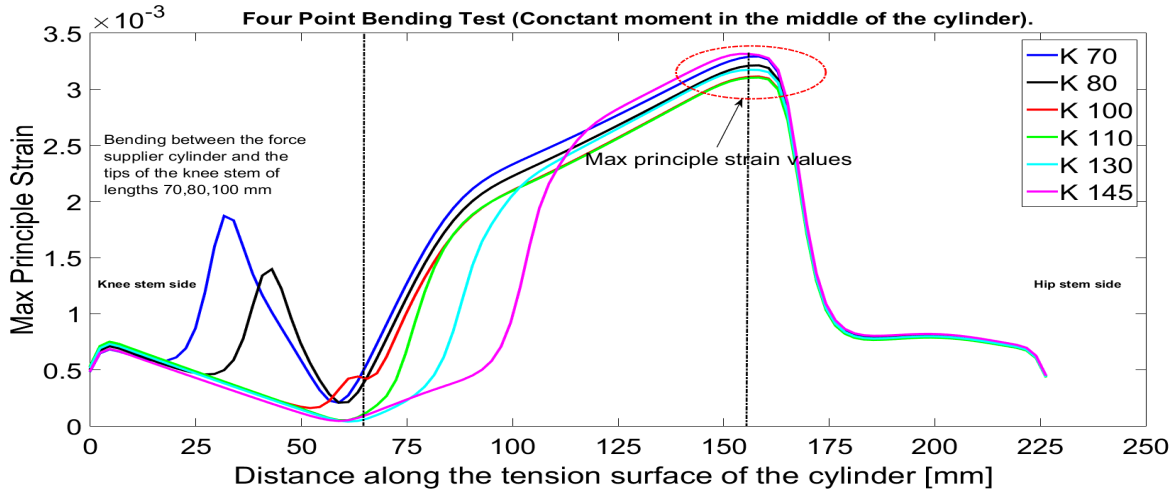

Figure 2.4.2: Influence of gap size on Max principal strains on the tensile side of the shaft

The values of the maximum strain shows a discontinuity at a particular value of the distance between the stem tips, especially in the zone between the loading support and the tip on each knee stem (left marked square in the (figure.2.4.2)). If the distance between the stem tips is lower than 110 mm, the bending moment will be only in zone between the two cylindrical force suppliers. However, if the distance between the two tips is higher than 110 mm, the resultant bending will compose two bending moment zones: one in the zone between the two cylindrical force suppliers and the other in the zone between the knee tip stem and the cylindrical force supplier close to the knee tip prosthesis.

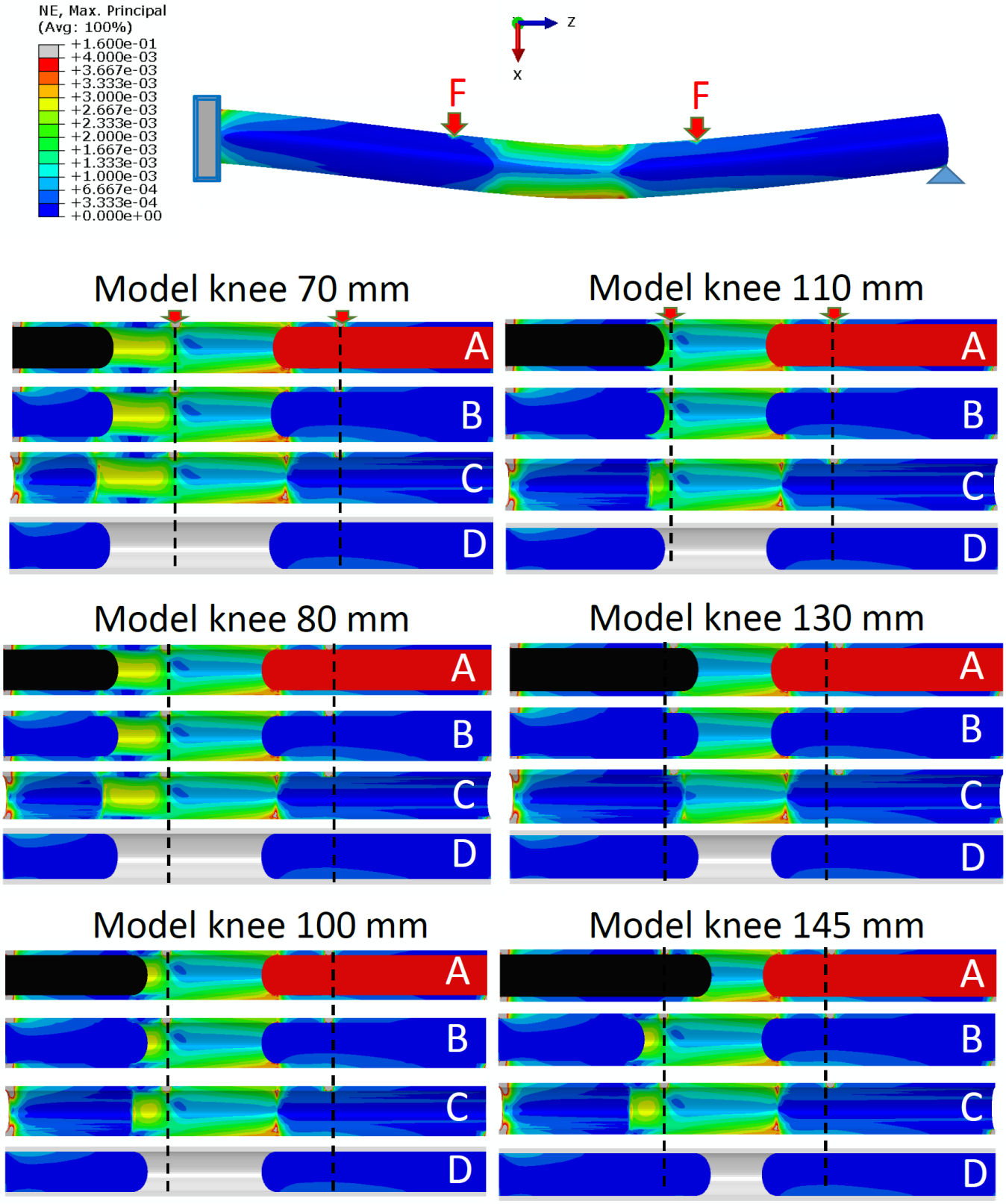

*Figure 2.4.3: A schematic represent the maximum principal strains at the cross-section along the length of the implanted stems and the cylindrical shaft under the four-point bending test with a constant moment throughout the mid-diaphysis of the cylindrical shaft under the four-point bending test with a constant moment throughout the mid-diaphysis of the cylindrical shaft: while **A** represent the deformation of the shaft without showing it in the stems, **B** represent the deformation on both of the cylindrical shaft and the implanted stems, **C** represent the deformation on the cylindrical shaft only and **D** represent the deformation on the implanted stems only.*

2.4.2 Four-point bending test with a constant moment through out the total shaft:

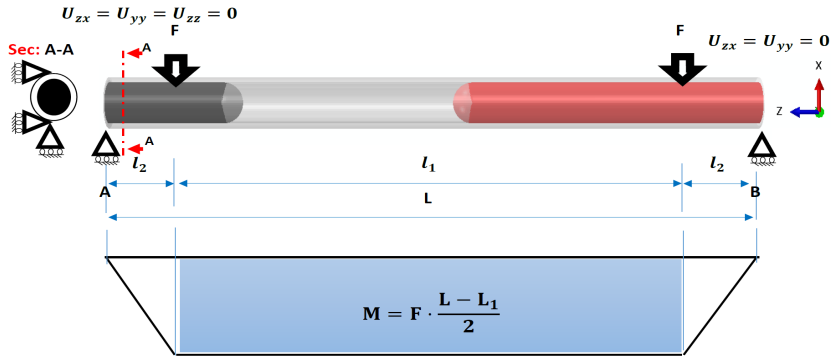

Figure 2.4.4: *Moment in the four-point bending test with a constant moment throughout the etotalcylindrical shaft, While L is the distance between the two outer cylinders and L_1 is the distance between the two inner loading cylinders .*

In this loading condition, the maximum moment area is always located between the two loading forces which induce a fixed moment throughout the total shaft, whatever was the IP gap (figure.2.4.4). The two loading cylinders are pushing a side of the cylindrical shaft to generate tension at the other side. The maximum principal strains values were located in the IP gaps region. The maximum principal strains for the different models are almost identical (figure.2.4.5). Figure.2.4.6 shows the maximum-principal strains at the cross-section along the length of the implanted stems and the cylindrical shaft obtained in all FE analyses. The inner loading cylinders create a bending moment. The loading is the same for the different configurations of the knee stem length and the resultant maximum principal strains are keeping the same value in the gap regions.

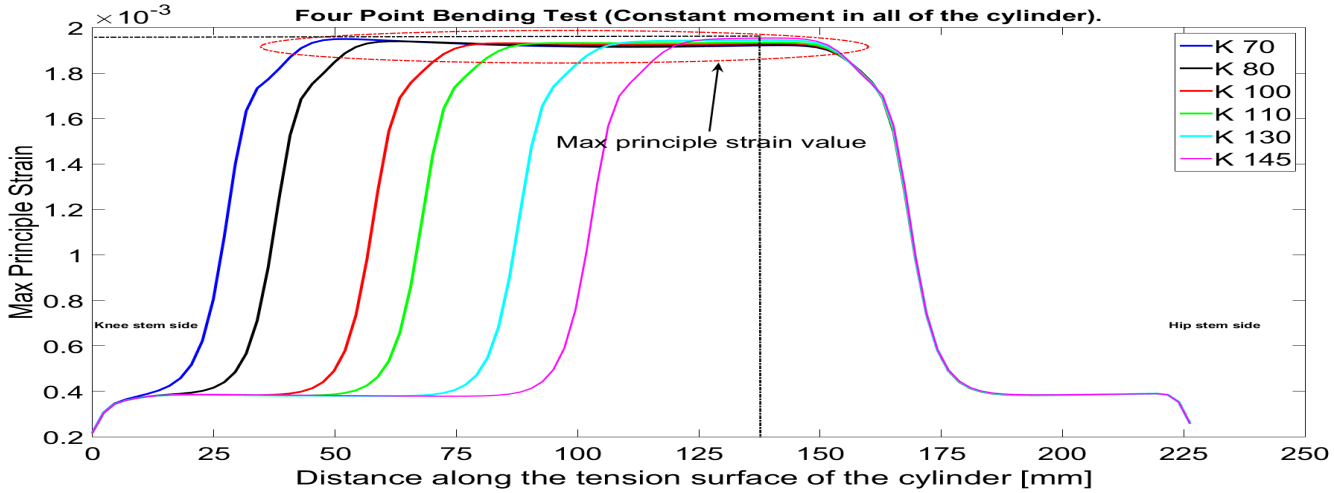

Figure 2.4.5: *Influence of gap size on Max principal strains on the tensile side of the shaft*

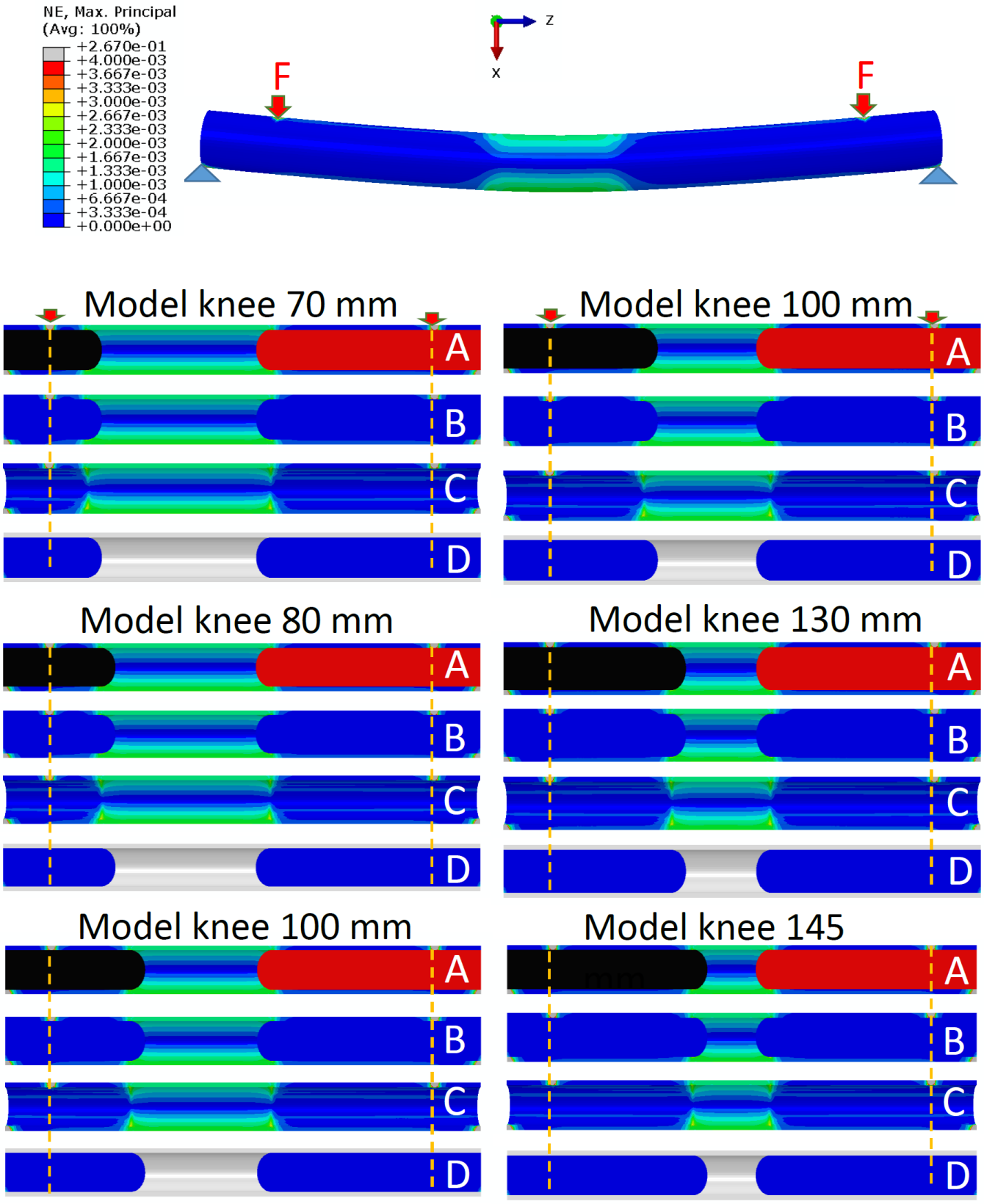

*Figure 2.4.6: A schematic represent the maximum principal strains at the cross-section along the length of the implanted stems and the cylindrical shaft under the four point bending test with a constant moment throughout the total cylindrical shaft: while **A** represent the deformation of the shaft without showing it in the stems, **B** represent the deformation on both of the cylindrical shaft and the implanted stems, **C** represent the deformation on the cylindrical shaft only and **D** represent the deformation on the implanted stems only.*

2.4.3 Two-point bending test with a symmetric configuration:

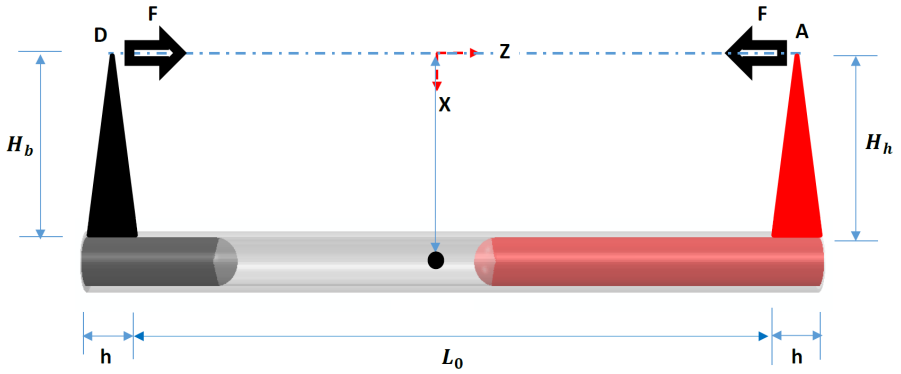

Figure 2.4.7: *Moment in the two-point bending test with a symmetric configuration*

For this configuration, with symmetry of the lengths of the two parallel arms ($H_h = H_b$) (figure.2.4.7), the loading induces a constant bending. The goal was to perform the test using pure compression loading of the total structure ensured by the use of two spherical plain bearings at the load points: A and D (figure.2.4.7). The maximum principal strains values were located in the IP gaps region. The strains patterns for the different models are similar and the maximal strains values located on the lateral surface are almost identical (figure.2.4.8).

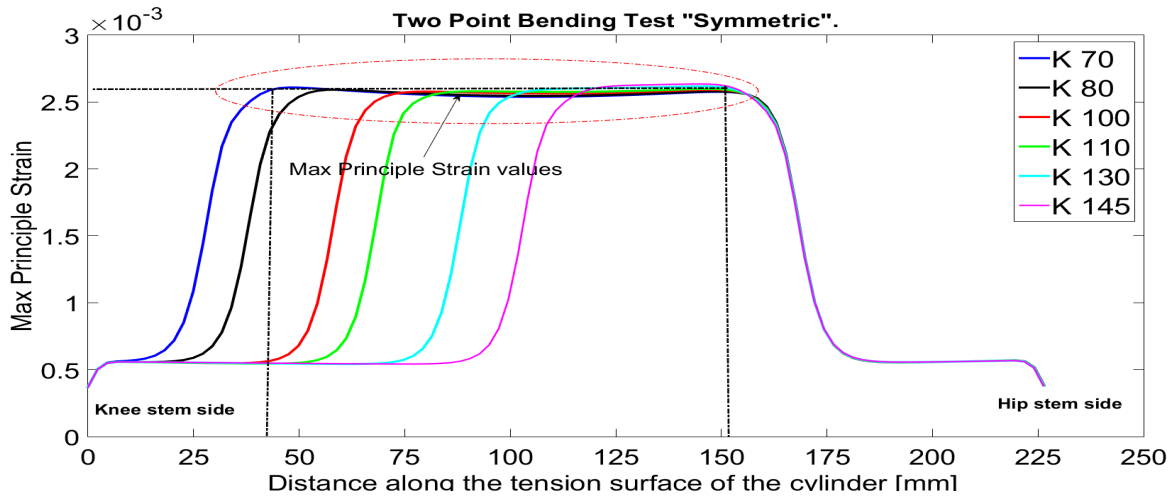

Figure 2.4.8: *Influence of gap size under two-point bending test with a symmetric configuration*

Figure(2.4.9) shows the maximum-principal strains at the cross-section along the length of the implanted stems and the cylindrical shaft obtained in all FE analyses. The two moment arms create a bending moment. The bending moment is the same for the differnt configurations of the knee stem length and the resultant maximum principal strains are almost identical in all the gap regions.

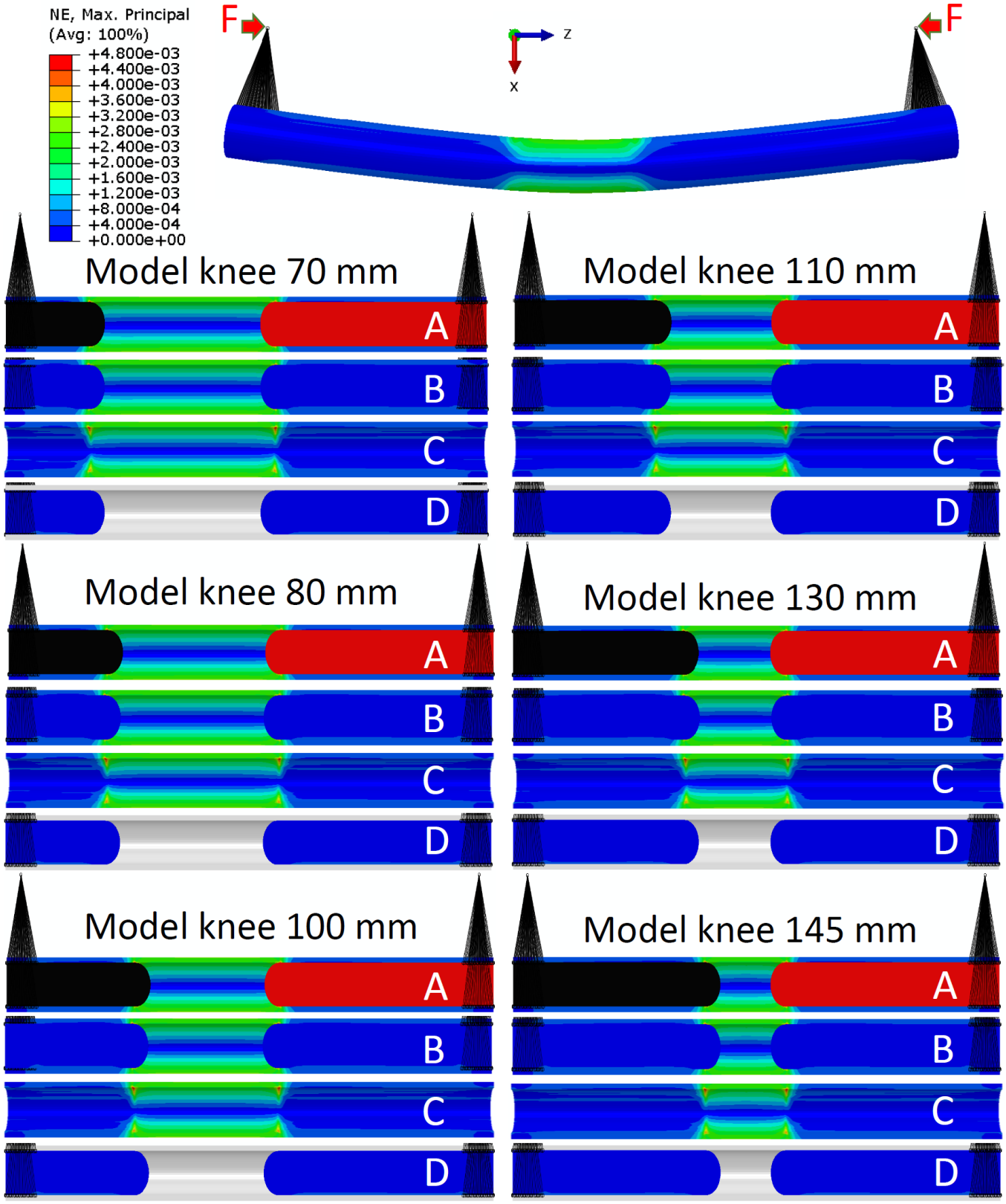

*Figure 2.4.9: A schematic represent the maximum principal strains at the cross-section along the length of the implanted stems and the cylindrical shaft under the two point bending test with a symmetric configuration: while **A** represent the deformation of the shaft without showing it in the stems, **B** represent the deformation on both of the cylindrical shaft and the implanted stems, **C** represent the deformation on the cylindrical shaft only and **D** represent the deformation on the implanted stems only.*

2.4.4 Two-point bending test with a non-symmetic configuration:

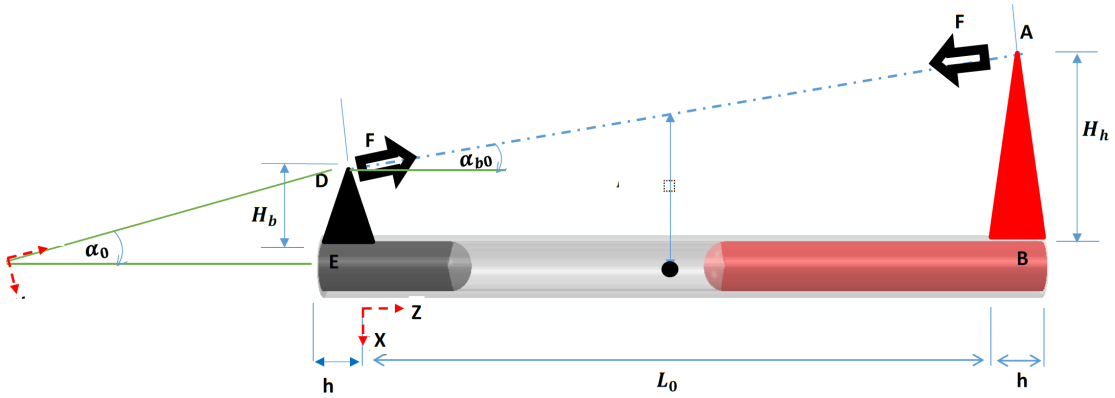

Figure 2.4.10: *Moment in the two-point bending test with a symmetric configuration*

For this test, there is no symmetry in the lengths of the two parallel arms ($H_h \neq H_b$) (figure.2.4.10), while the moment zone can be controlled by the length and the direction of the bending arms. The maximum principal strain pattern was located in the IP gaps region. The goal was to perform the test using pure compression loading of the total structure ensured by the use of two spherical plain bearings at the load points: A and D (figure.2.4.10). The strains patterns for the different models are comparable and the maximal strain values located on the tensile surface are almost identical (figure.2.4.11).

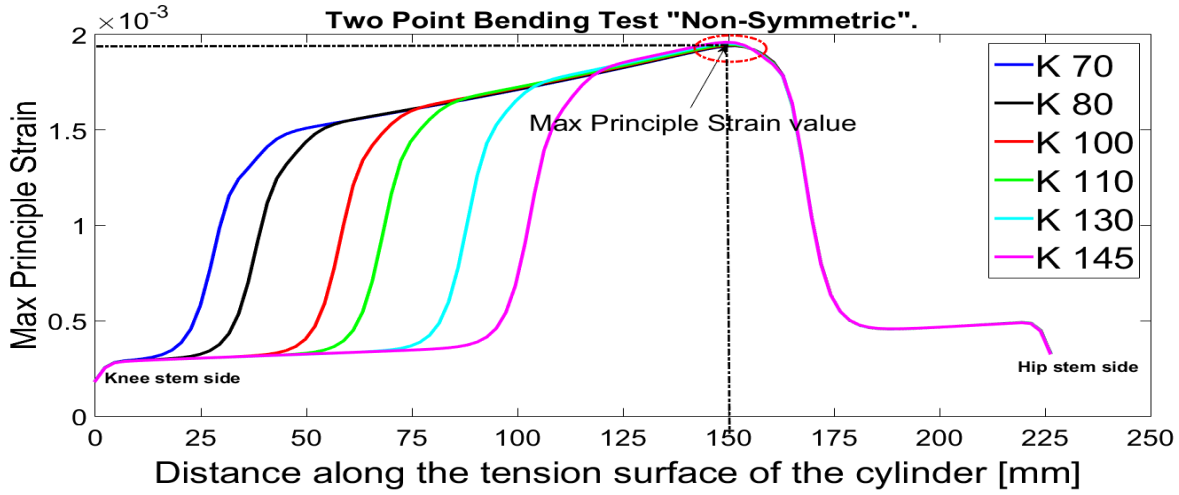

Figure 2.4.11: *Influence of gap size under two-point bending test with a non-symmetric configuration*

Figure(2.4.12) shows the maximum-principal strains at the cross-section along the length of the implanted stems and the cylindrical shaft obtained in all FE analyses. The two moment arms creat a bending moment. The bending moment is the same for the different configurations of the knee stem length and the resultant maximum principal strains are almost identical in all the gap regions.

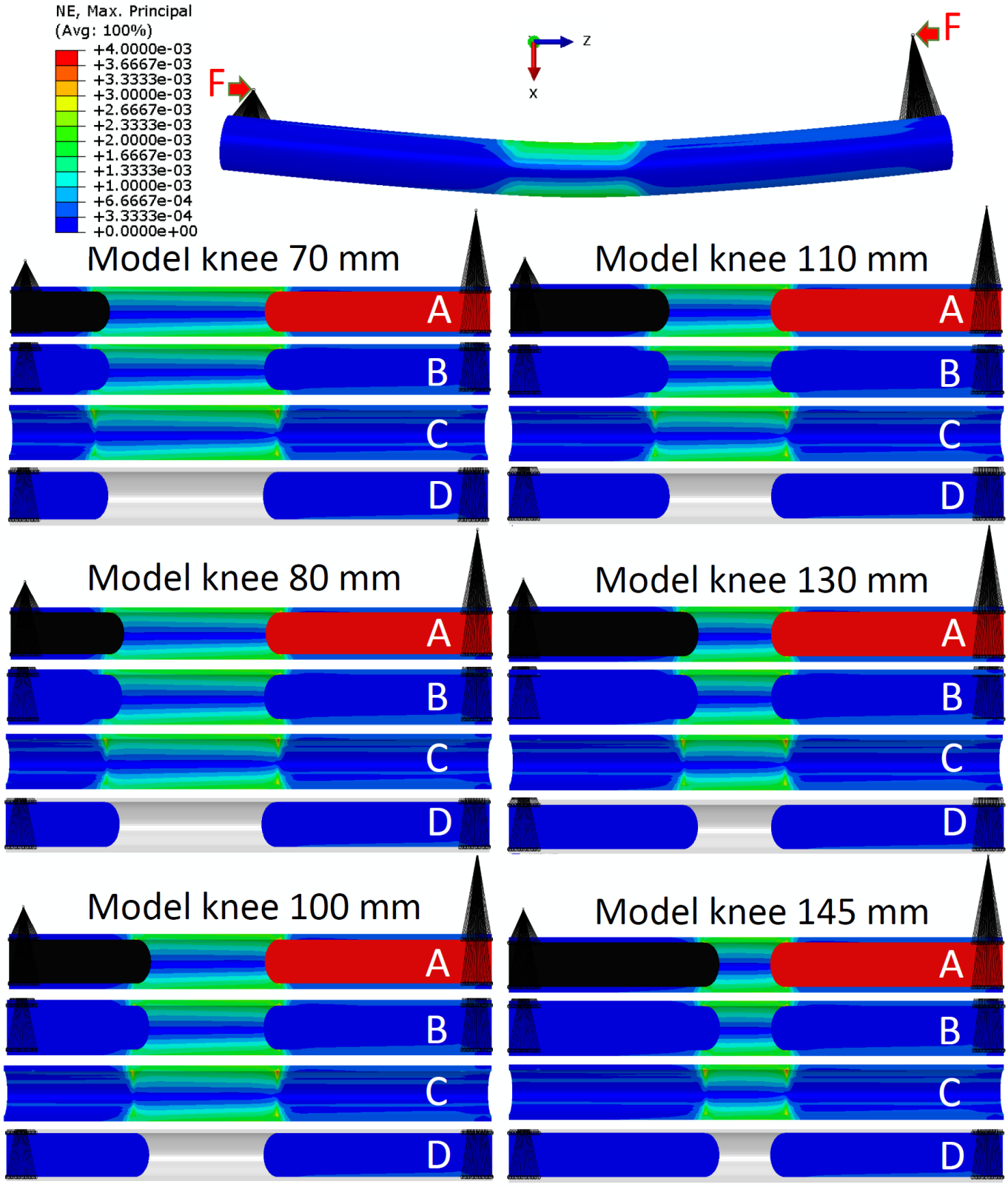

*Figure 2.4.12: A schematic represent the maximum principal strains at the cross-section along the length of the implanted stems and the cylindrical shaft under the two point bending test with a non-symmetric configuration: while **A** represent the deformation of the shaft without showing it in the stems, **B** represent the deformation on both of the cylindrical shaft and the implanted stems, **C** represent the deformation on the cylindrical shaft only and **D** represent the deformation on the implanted stems only.*

2.5 Discussion and conclusion

By using simplified geometry, four simulation tasks were performed in this work, with the aim of getting deeper into the understanding of the factors involved in the risk of fracture (RF) in the human femur bone. The results show the effect of the different stem sizes during several bending tests. Nevertheless, judging these simulation tasks as still too simplistic to draw conclusive results. The distance between the tips of hip and knee prostheses, has been thought to be related with an increased risk of IP fracture. The results of this study showed that the inter-prosthetic distance does not have a significant effect on the risk of developing an IP fracture of the femur. By using a different stem length, the elasticity of the femur changes. Hence the region where the prosthetic stem is present the stiffness was higher, thus bending deformation was lower than in the gap region. The existence of the prosthetic stem leads to lower strain in the prosthetic regions than in the IP gap regions. The fracture is expected to occur in the gap region depending on the load condition. In recent works, such as [Weiser et al., 2014] or [Quirynen et al., 2016], it has already been discussed that the IP distance plays a minor role in the RF. There was statistical evidence that the cortical cross-section area might be the most critical factor that could lead to such increased RF in the human bi-prosthetic femur bones. In a reluctant conclusion of the study done by [Soenen et al., 2013], they show the importance of the gap size in the IP fractures. So, it was necessary to perform the four-point bending test with a constant load in the middle of the simplified femur shaft. Thus, we could study and analyze this variance in the results. In this test using the boundary conditions used by [Soenen et al., 2013], The maximum bending moment were located in the area between the loading cylinders. However, due to the differences in the stem lengths, there is 3 stems length out of the bending zone provided by the loading cylinders. In fact, the advantage of the 4-point bending test is to have a pure and constant bending moment between the two central supports. Unfortunately, in the setup and use of the 4-point bending test which is presented in this article [Soenen et al., 2013], the information on the transition of the fracture risk is just the passage of the stem tip from one side to the other of the distal central support and therefore to a variation of the local load. The position of the over-stress is not exactly at the end of the inner shaft of the prosthesis. The models of stems tip located between the loading support are subjected to over-stress is placed in the central zone of the maximum moment, While the models of stem tips located before the loading support are in zones of less moment. So, there is no an uniformity of the load in the transfer zone by using this way of the 4-point bending test with central supports which are close together. This explains the slight variance in the maximum principal strains in the IP gaps. And therefore, by using the real geometry of the femur bone the variance optioned by [Soenen et al., 2013] could be configured.

Despite the results obtained in this chapter, it must be kept in mind that all of these simulations works were only of a qualitative nature: no real bone geometries were used.

Chapter 3

Finite element analysis on a human femur geometry to investigate the risk of the fracture after the THA and the TKA

Abstract: The femur geometry is non-homogenous, the thickness of the cortical bone is not constant along the femur diaphysis, while the thickness of the cortical wall is changing through the femur shaft. In order to integrate the femur's geometrical variabilities, we will analyze the effect of a real geometry on the stress distribution for quasi-static loading cases. The main goal is to understand how the stress distribution varies by varying the loading cases (4-point bending tes, 2-point symmetrical bending test and 2-pint non-symmetrical bending test) while keeping the same interprosthetic distance. Then we will modify the length of the knee stem to vary the interprosthetic distance for the same loading case. In order to perform these calculations, we created an anatomically relevant FEM to evaluate the risk of fracture of a femur with total hip arthroplasty and total knee arthroplasty based on different numerical simulations. The loading conditions were applied mimicking load of four-point bending test throughout all the femur shaft, 2-point bending test and the gqit cycle test. For the effect of the thickness of the cortical wall, three a different thicknesses of the cortical wall have been used.

Résumé: La géométrie du fémur n'est pas homogène, l'épaisseur de l'os cortical n'est pas constante le long de la diaphyse, tandis que l'épaisseur de la paroi corticale change à travers la tige du fémur. Afin d'intégrer ses variabilités géométriques, nous allons analyser l'effet d'une géométrie réelle sur la distribution des contraintes pour des cas de chargement quasi-statique. L'objectif principal est de comprendre comment la distribution des contraintes varie en faisant varier les cas de chargement (flexion 4pt, flexion 2pt symétrique et non symétrique) tout en gardant la même distance interprothétique. Ensuite, nous modifierons la longueur de la tige du genou pour faire varier la distance interprothétique pour le même cas de charge. Afin d'effectuer ces calculs, nous avons créé une FEM anatomiquement pertinente pour évaluer le risque de fracture d'un fémur avec une arthroplastie totale de la hanche et une arthroplastie totale du genou sur la base de différentes simulations numériques. Les conditions de chargement ont été appliquées en imitant la charge de l'essai de flexion à quatre points sur toute la tige du fémur, l'essai de flexion à deux points et l'essai de cycle gqit. Pour l'effet de l'épaisseur de la paroi corticale, trois épaisseurs différentes de la paroi corticale ont été utilisées.

3.1 Introduction

In order to create a successful FEM, there are many important variables that should be first adapted, such as implant design geometry, bone geometry, cement geometry, material properties, direction and magnitude of applied loads, and bone-implant relative position that can affect performance [Browne et al., 1999],[Nicolella et al., 2001],[Bah and Browne, 2003],[Easley et al., 2007],[Speirs et al., 2007]. The femur geometry and the prosthesis geommetry have been obtained by converting the Digital Imaging and Communications in Medicine (DICOM) to a 3D model. The goal to achieve in this chapter is to create an accurate geometrical model of a real human femur bone. This geometry will be used for evaluating the mechanical response and the fracture risk of a femur with a total hip arthroplasty (THA) and total knee arthroplasty (TKA) under a different finite element analysis (FEA) of the four-points bending test, two-points bending test and the gait cycle test. We will evaluate in terms of strains the effect of IP gaps, and the cortical thickness on the fracture risk. After that we will analyze the distribution of the maximum principal strains between the bone and the prosthesis for quasi-static loading cases. We will calculate the fracture risk under each test using different IP distances between the two prostheses. Thus the results obtained will guide us to identify the zones which have the highest fracture risk and therefore these could help in the decision making of a preventive plate.

3.2 Materials and methods

A geometrical data of real human left femur bone in the form of DICOM files using GE Ultrafast High-Resolution Multi-slice CT Scanner has been obtained from the Hopitaux Universitaires de Strasbourg (HUS). This DICOM data have been converted to a three dimensional FE models using a 3D Image Segmentation, Processing and Meshing Software (Synopsys Simpleware Software) (figure.3.2.1).

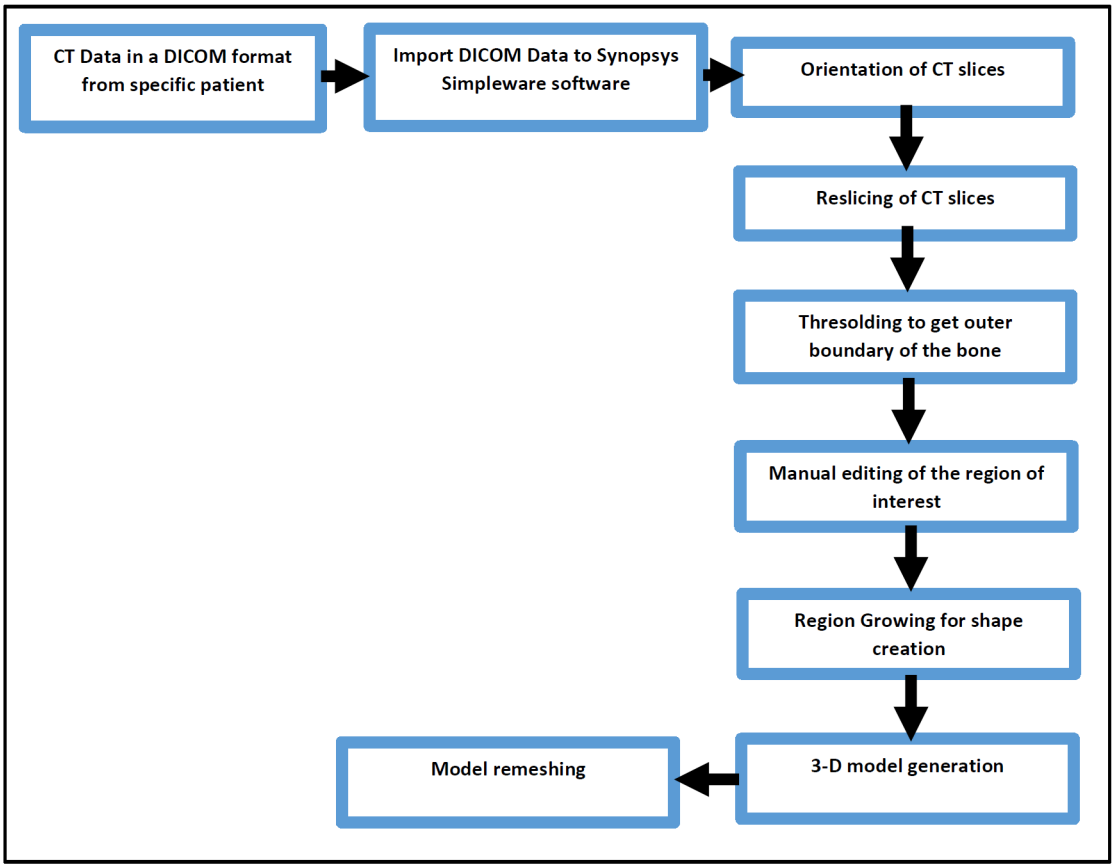

Figure 3.2.1: The steps involved for processing the CT-data from a specific patient of a femur bone.

The Hounsfield Units (HU), which are used to express the density of any tissue in a CT scan, are used to define the type of tissue. The bone which has a HU between 148 and 661 is for trabecular bone. Cortical bone has a HU between 662 to 1893 and the hip prosthesis has a HU between 800 ro 1893. Based on Hounsfield units the image data were segmented into different bone layers and the intramedullary canal (figure.3.2.2). The segmentation is a method that helps one to extract the bony structures from a CT image. A semi-automatic segmentation method using (Synopsys Simpleware Software®) has been used to obtain the femur and the hip prosthesis geometry. In order to obtain a good segementation the region of interest (the femur bone) was manually selected.

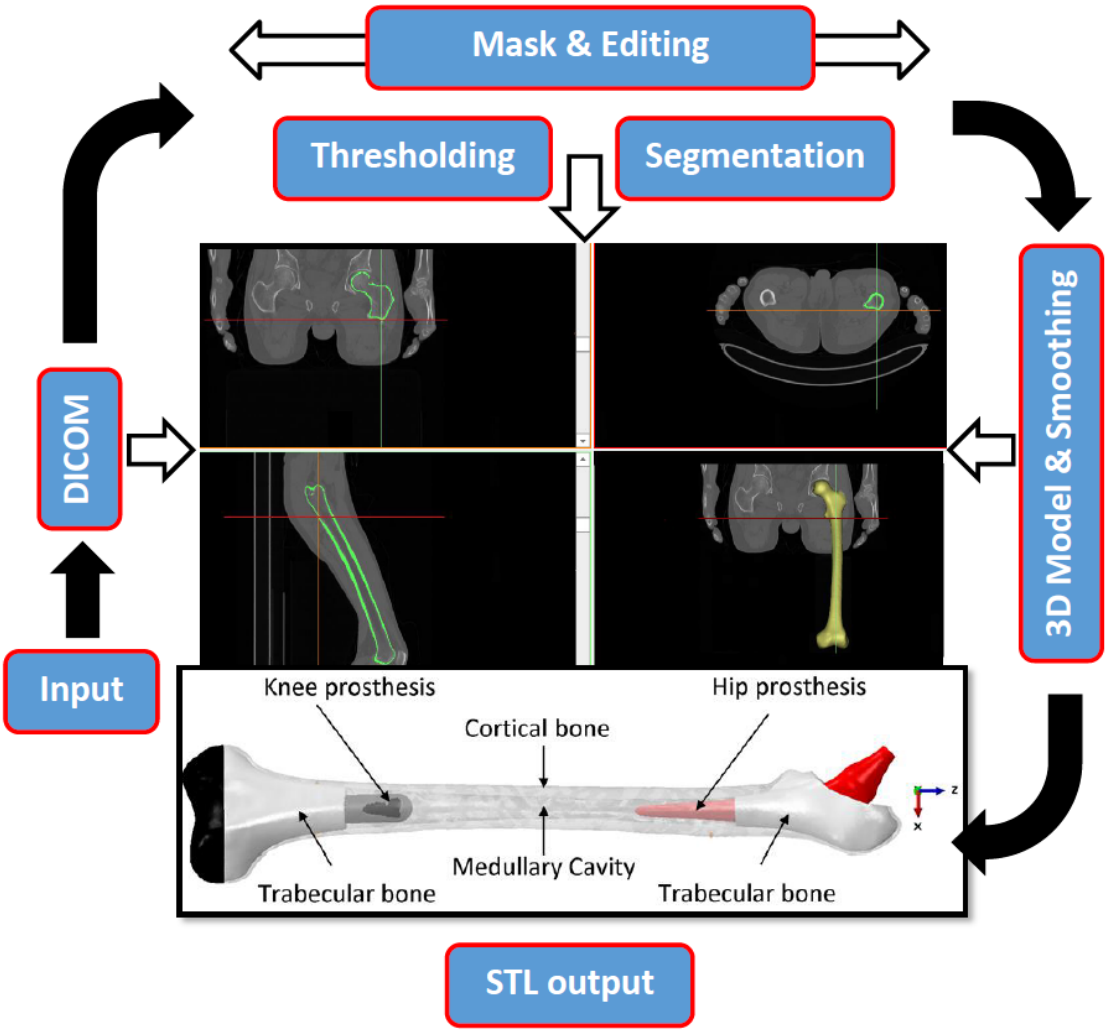

Figure 3.2.2: Converting of the DICOM data to 3d-model of the femur (Cortical bone, Trabecular bone and prostheses)

The data used in analysis belongs to a 56-year-old male with 61 kilograms with a total femur length of 440 mm. Charnley low-frictional total hip replacement was used with a stem length of 145 mm. The hip prosthesis placed and verified by the orthopedic surgeon such as the center of the prosthesis head was matched to the center of the healthy femoral head. The knee prosthesis was modelled as a cylinder with spherical tip attached to a part from the knee condyle (Femoral component). The knee prosthesis cylinder (stem) placed in to the femur diaphysis to create the different IP gaps depending on the cylinder length. Six different stem lengths and diameters were modeled (table.3.2.1): three commercially lengths in the market (120, 160 and 220 mm), and three intermediate, not commercially available, stem lengths (140, 180 and 200 mm) [Soenen et al., 2013]]. The size of the inter-prosthetic gap was defined by the distance between the distal tip of the hip stem and the proximal tip of the knee stem.

THA Stem length [mm]	TKA stem length [mm]	TKA stem diameters [mm]	Interprosthetic distance [mm]
145	120	22	130
145	140	22	110
145	160	20	90
145	180	18	70
145	200	16	50
145	220	15	30

Table 3.2.1: Different models geometry used in the FE studies.

All the models were meshed uniformly using the (Synopsys Simpleware Software®). To obtain a good meshing, the sofware uses proprietary algorithms to generate multi-part meshes to guarantees conforming interfaces and shared nodes between an implant and bone and between the different bone layers. All the multiple triangles after meshing have been modified and processed using the manual mesh editing, smoothening and filtering. A quadratic tetrahedral element, type C3D10 with an approximate element size of 1.2 mm has been used for all the models. For the stress-strain calculations the quadratic tetrahedron behaves significantly better than the four-node (linear) tetrahedron . Subsequently the volume mesh created and finally the mesh has been splitter into remeshed parts using the splitting tool of the volume mesh in (Synopsys Simpleware Software®) . All the meshed parts were then imported to Abaqus® CAE 6.14-1 (Dassault Systèmes ©).

The material properties were assigned to all elements. The bone material properties were simulated as a left mechanical-equivalent synthetic femur bone [Kayabasi et al., 2007], [Soenen et al., 2013].

The cortical bone materials properties were considered transversely isotropic: $E_1 = E_2 = 11.5$ GPa, $E_3 = 17$ GPa, $\nu_{12} = 0.51$, $\nu_{23} = \nu_{13} = 0.31$. To assign the material properties orientation, the Z axis was taken parallel with the anatomical axis of the femur. The trabecular bone materials behavior is considered linear isotropic with the following mechanical properties: $E = 2.13$ GPa, $\nu = 0.3$. The hip prosthesis is made from Cobalt Chrome alloy which is considered to be linear isotropic material with the following mechanical properties: $E = 220$ GPa, $\nu = 0.3$. The Knee prosthesis is made from Titanium alloy which is considered as a linear isotropic material with the following mechanical properties: $E = 110$ GPa, $\nu = 0.3$. No cement layer has been added while it has been considered that the prosthesis fully bonded (tie contact) to the bone surface. There is no any tolerance between the bone surface and the prosthesis. A coefficient of friction of 0.2 was considered for the contact between the hip prosthesis and the bone, while it is 0.6 between the Knee prosthesis and the bone [Soenen et al., 2013]. The Finite element analysis was performed using (Abaqus 6.13, Dassault Systèmes Corp., Providence, RI, USA).

3.3 Boundary Conditions

- Three different FE models were used to study the strain distribution

  - Four-point bending test with a constant moment throughout the femur diaphysis:
  - Two-point bending test
  - Gait cycle test.

- One FE model used to study the effect of the cortical thickness using the four-point bending test.

- One FE model used to study the effect of the bone quality considering both physiological and osteoporotic material properties using the four-point bending test.

- ### 3.3.1 Four-point bending test with a constant moment throughout the femur diaphysis

The boundary conditions were based on the study of [Weiser et al., 2014]. After implantation of both prostheses, the femur was embedded in aluminum pots at the proximal and distal ends.

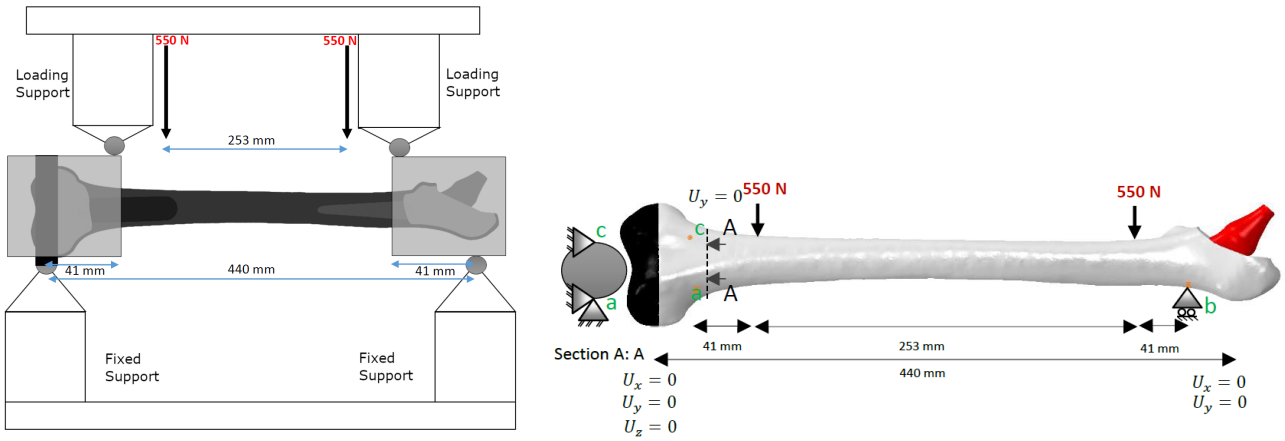

(a) Set-up used for the four point bending test *(b) FE model of the 4 point bending test with the boundary conditions*

Figure 3.3.1: Boundary conditions of the four-point bending test with a constant moment throughout the femur diaphysis

The four point bendint test is used to measure the strength and the bending stiffness of slender structures such as the femur bone[Cristofolini et al., 1996],[McNamara et al., 1994],[Soenen et al., 2013]. From the clinical point of view, the four point bending test may simulate a loading condition that occurs during falling on top of an object[Soenen et al., 2013]. From the mechanical point of view, the test is used to investigate the fracture resistance while, the loading can induce a fracture on the center of the bone shaft .The experimental setup (figure.3.3.1a) consists of 4 cylinders mounted in the loading frame, 253 mm is the distance between the inner cylinders and 440 mm is the distance between the outer cylinders. The two outer cylinders are used for holding and aligning the femur and the inner cylinders are used as a loading supports. The distal side of the femur was constrained by the distal cylinder to lock all distal side displacement iso-statically, and lock the rotational around the femur axis. The proximal side of the femur was constrained by the proximal cylinder in the load direction (figure.3.3.1b). A constant load of 550 N is applied at each of the two internal cylinders, while this loading is not enough to break the femur for all the different distances . The load is applied pushing from the medial femoral side to generate tension at the lateral side (figure.3.3.1).

• 3.3.2 Two-point bending test

As described in chapter two, this alternative test of the two point bending test which is developed by Dr.CLUZEL is a versatile way to apply a flexural moment (with a compressive component which can be managed with the arms' length). A symmetric test and, non-symmetric test (figure.3.3.2) have been applied in the femur geometery with a constant load of 550 N.

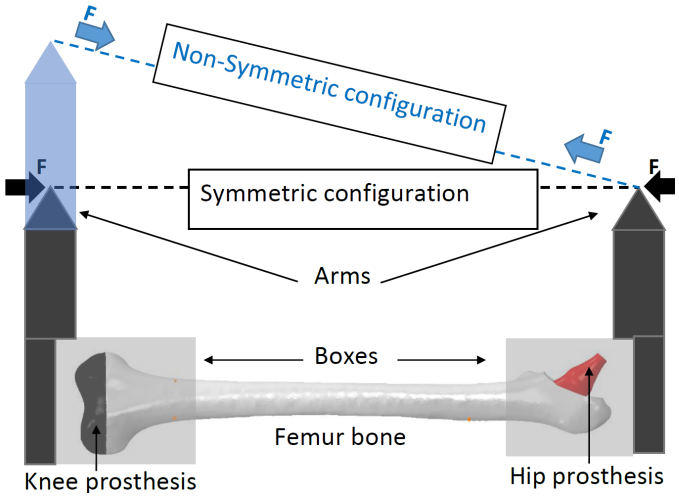

Figure 3.3.2: FEM representing the 2-points bending test for the symmetric and non-symmereic configurations

To perform a test on the interaction between a prosthesis and a femur, it is necessary to be able to impose boundary conditions that generate the required load without interfering with the study area. In order to implement this boundary conditions in the ABAQUS® software, it was decided to mimicry the lids (boxes) with the arms proposed in the configuration description and rather use a structural distributing coupling that would transfer the forces applied at the tip of the arm in a flexural moment. Taking advantage of the distributing nature of this coupling, it was decided to couple only the translational degrees of freedom from the reference node to the coupling nodes. Thus, although the reference node is free to rotate (e.g. to roll), the coupling nodes are translated following the equivalent displacement applied at the reference node. Using this approach, it was possible to save the use of more elements in the simulation, and hence, it was kept a low computational cost. A constant load of 550 N is applied at each of the two-moment arms on the symmetric configuration and nonsymmetric configuration.

3.3.3 Gait cycle loading test

For walking in a flat land, the boundary conditions and load application points as described in [Heller et al., 2005] were applied. It was necessary to develop a load profile for the femur that improves the simulation of in vivo loading conditions of patient with a THR and TKR in the same femur and considers the relationship between muscle and joint forces. These loading conditions are considered to be the major simplification of the actual in vivo loading situation and result generally in bending loads on the femur. The musculoskeletal loading conditions were calculated throughout the complete cycle of the single instant of maximum in vivo hip prosthesis contact force of the walking cycle, assuming a body weight of 81.5 kg (800 N). The total force in the hip joint is considerthe interdependence of muscle and joint contact forces and the musculoskeletal loading[Heller et al., 2005].

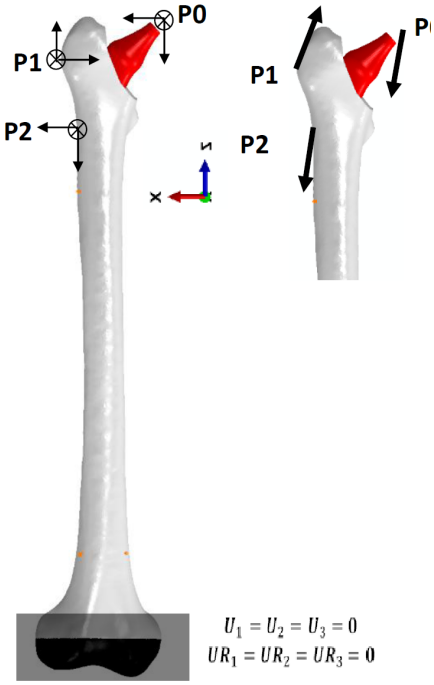

Figure 3.3.3: Boundary conditions of the Gait cycle during walking

Point	P_0	P_1	P_2
F_x	518.3	-543.4	7.5
F_y	381.2	-133.8	-154.7
F_z	-2570	-677.2	-776.6

Table 3.3.1: Force Values Used for the Gait Simulation.

The maximum load condition during the gait cycle was applied in three regions in the proximal part of the femur. The loading at point (P_0) is the hip prosthesis head forces, the loading at (P_1) is the Great Trochanteric muscle forces and the loading at (P_2) is the vastus lateralis forces and the distal part of the model translation and rotation were fully constrained(figure.3.3.3). The force components of the three loading conditions (table.3.3.1) were oriented based on the coordinate system.

3.4 Results

For the pure bending loads, the risk of fracture is always on the tension side since the value of the ultimate tensile strengh 30 % lower than that of compression [Bayraktar et al., 2004]. Therefore, the comparisons only involve the positive stress differences from one simulation to another. In contrast, when analyzing with a loading representing walking, the higher compressive than tensile stress component may generate a fracture of the compressed face which must then also be checked. To quantify the risk of fracture (RF), some authors [Bayraktar et al., 2004], [Schileo et al., 2008a],[Soenen et al., 2013] use a criterion based on the maximum principal strain. In our analyses, we use this criteria as described in [Nalla et al., 2003],[Schileo et al., 2008b]

$$\boxed{RF = \epsilon_{max}/\epsilon_{ultim_{(compression,tensile)}}}$$

ϵ_{max} is the resultant maximum principal strain in the cortical bone;
$\epsilon_{ultim_{(compression)}}$ is the compressive ultimate strain for cortical bone;
$\epsilon_{ultim_{(tensile)}}$ is the tensile ultimate strain for cortical bone.
With: $\epsilon_{ultim_{(compression)}}$=0.0104, $\epsilon_{ultim_{(tesile)}}$=0.0073 [Ford et al., 2009], [Bayraktar et al., 2004]. Therefor

this formula can be used as an indication comparison tool for the fracture. The close RF value to 1 indicates a higher fracture risk.

Note: this indicator assumes a linear behavior and independent of the strain rate.

3.4.1 Four-point bending test with a constant moment throughout the total femur

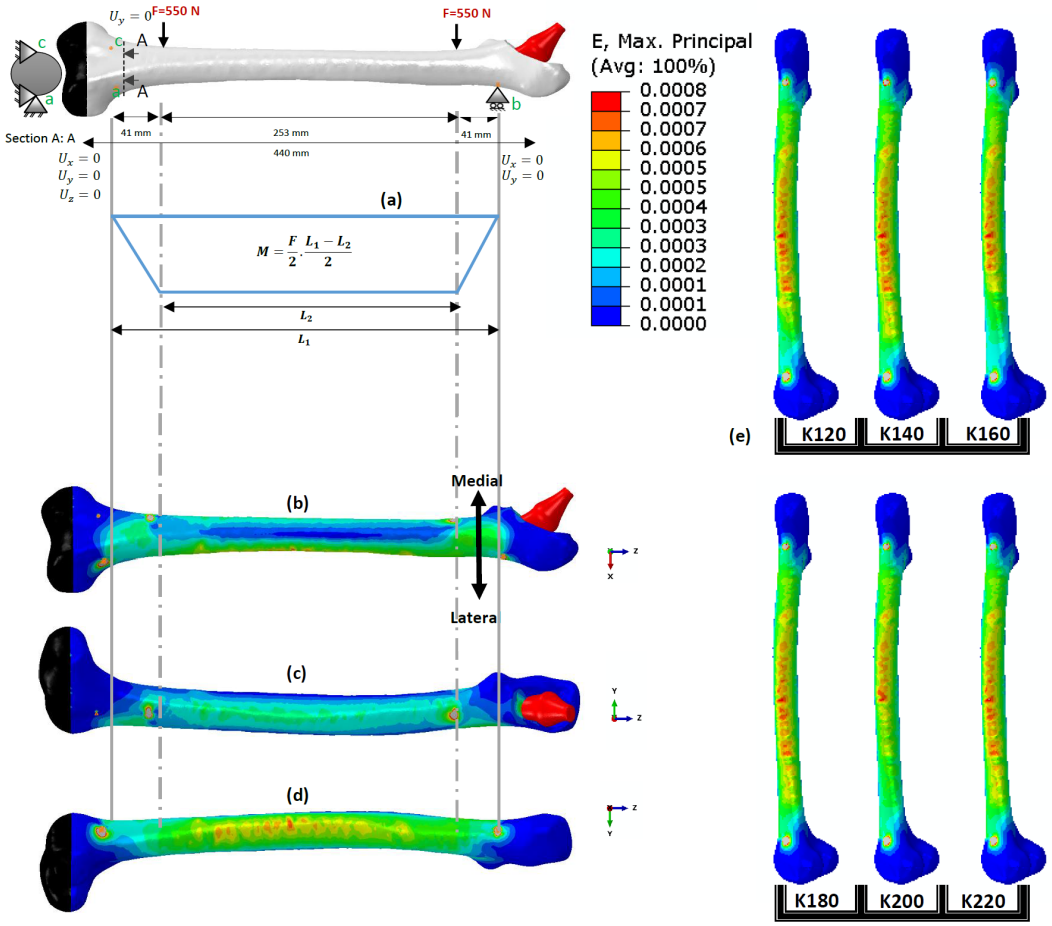

Figure 3.4.1: Max principal strain distribution obtained in the several modes during the Four-point bending test with a constant moment through out the total femur. (a) represents the bending moment diagram: The femur was loaded with a constant bending moment between the inner supports; L_1: distance between the outer supports; L_1: distance between the inner supports; F: applied force; M: bending moment. (b) represents the anterior view of the femur. (c) represents the medial view of the femur (the compression part due to the bending). (d) represents the lateral view of the femur (the tensile part due to the bending). (e) represents the max principal strain distribution obtained in the several modes during the four point bending test (The model name is reported, for each configuration, below each picture).

Under this four-point bending condition, the maximum deformation of the cortical bone is always located between the two inner loading supports which induces a constant moment in this area with or without prostheses, whatever was the IP gap. In the presented four-point bending test, the inner loading supports are pushing from the medial side to generate tension at the lateral side. (figure.3.4.1). The maximum principal tensile strains pattern was located in the lateral side in the IP gap region, while the compressive strains had mainly appeared in the medial part. The strains patterns for the different models are comparable and the maximal principle strains values located on the lateral surface are the same (figure.3.4.1.e)

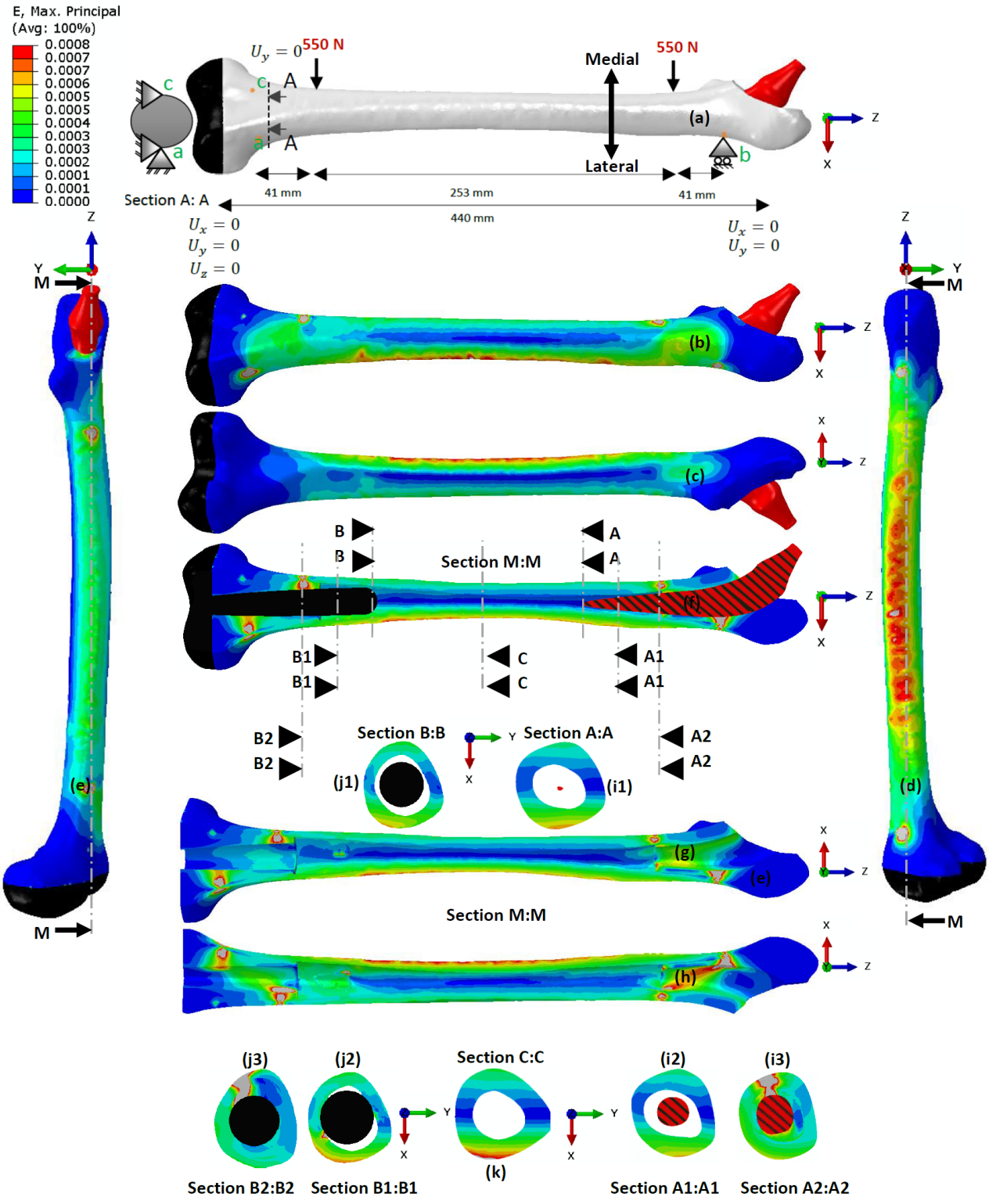

Figure 3.4.2: *Maximum principle strain values on the lateral side of the femur (Four-point bending test with a constant moment through out the total femur). (a) represents the boundary conditions of the four-point bending test with a constant moment throughout the femur diaphysis. (b) represents the maximum principle strain on bothe of the fmur and prostheses. (d) represents the maximum principle strain distribution on the fmeur only, while the colors for thip and knee prostheisis do not follow the diformation legend . (e) represents the deofmed femur after the four point bending test while the cuts to represent the three difrerrent parts of the femur: deformation of the promiamal side , middel shaft and distal side. (f1) a cross section represent the dofmation on the tip of the hip prosthesis. (f2) a cross section represents the deformation on the cortical bone due to the exsitence of the hip prostheis. (f3) a cross section represents the full contact between the proximal fmeur and the hip prosthesis. (g1) a cross section represent the dofmation on the tip of the knee prosthesis. (g2) a cross section represents the deformation on the cortical bone due to the exsitence of the knee prostheis. (g3) a cross section represents the full contact between the distal fmeur and the knee prosthesis. (h) represents the maximum deformation on the femur shaft. (l1,l2) represens the deformation on the lateral and medial sides of the femur*

Implantation of hip and knee prostheses causes the load transfer and the deformation state within the treated femur to be altered. The full contact between the prostheses and the femur is awlays where the trabecular bone is existing (figure.3.4.2). Thus, the nature of the trabecular bone reduces the deformations on the cortical bone. Along the lateral side of the femur, the maximum principal strain value was appearing in the middle of the shaft. The max principal strain values were ranged between 0.000802 (for the model with a knee stem length of 120 mm) and 0.00082 (for the model of the knee stem length of 220mm). Consequently the RF for each model was almost the same value of 0.1.

3.4.2 Two-point bending "Rigid-Orthogonal-Heels flexion" symmetric test configuration

The two-moment arms are equal and parallel, Thus there is no shear component. The maximum principal strain pattern was located in the IP gaps region. The strain patterns for the different models are comparable and the maximal strain values located on the lateral surface are almost identical(figure.3.4.3)

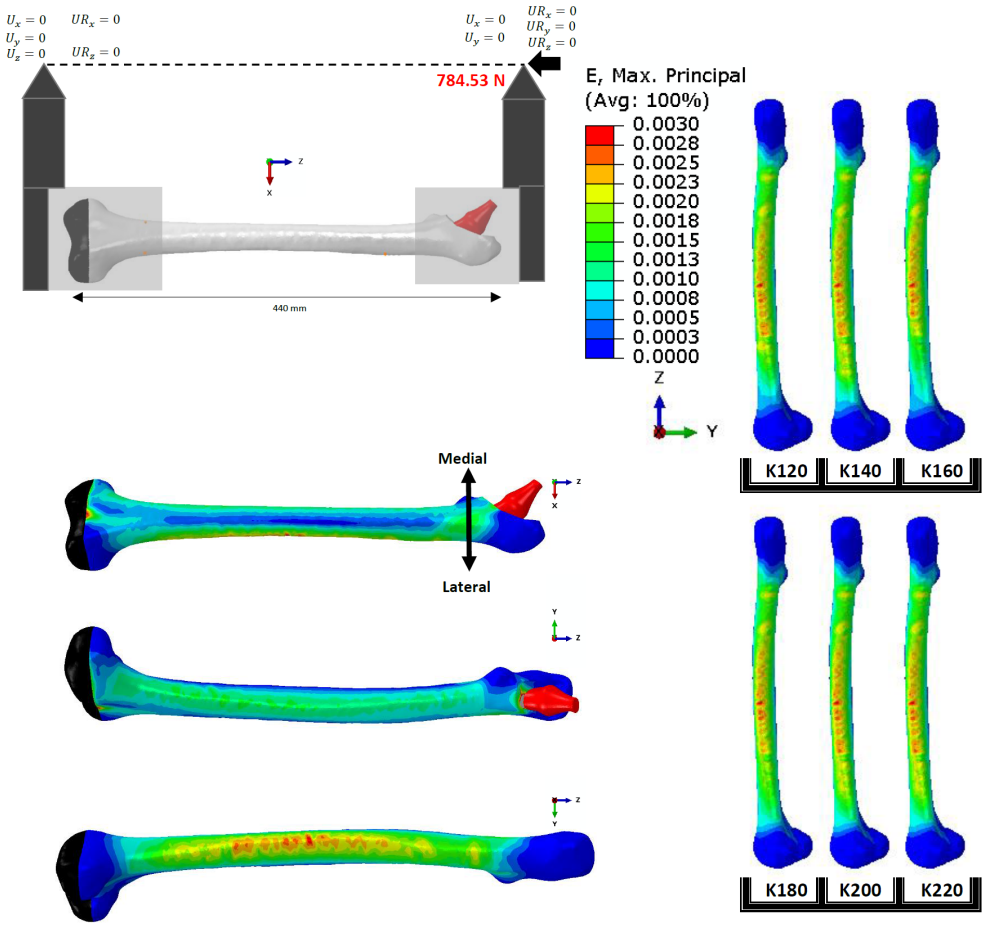

Figure 3.4.3: Max principal strain distribution obtained in the several modes during the Two-point bending test with a symmetric congifuration.

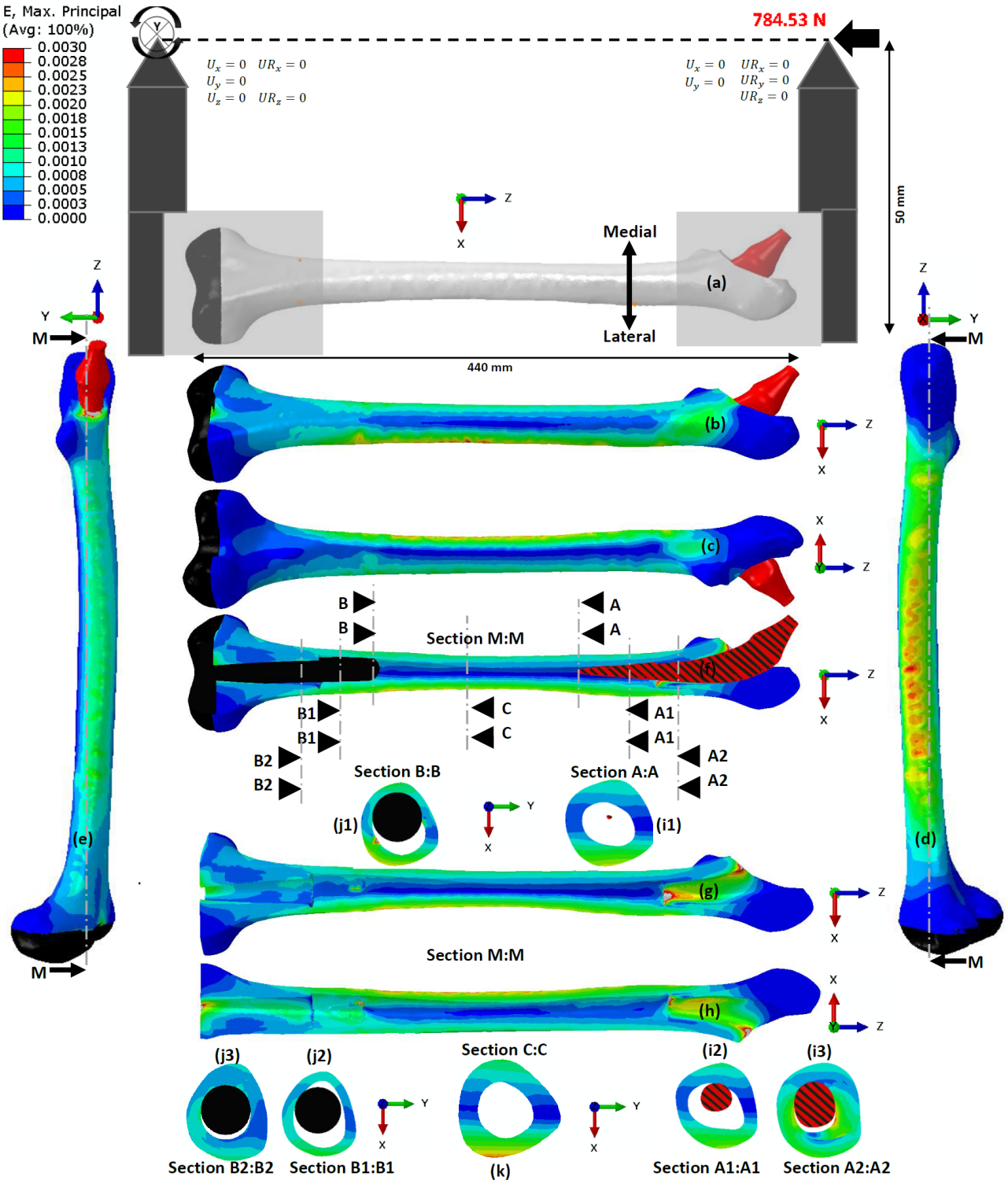

Figure 3.4.4: *Maximum principle strain values on the lateral side of the femur (Four-point bending test with a constant moment through out the total femur). (a) represents the boundary conditions of the four-point bending test with a constant moment throughout the femur diaphysis. (b) represents the maximum principle strain on bothe of the fmur and prostheses. (d) represents the maximum principle strain distribution on the fmeur only, while the colors for thip and knee prostheisis do not follow the diformation legend . (e) represents the deofmed femur after the four point bending test while the cuts to represent the three difrerrent parts of the femur: deformation of the promiamal side , middel shaft and distal side. (f1) a cross section represents the dofmation on the tip of the hip prosthesis. (f2) a cross section represents the deformation on the cortical bone due to the exsitence of the hip prostheis. (f3) a cross section represents the full contact between the proximal fmeur and the hip prosthesis. (g1) a cross section represents the dofmation on the tip of the knee prosthesis. (g2) a cross section represents the deformation on the cortical bone due to the exsitence of the knee prostheis. (g3) a cross section represent the full contact between the distal fmeur and the knee prosthesis. (h) represents the maximum deformation on the femur shaft. (l1,l2) represents the deformation on the lateral and medial sides of the femur*

Along the lateral side of the femur, the maximum strains values were highest in the IP gap region.

While, the maximum strain vlaue for all the models was varying from 0.0028 to 0.0030. Consequently, the RF for each model was almost the same value of 0.42.

3.4.3 Two-point bending "Rigid-Orthogonal-Heels flexion" symmetric test configuration:

The two-moment arms are not equal (the moment arm length in the knee side is double in the length of the one the hip side), and parallel, Thus there is no shear component. The maximum principal strain pattern was located in the IP gaps region but more proximally. The strains patterns for the different models are comparable and the maximal strains values located on the lateral surface are almost identical(figure 3.4.5)

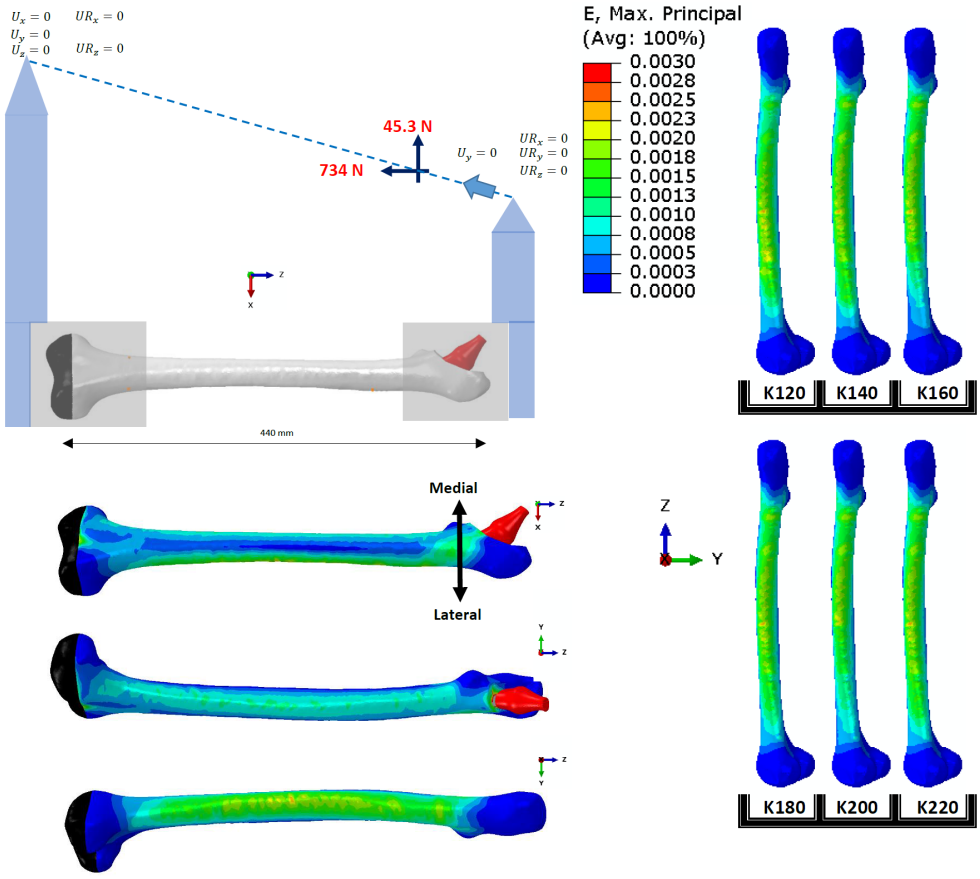

Figure 3.4.5: Max principal strain distribution obtained in the several modes during the Two-point bending test with a nonsymmetric congifuration.

Along the lateral side of the femur, the maximum strains values were highest in the IP gap region. While, the maximum strain value for all the models was varying from 0.0020 to 0.0023. Consequently, the RF for each model was almost the same value of 0.315.

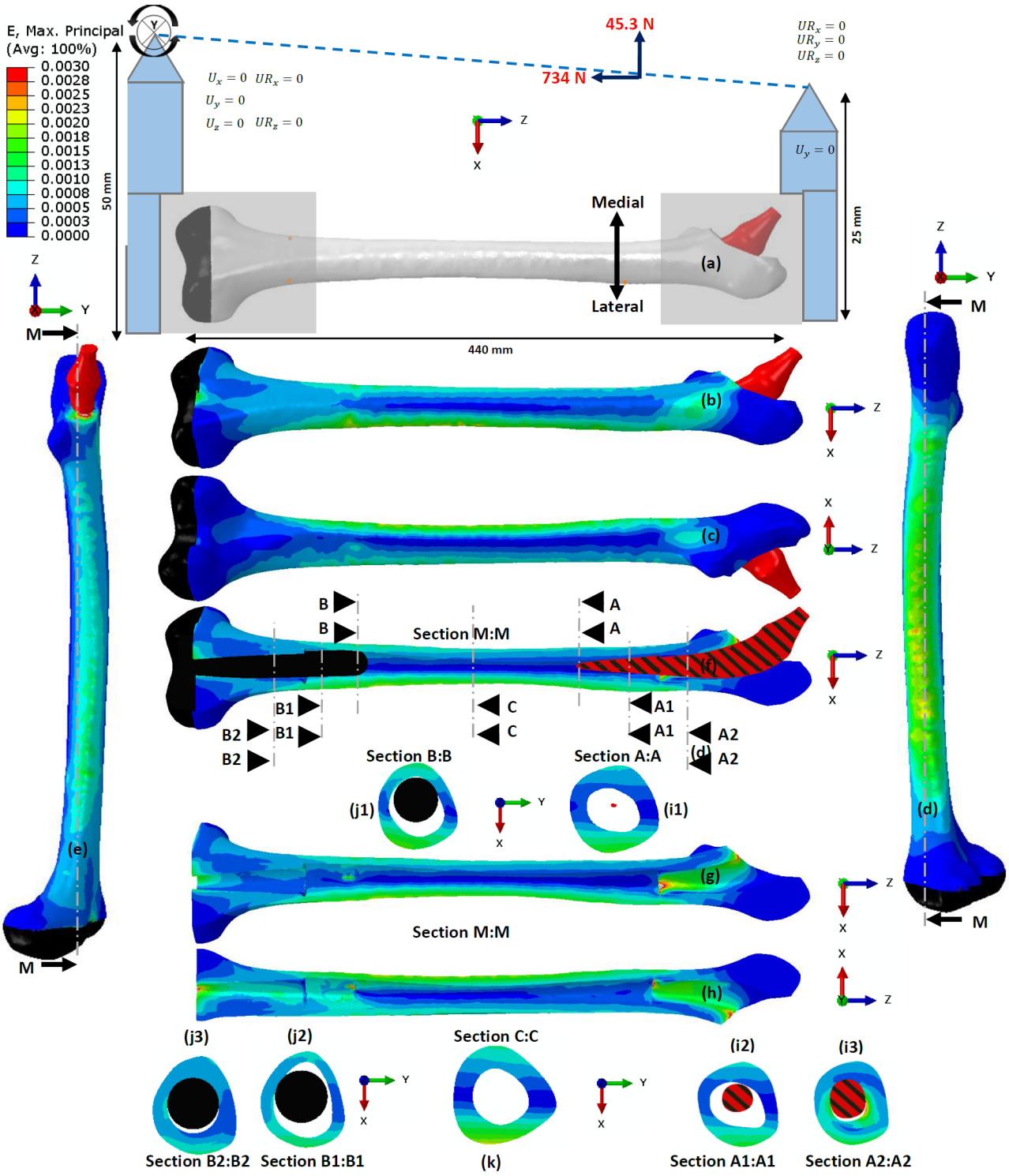

Figure 3.4.6: *Maximum principle strain values on the lateral side of the femur (Four-point bending test with a constant moment through out the total femur). (a) represents the boundary conditions of the four-point bending test with a constant moment throughout the femur diaphysis. (b) represents the maximum principle strain on bothe of the fmur and prostheses. (d) represents the maximum principle strain distribution on the fmeur only, while the colors for thip and knee prostheisis do not follow the diformation legend . (e) represents the deofmed femur after the four point bending test while the cuts to represent the three difrerrent parts of the femur: deformation of the promiamal side , middel shaft and distal side. (f1) a cross section represents the dofmation on the tip of the hip prosthesis. (f2) a cross section represents the deformation on the cortical bone due to the exsitence of the hip prostheis. (f3) a cross section represents the full contact between the proximal fmeur and the hip prosthesis. (g1) a cross section represents the dofmation on the tip of the knee prosthesis. (g2) a cross section represents the deformation on the cortical bone due to the exsitence of the knee prostheis. (g3) a cross section represents the full contact between the distal fmeur and the knee prosthesis. (h) represents the maximum deformation on the femur shaft. (l1,l2) represents the deformation on the lateral and medial sides of the femur*

3.4.4 Gait cycle loading test

The maximum strains were located more distally in the gap due to a change in resulting moment compared to the 4-point bending test. Anatomical loading causes torsion and bending, while the 4-point bending test causes bending only (3.4.7).

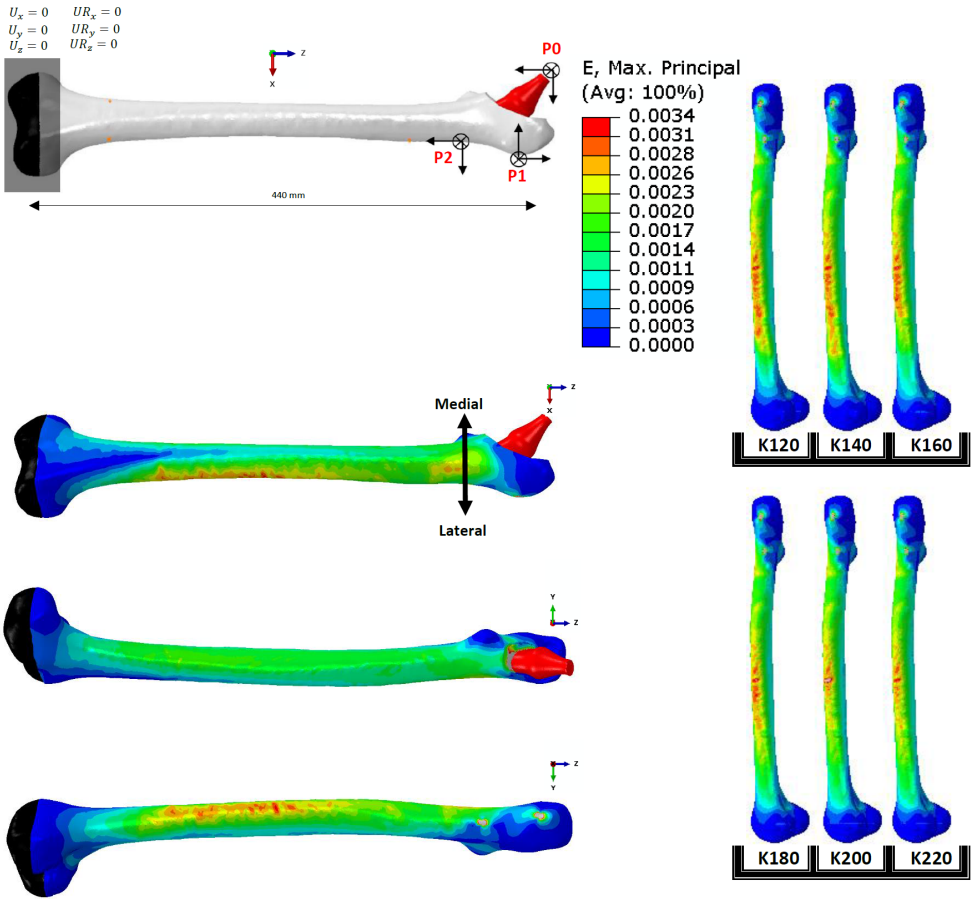

Figure 3.4.7: Max principal strain distribution obtained in the several modes during the gait cycle during walking activity.

Along the lateral side of the femur, The maximum strains values were highest in the IP gap region. While, the maximum strain vlaue for all the models was varying from 0.0031 to 0.0034. Consequently the RF for each model was almost the same value of 0.465.

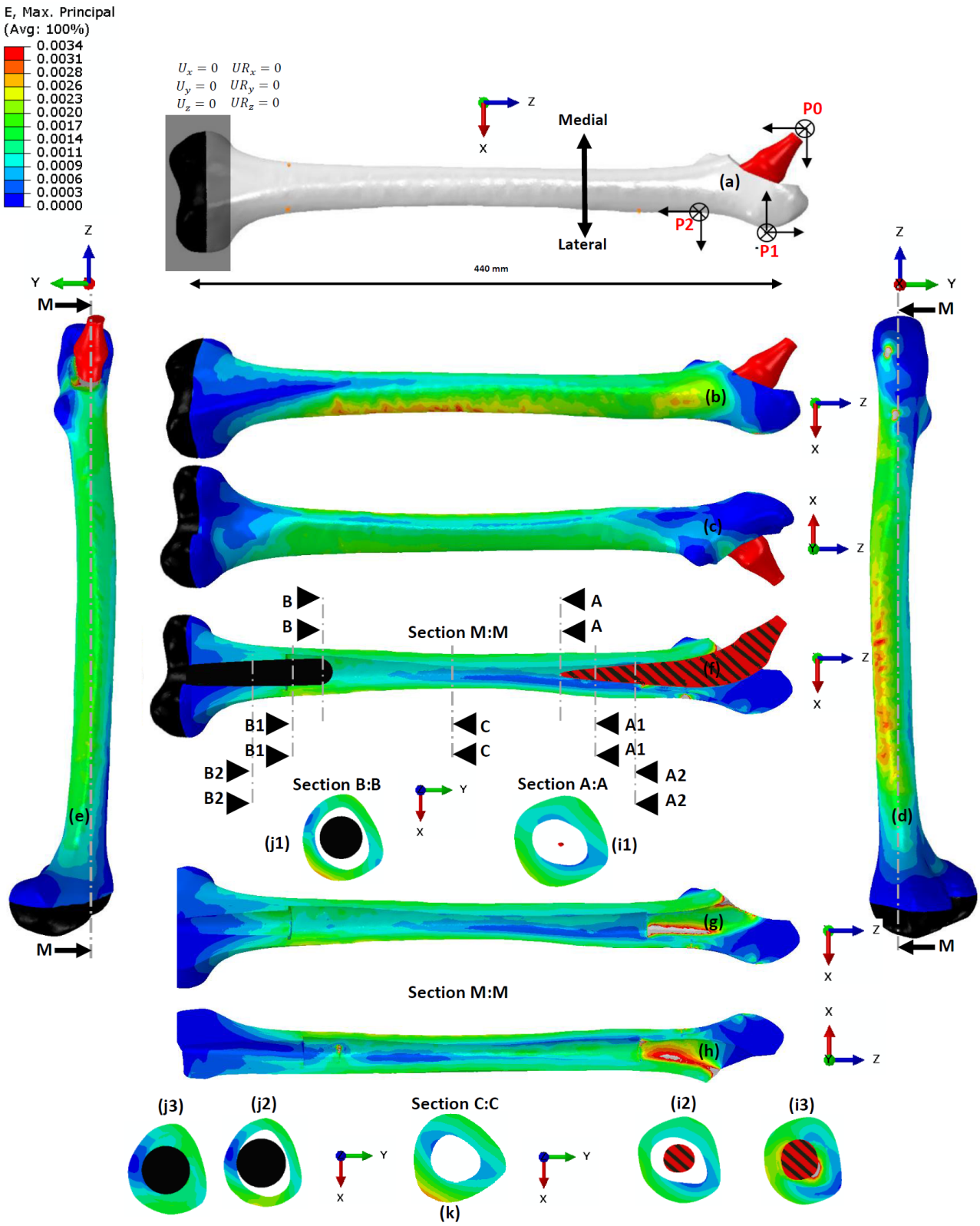

Figure 3.4.8: *Maximum principle strain values on the lateral side of the femur (Four-point bending test with a constant moment through out the total femur). (a) represents the boundary conditions of the four-point bending test with a constant moment throughout the femur diaphysis. (b) represents the maximum principle strain on bothe of the fmur and prostheses. (d) represents the maximum principle strain distribution on the fmeur only, while the colors for thip and knee prostheisis do not follow the diformation legend . (e) represents the deofmed femur after the four point bending test while the cuts to represent the three difrerrent parts of the femur: deformation of the promiamal side , middel shaft and distal side. (f1) a cross section represents the dofmation on the tip of the hip prosthesis. (f2) a cross section represents the deformation on the cortical bone due to the exsitence of the hip prostheis. (f3) a cross section represents the full contact between the proximal fmeur and the hip prosthesis. (g1) a cross section represents the dofmation on the tip of the knee prosthesis. (g2) a cross section represents the deformation on the cortical bone due to the exsitence of the knee prostheis. (g3) a cross section represents the full contact between the distal fmeur and the knee prosthesis. (h) represents the maximum deformation on the femur shaft. (l1,l2) represents the deformation on the lateral and medial sides of the femur*

3.4.5 Cortical thickness effect using the four-point bending test with a constant moment through the middel of the femur shaft

Variation of cortical thickness along the femur model has been icluded in FEM calculaion with a model of knee prosthesis length of 120 mm and a model of knzz peosthesis length of 220 mm. A significant influence of cortical thickness on femoral strains has been observed. A smaller cortical thickness shows higher strains (3.4.9),(3.4.10).

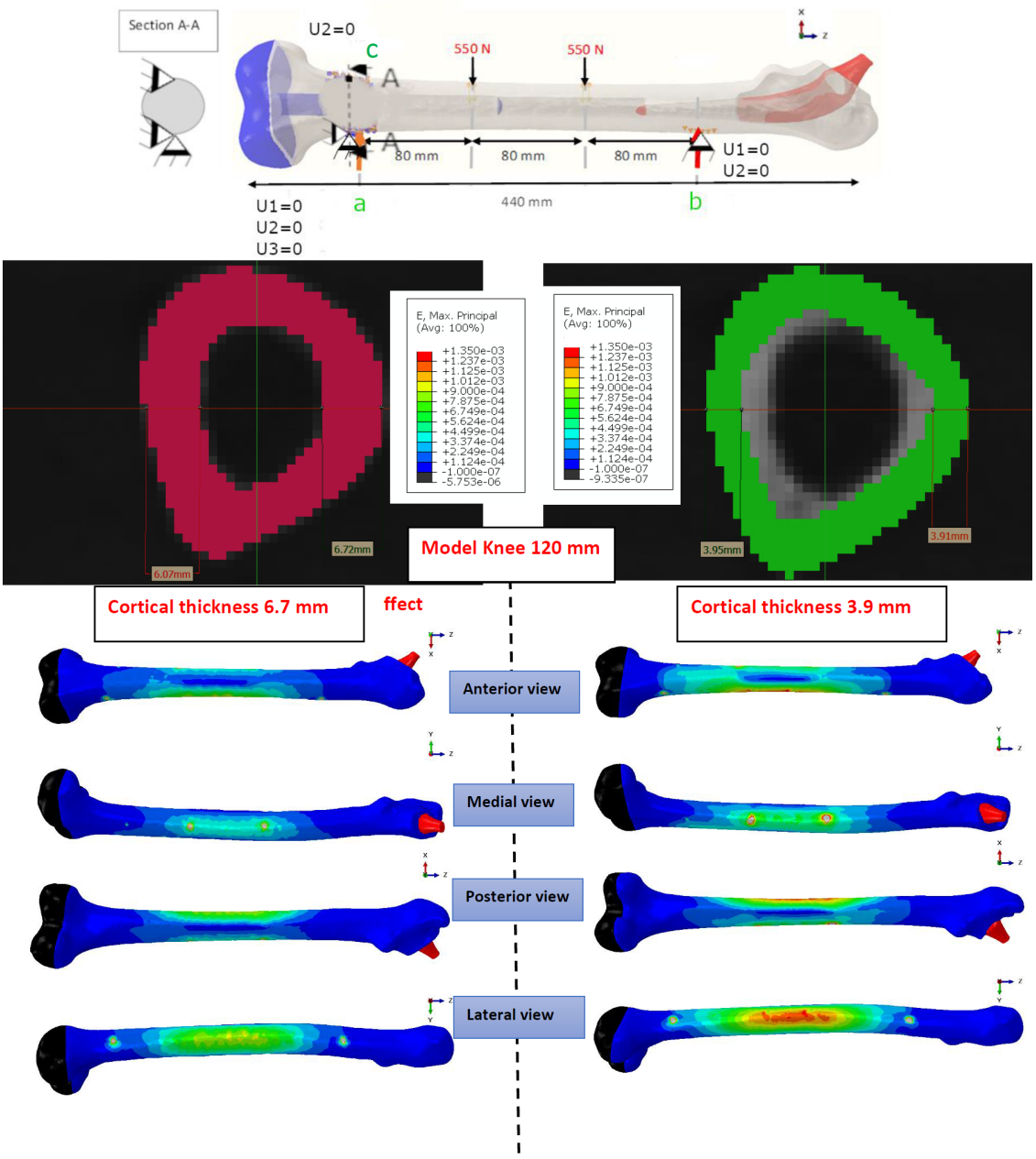

Figure 3.4.9: Max principal strain distribution showing the effect of the cortical wall thickness for an avrage thickness of the cortical femur shaft of 6.7mm and 3.9 mm.

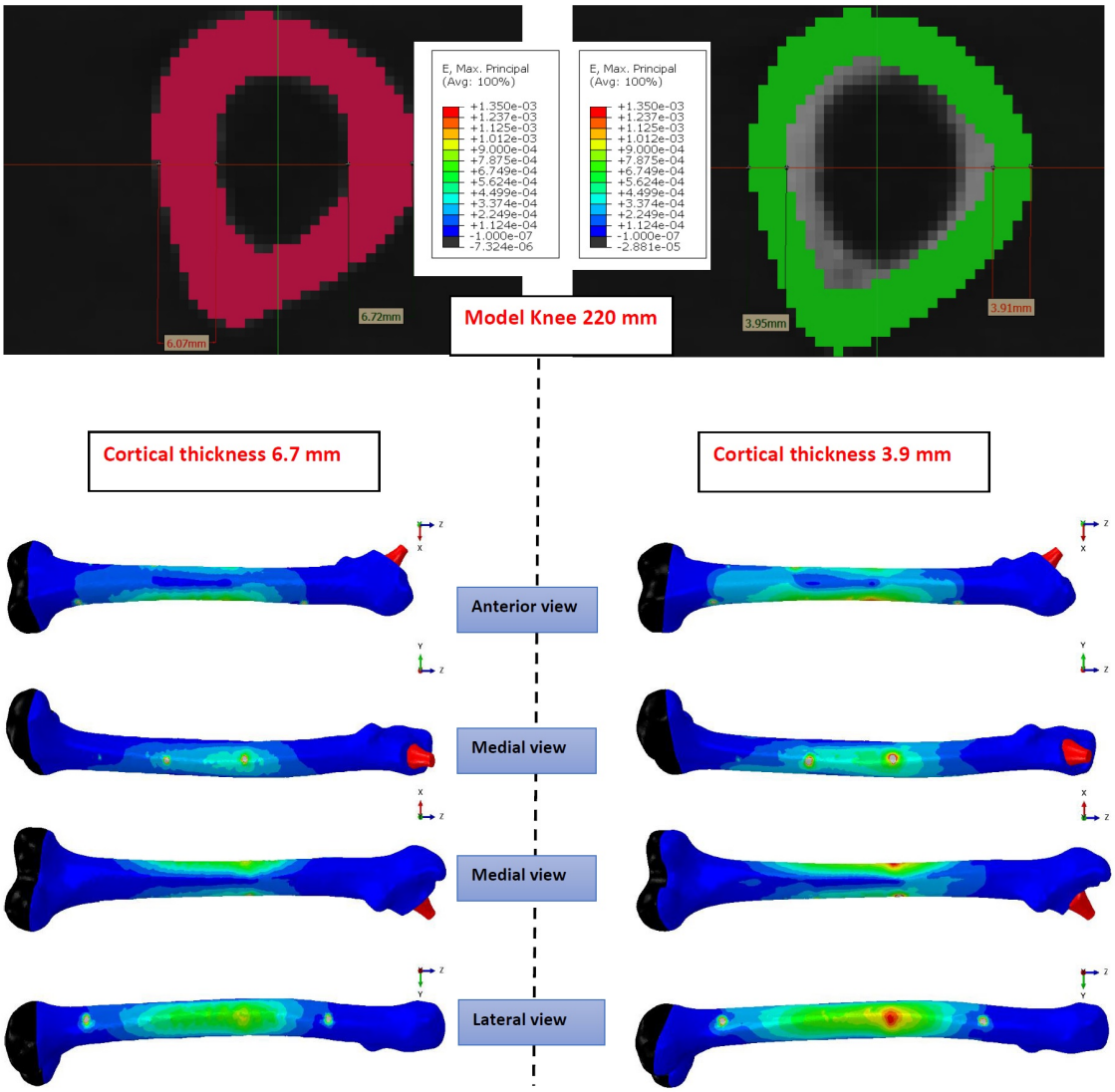

Figure 3.4.10: *Max principal strain distribution showing the effect of the cortical wall thickness for an avrage thickness of the cortical femur shaft of 6.7mm and 3.9 mm.*

For the model with a knee prosthesis of 120 mm length, the maximum strain value was 0.001 with an average cortical thickness of 3.9 mm and 0.0019 with an average cortical thickness of 6.7 mm. For the model with a knee prosthesis of 220 mm length, the maximum strain vlaue was 0.001825 with an average cortical thickness of 3.9 mm and 0.0025915 with an avrage cortical thickness of 6.7 mm Consequently the RF for each models with lower thcikness of the cortical wall is higher than the models with the lower thickess (3.4.11). These results are in agreement with the results of [Iesaka et al., 2005].

Figure 3.4.11: *Fracture risk calculations showing the effect of the cortical wall thickness for an avrage thickness of the cortical femur shaft of 6.7mm and 3.9 mm.*

3.4.6 Preventive plate effect using the four-point bending test with a constant moment through out the total femur

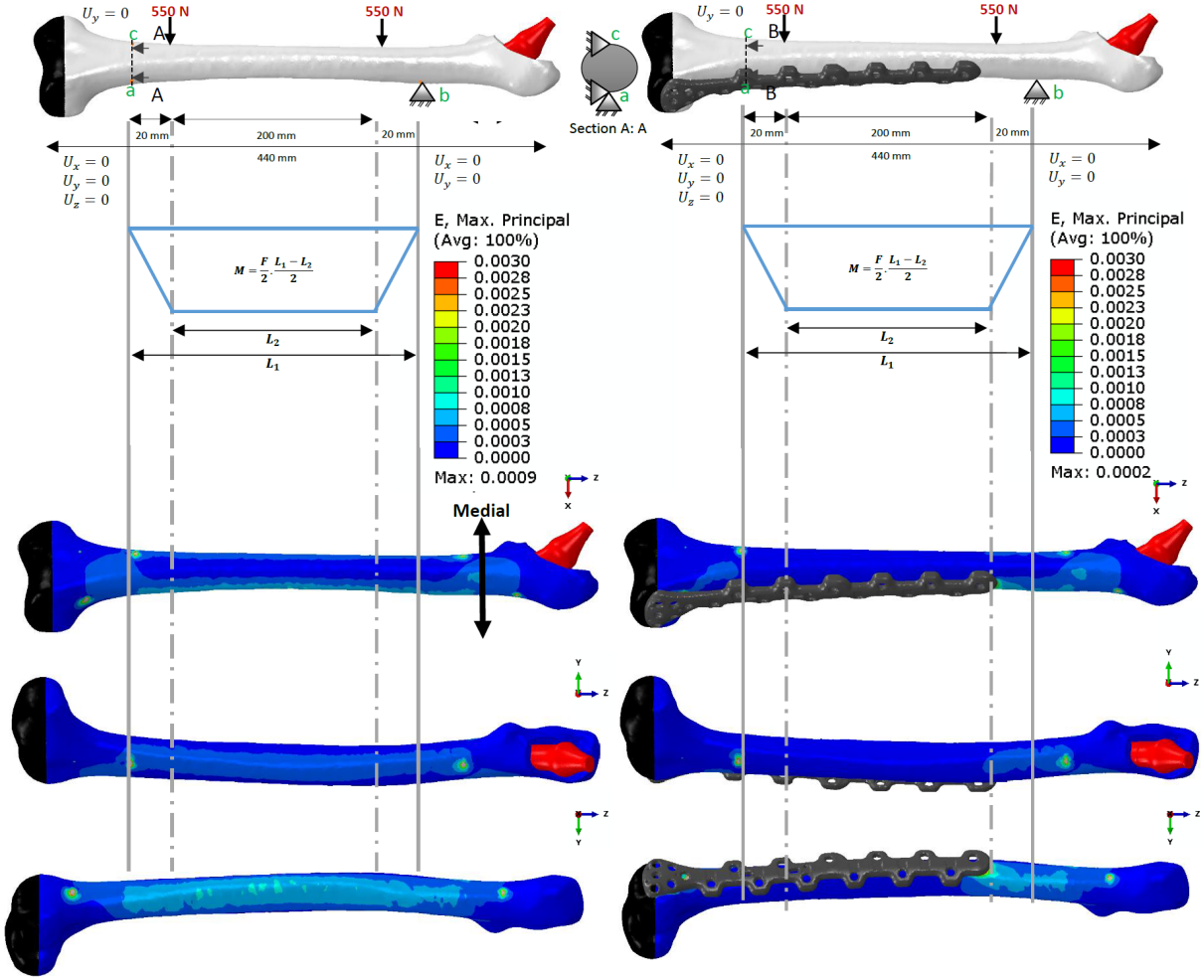

Figure 3.4.12: *Max principal strain distribution obtained in the several modes during .*

In this loading condition, the maximum momentum area is always located between the two loading forces which induce a constant moment in this area, Whatever was the IP gap. The loading is applied to generates tension at the lateral side. a fracture plate has been used as a preventive plate. the positioning and the orientation of the plate have been done and it has been reviewed by Pr. Matthieu EHLINGER. it has been considered a tied contact between the femur surface and the plate. With using a preventive plate in the lateral side of the femur, the maximum principal strain value drops in the IP gap area, which gives a significant effect of using the preventive plate in a femur with a THR and a TKR (3.4.12).

3.5 Discussion and conclusion

The understanding of the potential of the fracture risk affiliated with factors such as aging, disease, different loads, and how they linked with fracture, is still relatively limited. The bone material and its geometry has a complex mechanical properties and structure. Therefore, the problem of understanding the fracture risk of femur bone with a TKR and THR is equally complex. The presence of the prostheses change the elasticity of the whole model. The present chapter shows several investigations of FE models of a femur bone fracture risk under diffrenet tests. A 3D model of a real femur bone geometery has been generated by converting the CT scan images. The 3D model of the femur has been edited by removing the hip and the knee joints. The 3D model of the hip prosthesis and the knee prosthesis have been placed and oriented in the femur bone model under the supervision and the acceptance of professor Matthieu EHLINGER and professor Sybille FACCA.

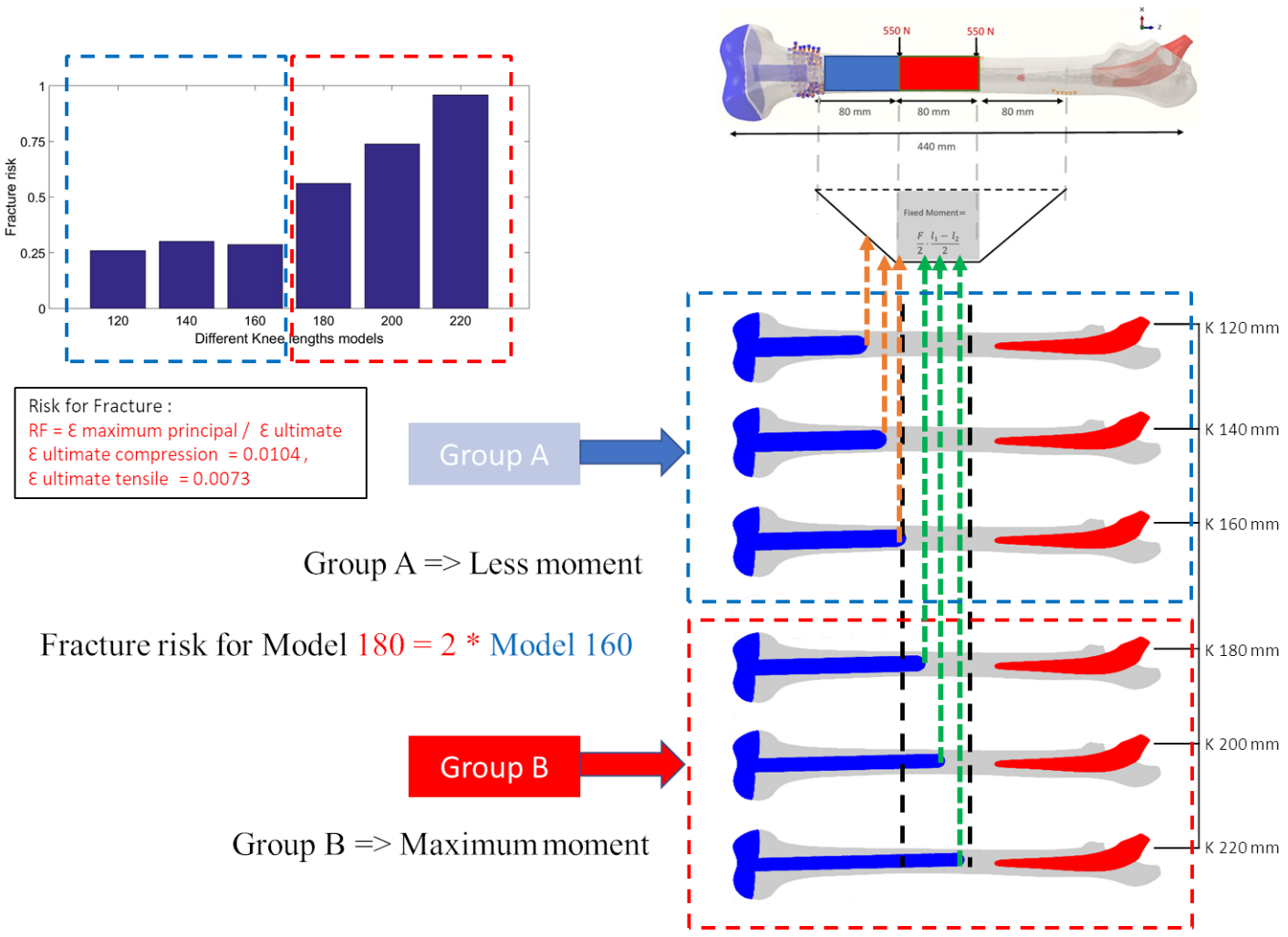

Figure 3.5.1: Analysis of the four-point bending test proposed by [Soenen et al., 2013], while the red colored zone (group A) represent the fixed moment area between the two loadings supports and the blue area zone (group A) represents the varied moment area in the distal part of the femur. the strains obtained in the red zone is about doubl the ones in the blue zone. Consequence, the fracture risk in the middel of the femur shaft with present of the the knee stems is higher

Under a quasi-static loading condition, five different FE models with different loading conditions have been used to study the sensitivity on the IP distance, the cortical thickness and effect of using a fracture plate as a preventive one with the presence of the two prostheses. To validate the FE modeling without having experiments results on anatomical parts, several simulations presented in [Soenen et al., 2013], [Weiser et al., 2014], [Quirynen, 2016], were replicated with similar boundary conditions, except for the 4-point bending tests in [Soenen et al., 2013], which give similar results but different conclusions. It has been hypothesised that the small interprosthetic gaps increase the fracture risk [Soenen et al., 2013]. The results obtained in this chapter do not comply with this argument. Infact the transition of the fracture risk is just the position of the stem tip from one side to the other of the distal central support and therefore the displacement of the maximum moment. The position of the over-stress is not exactly at the end of the inner shaft of the prosthesis. The models of stem tips located between the loading support are subjected to over-stress which is placed in the central zone of the maximum moment, While the models of stem tips located before the loading support are in zones of less moment . So, there is no uniformity of the load in the transfer zone by using the 4-point bending test with central supports which are close together. This explains the slight variance in the maximum principal strains in the IP gaps. Therefore by using the real geometry of the femur bone the variance optioned by [Soenen et al., 2013] could be clearly observed in figure.(3.5.1).

For the different loading conditions in all configurations tested, if the loading imposed is an instantaneous force in pure bending or in loading equivalent to a gait cycle, the length of the knee prosthesis stem is not decisively related to the risk of fracture. The models with hip and knee prostheses had lower strains than a model with out prosthesis. The presence of the hip and the knee stems inside the femur increase the stiffness of the structure and so on the bending deformation is lower. Therefore the strains in the zones which the prothesis stem present are lower than the strains in the IP gaps. This shows that the IP gap is the weakest section of the structure. Thus our results are consistent with the results of [Iesaka et al., 2005], [Weiser et al., 2014], [Quirynen, 2016] while, the prosthesis placement does not act as a stress riser, nor increases fracture risk. In addition, in our simulations we used a different diameters and lengths of the knee stems, the increase of the cortical wall from the distal metaphysis to the middle diaphysis of the femur shaft seems to be able to absorb the energy resulted by the loading forces and the fracture risk in this area is kept low. For the FE simulations of the cortical thickness effect, the cortical thickness and especially the cortical area in the femur shaft, correlates significantly with fracture risk. In all configurations tested, the IP gap between the fixed hip prosthesis length and the varied knee prosthesis length is not decisively related to the risk of fracture but, it must be clarified that through the stiffness of the structure; lower

distance between the prosthesis tips will be more preferred but not better in terms of the resultant strains, while higher IP gaps lead to larger zones of low stiffness compared to the regions where a prosthesis was present. Finally, it will be recommended suggestion that the tip of any prosthesis should be located in a zone with a sufficient cortical wall thickness since the selection criteria of the IP gap should be based on the femoral morphology, and the bone quality. The use of a fracture plate as a preventive plate in the IP gap zone shows that the locked plate significantly enhances the resistance to peri-implant fracture risk of a bone–plate construct. The use of the plate with the the hip and the knee prostheses decreases the peak bending moment and failure energy.

Chapter 4

Dynamic simulation of a forward fall for a human femur bone to investigate the critical fracture zone"

Abstract:

During a forward fall, the shock on the knee occurs. Defining the boundary conditions to apply to the simulation to represent this shock is complex. The goal of this numerical study is to investigate and model the loading leading to risk of fracture in a synthetic human femur during a forward falling.

Résumé:

Lors d'une chute avant, il peut y avoir un choc sur le genou. Définir les conditions aux limites à appliquer à la simulation pour représenter ce choc est complexe. L'objectif de cette étude numérique est d'étudier et de modéliser le chargement menant au risque de fracture dans un fémur humain synthétique lors d'une chute en avant.

4.1 Introduction

Fractures related to falls are a common and serious health issue faced by older people. Nearly one-third of the elderly population suffer falls every year [Rubenstein et al., 1994]. The statistical studies report that 59% of the elderly over the age of 65 years have at least one fall per year and almost all the fractures are due to the falling [Tinetti et al., 1994], [D.Bell and Goncalves, 2020]. In France, more than 80 percent of accidental injuries among elderly people is due to falling. In 2005, an estimated 450,000 falls requiring emergency care suffering a fall for adults aged between 65 and 75 [Danet, 2011]. These injuries make the elderly beat-heavy costs, direct costs for medical treatment and care, and indirect costs such as loss of productivity and independence. Falling or being exposed to a low energy shock in a femur with THR and TKR in the same leg could cause fractures while the femoral shaft is compressed between two ipsilateral implants with most of these fractures being located on the supracondylar femoral shaft [Solarino et al., 2014]. The treatment of these fractures is still challenging and it is associated with serious complications such as the type of fracture, the bone quality, and the prosthesis stability. In addition, the treatment will require a surgical intervention. The purpose of this chapter was to predict the fracture location due to a forward falling of an elderly on a flat floor, therefore this information of the predicted fracture location will be used to design and optimize a preventive plate.

4.2 Materials and methods

A geometrical data of cadaveric human left femur bone in the form of DICOM files obtained from GE Ultrafast High-Resolution Multi-slice CT Scanner (Hôpitaux Universitaires de Strasbourg (HUS)). This DICOM data have been converted to a three-dimensional FE models using a 3D Image Segmentation, Processing and Meshing Software (Synopsys Simpleware Software). The data used in analysis belongs to a 56-year-old male with 61 kilograms with a total femur length of 440 mm. Charnley low-frictional total hip replacement was used with a stem length of 145 mm. The hip prosthesis was placed and verified by the orthopedic surgeon such as the center of the prosthesis head was matched to the center of the healthy femoral head. The knee prosthesis was modelled as a cylinder with spherical tip attached to a part from the knee condyle (Femoral component). The knee prosthesis cylinder (stem) was placed in to the femur diaphysis to create the different IP gaps depending on the cylinder length. The size of the inter-prosthetic gap was defined by the distance between the distal tip of the hip stem and the proximal tip of the knee stem (figure.4.2.1).

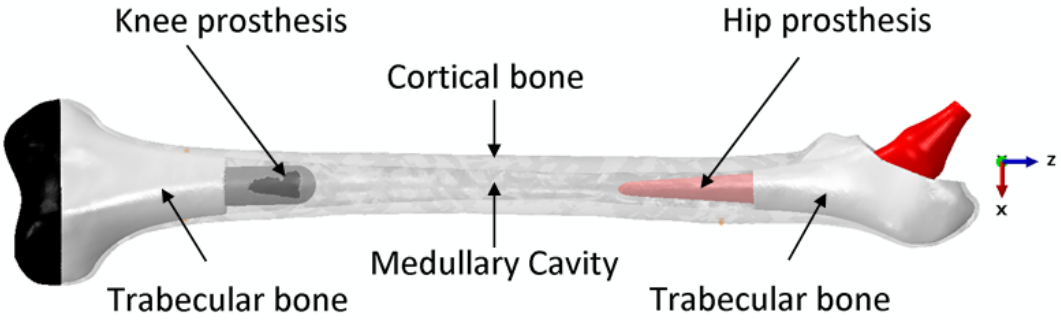

Figure 4.2.1: A 3d-model of the femur with TKR anf THR (Cortical bone, Trabecular bone and prostheses)

All the models were meshed uniformly using the Synopsys Simpleware Software®. To obtain a good meshing, the sofware uses proprietary algorithms to generate multi-part meshes to guarantees conforming interfaces and shared nodes between an implant and bone and between the different bone layers. All the multiple elements after meshing were modified and processed using the manual mesh editing, smoothening and filtering. elementsquadratic tetrahedral element, type C3D10 with an approximate element size of 2 mm have been used. For the stress-strain calculations the quadratic tetrahedron behaves significantly better than the four-node (linear) tetrahedron . Subsequently the volume mesh was created (figure.4.2.2) and finally the mesh was splitted into remeshed parts using the splitting too or the volume mesh in (Synopsys Simpleware Software®) .The resulted volume mesh in total number of elements over the whole femur and prostheses is ranging from 147539 to 152310 elements (average: 149925) All the meshed parts were then imported to Abaqus® CAE 6.14-1 (Dassault Systèmes ©).

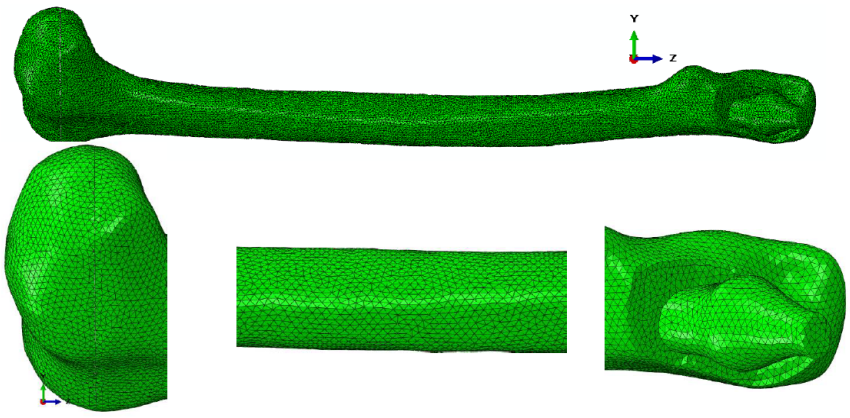

Figure 4.2.2: Volume meshing of the femur bone and the prostheses : The zoomed image shows the non manifold assembly technique which is used to mesh the different parts.

The material properties were assigned to all elements and we did not take in to account the strain rate sensitivity of the bone (cortical and trabecular) and the strain rate sensitivity of the prostheses. The bone material properties were based on the data described in [Kayabasi et al., 2007],

[Soenen et al., 2013]. The cortical bone materials properties were considered transversely isotropic: $E_1 = E_2 = 11.5$ GPa, $E_3 = 17$ GPa, $\nu_{12} = 0.51$, $\nu_{23} = \nu_{13} = 0.31$. To assign the material properties orientation, the Z axis was taken parallel with the anatomical axis of the femur. The trabecular bone materials behavior was considered linear isotropic with the following mechanical properties: $E = 2.13$ GPa, $\nu = 0.3$. The hip prosthesis was made of Cobalt Chrome alloy which is considered to be linear isotropic material with the following mechanical properties: $E = 220$ GPa, $\nu = 0.3$. The Knee prosthesis was made of Titanium alloy which was considered as a linear isotropic material with the following mechanical properties: $E = 110$ GPa, $\nu = 0.3$. No cement layer were added while it was considered that the prosthesis fully bonded (tie contact) to the bone surface thus there was no any tolerance between the bone surface and the prosthesis. A coefficient of friction of 0.2 was considered for the contact between the hip prosthesis and the bone, while it is 0.6 between the Knee prosthesis and the bone [Soenen et al., 2013]. The Finite element analysis was performed using (Abaqus 6.13, Dassault Systèmes Corp., Providence, RI, USA). The cortical wall thickness was varying from the distal part to the proximal part crossing with the femur shaft (figure.4.2.3).

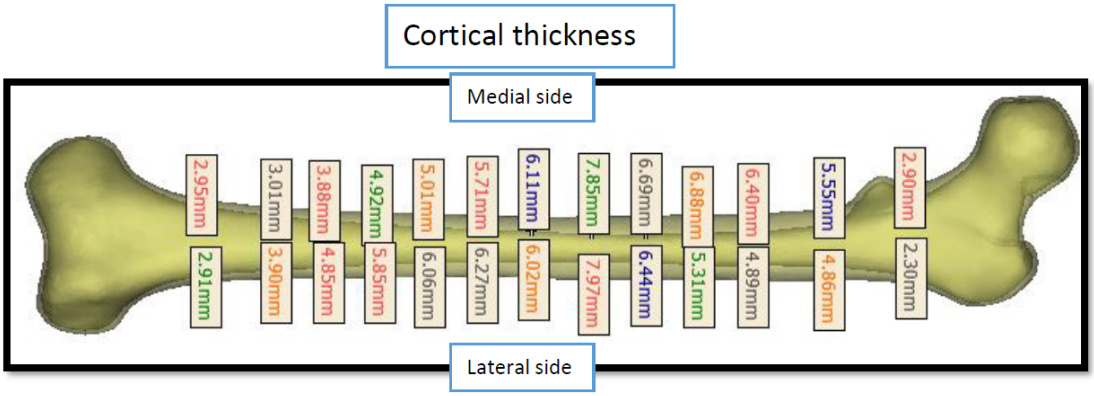

Figure 4.2.3: Cortical wall thickness along the femur on both lateral and medial sides.

4.3 Boundary Conditions

The boundary conditions were selected based on the experimental study of [Choi et al., 2015] for a voluntary forward falling. The characterization of the impact velocity is measured at a point on the hip (figure.4.3.1). The first step is the analysis of the images. The correspondence between the number of images and the time is done by assuming that the images are taken at regular time intervals, that the first one is after the first interval and that the last one is the number 22 which corresponds to a time of 533ms. This last point is consistent with the zero of the horizontal and vertical velocities. In figure (1) taken from [Choi-2015], between frames 5 and 11, the calculated interval is 22.3ms, while between 11 and 22, it is 24.2ms. Thus, there is some variability in the

measurement. A conversion is therefore proposed to the best of the values with the two scales (figure.4.3.1).The data are provided at point A and the corresponding velocities are presented as a function of time figure 1. However, the two average functions describing the horizontal and vertical velocities are derived from the experimental data of each image with a non-negligible noise. The curves are given in (figure.4.3.2)..

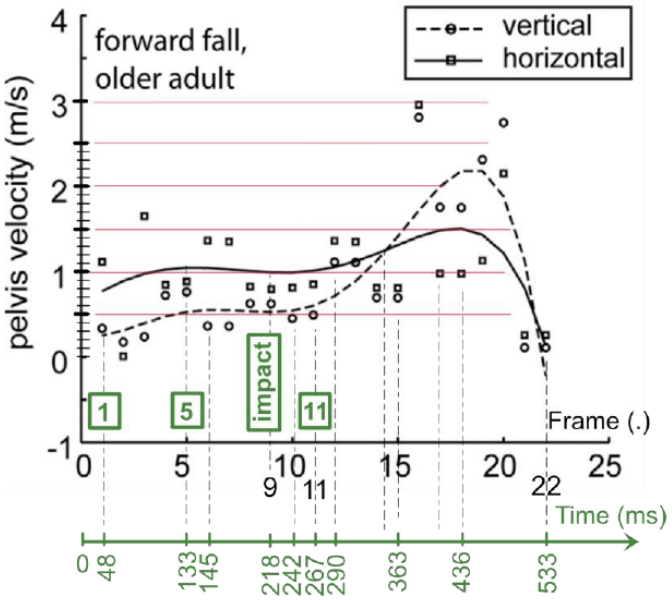

Figure 4.3.1: Speeds of the pelvis during a voluntary fall on the knee. Images extracted from [Choi et al., 2015]

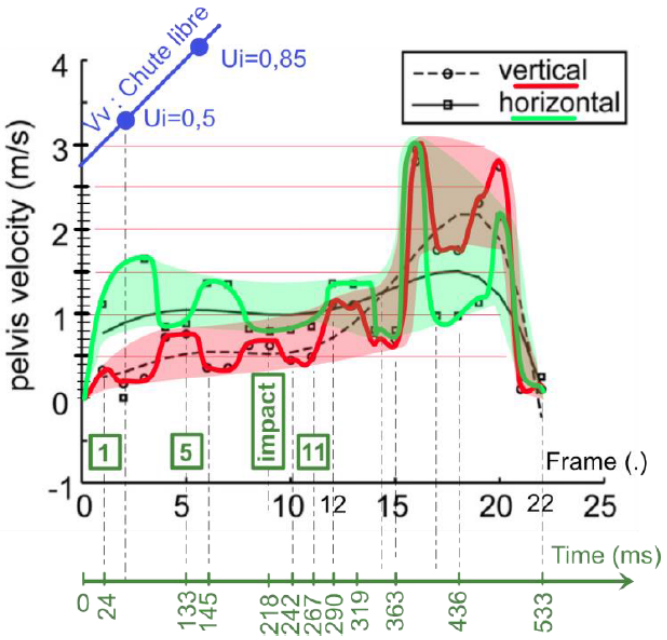

Figure 4.3.2: Envelopes of velocity curves from curves from [Choi et al., 2015]

The first image does not correspond to the beginning of the fall, this is why the free fall curve is shifted. The offset is calculated from the angle of the tibia of the first image. To perform a transfer of the measurement points and avoid the use of the average curves of figure 1, an option is to calibrate the images. This calibration is performed from the calibration grid of the article with a step of 40cm. By drawing a skeleton on the different images, it is possible to plot the jumps in displacement between two pictures. Via the corresponding time jumps, it is possible to find average values of the velocities which are reasonable if they vary little between the two considered instants. The displacement jumps are plotted in blue on (figure.4.3.3).

With the assumption of the speeds of point $B_{1\to9}$ is quite regular until the moment of impact, the moment of the shock is estimated in relation to t_5 with : $\Delta t_{5\to9} = \Delta t_{1\to5}\left(\frac{U_{5\to9}}{U_{1\to5}}\right) = 78ms.$

So the time at the moment of the shock is: $t_5 = 211.6$ ms. This value allows us to correctly place the point A_9 between A_5 and A_{11} and thus to add the position of the skeleton at the time of the shock (in yellow (figure.4.3.3).

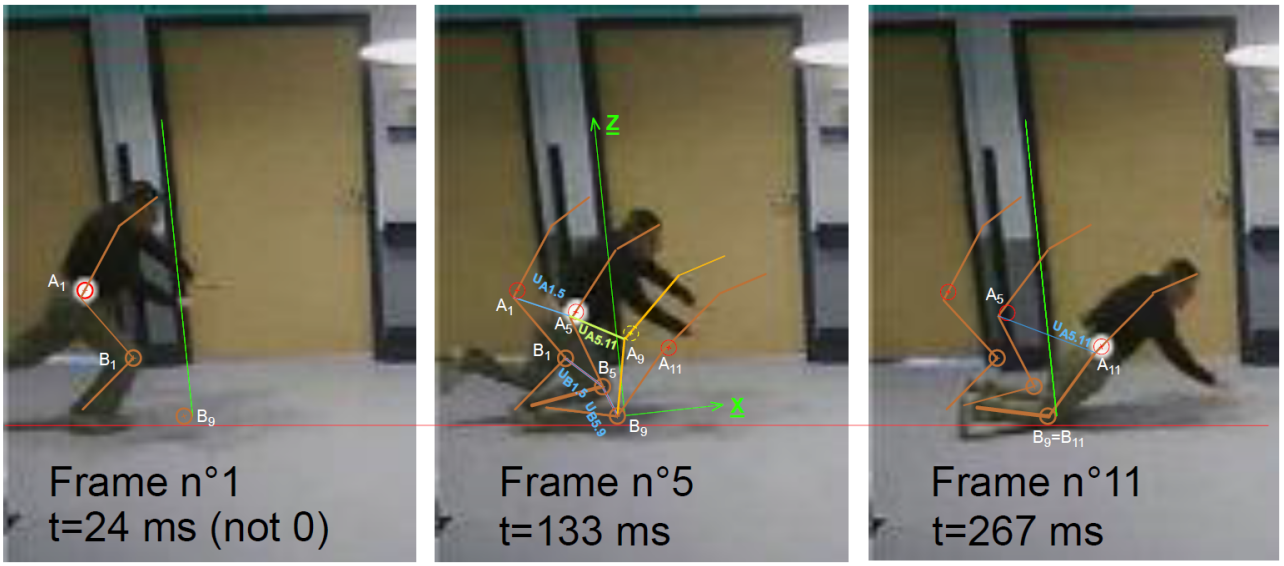

Figure 4.3.3: Kinematics of the fall via the images extracted from [Choi et al., 2015]

The obtained velocities are given in table 1. The average velocities given in table 1 are then calculated at a point P, between the two moments i and j, by :

$$V_{PH_i\cdot i} = \frac{\Delta U\rho_{i\cdot j}}{\Delta t_{i\cdot j}}\cos\left(AP_{i\cdot j}\right) \text{ and } V_{PV_i\cdot i} = \frac{\Delta U\rho_{i\cdot j}}{\Delta t_{i\cdot j}}\sin\left(AP_{i\cdot j}\right)$$

	Δt (s)	V (m/s)	V_H (m/s)
A1.5	0.109	2.669	-1.222
A5.11	0.134	3.751	-1.895
A5.9	0.078	3.75	-2.0
B1.5	0.109	1.683	-1.570
B5.9	0.078	0.38	-1.2

Table 4.3.1: Average velocities of A and B between different times. V_H represents the horizontale. velocity and V_V represents the verical velocity .

The projection of the velocity of point A of the femur versus time from [Choi et al., 2015] (Figure.4.3.4) is 3.75 m/s in X-direction and - 2 m/s in Y-direction

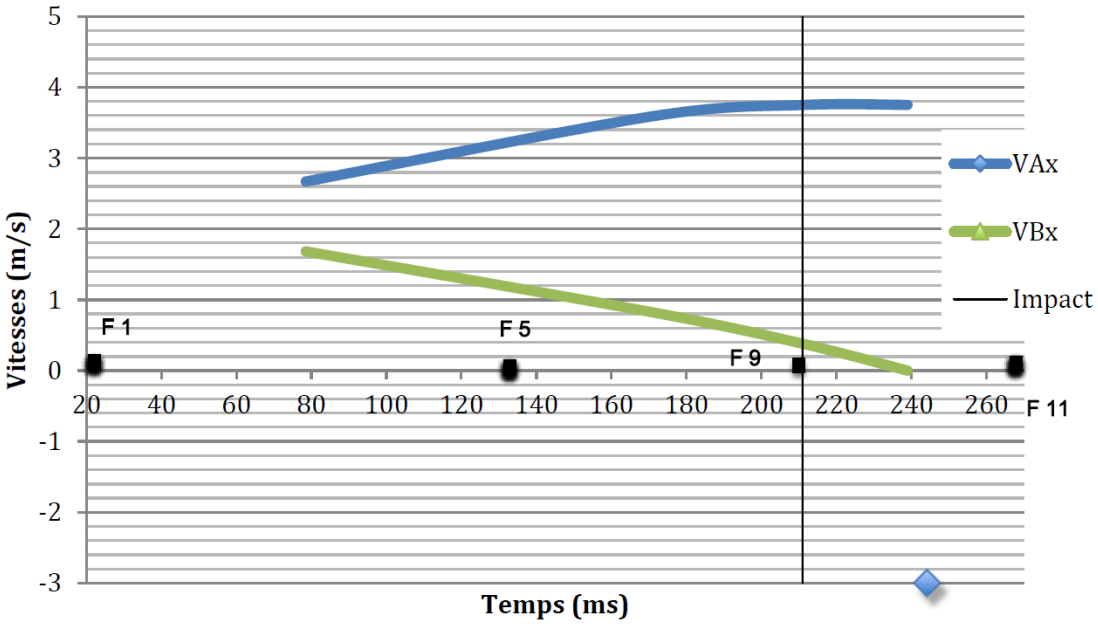

Figure 4.3.4: Projections of the velocity of point A of the femur versus time from [Choi et al., 2015]

The speed of A is very regular even after the impact. This allows a correct interpolation of this velocity at the time of impact. On the other hand, point B shows a value with a gradient before the impact and a value affected by the impact. It is therefore easier to use the femur rotation speed. Considering all the kinematics, there appears to be a change in the position of the femur at the time of impact (t_9) compared to the position at time t_5. The reading in (figure.4.3.5) of the angle between (-x) and (B_9A_9) gives: 102.5°.

The coordinates of the vector $\underline{BA}$ give the orientation of the femur:

$$\underline{BA}^t = \text{(-0.03668 m ; 0 ; -0.42432 m)} \qquad \underline{n}^t = \frac{BA^t}{\|\underline{BA}\|} = \text{(0.2213 ; 0 ; 0.9752)}$$

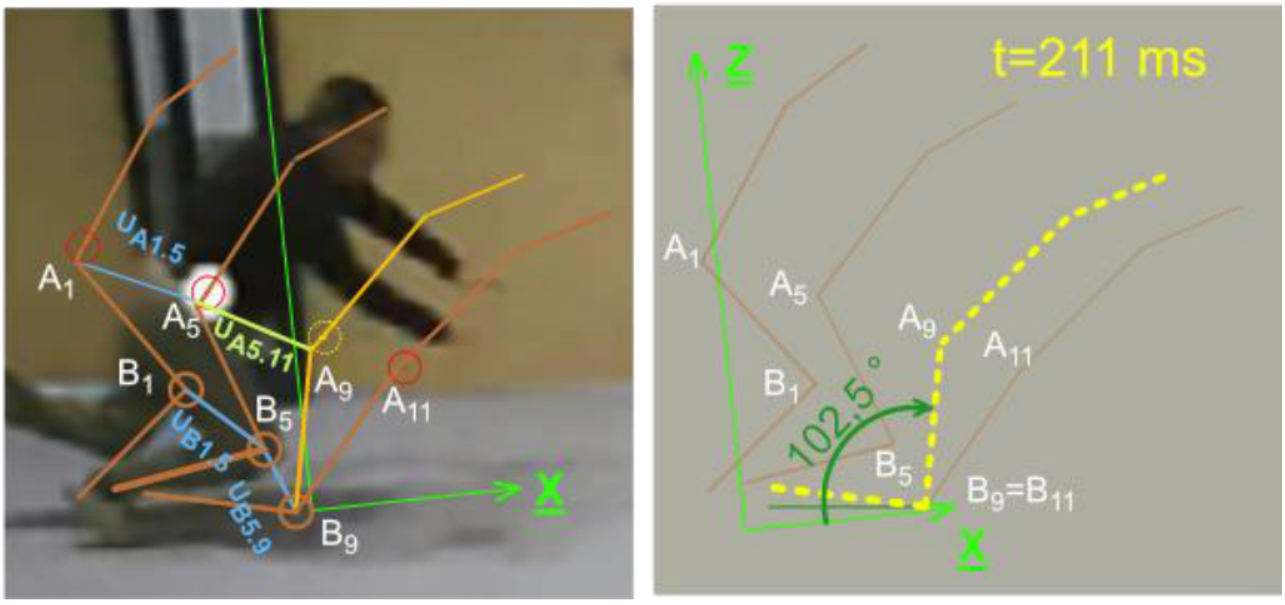

Figure 4.3.5: Angle of the femur during a voluntary fall on the knee on images extracted from [Choi et al., 2015]

The angle of the femur for each frame (1, 5, 9, 11) is obtained by direct measurements on the graphs and plotted below against times (figure.4.3.6. The angular velocities are given by the discrete slopes between two points (figure.4.3.6. The angular velocity of the femur (in rd/s) : ω $\underline{y}$ (here, rotation of z to x so ω>0).

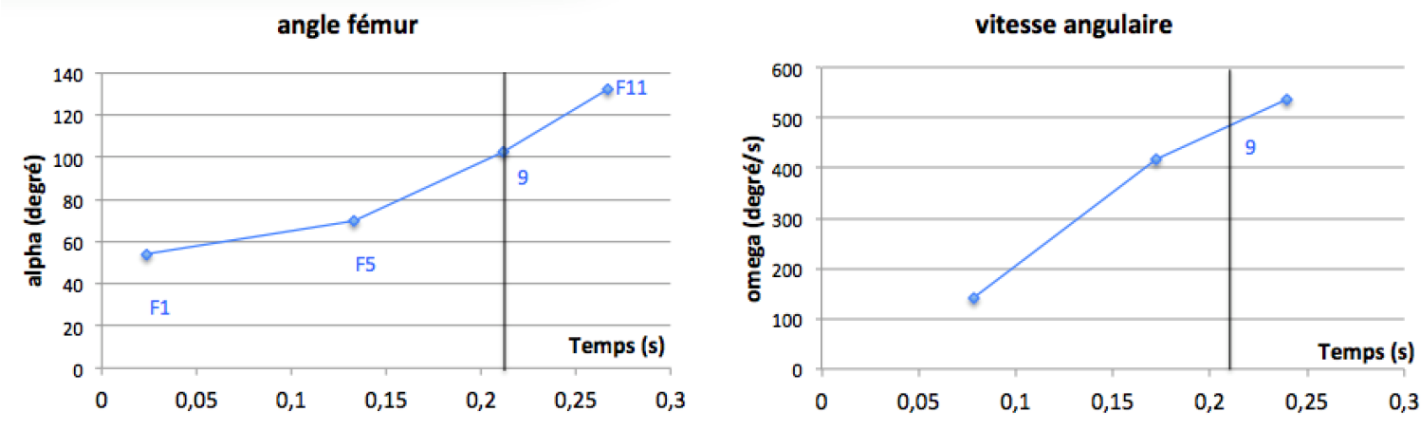

Figure 4.3.6: Angles and angular velocities of the femur versus time

At the moment of impact, we find an angular velocity of : $\omega_9 = 487°/s = 8.50$ rd/s.
To enter this simulation data of the impact on the knee which is consistent with a solid displacement, it is therefore based on the following kinematic torsor:

$$\varepsilon_{femur} = \begin{cases} \omega_{femur}\underline{y} \\ \underline{V}_A \end{cases}$$

$$\text{The velocity at point A: } \underline{V_A} = \begin{pmatrix} v_{Ax} \\ v_{Ay} \\ v_{Az} \end{pmatrix} = \begin{pmatrix} 3 \cdot 75m/s \\ 0 \\ -2 \cdot 0m/s \end{pmatrix}$$

$$\text{Angular velocity : } \omega_{femur} = 8.50 \text{ rd/s}$$

$$\text{Impact angle : } \theta_{femur} = 102.5 \text{ degree}$$

Finally, in order to implement the model in the FE simulation, the floor was assumed to be a rigid surface and the gap between the knee prosthesis and the floor is 0.07mm. The total mass of the femur was assumed to be 6 kg [NASA link]

4.4 Results

We analyzed the distribution of the equivalent stress at the time of the collision, the stress analysis allows us to know well the stress concentration area. In the presented results, we will determine the distribution of the stresses for four different cases of impact as following:

- Forward falling of a full femur bone.
- Forward falling of a femur bone with a TKR (only knee component).
- Forward falling of a femur bone with THR and TKA (with a knee prosthesis of 180 mm length).
- Forward falling of a femur bone with THR and TKA (with a knee prosthesis of 220 mm length).

We note the distribution of the stresses for the four models of impact at the moment of collision of 0.34 ms

For all the simulations the results (figure.4.4.1), (figure.4.4.4), (figure.4.4.7), (figure.4.4.8), (figure.4.4.11), (figure.4.4.12) show that the maximum stresses are concentrated distally around the femur shaft near to the knee. The distal part receives the first load of the impact. In order to plot the resultant moment across the femur for each case (figure.4.4.2, (figure.4.4.6, (figure.4.4.10, (figure.4.4.14; the femur bone has been divided to 73 section and the moment is calulcated at each section (figure.4.4.3), (figure.4.4.5), (figure.4.4.9), (figure.4.4.13).

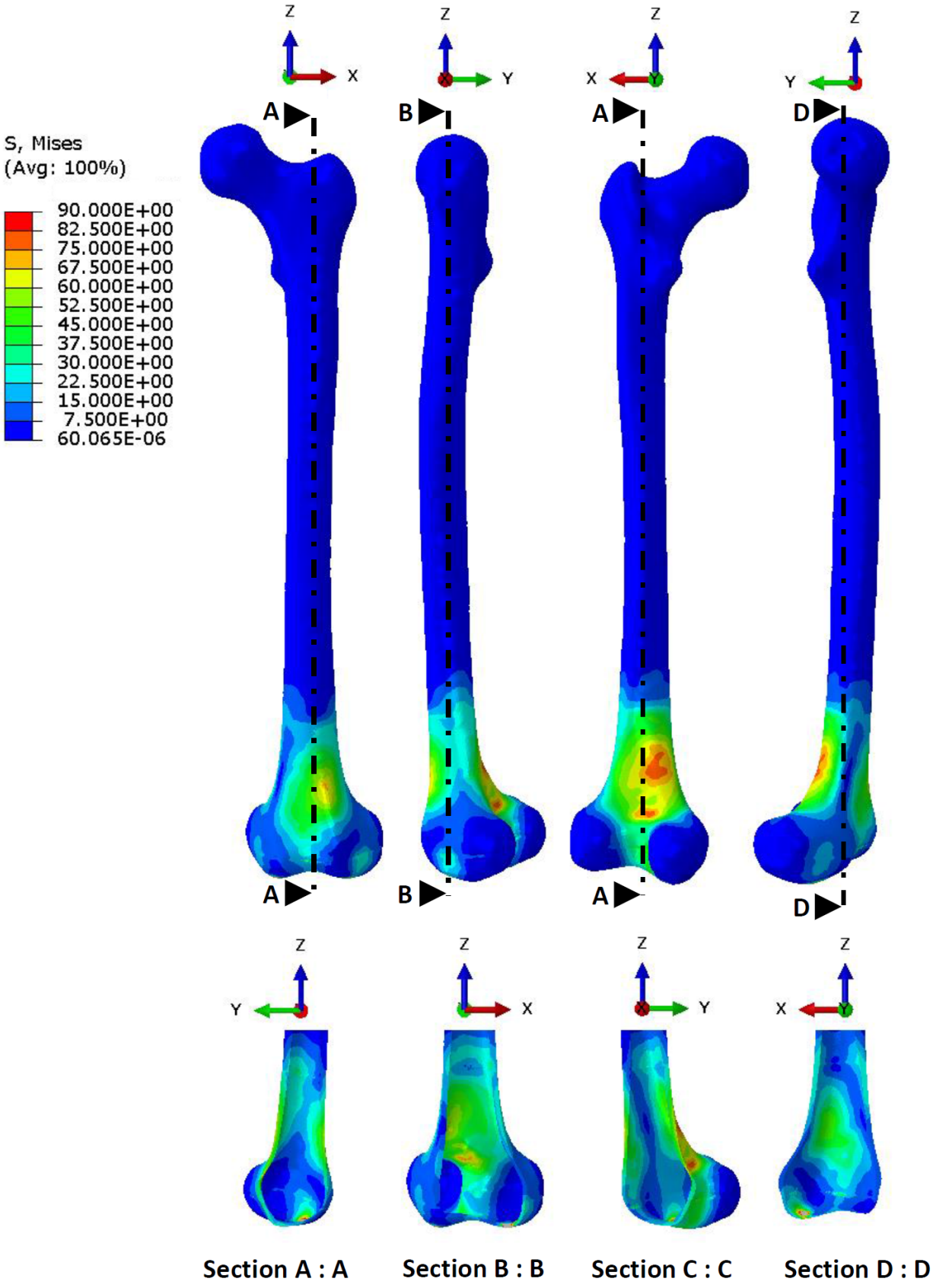

Figure 4.4.1: Distribution of the equivalent Von Mises stress [MPa] outside and inside the cortical layer of a femur without any prosthesis under a forward falling impact simulation at the moment of impact.

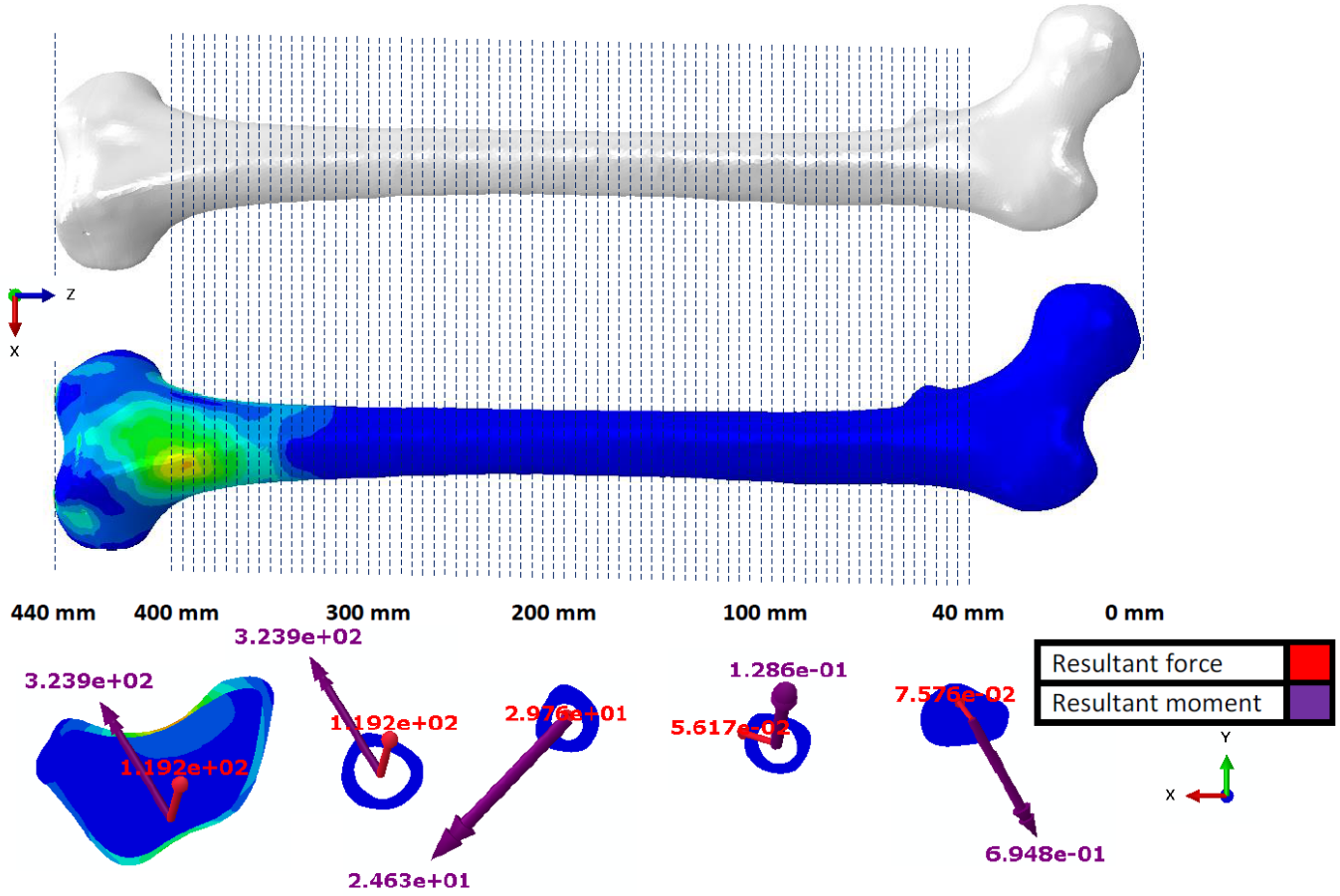

Figure 4.4.2: The full femur surface has been divided in 73 section from 40 mm to 400 mm with a step of 5 mm to calculate the moment in each step.

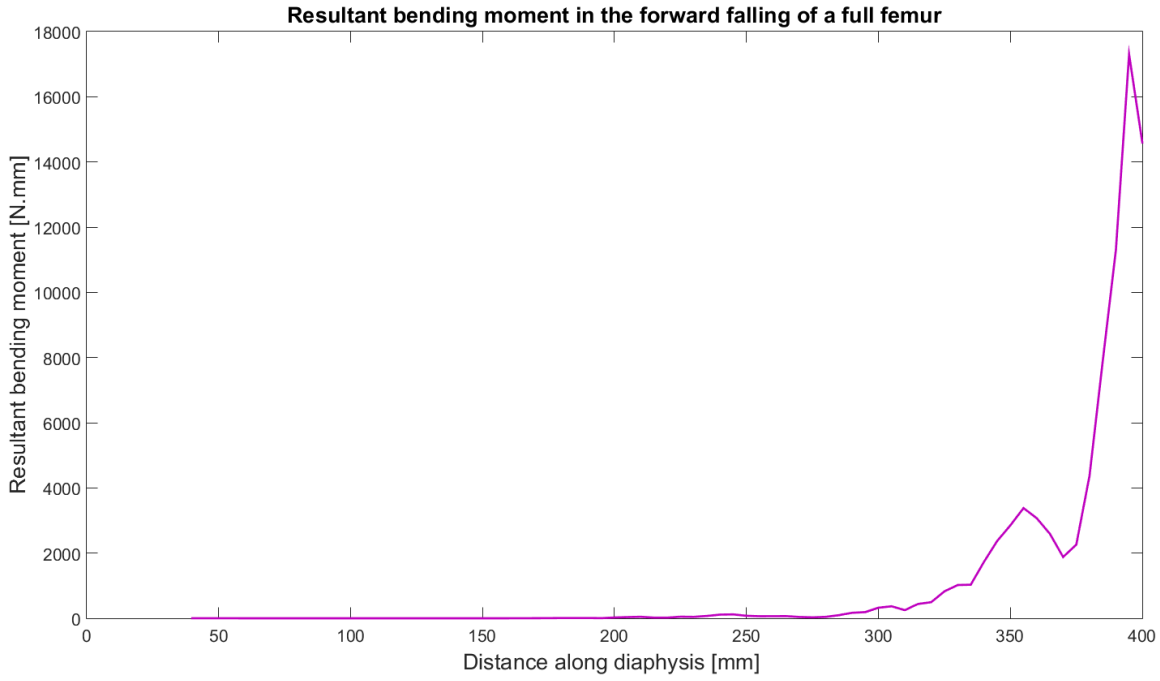

Figure 4.4.3: Resultant moment across a femur without any prosthesis after a forward falling impact at the moment of the impact

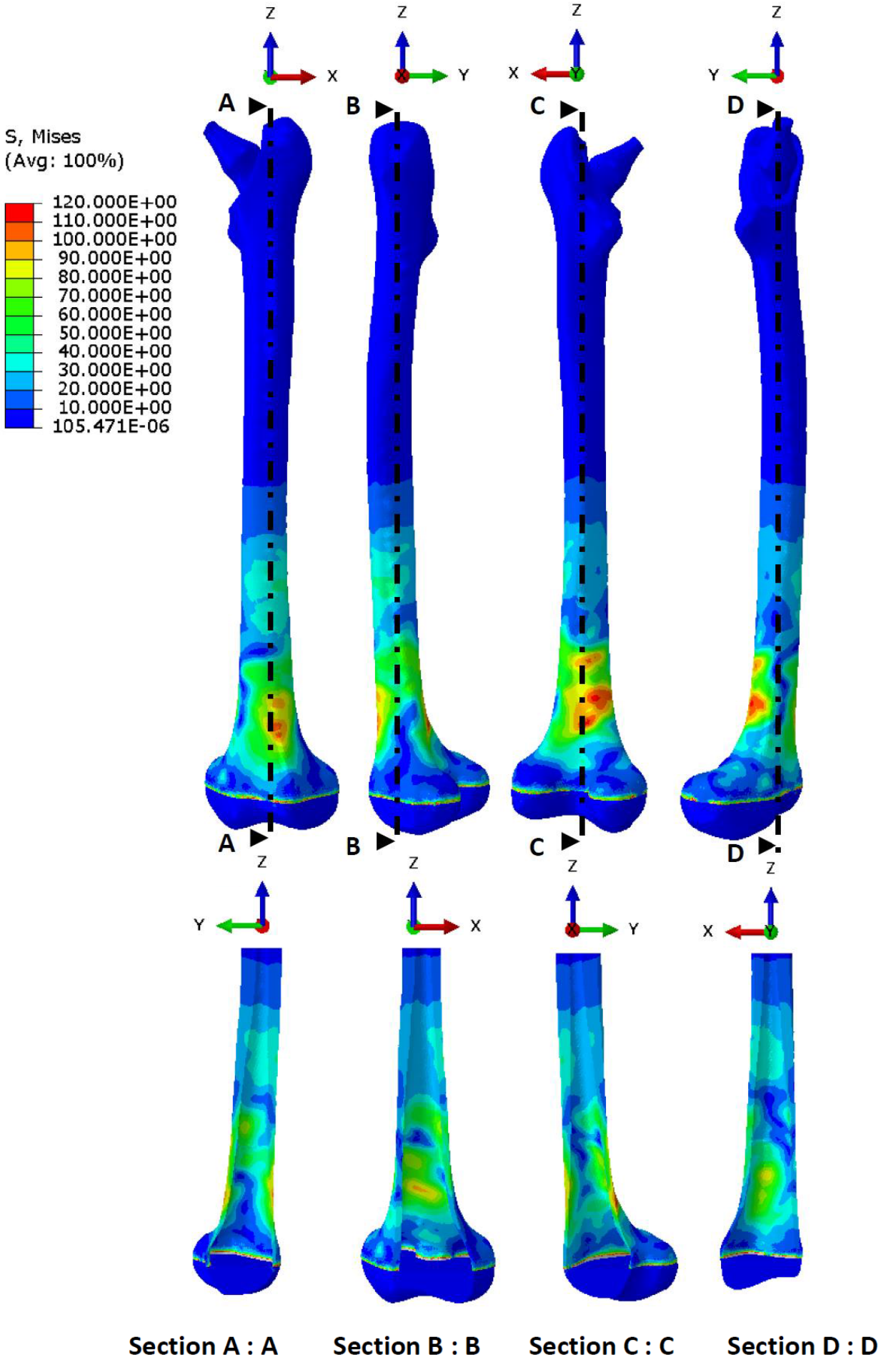

Figure 4.4.4: Distribution of the equivalent Von Mises stress [MPa] outside and inside the cortical layer of a femur with a knee prosthesis replacement (only knee component) under a forward falling impact simulation at the moment of impact

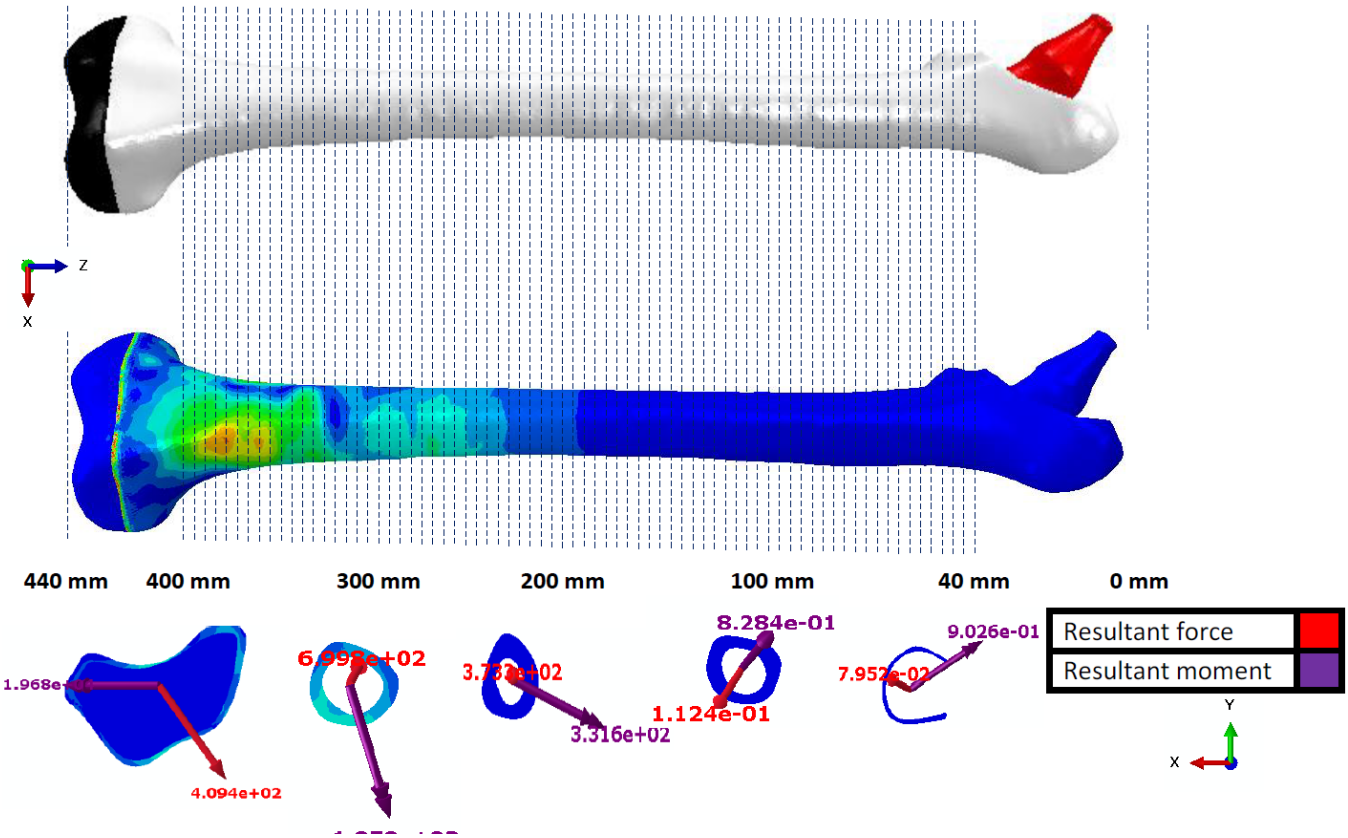

Figure 4.4.5: The femur with only knee component has been divided in 73 section from 40 mm to 400 mm with a step of 5 mm to calculate the moment in each step.

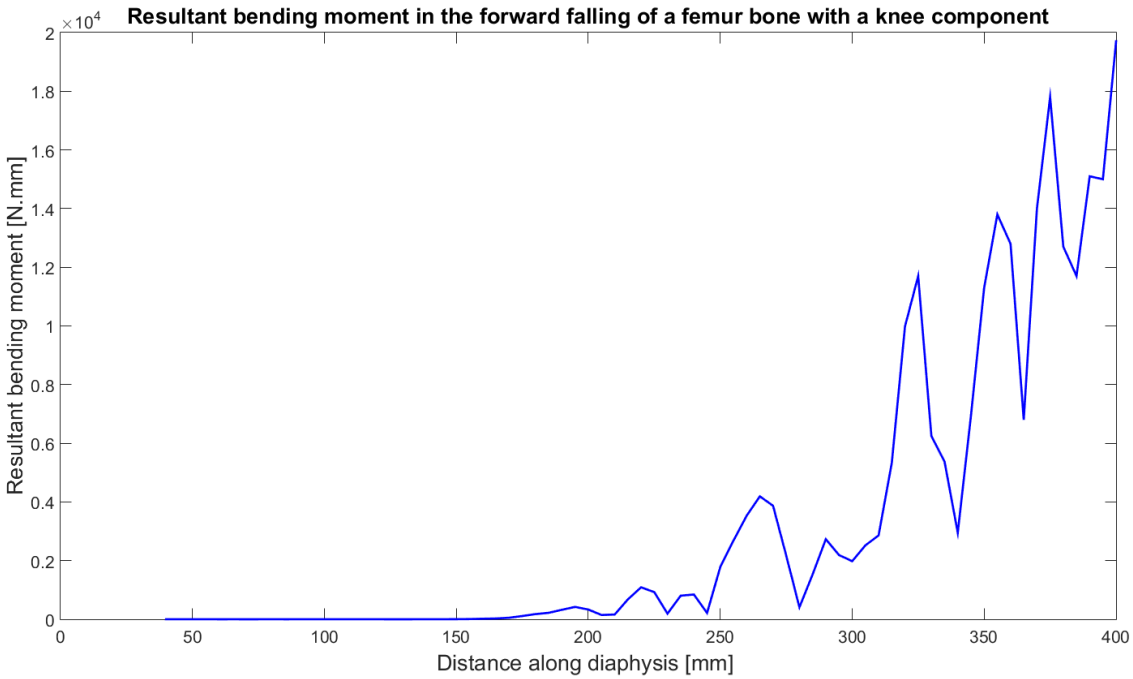

Figure 4.4.6: Resultant moment across a femur with a knee prosthesis replacement (only knee component) under a forward falling impact simulation at the moment of impact

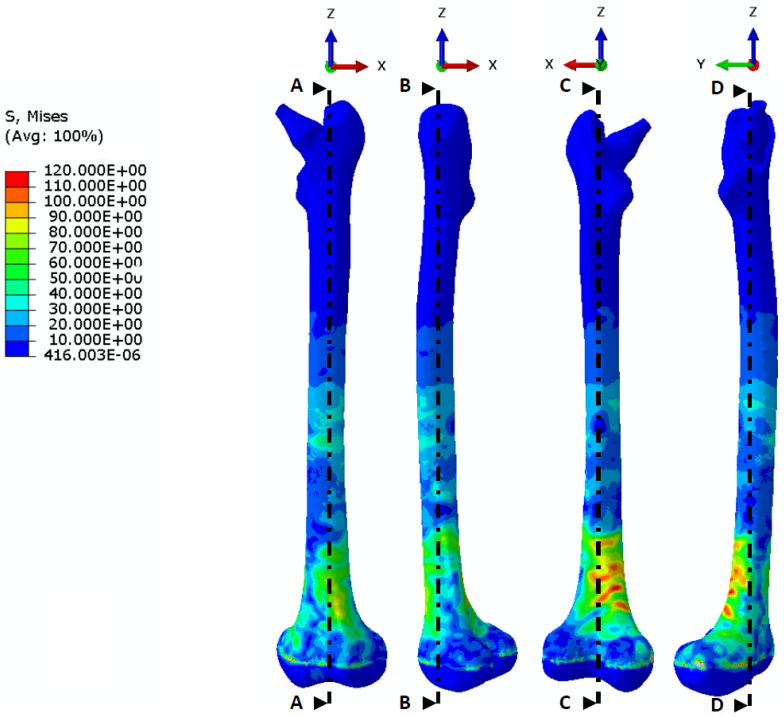

Figure 4.4.7: Distribution of the equivalent Von Mises stress [MPa] in the outer surface of the cortical layer of a femur with a THR and TKR replacement (knee prosthesis of 180 mm length) under a forward falling impact simulation at the moment of impact

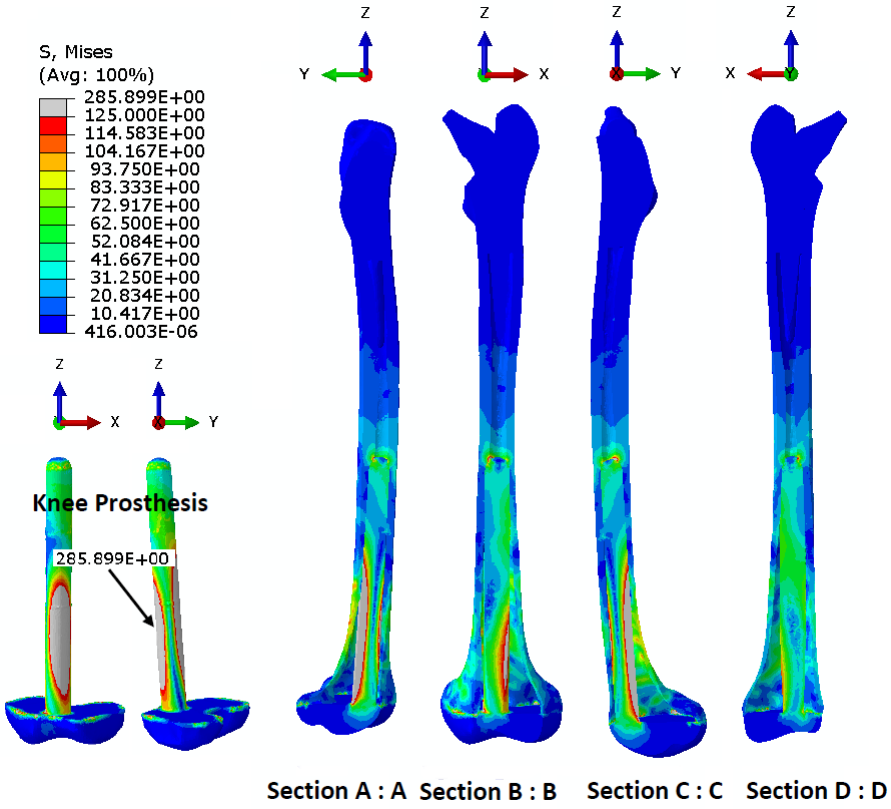

Figure 4.4.8: Cross sections of the femur with a THR and TKR (knee prosthesis of 180 mm length) shows the equivalent Von Mises stress [MPa] inside the cortical bone layer and the equivalent Von Mises stress [MPa] on the kne prosthesis.

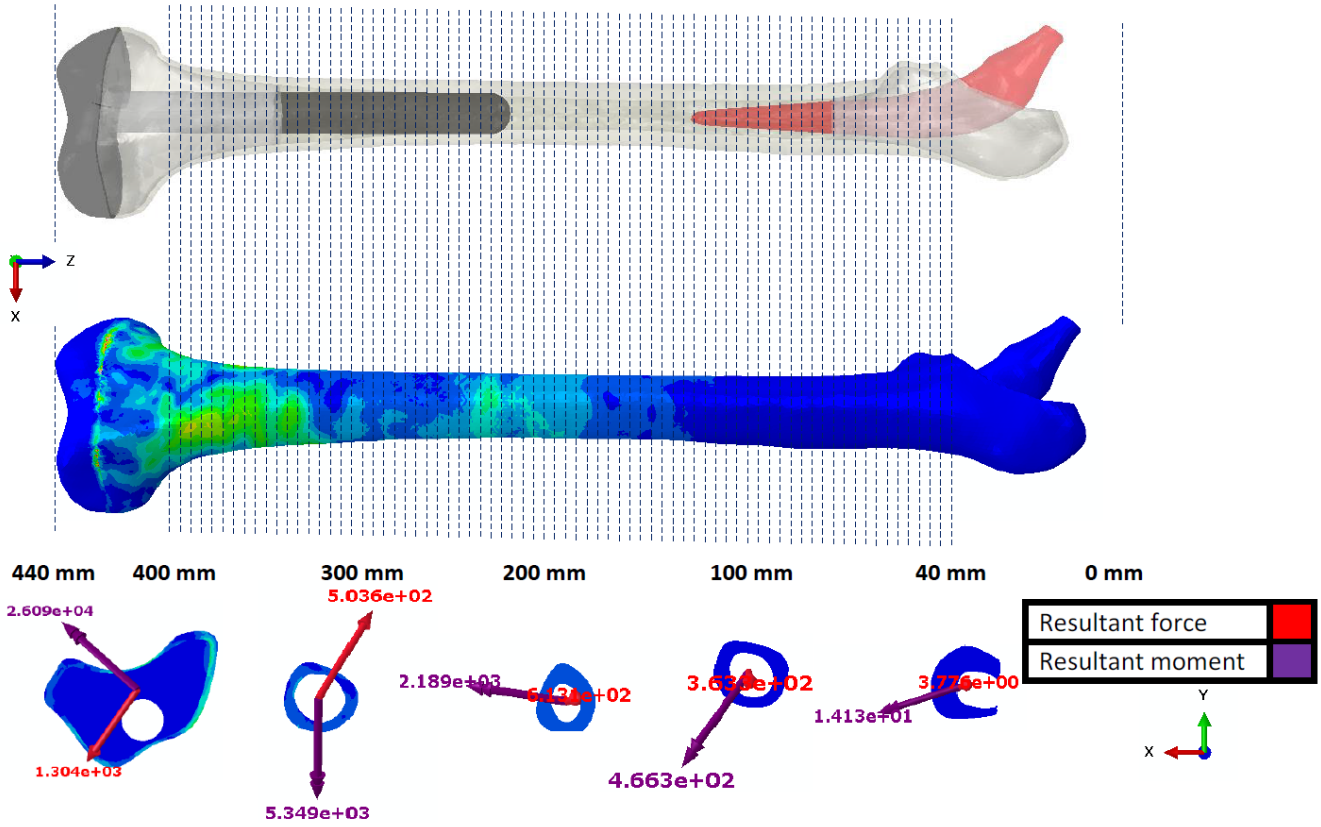

Figure 4.4.9: The femur with a THR and TKR (knee prosthesis of 180 mm length) has been divided in 73 section from 40 mm to 400 mm with a step of 5 mm to calculate the moment in each step

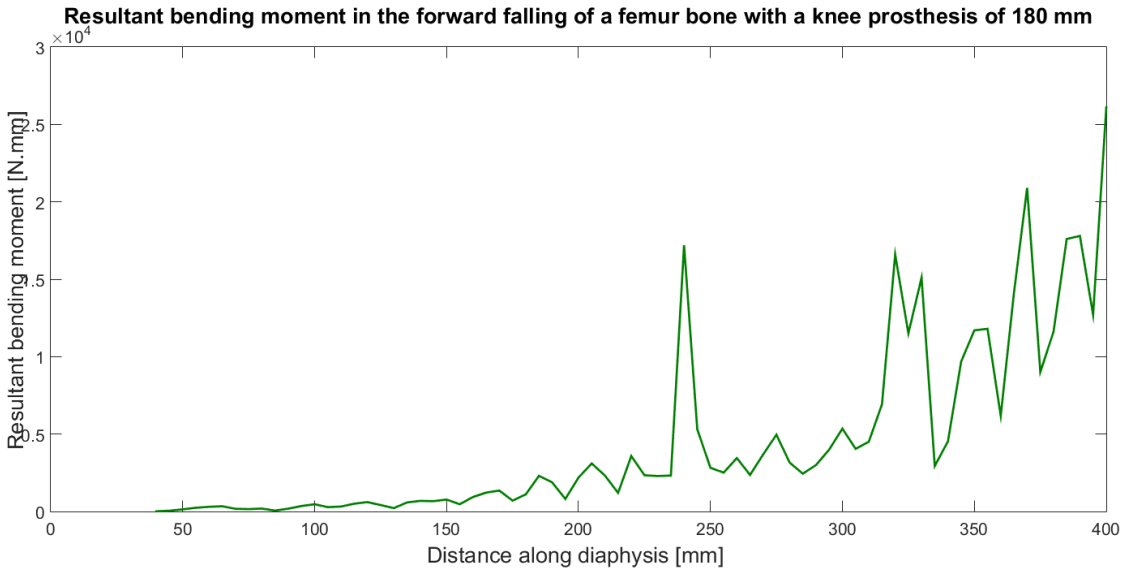

Figure 4.4.10: Resultant moment across a femur with a THR and TKR (knee prosthesis of 180 mm length) under a forward falling impact simulation at the moment of impact

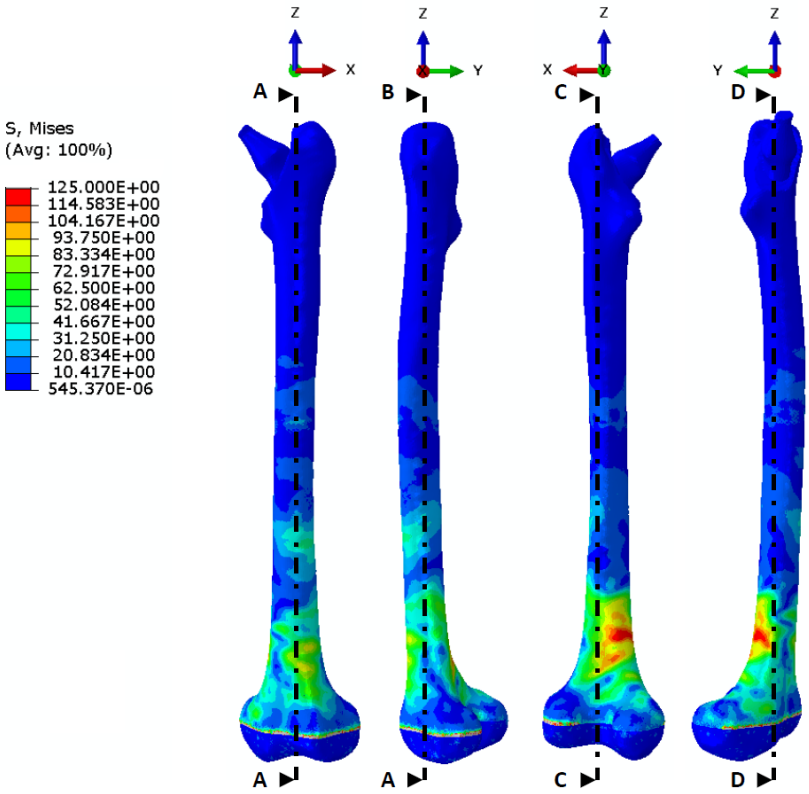

Figure 4.4.11: Distribution of the equivalent Von Mises stress [MPa] in the outer surface of the cortical layer of a femur with a THR and TKR replacement (knee prosthesis of 220 mm length) under a forward falling impact simulation at the moment of impact

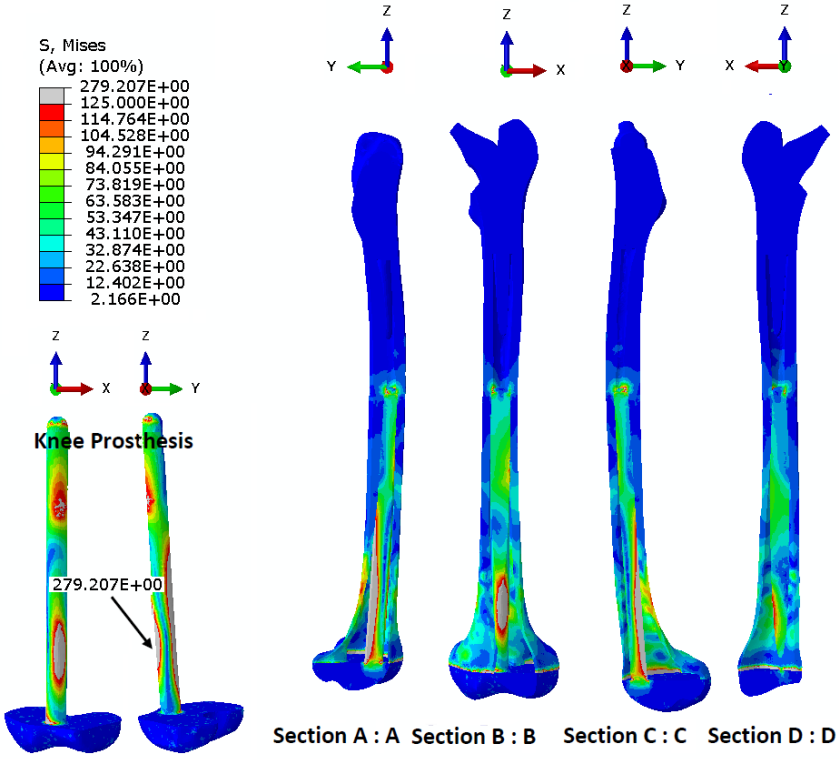

Figure 4.4.12: Cross sections of the femur with a THR and TKR (knee prosthesis of 220 mm length) shows the equivalent Von Mises stress [MPa] inside the cortical bone layer and the equivalent Von Mises stress [MPa] on the kne prosthesis.

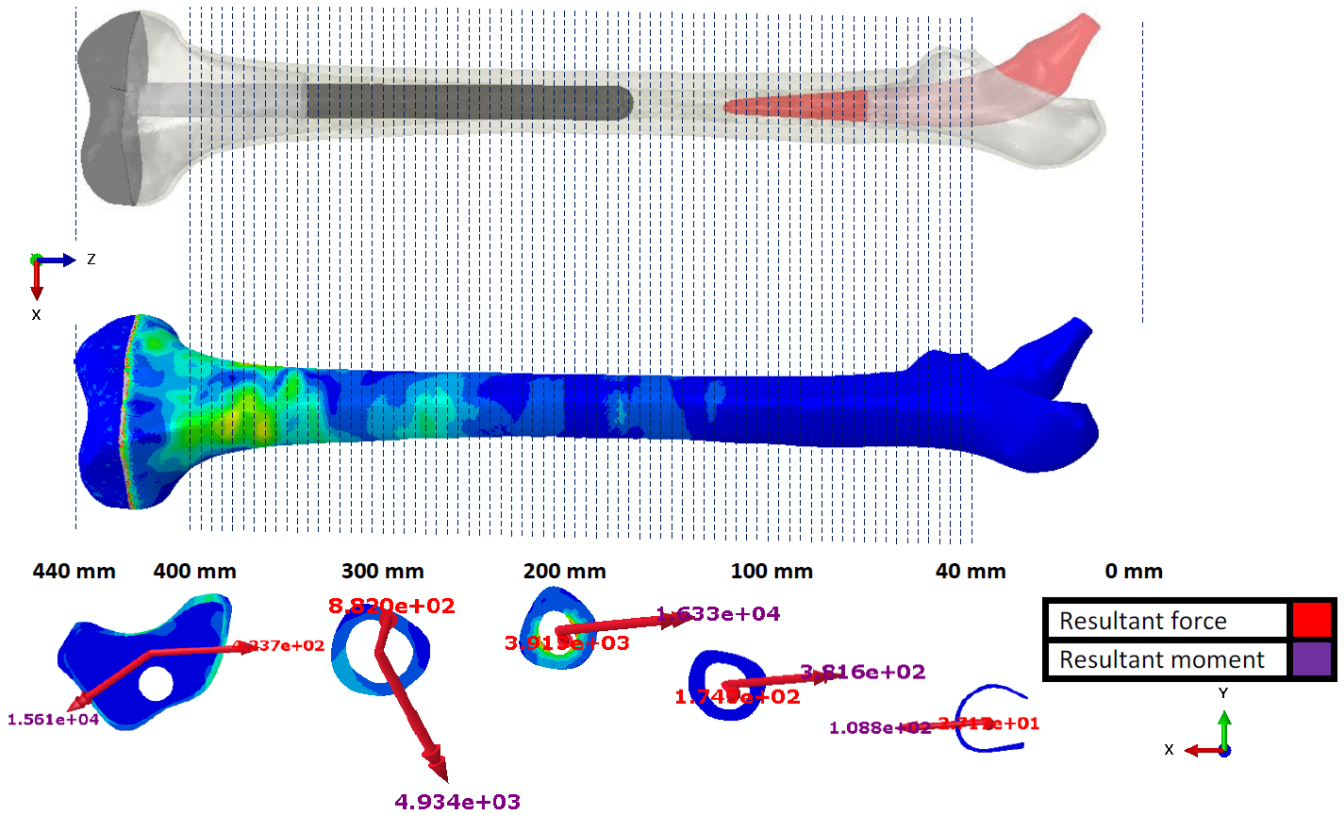

Figure 4.4.13: The femur with a THR and TKR (knee prosthesis of 220 mm length) has been divided in 73 sections from 40 mm to 400 mm with a step of 5 mm to calculate the moment in each step

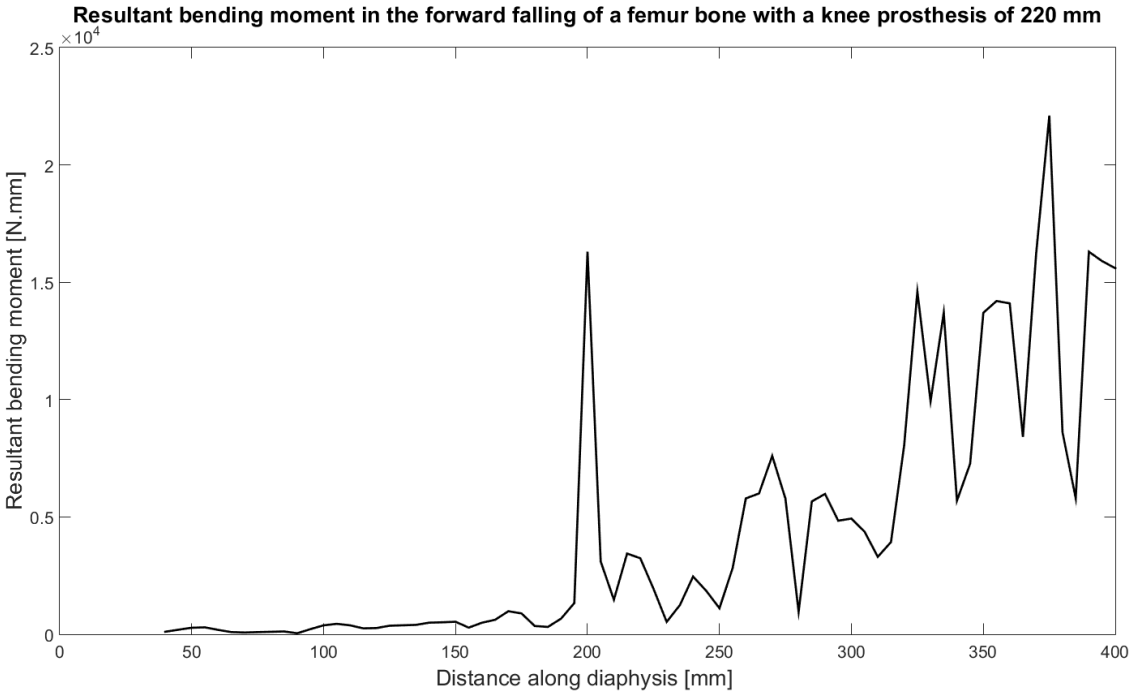

Figure 4.4.14: Resultant moment across a femur with a THR and TKR (knee prosthesis of 220 mm length) under a forward falling impact simulation at the moment of impact

For all the simulations the results in (figure.4.4.1), (figure.4.4.4), (figure.4.4.7), (figure.4.4.8),

(figure.4.4.11), (figure.4.4.12) shows the maximum stresses are concentrated distally around the femur shaft near to the knee, while the distal part receives the first load of the impact. In order to plot the resultant moment across the femur for each case (figure.4.4.2, (figure.4.4.6, (figure.4.4.10, (figure.4.4.14; the femur bone has been divided to 73 section and the moment is calculated at each section (figure.4.4.3), (figure.4.4.5), (figure.4.4.9), (figure.4.4.13).

4.5 Conclusion

These results are in agreement with the medical point of view while the forward falling in a femur with both total hip and total knee replacement causes a fracture in the distal part around the knee prosthesis. The maximum bending moment always appears in the distal zones. Installing a preventive plate around the area of the high bending moment will reduce the risk of fracture and thus prevent additional operations.

General conclusion

Due to the increasing ageing population, it has been observed that there is a significant increase in the number of operations leading to knee prosthesis and then, a few years later, to hip prosthesis. Few studies have been done on the influence of the presence of these prostheses on the risk of femur fracture and even fewer on how to prevent it. The literature review identified existing contradictions in the identification and calculation of the risk of fracture of biprosthetic femurs. In this context, our study focused on the risk of fracture of biprosthetic femurs by analyzing different loading cases. For this purpose, we used numerical tools to study the risk of fracture of bi-prosthetic femurs. After evaluating the literature, the objective of the next two chapters is to identify the influence of IP distances using different loading conditions and to predict in terms of deformation patterns the critical locations that may be exposed to fracture. One of the solutions to prevent this risk of fracture would be the implementation of a preventive locked plate.

Using a simplified geometry of the femur, four load cases were simulated in this work, with the aim of better understand the factors involved in fracture risk (FR) in the human femur. The results show the effect of different stem lengths in several bending tests. Nevertheless, these simulations are still considered too simplistic to draw conclusive results. The results of this study show that with a constant fixed imposed moment, the inter prosthetic distance has no significant effect on the risk of developing an IP fracture of the femur. By using a different stem length, the elasticity of the femur changes. Thus, in the region where the prosthetic stem is present, the stiffness is higher, and the bending deformation is therefore lower than in the region without the stem. The existence of the prosthetic stem results in lower deformation in the prosthetic regions than in the IP regions. Fracture is expected to occur in the space region depending on the loading condition.

Then, we have analyzed the effect of a real femur geometry on the stress distribution for quasi-static loading cases. We have also analyzed how this distribution varied by varying the loading cases (4pt bending, 2pt symmetrical and non-symmetrical bending) while keeping the same inter prosthetic distance. Then we have modified the length of the knee stem to vary the inter prosthetic distance for the same loading case. The parameters set for the comparisons were Maximum Force, Maximum Displacement, Maximum Energy. In all configurations tested, if the loading imposed is an instantaneous force in pure bending or in loading equivalent to a gait cycle, the length of the knee prosthesis stem is not decisively related to the risk of fracture. By using a different stem length, the elasticity of the femur changes. Thus, in the region where the prosthetic stem is present, the stiffness was higher, so that the bending deformation was lower than in the gap region. The existence of the

prosthetic stem leads to less strain in the prosthetic regions than in the PI regions. Fracture should occur in the IP gap region depending on the loading condition. To validate the modeling without having test results on anatomical parts, several simulations presented in [Soenen et al., 2013], [Weiser et al., 2014] and [Quirynen, 2016], were replicated with similar conclusions, except for the 4-point bending tests in [Soenen 2013], which gave identical results but different conclusions. Indeed, the results of the modeling agree with those of the literature for both group 1 and group 2 of knee prosthesis stems. It is therefore reasonable to use this tool for the study of bi prosthetic femurs. Our conclusions are that, for the classical loads of walking or pure flexion, the variations of prosthesis implantations and in particular of knee prosthesis stem length, with a constant imposed force, do not modify the fracture risk. On the other hand, the use of the model shows that the risk of fracture is strongly dependent on the bone quality and the thickness of the cortical part of the diaphysis. If this criterion is used as a basis for implanting or not implanting a reinforcement plate, the results show that the customization of the geometric model implanted in our approach is essential. Another use of this linear elastic modeling, is the possibility to change the fixed parameter for RF comparisons with different knee prosthesis stem lengths. The loading can be quantified by kinetic energy when it corresponds to a forward fall or a small shock. Double prosthesis implantation is often performed on elderly people whose fall from a standing position is very common and frequently results in fractures. With this case of low energy load, to estimate the risk of fractures, it is more reasonable to consider that it is the elastic energy level before rupture that is a constant quantity and not the force imposed which does not correspond in bending to a physiological situation. In this case, the finite element calculations are identical, but a quantification of the displacement of the loading points allows to measure the energy introduced. The use of the linearity of the behavior allows to correct the stresses obtained for a given energy level. In this case, our model allows a different interpretation of the results because the reduction of the inter prosthetic distance is then directly linked to an increase in the risk of fracture. This shows that the bone between the two prostheses is the weakest section of the construct. Thus, our results are consistent with the results of [Iesaka et al., 2005], [Weiser et al., 2014], [Quirynen, 2016] when the prosthesis does not act as a stress concentrator, nor does it increase fracture risk. Furthermore, our results suggest that the tip of any prosthesis should be located in an area with sufficient cortical wall thickness. Accordingly, we noted that the criteria for selecting the IP space should be based on femoral morphology, and bone quality. If the elastic energy of the femur before fracture is the fixed parameter of the study, it is obvious that the presence of a plate increases the moment to be transmitted, but decreases the stress seen by the cortical bone. However, in order to quantify the risk of fracture, it would be necessary to ensure that the fixation screws can effectively transmit the loads from the plate to the bone. This section is not complete and should be

placed in the context of this work.

The last part of the thesis was dedicated to numerical study to investigate and detect the areas of high bending moment in a human femur during a low energy impact of a forward fall. The detection of these areas of maximum moment will give us the ability to impose these moments using an experimental setup developed in-house of a two-point bending test. The validation between the numerical simulations and the experimental work will give significant information about the possible fracture zones around the knee implant, so it will be used to achieve the research objective by designing and optimizing a preventive fracture plate that can be used in a femur with ATH and ATG. The results show that the stress concentration area always appeared in the distal zones around the knee joint. These results agree with the medical point of view while the forward falling in a femur after a forward falling on the knee prosthesis. The presence of the hip's prosthesis nor the length of the knee stem showed any changing in the resultant maximum bending moment around the knee stem. It will be recommended to put in consideration this area in the design of the preventive plate. The validation of all the presented results will be a future step by using the ROHF test designed by Dr. Christophe CLUZEL, LMT Paris Saclay, in collaboration with this study.

Bibliography

[Agarwal, 2004] Agarwal, S. (2004). Osteolysis—basic science, incidence and diagnosis. *Current Orthopaedics*, 18(3):220–231. 70

[Albareda et al., 2017] Albareda, J., Gómez, J., Ezquerra, L., and Blanco, N. (2017). Interprosthetic femoral fractures: Treatment with a lateral angular-stable plate. *Revista Española de Cirugía Ortopédica y Traumatología (English Edition)*, 61(1):1–7. 72

[An et al., 2000] An, Yuehuei, A. D., and Robert (2000). *Mechanical Testing of Bone and the Bone–Implant Interface*. 54

[Arneson et al., 1988] Arneson, T. J., Melton, L. J., Lewallen, D. G., and O'Fallon, W. M. (1988). Epidemiology of diaphyseal and distal femoral fractures in rochester, minnesota, 1965-1984. *Clinical orthopaedics and related research*, (234):188–94. 60

[Ashman et al., 1988] Ashman, Richard.B, R., and Young, J. (1988). Elastic modulus of trabecular bone material. *Journal of biomechanics*, 21(3):177–181. 56

[Ashman and Rho, 1988] Ashman, R. B. and Rho, J. Y. (1988). Elastic modulus of trabecular bone material. *Journal of Biomechanics*, 21(3):177 – 181. 57

[Bah and Browne, 2003] Bah, M. and Browne, M. (2003). Probabilistic analysis of a cemented hip implant. 104

[Bayraktar et al., 2004] Bayraktar, H. H., Morgan, E. F., Niebur, G. L., Morris, G. E., Wong, E. K., and Keaveny, T. M. (2004). Comparison of the elastic and yield properties of human femoral trabecular and cortical bone tissue. *Journal of Biomechanics*, 37(1):27–35. 55, 56, 74, 90, 112

[Beck et al., 2009] Beck, T. J., Petit, M. A., Wu, G., LeBoff, M. S., Cauley, J. A., and Chen, Z. (2009). Does Obesity Really Make the Femur Stronger? BMD, Geometry, and Fracture Incidence in the Women's Health Initiative-Observational Study. *Journal of Bone and Mineral Research*, 24(8):1369–1379. 58

[Bengnér et al., 1990] Bengnér, U., Ekbom, T., Johnell, O., and Nilsson, B. E. (1990). Incidence of femoral and tibial shaft fractures. epidemiology 1950-1983 in malmö, sweden. *Acta orthopaedica Scandinavica*, 61(3):251–4. 60

[Berry, 1999] Berry, D. J. (1999). EPIDEMIOLOGY: Hip and Knee. *Orthopedic Clinics of North America*, 30(2):183 – 190. 62

[Bettamer et al., 2017] Bettamer, A., Hambli, R., Allaoui, S., and Almhdie, A. (2017). Using visual image measurements to validate a novel finite element model of crack propagation and fracture patterns of proximal femur. *Computer Methods in Biomechanics and Biomedical Engineering: Imaging and Visualization*, 5:251–262. 71

[Bras et al., 2004] Bras, A., Laporte, S., Bousson, V., Mitton, D., de Guise, J., D Laredo, J., and Skalli, W. (2004). 3d reconstruction of the proximal femur with low-dose digital stereoradiography. *Computer aided surgery : official journal of the International Society for Computer Aided Surgery*, 9:51–7. 71

[Brown et al., 2013] Brown, J. L., Kumbar, S. G., and Laurencin, C. T. (2013). Chapter ii.6.7 - bone tissue engineering. In Ratner, B. D., Hoffman, A. S., Schoen, F. J., and Lemons, J. E., editors, *Biomaterials Science (Third Edition)*, pages 1194 – 1214. Academic Press, third edition edition. 57

[Browne et al., 1999] Browne, M., Langley, R., and Gregson, P. (1999). Reliability theory for load bearing biomedical implants. *Biomaterials*, 20(14):1285–1292. 104

[Bruyère Garnier et al., 1999] Bruyère Garnier, K., Dumas, R., Rumelhart, C., and Arlot, M. (1999). Mechanical characterization in shear of human femoral cancellous bone: torsion and shear tests. *Medical Engineering & Physics*, 21(9):641–649. 57

[Caeiro et al., 2013] Caeiro, J., González, P., and Guede, D. (2013). Biomechanics and bone (ii): Trials in different hierarchical levels of bone and alternative tools for the determination of bone strength. *Rev. Osteoporosis Metab. Miner.*, 5:1–13. 57

[Carballido-Gamio et al., 2015] Carballido-Gamio, J., Bonaretti, S., Saeed, I., Harnish, R., Recker, R., Burghardt, A., H. Keyak, J., Harris, T., Khosla, S., and Lang, T. (2015). Automatic multi-parametric quantification of the proximal femur with quantitative computed tomography. *Quantitative Imaging in Medicine and Surgery*, 5:552–568. 71

[Carter et al., 1977] Carter, Dennis.R, H., and Wilson.C (1977). Bone compressive strength: The influence of density and strain rate. *Science (New York, N.Y.)*, 194:1174–6. 54

[Choi et al., 2010] Choi, J. K., Gardner, T. R., Yoon, E., Morrison, T. A., Macaulay, W. B., and Geller, J. A. (2010). The Effect of Fixation Technique on the Stiffness of Comminuted Vancouver B1 Periprosthetic Femur Fractures. *The Journal of Arthroplasty*, 25(6):124–128. 65

[Choi et al., 2015] Choi, W., Wakeling, J., and Robinovitch, S. (2015). Kinematic analysis of video-captured falls experienced by older adults in long-term care. *Journal of Biomechanics*, 48(6):911–920. xiii, 132, 133, 134, 135, 136

[Cristofolini et al., 1996] Cristofolini, L., Viceconti, M., Cappello, A., and Toni, A. (1996). Mechanical validation of whole bone composite femur models. *Journal of biomechanics*, 29(4):525–535. 109

[Currey, 2010] Currey, J. (2010). Mechanical properties and adaptations of some less familiar bony tissues. *Journal of the Mechanical Behavior of Biomedical Materials*, 3(5):357–372. 54

[Currey, 2004] Currey, J. D. (2004). Tensile yield in compact bone is determined by strain, post-yield behaviour by mineral content. *Journal of Biomechanics*, 37(4):549–556. 55

[Danet, 2011] Danet, S. (2011). L'état de santé de la population en France - 2011. page 342. 130

[D.Bell and Goncalves, 2020] D.Bell, E. and Goncalves (2020). Why do falls and lower limb fractures occur more frequently in the diabetic patient and how can they be prevented? *Diabetes Therapy*, 11:1687 – 1694. 130

[Donald et al., 1975] Donald, T. Reilly, A., and Burstein, H. (1975). The elastic and ultimate properties of compact bone tissue. *Journal of Biomechanics*, 8(6):393 – 405. 54

[Du et al., 2006] Du, C., ma, H., Ruo, M., Zhang, Z., Yu, X., and Zeng, Y. (2006). An experimental study on the biomechanical properties of the cancellous bones of distal femur. *Bio-medical materials and engineering*, 16:215–22. 56

[Duncan and Masri, 1995] Duncan, C. and Masri, B. (1995). Fractures of the femur after hip replacement. *Instructional course lectures*, 44:293–304. 63

[D.Woolf et al., 2003] D.Woolf, Anthony, P., and Bruce (2003). Burden of major musculoskeletal conditions. *Bulletin of the World Health Organization*, 81(9):646–56. 61

[Easley et al., 2007] Easley, S. K., Pal, S., Tomaszewski, P. R., Petrella, A. J., Rullkoetter, P. J., and Laz, P. J. (2007). Finite element-based probabilistic analysis tool for orthopaedic applications. *Computer methods and programs in biomedicine*, 85(1):32–40. 104

[Ehlinger et al., 2013] Ehlinger, M., Czekaj, J., Adam, P., Brinkert, D., Ducrot, G., and Bonnomet, F. (2013). Minimally invasive fixation of type B and C interprosthetic femoral fractures. *Orthopaedics & Traumatology: Surgery & Research*, 99(5):563–569. 63

[Ehlinger et al., 2019] Ehlinger, M., Soenen, M., Bahlouli, N., and Bonnevialle, P. (2019). Interprosthetic femoral fracture: Crime or punishment? *Orthopaedics & Traumatology: Surgery & Research*, 105(4):577–578. 63

[F. Morgan et al., 2001] F. Morgan, E., C. Yeh, O., C. Chang, W., and M. Keaveny, T. (2001). Nonlinear behavior of trabecular bone at small strains. *Journal of biomechanical engineering*, 123:1–9. 57

[Ford et al., 2009] Ford, C. M., Keaveny, T. M., and Hayes, W. C. (2009). The effect of impact direction on the structural capacity of the proximal femur during falls. *Journal of Bone and Mineral Research*, 11(3):377–383. 112

[Forwood, 2001] Forwood, M. (2001). Mechanical effects on the skeleton: Are there clinical implications? *Osteoporosis international : a journal established as result of cooperation between the European Foundation for Osteoporosis and the National Osteoporosis Foundation of the USA*, 12:77–83. 57

[Garellick et al.,] Garellick, G., Kärrholm, J., Rogmark, C., Rolfson, O., and Herberts, P. Swedish Hip Arthroplasty Register - Annual reporrt 2011. page 136. 62

[Goldstein, 1987] Goldstein, S. A. (1987). The mechanical properties of trabecular bone: dependence on anatomic location and function. *Journal of biomechanics*, 20(11-12):1055–1061. 56

[Grassi et al., 2017] Grassi, L., Väänänen, S. P., Ristinmaa, M., Jurvelin, J. S., and Isaksson, H. (2017). Prediction of femoral strength using 3d finite element models reconstructed from dxa images: validation against experiments. *Biomechanics and Modeling in Mechanobiology*, 16(3):989–1000. 71

[Gwathmey et al., 2010] Gwathmey, W. F., Jones-Quaidoo, S. M., Kahler, D., Hurwitz, S., and Cui, Q. (2010). Distal Femoral Fractures: Current Concepts:. *American Academy of Orthopaedic Surgeon*, 18(10):597–607. 61

[Hansen et al., 2008] Hansen, U., Zioupos, P., Simpson, R., Currey, J. D., and Hynd, D. (2008). The Effect of Strain Rate on the Mechanical Properties of Human Cortical Bone. *Journal of Biomechanical Engineering*, 130(1):011011. 55

[Heller et al., 2005] Heller, M., Bergmann, G., Kassi, J.-P., Claes, L., Haas, N., and Duda, G. (2005). Determination of muscle loading at the hip joint for use in pre-clinical testing. *Journal of Biomechanics*, 38(5):1155–1163. 81, 111

[Ho Ba Tho et al., 2012] Ho Ba Tho, M., Mazeran, P.-E., Kirat, K., and Bensamoun, S. (2012). Multiscale characterization of human cortical bone. *CMES - Computer Modeling in Engineering and Sciences*, 87:557–577. 52

[Hong et al., 2007] Hong, J., Cha, H., Park, Y., Lee, S., Khang, G., and Kim, Y. (2007). Elastic moduli and poisson's ratios of microscopic human femoral trabeculae. In Jarm, T., Kramar, P., and Zupanic, A., editors, *11th Mediterranean Conference on Medical and Biomedical Engineering and Computing 2007*, pages 274–277, Berlin, Heidelberg. Springer Berlin Heidelberg. 57

[Hou et al., 2011a] Hou, Z., Moore, B., Bowen, T. R., Irgit, K., Matzko, M. E., Strohecker, K. A., and Smith, W. R. (2011a). Treatment of interprosthetic fractures of the femur. *The Journal of trauma*, 71(6):1715–9. 62, 66

[Hou et al., 2011b] Hou, Z., Moore, B., Bowen, T. R., Irgit, K., Matzko, M. E., Strohecker, K. A., and Smith, W. R. (2011b). Treatment of interprosthetic fractures of the femur. *Journal of Trauma and Acute Care Surgery*, 71(6):1715–1719. 64, 65

[Hunt et al., 1998] Hunt, K. D., O'Loughlin, V. D., Fitting, D. W., and Adler, L. (1998). Ultrasonic determination of the elastic modulus of human cortical bone. *Medical & Biological Engineering & Computing*, 36(1):51–56. 55

[Iesaka et al., 2005] Iesaka, K., Kummer, F. J., and Di Cesare, P. E. (2005). Stress risers between two ipsilateral intramedullary stems. 20(3):386–391. x, xi, 72, 73, 76, 81, 84, 122, 126, 150

[Johnson et al., 2010] Johnson, T., Socrate, S., and Boyce, M. (2010). A viscoelastic, viscoplastic model of cortical bone valid at low and high strain rates. *Acta Biomaterialia*, 6(10):4073–4080. 55

[Katz and Ukraincik, 1971] Katz, J. and Ukraincik, K. (1971). On the anisotropic elastic properties of hydroxyapatite. *Journal of Biomechanics*, 4(3):221 – 227. 54

[Kayabasi et al., 2007] Kayabasi, Oguz, E., and Bulent (2007). The effects of static, dynamic and fatigue behavior on three-dimensional shape optimization of hip prosthesis by finite element method. *Materials & Design*, 28(8):2269–2277. 107, 131

[Keaveny et al., 1994] Keaveny, T. M., Wachtel, E. F., Ford, C. M., and Hayes, W. C. (1994). Differences between the tensile and compressive strengths of bovine tibial trabecular bone depend on modulus. *Journal of Biomechanics*, 27(9):1137–1146. 57

[Kefalas et al., 2012] Kefalas, V., D., and Eftaxiopoulos (2012). Experimental study of cancellous bone under large strains and a constitutive probabilistic model. *Journal of the Mechanical Behavior of Biomedical Materials*, 6:41 – 52. 56

[Keller, 1994] Keller, T. S. (1994). Predicting the compressive mechanical behavior of bone. *Journal of Biomechanics*, 27(9):1159 – 1168. 55

[Kenny et al., 1998] Kenny, P., Rice, J., and Quinlan, W. (1998). Interprosthetic fracture of the femoral shaft. *The Journal of Arthroplasty*, 13(3):361–364. 72

[Keyak, 2001] Keyak, J. (2001). Improved prediction of proximal femoral fracture load using non-linear finite element models. *Medical Engineering & Physics*, 23(3):165–173. 71

[Kulin et al., 2011] Kulin, R. M., Jiang, F., and Vecchio, K. S. (2011). Effects of age and loading rate on equine cortical bone failure. *Journal of the Mechanical Behavior of Biomedical Materials*, 4(1):57–75. 53

[Kurtz et al., 2007] Kurtz, S., Ong, K., Lau, E., Mowat, F., and Halpern, M. (2007). Projections of primary and revision hip and knee arthroplasty in the united states from 2005 to 2030. 89(4):780–785. 59

[Lakatos et al., 2014] Lakatos, v., Magyar, L., and Bojtár, I. (2014). Material Properties of the Mandibular Trabecular Bone. *Journal of Medical Engineering*, 2014:1–7. 56

[Laporte et al., 2003] Laporte, S., Skalli, W., de Guise, J., Lavaste, F., and Mitton, D. (2003). A biplanar reconstruction method based on 2d and 3d contours: Application to the distal femur. *Computer methods in biomechanics and biomedical engineering*, 6:1–6. 71

[Lau et al., 2011] Lau, A. N., Adachi, J., and D. (2011). Bone Aging. In Nakasato, Y. and Yung, R. L., editors, *Geriatric Rheumatology*, pages 11–16. Springer New York, New York, NY. 59

[Lehmann et al., 2012] Lehmann, W., Rupprecht, M., Nuechtern, J., Melzner, D., Sellenschloh, K., Kolb, J., Fensky, F., Hoffmann, M., Püschel, K., Morlock, M., and Rueger, J. M. (2012). What is the risk of stress risers for interprosthetic fractures of the femur? A biomechanical analysis. *International Orthopaedics*, 36(12):2441–2446. xi, 77, 79, 81, 84

[Lotz et al., 1991] Lotz, J., J Cheal, E., and Hayes, W. (1991). Fracture prediction for the proximal femur using finite element models: Part i - linear analysis. *Journal of biomechanical engineering*, 113:353–60. 71

[Lotz et al., 1990] Lotz, J. C., Gerhart, T. N., and Hayes, W. C. (1990). Mechanical properties of trabecular bone from the proximal femur: a quantitative ct study. *Journal of computer assisted tomography*, 14 1:107–14. 57

[Luo, 2017] Luo, Y. (2017). *Finite Element Modeling of Femur Stresses/Strains Induced by Impact Force*, pages 97–109. 71

[Mamczak et al., 2010] Mamczak, C. N., Gardner, M. J., Bolhofner, B., Borrelli, J., Streubel, P. N., and Ricci, W. M. (2010). Interprosthetic Femoral Fractures:. *Journal of Orthopaedic Trauma*, 24(12):740–744. 62, 64, 66, 72

[McElhaney, 1966] McElhaney, J. H. (1966). Dynamic response of bone and muscle tissue. *Journal of Applied Physiology*, 21(4):1231–1236. 55

[McNamara et al., 1994] McNamara, B. P., Cristofolini, L., Toni, A., and Taylor, D. (1994). Evaluation of experimental and finite element models of synthetic and cadaveric femora for pre-clinical design-analysis. *Clinical materials*, 17(3):131–140. 109

[M.Dowsey et al., 2013] M.Dowsey, Michelle, M., and F., P. (2013). Predictors of Pain and Function Following Total Joint Replacement. In Kinov, P., editor, *Arthroplasty - Update*. InTech. 61

[Mercer et al., 2006] Mercer, C., He, M., Wang, R., and Evans, A. (2006). Mechanisms governing the inelastic deformation of cortical bone and application to trabecular bone. *Acta Biomaterialia*, 2(1):59–68. 54

[Mirzaei et al., 2012] Mirzaei, M., Samiezadeh, S., Khodadadi, A., and Ghazavi, M. (2012). Finite element prediction and experimental verification of the failure pattern of proximal femur using quantitative computed tomography images. 71

[Mu Jung and Sang Kim, 2014] Mu Jung, J. and Sang Kim, C. (2014). Analysis of stress distribution around total hip stems custom-designed for the standardized asian femur configuration. *Biotechnology & Biotechnological Equipment*, 28(3):525–532. 70, 71

[Muller, 1990] Muller, M. E. (1990). *The comprehensive classification of fractures of long bones*. Springer-Verlag, Berlin New York. 60, 61

[Nalla et al., 2003] Nalla, R., Kinney, J., and Ritchie, R. (2003). Mechanistic fracture criteria for the failure of human cortical bone. *Nature Materials*, 2(3):164–168. 74, 112

[Neil et al., 2004] Neil, Dong, X., and Guo (2004). The dependence of transversely isotropic elasticity of human femoral cortical bone on porosity. *Journal of Biomechanics*, 37(8):1281–1287. 55

[Nelson et al., 2000] Nelson, D. A., Barondess, D. A., Hendrix, S. L., and Beck, T. J. (2000). Cross-Sectional Geometry, Bone Strength, and Bone Mass in the Proximal Femur in Black and White Postmenopausal Women. *Journal of Bone and Mineral Research*, 15(10):1992–1997. 58

[Nelson et al., 2004] Nelson, D. A., Pettifor, J. M., Barondess, D. A., Cody, D. D., Uusi-Rasi, K., and Beck, T. J. (2004). Comparison of Cross-Sectional Geometry of the Proximal Femur in White and Black Women from Detroit and Johannesburg. *Journal of Bone and Mineral Research*, 19(4):560–565. 58

[Neumann et al., 2015] Neumann, M. V., Südkamp, N. P., and Strohm, P. C. (2015). Management of Femoral Shaft Fractures. page 11. 60

[Nicolella et al., 2001] Nicolella, D. P., Thacker, B. H., Katoozian, H., and Davy, D. T. (2001). Probabilistic risk analysis of a cemented hip implant. *ASME-PUBLICATIONS-BED*, 50:427–428. 104

[Novitskaya et al., 2011] Novitskaya, E., Chen, P.-Y., Lee, S., Castro-Ceseña, A., Hirata, G., Lubarda, V. A., and McKittrick, J. (2011). Anisotropy in the compressive mechanical properties of bovine cortical bone and the mineral and protein constituents. *Acta Biomaterialia*, 7(8):3170–3177. 54

[Oftadeh et al., 2015] Oftadeh, R., Perez-Viloria, M., Villa-Camacho, J. C., Vaziri, A., and Nazarian, A. (2015). Biomechanics and Mechanobiology of Trabecular Bone: A Review. *Journal of Biomechanical Engineering*, 137(1):010802. 56

[Op Den Buijs and Dragomir-Daescu, 2011] Op Den Buijs, J. and Dragomir-Daescu, D. (2011). Validated finite element models of the proximal femur using two-dimensional projected geometry and bone density. *Computer Methods and Programs in Biomedicine*, 104(2):168 – 174. 7th IFAC Symposium on Modelling and Control in Biomedical Systems. 71

[Oryan et al., 2015] Oryan, A., Monazzah Harsini, S., and Bigham Sadegh, A. (2015). Bone injury and fracture healing biology. *Biomedical and environmental sciences : BES*, 28:57–71. 58

[Peng et al., 2006] Peng, L., Bai, J., Zeng, X., and Zhou, Y. (2006). Comparison of isotropic and orthotropic material property assignments on femoral finite element models under two loading conditions. *Medical Engineering & Physics*, 28(3):227–233. 54

[Pires et al., 2014] Pires, R. E. S., de Toledo Lourenço, P. R. B., Labronici, P. J., da Rocha, L. R., Balbachevsky, D., Cavalcante, F. R., and de Andrade, M. A. P. (2014). Interprosthetic femoral fractures: proposed new classification system and treatment algorithm. *Injury*, 45:S2–S6. 64, 66

[Pivonka and Dunstan, 2012] Pivonka, P. and Dunstan, C. R. (2012). Role of mathematical modeling in bone fracture healing. *BoneKEy reports*, 1. 71

[Platzer et al., 2011] Platzer, P., Schuster, R., Luxl, M., Widhalm, H. K., Eipeldauer, S., Krusche-Mandl, I., Ostermann, R., Blutsch, B., and Vécsei, V. (2011). Management and outcome of interprosthetic femoral fractures. *Injury*, 42(11):1219–1225. 64, 66

[Quirynen, 2016] Quirynen, T. (2016). The interprosthetic gap as a risk factor for interprosthetic fractures of the femur. 73, 75, 81, 126, 150

[Quirynen et al., 2016] Quirynen, T., Corten, K., Segal, O., Simon, J.-P., Sloten, J. V., and Lenthe, H. G. v. (2016). Small interprosthetic gaps do not increase femoral peri-prosthetic fracture risk. An in vitro biomechanical analysis. *Acta Orthopaedica Belgica*, 83(2). xi, 78, 79, 99

[Reginster et al., 1999] Reginster, J.-Y., Gillet, P., Sedrine, W. B., Brands, G., Ethgen, O., defroidmont, C., and Gosset, C. (1999). Direct Costs of Hip Fractures in Patients Over 60 Years of Age in Belgium:. *PharmacoEconomics*, 15(5):507–514. 59

[Rho et al., 1993] Rho, J. Y., Ashman, R. B., and Turner, C. H. (1993). Young's modulus of trabecular and cortical bone material: Ultrasonic and microtensile measurements. *Journal of Biomechanics*, 26(2):111 – 119. 57

[Rho et al., 1998] Rho, J.-Y., Kuhn-Spearing, L., and Zioupos, P. (1998). Mechanical properties and the hierarchical structure of bone. *Medical Engineering & Physics*, 20(2):92–102. 51, 52, 54

[Rorabeck et al., 1998] Rorabeck, C. H., Angliss, R. D., and Lewis, P. L. (1998). Fractures of the femur, tibia, and patella after total knee arthroplasty: decision making and principles of management. *Instructional course lectures*, 47:449–58. 62

[Rorabeck and Taylor, 1999] Rorabeck, C. H. and Taylor, J. W. (1999). Classification of periprosthetic fractures complicating total knee arthroplasty. *Orthopedic Clinics of North America*, 30(2):209–214. 63

[Rubenstein et al., 1994] Rubenstein, L. Z., Josephson, K. R., and Robbins, A. S. (1994). Falls in the nursing home. *Annals of internal medicine*, 121(6):442–451. 130

[Salminen et al., 1997] Salminen, S., Pihlajamäki, H., Avikainen, V., Kyrö, A., and Böstman, O. (1997). Specific features associated with femoral shaft fractures caused by low-energy trauma. *The Journal of trauma*, 43(1):117–22. 60

[Schileo et al., 2008a] Schileo, E., Dall'Ara, E., Taddei, F., Malandrino, A., Schotkamp, T., Baleani, M., and Viceconti, M. (2008a). An accurate estimation of bone density improves the accuracy of subject-specific finite element models. *Journal of Biomechanics*, 41(11):2483–2491. 74, 112

[Schileo et al., 2008b] Schileo, E., Taddei, F., Cristofolini, L., and Viceconti, M. (2008b). Subject-specific finite element models implementing a maximum principal strain criterion are able to estimate failure risk and fracture location on human femurs tested in vitro. *Journal of Biomechanics*, 41(2):356–367. 112

[Scolaro et al., 2017] Scolaro, John A., S., and Ran (2017). Management of Interprosthetic Femur Fractures:. *Journal of the American Academy of Orthopaedic Surgeons*, 25(4):e63–e69. 62

[Soenen et al., 2013] Soenen, M., Baracchi, M., De Corte, R., Labey, L., and Innocenti, B. (2013). Stemmed TKA in a Femur With a Total Hip Arthroplasty. *The Journal of Arthroplasty*, 28(8):1437–1445. x, xii, 72, 73, 74, 79, 81, 84, 86, 87, 99, 106, 107, 109, 112, 125, 126, 132

[Soenen et al., 2006] Soenen, M., Lautridou, C., Lebel, B., Hulet, C., Migaud, H., May, O., Laffargue, P., and Burdin, P. (2006). [periprosthetic fractures around total hip and knee arthroplasty. review of the literature]. *Revue de chirurgie orthopédique et réparatrice de l'appareil moteur*, 92:2S44–2S51. 63

[Soenen et al., 2011] Soenen, M., Migaud, H., Bonnomet, F., Girard, J., Mathevon, H., and Ehlinger, M. (2011). Interprosthetic femoral fractures: Analysis of 14 cases. Proposal for an additional grade in the Vancouver and SoFCOT classifications. *Orthopaedics & Traumatology: Surgery & Research*, 97(7):693–698. 62, 64

[Solarino et al., 2014] Solarino, G., Vicenti, G., Moretti, L., Abate, A., Spinarelli, A., and Moretti, B. (2014). Interprosthetic femoral fractures—A challenge of treatment. A systematic review of the literature. *Injury*, 45(2):362–368. 62, 65, 72, 130

[Speirs et al., 2007] Speirs, A. D., Heller, M. O., Taylor, W. R., Duda, G. N., and Perka, C. (2007). Influence of changes in stem positioning on femoral loading after thr using a short-stemmed hip implant. *Clinical biomechanics*, 22(4):431–439. 104

[Stoffel et al., 2016] Stoffel, K., Sommer, C., Kalampoki, V., Blumenthal, A., and Joeris, A. (2016). The influence of the operation technique and implant used in the treatment of periprosthetic hip and interprosthetic femur fractures: a systematic literature review of 1571 cases. *Archives of Orthopaedic and Trauma Surgery*, 136(4):553–561. 65

[Talbot et al., 2008] Talbot, M., Zdero, R., and Schemitsch, E. H. (2008). Cyclic Loading of Periprosthetic Fracture Fixation Constructs:. *The Journal of Trauma: Injury, Infection, and Critical Care*, 64(5):1308–1312. 81

[Testi et al., 1999] Testi, D., Viceconti, M., Baruffaldi, F., and Cappello, A. (1999). Risk of fracture in elderly patients: a new predictive index based on bone mineral density and finite element analysis. *Computer methods and programs in biomedicine*, 60(1):23—33. 71

[Tinetti et al., 1994] Tinetti, M., Baker, D., Mcavay, G., Claus, E., Garrett, P., Gottschalk, M., Koch, M., Trainor, K., and Horwitz, R. (1994). A multifactorial intervention to reduce the risk of falling among elderly people living in the community. *The New England journal of medicine*, 331:821–7. 130

[Travison et al., 2008] Travison, T. G., Beck, T. J., Esche, G. R., Araujo, A. B., and McKinlay, J. B. (2008). Age trends in proximal femur geometry in men: variation by race and ethnicity. *Osteoporosis International*, 19(3):277–287. 58

[Turner et al., 1999] Turner, C. H., Rho, J., Takano, Y., Tsui, T. Y., and Pharr, G. M. (1999). The elastic properties of trabecular and cortical bone tissues are similar: results from two microscopic measurement techniques. *Journal of Biomechanics*, 32(4):437 – 441. 57

[Valle Cruz et al., 2016] Valle Cruz, J. A., Urda, A. L., Serrano, L., Rodriguez-Gonzalez, F. A., Otero, J., Moro, E., and López-Durán, L. (2016). Incidence of and risk factors for femoral fractures in the gap between hip and knee implants. *International Orthopaedics*, 40(8):1697–1702. 72

[Vanderoost et al., 2011] Vanderoost, J., Jaecques, S. V., der Perre, G. V., Boonen, S., D'hooge, J., Lauriks, W., and van Lenthe, G. (2011). Fast and accurate specimen-specific simulation of trabecular bone elastic modulus using novel beam–shell finite element models. *Journal of Biomechanics*, 44(8):1566 – 1572. 56

[Vashishth et al., 2001] Vashishth, D., Gibson, G., Khoury, J., Schaffler, M., Kimura, J., and Fyhrie, D. (2001). Influence of nonenzymatic glycation on biomechanical properties of cortical bone. *Bone*, 28(2):195 – 201. 53

[Verhulp et al., 2008] Verhulp, E., Van Rietbergen, B., Muller, R., and Huiskes, R. (2008). Micro-finite element simulation of trabecular-bone post-yield behaviour - effects of material model, element size and type. *Computer methods in biomechanics and biomedical engineering*, 11:389–95. 56

[Wagner, 2003] Wagner, M. (2003). General principles for the clinical use of the LCP. *Injury*, 34:31–42. 65

[Wang et al., 2019] Wang, K., Kenanidis, E., Miodownik, M., Tsiridis, E., and Moazen, M. (2019). Periprosthetic fracture fixation of the femur following total hip arthroplasty: A review of biomechanical testing – Part II. *Clinical Biomechanics*, 61:144–162. 65, 71

[Wang et al., 2009] Wang, Y., Simpson, J., Wluka, A. E., Teichtahl, A. J., English, D. R., Giles, G. G., Graves, S., and Cicuttini, F. M. (2009). Relationship between body adiposity measures and risk of primary knee and hip replacement for osteoarthritis: a prospective cohort study. *Arthritis Research & Therapy*, 11(2):R31. 61

[Weiser et al., 2014] Weiser, L., Korecki, M. A., Sellenschloh, K., Fensky, F., Püschel, K., Morlock, M. M., Rueger, J. M., and Lehmann, W. (2014). The role of inter-prosthetic distance, cortical thickness and bone mineral density in the development of inter-prosthetic fractures of the femur: a biomechanical cadaver study. 96-B(10):1378–1384. xi, 73, 77, 78, 79, 81, 84, 87, 88, 99, 109, 126, 150

[Weiss et al., 2009] Weiss, R. J., Montgomery, S. M., Al Dabbagh, Z., and Jansson, K.-k. (2009). National data of 6409 Swedish inpatients with femoral shaft fractures: Stable incidence between 1998 and 2004. *Injury*, 40(3):304–308. 60

[Wähnert et al., 2014] Wähnert, D., Schröder, R., Schulze, M., Westerhoff, P., Raschke, M., and Stange, R. (2014). Biomechanical comparison of two angular stable plate constructions for periprosthetic femur fracture fixation. *International Orthopaedics*, 38(1):47–53. 65

[World Report on Disability, 2012] World Report on Disability (2012). *: WHO; 2011 cited 06/08/2012.* [Online]. Available from: http://www.who.int/disabilities/world_report/2011/en/index.html. 61

[Yoon and Katz, 1976] Yoon, H. S. and Katz, J. L. (1976). Ultrasonic wave propagation in human cortical bone—i. theoretical considerations for hexagonal symmetry. *Journal of Biomechanics*, 9(6):407 – IN3. 54

[Zhang et al., 2010] Zhang, F., Tan, L.-J., Lei, S.-F., and Deng, H.-W. (2010). The differences of femoral neck geometric parameters: effects of age, gender and race. *Osteoporosis International*, 21(7):1205–1214. 58

[Zioupos et al., 2008] Zioupos, P., Hansen, U., and Currey, J. D. (2008). Microcracking damage and the fracture process in relation to strain rate in human cortical bone tensile failure. *Journal of Biomechanics*, 41(14):2932 – 2939. 55

Maximum bending force

The maximum force related to the fracture risk of the femur bone was determined by performing a two-point bending test with a symmetric and non-symmetric configuration. The femur bone stiffness as measured in the bending tests depends on bone structure (shape, thickness, and internal architecture) and bone tissue level material properties. The femur is the longest bone, so that it is highly sensitive to bending loads, that too in the mid-shaft region. Accordingly, the femur bone was prepared to be loaded under the two-point bending test out of the midshaft region, within a controlled loading condition. Firstly, a finite element simulation of the bending test has been applied on the cylindrical tube which representing the femur without any prostheses to detect the extent of the loads without approaching the fracture risk of the femur. While the placement of the prostheses changes the construction elasticity and increases the stiffness. Then the cylindrical tube was loaded with the presence of the hip prosthesis and the different lengths of the knee prosthesis. Seven random loads have been applied and the fracture risk has been calculated.

The results show that deformation of the cylindrical shaft without the presence of the prostheses is higher than the one with the prostheses (figure.4.5.3), (figure.4.5.2).

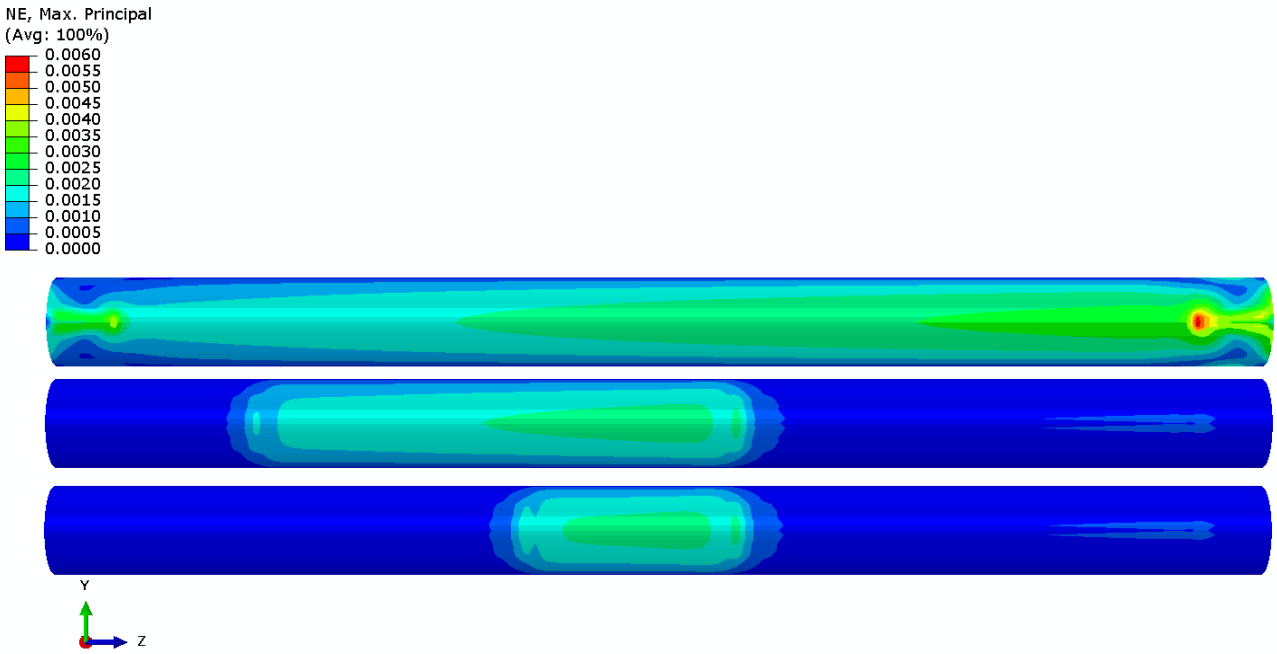

Figure 4.5.1: Maximum principle strains distribution under the two-point bending test : (A) represent the cylindrical tube model without any prostheses, (B) represent the cylindrical tube model with the presence of hip prothesis and knee prothesis of 70 mm in length, (C) represent the cylindrical tube model with the presence of hip prothesis and knee prothesis of 145 mm in length

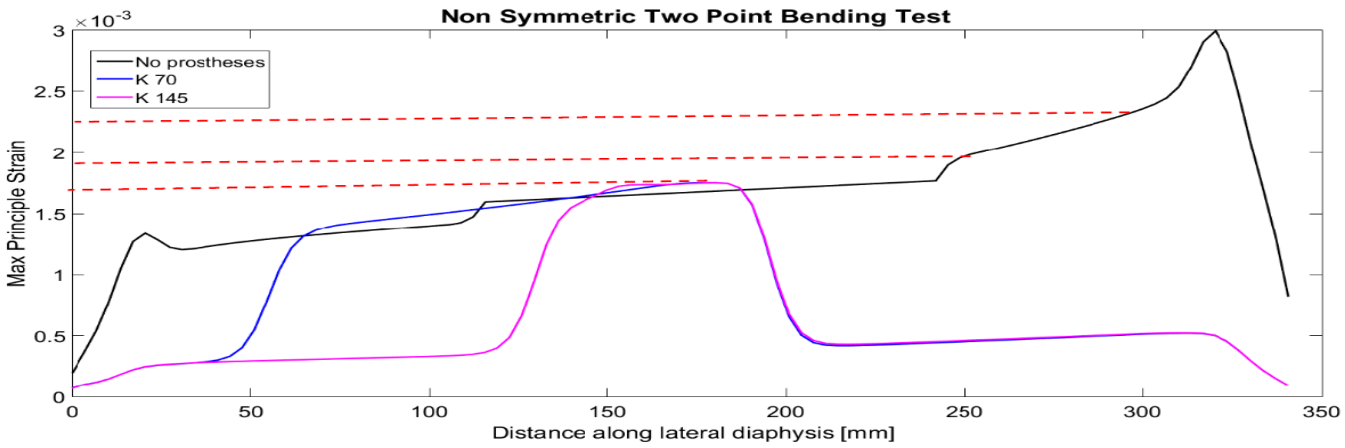

Figure 4.5.2: A comparison of the presence and the nonpresence of the prostheses under a two-point bending test with a non-symmetric configuration

The results shows that the maximum load that should be use has to be under 4325, while the fracture risk value is 1 in this load. In our simulations in thesis, we used a load of 550 N so that it s a safe load to perform the test without any risk of fracture (figure.4.5.3).

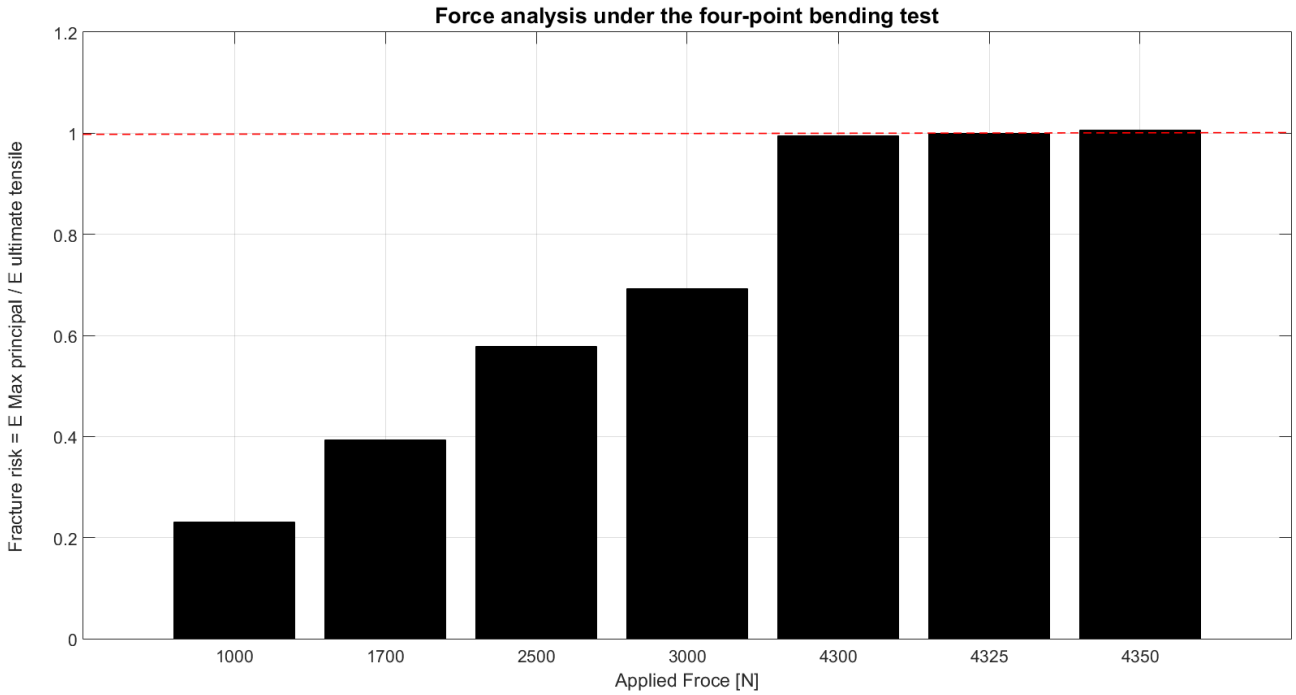

Figure 4.5.3: Maximum force analysis under the four-point bending test

List of conferences and publications

The List of the conferences:

- 23rd Congress of the European Society of Biomechanics, July 2 - 5, 2017, Seville, Spain.
- 92ème Congrès de la Société Française de Chirurgie Orthopédique et Traumatologique – SOFCOT 2017, 06-09 Novembre 2017, Paris, France https://doi.org/10.1016/j.rcot.2017.09.276.
- Journée des posters de l'école doctorale,2017, l'école doctorale MSII, Strasbourg, France.
- Fédération de Médecine Translationnelle de Strasbourg (FMTS), Jeudi 27 AVRIL 2017.
- 7ème journée de mécanique ICUBE mai 2018.
- 10ème réunion annuelle de l'ITS – 6 & 7 novembre 2018 Strasbourg, Faculté de Chirurgie dentaire.
- Fédération de Médecine Translationnelle de Strasbourg (FMTS), Jeudi 26 AVRIL 2019.

The List of the publications:

- Conference paper at 92ème Congrès de la Société Française de Chirurgie Orthopédique et Traumatologique – SOFCOT 2017

Figure 4.5.4: Conferance paper